MODELING SOLUTE DYNAMICS IN AQUIFERS: CASE STUDY OF IRON DISPERSION IN CHYULU AQUIFER, KENYA

STANLEY KIBE NG'ANG'A
MSc. (JKUAT)
EECX0650P/2016

A Thesis Submitted in Partial Fulfillment of the Requirements for the Award of the Degree of Doctor of Philosophy in Civil Engineering

in

The School of Civil and Resources Engineering

of

The Technical University of Kenya

2022

DECLARATION

This thesis is my original work and has not been presented in any other institution for a degree award or other qualification.

Signature …… Date ……..

STANLEY KIBE NG'ANG'A

REG. NO. EECX 0650P/2016

This thesis has been submitted with our approval as supervisors:

Signature …… Date ……..

PROF. GEORGE MUTURI THUMBI

PROFESSOR OF CIVIL ENGINEERING

THE TECHNICAL UNIVERSITY OF KENYA

Signature …… Date ……..

PROF. MAURICE OMONDI NYADAWA

PROFESSOR OF CIVIL ENGINEERING

JARAMOGI OGINGA ODINGA UNIVERSITY OF SCIENCE AND TECHNOLOGY

Signature …… Date ……..

DR. GEORGE OGINGA OKWADHA

SENIOR LECTURER IN CIVIL ENGINEERING

TECHNICAL UNIVERSITY OF KENYA

DEDICATION

This research work is dedicated to God who gives me strength, grace, patience and provides for all my needs. May this work reduce, even in a very small way, the suffering of the residents of arid and semi-arid lands who continue to suffer hunger, disease and poverty in a world full of resources.

ACKNOWLEDGEMENTS

I would like, first and foremost, to thank Prof. Thumbi, Prof. Nyadawa and Dr. Oginga Okwadha for supervising this work. I also thank B. Ngula, P. Njuguna and J. Kamathi as my research assistants for making long hours in the collection of huge amount of data that forms part of this work. Special thanks to Makueni County Government and Water Resources Authority (WRA) for availing their data bank to this research. I also thank my colleagues G. Hinga and Lydia E. for reading this manuscript.

The most special thanks goes to my wife Patricia and children; Njeri, Ng'ang'a and Simon who have always been there for me in this journey.

ABSTRACT

Chyulu in Makueni County falls in the Arid and Semi-Arid Lands (ASAL) parts of southeastern Kenya. The main source of water is boreholes whose water is mostly saline, harmful to human health and environment and sometimes fail to produce enough water to justify the high cost of drilling. Availability of both the groundwater potential and water quality index (WQI) maps would be paramount. Water quality parameters such as pH, turbidity, iron, fluoride, electrical conductivity, total dissolved solids, were used in assessment of the impact of stratum geochemistry on the groundwater quality. The results showed water whose parameters far exceeded the upper limits as per World Health Organization (WHO) standards. The negative impact of iron to storage and plumbing facilities was notable with tanks leaking by the third year of use due to corrosion and therefore reduction of iron using appropriate technology in the water would be a notable improvement of water quality. These parameters included iron, fluoride and nitrates among others and to understand their behavior in the aquifer/stratum, groundwater models are used. These models require modification to suite particular parameter because different ions react differently in the stratum. This study sought to develop tools for solute characterization that address strata like the Chyulu aquifer one that have excess iron among other salts. The study mapped groundwater in terms of quantity using drainage, rainfall, aspect, slope, topography, impact of the vadoze zone, and conductivity of the aquifer as inputs in (DRASTIC) modeling which utilizes both GIS and remote sensing techniques. The groundwater quality index (WQI) and quality map was also developed using the corresponding parameters' concentrations. The study also tested a non-motorized aeration/filtration process using a fabricated unit that was used for aeration of feed water and its filtration. A user-defined Reactive Three–Dimensional Multi-Species Transport (RT3D) sub-routine that was linked to the Groundwater Modeling System (GMS) software that depicted the oxygenation of ferrous iron (II) at neutral pH was developed and tested using the non-motorized aeration filtration unit that now acted as batch reactor to predict chemical reactions in the aquifer. To validate the user-defined RT3D subroutine ferrous and ferric ions were measured every six months from June 2016 to December 2019. These test results were compared with those that were obtained from GMS/RT3D model after the subroutine had been linked to GMS software. This study concludes that the main consideration in deciding the site of a borehole in the study area be water quality because only 10% of the whole study area had portable water while 91 % of the area has either high or moderate groundwater potential. The non-motorized aeration/filtration system reduced the iron in groundwater by 58.3% and therefore this oxygenation process improves water quality. The other conclusion is that the User-defined RT3D subroutine predicted the iron flow through the stratum very accurately because the coefficient of correlation for ferrous ions was 0.8 while that for ferric ions was 0.82 which meant that the proposed subroutine as linked to the GMS model can be used to predict the solute (ferrous and ferric ions) in the Chyulu stratum/aquifer at Makindu. This study recommends that this user-defined model be tested and calibrated for use in other aquifers and that the model be tailor made/adopted to investigate the flow of calcium and its derivatives in aquifers.

TABLE OF CONTENT

LIST OF TABLES

Page.

LIST OF FIGURES

Page.

LIST OF PLATES

Page.

LIST OF ABBREVIATIONS

3DFEMFAT	3-D Finite-Element Model of Flow and Transport through Saturated-Unsaturated Media
AA	Action Aid
ANIS	American National Standards Institute
AQUA3D	3-D Groundwater Flow and Contamination Transport Model
ASAL	Arid and Semi -Arid Lands
BGS	British Geological Survey
BIOS	Basic Input and Output
ChemFlux	Finite Element Mass Transport Model
CO_2	Carbon Dioxide
DEM	Digital Elevation Model
DLL	Dynamic Link Library
DRASTIC	**D**rainage, **R**ainfall, **A**spect, **S**lope, **T**opography, **I**mpact of the Vadose Zone and **C**onductivity of the Aquifer Model
EC	Electrical Conductivity
EPA	Environmental Pollution Agency
ESRI	Environmental Systems Research Institute
FDM	Finite Difference Method
FR	Frequency Ratio
FORTRAN	FORmula TRANsilation
GFLOW	Analytical Element Model with Conjunctive Surface Water and Groundwater Flow and a MODFLOW Model Extract Feature
GIS	Geographical Information System
GMT	Generic Mapping Tool

GMS	Groundwater modeling System
GWPI	Groundwater Potential Index
GPS	Geographical Positioning System
GV	Groundwater Vistas
H_2CO_3	Carbonic acid
IBM	International Business Machines
ILRI	International Livestock Research Institute
IWMI	International Water Management Institute
JICA	Japan International Cooperation Agency
KEBS	Kenya Bureau of Standards
NTU	Nephelometric Turbidity Unit
MODFLOW	Modular Three-Dimensional Finite-Difference Groundwater Flow Model
MT3DMS	Modular Three-dimensional Multi-Species Transport Model
PNNL	Pacific Northwest National Laboratory
RCMRD	Regional Centre for Mapping and Remote Sensing
RT3D	Reactive Three–Dimensional Multi-Species Transport
TARDA	Tana and Athi River Development Authority
TCE	Trichloroethene
TCU	True Color Units
UNEP	United Nations Environment Programme
USGS	United States Geological Survey
VLEACH	One-Dimensional Finite-Difference Vadose Zone Leaching Model
VS2DT	Flow and Solute Transport in Variably-Saturated, Single-Phase Flow in Porous Media

WHO	World Health Organization
WQI	Water Quality Index
WRL	Water Rest Level
WRA	Water Resources Authority
WSL	Water Stuck Level

CHAPTER 1: INTRODUCTION

1.1 BACKGROUND

Globally, the available sources of domestic and agricultural water include surface water from rivers, pans, ponds, tanks, springs and groundwater from boreholes and wells (Shiklomanov, 1998; Rahmati et al., 2015; Priya et al., 2022). Surface water is scarce in the Arid and Semi-Arid Lands (ASAL) of the world and is inaccessible in the Polar regions due to presence of glaciers. There has been gross overuse of surface water sources in the Middle East, the Americas, Southwest and Southern Asia among other places which results in increased demand of groundwater (Abdel-lah et al., 2002; Patil and Chore, 2014). Here in Kenya as well as in other parts of Africa groundwater is becoming more prominent as a source of domestic water particularly in Urban centres (Kumar, 2004; Onyancha and Getenga, 2013; Mbithi et al., 2017; Gevera et al., 2020). Groundwater constitutes 30.1 % of all freshwater in the world and is seen as a viable solution to water supply in the future (Todd, 1980; Priya et al., 2022). According to Foster and Chilton, 2003, rapid exploration of groundwater in the developing world was realised between 1970 and 1990. In the world, ASAL groundwater brings larger economic benefit per unit volume than surface warer because of its high drought reliability (Burke and Moench, 2000). In this regard, groundwater becomes the only available option in the ASAL of Kenya and more so in the study area where surface water is scarce (Kithiia, 2009; Mbithi et al., 2017).

The chemistry and quality of surface water largely depends on the chemical composition of the stratum (Amadi et al., 2015) combined with the influence of the hydrophysical, hydrochemical and hydrobiologial aspects of the water body (Chapman et al., 2013; Jakeman et al., 2016; Volodymyr et al., 2016). The quality of groundwater on the other hand depends on the chemical composition of the stratum and boreholes are often abandoned due to the presence of obnoxious smell, color and taste among other unacceptable characteristics (Mailu, 1994; Amadi et al.,

2015). Water quality test results from the study area have shown high concentrations of iron, flourides, manganese, sulphates and carbonates that make the water saline, among other parameters such as electrical conductivity (EC), total suspended solids (TSS) which have also reported high values (Krhoda, 1989; Mwango et al., 2002; Kaluli and Gathenya, 2004; Gevera et al., 2020).

Presence of these ions and iron in particular in groundwater found in the study area is evident due to severe corroding and staining of metallic tanks and plumbing components such as taps and sinks that often collapse within the first three years of use. The decaying of teeth in people caused by excessive fluorides has also been reported in the study area after use of the groundwater (Mbithi et al., 2017; Gevera et al., 2020), while the folding of leaves upon irrigation with the groundwater is also experienced which is an indication of excess chloride (Ebrahimi and Bhatla, 2011).

Several studies on groundwater quality have been undertaken in the study area. They have mostly addressed the challenge posed by fluoride whose concentration have been found to be greater than 1.5 mg/L which is the maximum allowable by World Health Organization (WHO)(1994) and Kenya Bureau of Standards (KEBS)(1996). Concentrations of iron greater than 4.0 mg/L have been reported in samples from boreholes spread throughout the study area and are indicative of the presence of iron in the stratum. Such concentration far exceeds the allowable upper limit of 0.3 mg/L. Presence of iron in groundwater causes change of colour of water in storage tanks from colorless to brown to yellow which is evidence of oxygenation of ferrous ions to more stable iron hydroxide ($Fe(OH)_3$). According to Syazwan et al., (2020) iron ions while in water give it foul taste and makes the water aesthetically unacceptable.

The trivalent (ferric) form of iron is insoluble and sometime deposited in boreholes prompting the growth and flourishing of iron bacteria resulting in increase of turbidity and increase in pH (Singer and Stumm, 1969). The presence of iron bacteria even in low oxygen environment of

the stratum facilitates the change of ferrous iron (Fe (II)) to ferric iron (Fe (III)) (James and Ferris, 2004). The presence of iron in the aquifer/stratum poses challenges in groundwater abstraction because the pumped water has low turbidity on reaching the surface but changes immediately because of oxygenation of ferrous ions to ferric ions. This raises the turbidity because oxygenation results in formation of yellowish precipitate, ferric oxides (Ferris, 2005; Hansel et al., 2005).

Furthermore, organic substances found in groundwater can form soluble substances complexes with iron that may not oxidize to insoluble form without use of expensive oxidants. The process of oxygenation is kinetically slow and dependent on pH and would require large primary clarifiers and sedimentation basins and high financial out-lay that may not be available. Removal of iron from groundwater is achieved through a process of aeration, coagulation, sedimentation and filtration. This is an expensive undertaking where air must be pumped into the water in the oxygenation process (Kiviloog, and Fjall, 2001; Kapulu et al., 2013; Syazwan et al., 2020). Other ways of removal or reduction of concentration of iron in the groundwater must therefore be investigated and tested. This calls for understanding of physical and chemical characteristics of iron. Studies of behaviour of iron in groundwater have been undertaken for example the oxygenation of ferrous to ferric ions was investigated (Singer and Stumm, 1969). According to Makjik-Dursun et al., (2015) the expression of ferrous iron oxidation for mildly acid to neutral water (pH values between 6-8) was found to be first order and differential in nature. The oxidation of Fe(II) at these pH levels proceeds at a rate that is dependent upon the concentrations of Fe(II) and dissolved oxygen. The study of these processes in an aquifer is complex and require use of models to generate conditions in the aquifer to enhance understanding of ionic flow through the stratum (Chapelle et al., 1995; Harbaugh et al., 2000). In solute studies, the Modular Three-Dimensional Finite-Difference Groundwater Flow Model (MODFLOW) is usually employed to numerically solve solute movement problems. However,

in this study the more comprehensive groundwater study tool, the Groundwater Modeling System (GMS), that was developed in the United States by the Environmental Modeling Research Laboratory of Brigham Young University in partnership with the U.S. Army Engineers Waterways Experiment Station (Harbaugh, 2005) has been employed.

To study the behaviour of solute in the strata, modules are incorporated into the GMS that address the characteristics in question. For example, the issue maybe chemical reactions in the aquifer in which case the Reactive Three-Dimensional Multi-Species Transport (RT3D) will be activated. RT3D module does not provide solution for solute flow for all ions in the aquifers but offers possibility of a user-defined rate reaction chemical equations in form of a sub-routine which is then dynamically linked to GMS. Among the provided rate reaction chemical equations and their corresponding user- defined RT3D sub-routines available are the hydrocarbon ions such as trichloroethene (TCE) and its derivatives behaviours in the aquifers(Clement, 1997). However, the rate reaction chemical equations and sub-routine for iron and its derivatives are not provided. This study has developed the rate reaction chemical equations and the corresponding sub-routine for the iron and its derivatives that was incorporated in GMS as a user-defined package. The package allowed the estimation and prediction of iron concentration in the direction of flow.

The scope of this study entails sourcing data on boreholes' yield, depth, transimisivity, as well as groundwater quality in the study area which were then mapped on a Geographical Information System (GIS) platform. This was followed by the design of a non-motorized aeration/filtration unit which was used for reduction of iron, development and calibration of the rate reaction chemical equations of the iron. Finally, a user-defined RT3D FORTRAN sub-routine for iron in the Chyulu was developed that wss dynamically linked to GMS software. This sub-routine will be a contribution to solute dynamics studies of aquifers.

1.2 STATEMENT OF RESEARCH PROBLEM

The residents of the study area do not have adequate supply of water. Time is wasted in long queues as can be seen in Plate 1.1 where residents of the study area are seen queuing for water at a borehole. Provision of enough water would require sinking of many boreholes which is faced by lack of tools that would promote success of boreholes such as a groundwater potential map. The water that the residents obtain from the boreholes is likely to be poor quality because groundwater from the study area was reported to be saline by Kuria et al., 2012, Mbithi et al., 2017 and Gevera et al., 2020. The water from the study area has also been reported to be unfit for human consumption (Kaluli and Gathenya, 2004). For example, concentration of iron of 4.0 mg/L, which far exceeds the maximum allowable of 0.3 mg/L (WHO, 1994) have been reported.

Iron in groundwater has resulted in the abandoning of boreholes in the study area. Plates 1.2 and 1.3, for instance, show well-designed and appropriately powered boreholes that have been abandoned due to presence of excessive iron in the groundwater.

Plate 1.1 Residents of the study area queuing for water at a borehole in Komboyoo (by Author)

Plate 1.2 A borehole at Makindu designed to use wind power but abandoned when water became yellowish (by Author)

In instances where boreholes have been sunk and have enough yield, the possibility of the water being saline exist. The use of convectional treatment methods which are expensive would still not guarantee attainment of WHO standards for all parameters as groundwater quality varies greatly from one point to the other because of the geology, hydrogeology and the geochemistry of a given area. The treatment for removal of iron using convectional treatment must include addition of oxygen. This is normally achieved by use of motorized aerators that can be powerwed by solar, wind or electricity from the grid which is expensive for the local community in the study area. However, use of cheaper non-motorized aerators that attain high percentage reduction of iron using locally available materials would be welcome intervention.

Plate 1.3 A borehole designed to use solar energy but abandoned when the water became yellowish (by Author)

Experiments are required to study the behavior of solutes in groundwater (Chilton and Foster, 1995). Carrying out the experiments is time consuming, costly and also prone to human error in the data collection phase. Where there is need to study the solute behavior for conditions that are not present in the aquifer, it can be difficult to control parameters in the aquifer to fit the conditions required for the study (Anderson and Woessner, 1992). Most solute transport behavior in the aquifer are complex because they depend on a lot variables such as hydraulic conductivity, porosity, recharge, type of rocks and their reactive nature which are difficult to take account of during experiment. A solute flow model is a mathematical representation of solute flow through an aquifer, which is composed of saturated sediment and rock. In order to solve the equations that constitute the flow model, it is necessary to make simplifying assumptions about the aquifer and the physical processes governing solute flow (Anderson and Woessner, 1992; Clement, T. P., 1997). Some solute models exists but cannot be generalized for all the solutes availbale becase different solutes react differently in the aquifer. Development or modification of existing models is required to suite the solute under study.

Once a model has been developed for a particular solute it is faster to generate data, easy to consider different scenarios of the aquifer as parameters can be adjucted during simulations.

The study of iron and its derivatives in the stratum is faced by lack of a vasatile model that can be used to trace the flow of iron ions in the aquifer. Such a groundwater solute flow model would enhance the understanding of iron flow in aquifers and would help in spacing of boreholes in the aquifer because the user-defined model would indicate the time that pollution from one borehole would flow to a adjoining borehole.

1.3 JUSTIFICATION OF THE STUDY

To minimize chances of failure of boreholes in terms of yield and quality the modern methods of groundwater exploration and exploitation that entail generation of groundwater potential maps of the study area are needed. To achieve these potential maps, maps of drainage, rainfall, aspect, slope, topography, impact of the vadose and electrical conductivity are generated using Geographic Information System (GIS) and Remote Sensing techniques. The DRASTIC overlay scheme of ARCHVIEW GIS techniques is applied to groundwater potential map as well as the Water Quality Index map of the study area.

The groundwater quality in the study area is saline and chances of the drilled borehole having water that is fit for human consumption are low. The groundwater will more often than not require treatment. Affordable interventions that seek improvement of the groundwater are needed. These interventions include removal or lowering of iron levels in the water through a non - motorized natural aeration and filtration unit using non-corrosive and locally available materials, an intervention that will equip the local population with an answer to poor water quality. The materials that are required to fabricate the aeration/filtration unit ought to be easy to fabricate, use locally available materials and use appropriate technology.

Water quality results are important parameters in groundwater water exploitation. This calls for sampling and testing of samples periodically which is expensive in terms of time and

resources both human and materials. The option to testing all the time is the development of a transport model that can accurately predict the concentration of water quality parameters in the aquifer. Thorough understanding of flow of ions in the stratum is key in solving solute transport characteristics. Different ions will behave differently because of the different chemical reactions that take place despite the fact that the aquifer could have the same geology, recharge, topography and solute flow dynamics among other factors. Aquifer studies are very expensive because they entail establishment of observation wells that would again call for monitoring of several years before a conclusion can be drawn. Moreover, study of flow of ions in the stratum can only be undertaken by use of groundwater models such as the groundwater modeling system (GMS). This model can estimate the flow characteristics of many ions but in this study only iron and its derivatives has been studied because high concentration of iron remains one of the major challenge in groundwater in the study area. Groundwater Modeling System (GMS) is a versatile groundwater studies tool and has several modules, which include the modular 3-Dimensional transport module (MT3DMS) (Clement, 1997). The MT3DMS is a 3-dimensional transport module in the GMS that is used in the study of transport dynamics in aquifers. RT3D is a special form of MT3DMS that simulates solute transport that has reactive chemicals in the aqueous state. In this study a User – defined FORTRAN RT3D reaction module was written in form of sub-routine which was then dynamically linked to the GMS/RT3D software to simulate ferrous and ferric contamination in the Chyulu aquifer.

The solute transport understanding flow of cations and anions and in particular, iron flow behavior has expanded aquifer flow knowledge available to inform decision-making. The data generated by use of the model was compared with data that was obtained through laboratory testing over a period of four (4) years from 2016 to June 2019.

1.4 OBJECTIVES

1.4.1 Main Objective

Modeling solute dynamics in aquifers; Case study of iron dispersion in Chyulu aquifer, Kenya.

1.4.2 Specific Objectives

1) To develop groundwater potential and Water Quality Index (WQI) maps for the study area using GIS and remote sensing techniques.
2) To develop a physical non-motorized aeration model to oxygenate ferrous ions encountered in the Chyulu aquifer at Makindu.
3) To model dispersion of iron and its derivatives in the Chyulu aquifer using a user–defined sub-routine that is dynamically linked to solute transport modules of the groundwater modeling system (GMS)

1.5 RESEARCH QUESTIONS

1. How can GIS and remote Sensing techniques be used to generate groundwater potential and quality (WQI) maps of the Chyulu aquifer area of Makueni County?
2. What is the impact of non-motorized aeration in increasing ferric ion content in groundwater treatment by filtration?
3. How is dispersion of iron and its derivatives in the Chyulu aquifer, modelled using a user - defined sub-routine that is dynamically linked to solute transport modules of RT3D and the modular 3-Dimensional transport module (MT3DMS) of groundwater modeling system (GMS).

CHAPTER 2: LITERATURE REVIEW

2.1 INTRODUCTION TO LITERATURE REVIEW

This study focused on solute transport in the Chyulu aquifer. To undertake the study, groundwater characteristics are studied alongside the parameters that effect groundwater quality. The study has reviewed issues related to the rainfall, geology, soils, topography, land cover, geochemistry, and treatment options of groundwater. In an aquifer mineral salts are many and their dispersion dynamics vary from salt to salt and are therefore difficult to study in one research. In this study iron and its derivatives, its oxygenation and its transportation dynamics have been modelled using GMS and application of GIS and remote sensing techniques.

The area of study falls in Kenya's ASAL that is characterized by low rainfall that is lower than 200 mm in some places (Gevera et al., 2020). Surface water sources are almost non-existent or very inadequate. The water collected in pans that are been constructed in many places in the study area are an important source but such water may not be safe although this impounded water could be a source of recharge. According to Huisman and Wood (1974) safe water is water that cannot harm the consumer and does not mean water that is pleasant to drink or to use for domestic purposes.

2.1.1 Groundwater Recharge

Groundwater recharge is a hydraulic process where water infiltrates downwards into an aquifer. According to Allison et al., (1994) and Simmers (1997) recharge occurs through diffuse mechanism which is large area recharge and focused mechanism which refers to the movement of water from surface or canals to underlying aquifer. Focused recharge dominates in ASAL environments such as Makindu. Major factors that contribute groundwater recharge of an area are mainly rainfall, evapotranspiration and soil type (Chilton and Foster, 1995; Foster et al., 1997). Areas of increased aridity have much lower rate and frequency of downward flux to the

water table with rainfall becoming progressively less important than surface runoff and artificial recharge. Clearance of natural vegetation which leads to soil erosion, reduced infiltration, decreased aquifer recharge and decreased aquifer discharge. According to Herzog et al., (2007) and Kahsay (2008) seasonal river transmission loss represents an important groundwater surface water exchange in arid and semi-arid regions and is potentially a significant source of recharge at the watershed scale.

From a geological standpoint, seepage is a common phenomenon of the area as the underlying geology is affected by fracturing and cracks in the rocks that allow water flow in the ground but for the purpose of this study it is assumed that the indirect recharge from the seasonal streams is integrated in the areal recharge estimates. Recharge is a function of rainfall. It is taken as a percentage of rainfall and is taken to be between 5 and 10 %.

2.1.2 Groundwater Exploitation

Rapid expansion in groundwater exploration occurred during 1970-1990 in the developing world (Foster and Chilton, 2003) and the part played by groundwater is becoming more prominent. This rapid expansion in groundwater exploitation has generated major social and economic benefits but at the same time it is leading to aquifer degradation and environmental impact (Morris et al., 2003). All groundwater exploitation by boreholes and wells results in some decline in aquifers water level (water table or piezometric surface) over a certain area (Foster and Chilton, 2003). Slightly lowering of water table is desirable as it improves land drainage and maximizes groundwater recharge rates by providing additional subsurface storage space for excess wet season rainfall (Llamas and Custodio, 2002). If overall abstraction from part or all of an aquifer system exceeds the average rates of local recharge aquifer water levels may continue to decline which provokes expensive and inefficient cycle of well deepening leading to eventual abandonment of walls. Reports of abandonment of wells has already been registered in the study area which is not a positive sign (Kithiia, 2009).

2.2 DEVELOPMENT OF GROUNDWATER POTENTIAL AND QUALITY MAPS OF STUDY AREA

Groundwater potential and water quality maps are becoming integral tools of groundwater exploration and exploitation. The concept of groundwater exploitation using GIS and remote sensing is gaining ground in Kenya and several studies have been undertaken which include; study by Kuria et al. (2012), Kiplangat and Mutua (2016), Chepchumba et al., (2019), Ochungo et al., (2019) and Nyaberi et al, 2019. Kuria et al., (2012) generated a groundwater potential map of Kitui County using GIS and remote sensing while Kiplangat and Mutua (2016), Chepchumba et al., (2019) and Ochungo et al. (2019) carried out water quality studies for Juja Location, Embu County and Lang'ata Sub- County, Nairobi respectively. Nyaberi et al., (2019) on the other hand carried out a study titled "Mapping of groundwater through the integration of remote sensing and vertical sounding in ASALs; A case study of Turkana South Sub- County, Kenya" (Rusiniak et al., 2021). These researchers have demonstrated that GIS and remote sensing technologies are becoming useful tools in groundwater studies. Similar studies have been undertaken in many other parts of the world for example Rao et al., (2009) carried out hydrogeological mapping coupled with hydrogeological investigations for evaluating groundwater potential in Madhurawada, India using GIS. Ganapuram et al., (2009) mapped groundwater potential zones in the Musi basin, India using remote sensing data and GIS. Many other researches in groundwater have been undertaken such as Kamaraju et al., (1996) and Shahid et al., (2000) among others and all have demonstrated use of GIS in hydrogeological exploration using data that has been acquired through remote sensing.

2.2.1 Generation of Groundwater Potential Map Using DRASTIC Modeling

The generation of a groundwater potential map involves application of all the parameters that have an impact in groundwater accumulation or recharge. These parameters are slope, drainage, soil, land cover, rainfall distribution, surface drainage, topography, geology of the area, lineament density, lithology and electrical conductivity (Mohamad, 2013). Several methods for

generation of groundwater potential map exist. These include probabilistic based frequency ration (FR), the generic mapping tools (GMT), the groundwater potential index (GWPI) model, and the Bivariate statistical model that utilizes data from many boreholes and springs which include the DRASTIC model. The DRASTIC model was created through a partnership between the National Water Well Association and the United States Environmental Protection agency (EPA). It was initially designed to generate groundwater vulnerability and susceptibility to pollution but has now been modified to evaluate groundwater potential (Kuria et al., 2012; Chepchumba et al., 2019; Ahsen et al., 2020).

These parameters can be easily sources using GIS and remote sensing techniques. Lithology refers to rock formation while surface drainage refers to rivers and valleys be they permanent or seasonal. Soil map was sourced from Kenya Soil Survey. Rainfall of the area and the subsequent runoff from a basin are important in determining recharge rate (Lin and Yang, 1991; Murphy, 2000; Mullaney et al., 2009; Mohamad, 2013). Areas with low rainfall would have low recharge rate although rock types also play a more significant role in variation of borehole yield particularly where such rocks have faults, cracks and fractures (Neukum and Azzam, 2008; Kuria et al., 2012).

Topography refers to shapes, relief contours, roughness and other dimensions of the earth surface. On the other hand land cover is the physical material at the surface of the earth and includes grass, trees, shrubs bare ground and water. Lineament refers to linear features in a landscape, which is an expression of feature underlying geological structures such as joints and fractures. To generate a groundwater potential map for Chyulu aquifer area the DRASTIC modeling technique was used.

Use of DRASTIC Model for Generation of Groundwater Vulnerability

The factors that influence groundwater vulnerability are weighted according to the significance of each factor in determining pollution potential (Aller et al., 1987; Breaban and Paiu, 2012).

The resultant weighted overlay then depicts the groundwater vulnerability for each spatial region.

2.2.2 Development of Groundwater Quality Assessment Map

Until recently, groundwater assessment has been carried out based on laboratory testing and field incursions but the advent of Satellite technology and Geographical Information system (GIS) has made it easy to integrate various database (Ketata -Mouna et al., 2011; Kuria, 2012). The parameters used in the generation of groundwater water quality potential using DRASTIC model are Electrical conductivity, turbidity, Iron, fluoride, pH, colour, turbidity, total dissolved solids, calcium, magnesium, chloride, manganese, potassium, sodium, sulphates and nitrates. Data from many boreholes is required in the development of Water Quality Index (WQI) for a given area. This analysis allows good and bad water quality data to be quantified by reducing data on physical, chemical and biological variables into a single number in a simple, objective and reproducible manner (House and Newsome, 1989; Khan and Pieffer, 2003; Liou et al., 2004). The WQI concept is based on the comparison of the water quality parameter with respective regulatory standards (Khan and Pieffer, 2003) and provides a single number that express overall water quality at certain location based on several water quality parameters (Yogendra and Puittaiah, 2008).

Water Quality Index

According to House and Newsome, (1989) water quality index (WQI) is a measure by which water quality is summarized for reporting to the public in a consistent manner. Water quality index (WQI) provides a comprehensive picture of water quality for regional decision makers for better planning and management (Singh, 1992; Mohesn et al., 2009). Calculations produce a score between 0-100. The higher the score; the better the quality of water. Water Quality Index values are classified as shown in Table 2.1.

Table 2.1 Classification of water quality index (WQI) (National Sanitation Foundation Water Quality Index, 2002)

Class	Description	WQI Values Range	Remarks
1	Excellent	95-100	Water has no impairment. Pristine levels.
2	Very good	89-94	Water has slight impairment. Condition close to pristine levels.
3	Good	80-88	Minor impairment. Within desirable levels.
4	Fair	65-79	Occasionally impaired.
5	Marginal	45-64	Frequently impaired.
6	Poor	0-44	Always impaired.

2.3 DEVELOPMENT OF A PHYSICAL NON-MOTORIZED AERATION MODEL FOR OXYGENATION OF FERROUS IRON

To achieve this objective literature on general groundwater chemistry, iron and its derivatives, oxygenation of ferrous ions, aeration and filtration processes was reviewed. In the review of groundwater chemistry behaviour of parameters such as pH, Electrical conductivity, alkalinity, calcium and fluoride was carried out. These parameters have an effect on geochemistry of the study area because testing results of groundwater samples from boreholes from the study area showed that the concentration these parameters was way beyond the allowable upper limits.

2.4 STUDIES IN GROUNDWATER QUALITY

Many studies on groundwater quality and groundwater geochemistry have been undertaken in various part of the world. Luo et al, 2018 carried out a study titled geochemical processes controlling the groundwater chemistry and flouride contamination in the Yunchen Basin, China. One of the findings of this study was that evaporation and ion effect favour the enrichment of flourides in groundwater by encouraging the removal of calcium via precipitation and that the desorption of flouride from mineral/organic matter surfaces was enhanced under alkaline conditions accompanied by high HCO_3 content in groundwater. Here in Kenya a study by Gevera et al., (2020) studied the naturally occurring harmful salts in groundwater in Makueni South–Eastern Kenya and their effect on drinking water quality and agriculture, the study concluded that rock weathering, aquifer lithology, recharge rate and

evaporation were the primary controls of groundwater geochemical characteristics. Another study still here in Kenya by Nair et al.,(1984) looked at the occurrence and distribution of flouride in groundwater in Kenya. The research noted the extensive occurrence of flouride ions in Kenyan's groundwater particularly in the Rift Valley and in the study area. The high occurrence of was attributed to dissolution of flourites that are part of the geology of the East African region (Nanyaro et al., 1984; Coetsiers et al, 2008; Mbithi et al., 2017) carried out a similar study but on the impact of groundwater fluorides on human health while Mailu (1994) also carried out geological studies of the Chyulu area and noted the impact of geology on water quality. The Japan International Cooperation Agency (JICA)(2015) carried out a design study on the project for groundwater development in the counties of Lower Eastern Kenya that also covered the study area. The report showed that only few data and relevant studies touching on groundwater availability and its quality was available in the study area.

Studies of Iron and its Derivatives in Aquifers

SunpriyaAchary, (2014) carried out studies on groundwater pollution due to iron content in Bhubaneswar, Odisha, India. This study looked at the origin and distribution of iron in groundwater. The study found iron concentrations of between 0.32 mg/L and 7.7 mg/L, which were all above the allowable upper limit of 0.3 mg/L.

Studies on iron oxidation on shallow aquifers of the Velika Morava River of Serbia (Majkic-Dursun et al., 2015) concluded that iron precipitation was favourable under groundwater over-exploitation. Such conditions will develop as the population increases in the study area. This study observed that the dissolved oxygen in the groundwater varied from 0.1 to 7.1 mg/L. Raju (2006) carried studies on iron contamination in groundwater that covered Tirumala-Tirupati environs in India. Study by Saxena and Ahmed (2003) showed that an increase in pH was responsible for decrease of iron concentration in groundwater. This was because at higher pH, the $Fe^{2+/3+}$ were no longer stable and precipitated as oxides and hydroxides or as siderite ($FeCO_3$).

2.5 GROUNDWATER QUALITY

Groundwater quality is dependent on geology of a given area (Nanyaro, et al., 1984; Coetsiers et al., 2008; Onyancha and Getenga, 2013). It is defined in terms of physical, chemical and biological parameters (Singh and Khan, 2011; Ketata-Mouna et al., 2011). Groundwater in some areas is fresh depending on the chemical composition of the host rock and the retention time of the water in the aquifer.

Any groundwater that has been groundwater recently recharged either by rain or river water will have similar chemistry to its source. According to Freeze and cherry (1979), Domenico and Schwarz, 1997 and James and Ferries (2004) this recharged water is chemically dilute and has very low concentrations of salts. The groundwater quality changes gradually, driven by biochemical processes, as the infiltrating water leaches salts from the soil on its downward path to the water table. Major changes in groundwater quality occurs in the soil layer due to its ability to generate carbonic acid (H_2CO_3), formed when carbon dioxide (CO_2) combines with water.

Acidification of new recharge water lowers the pH of groundwater once it reaches the water table. In the water table zone and increased infiltration, oxygen becomes less and less as the natural diffusion of atmospheric gases slows down. Furthermore, microbes also consume oxygen in their quest for survival leading to the onset of anaerobic conditions. According Freeze and cherry (1979) microbes use nitrates, sulphates and iron complexes to sustain their metabolism. Additionally, cation exchange involving minerals in the groundwater and clay particles forming the aquifer also influence the groundwater chemical composition.

2.5.1 Chemical Composition of Groundwater

Groundwater contains many chemicals both naturally occurring and manufactured. Some of these are present in large quantities while others are in trace quantities. Iron is one of the most abundant chemical in the stratum and exists in the form of ferric oxides and pyrites (Singer and

Stumm, 1969; Hem and Cropper, 1959). The parameters that indicates groundwater status include pH, electrical conductivity, acidity and alkalinity. Table 2.2 shows the results of preliminary results of water quality parameters of forty-five boreholes (45) from the study area.

Table 2.2 Representative parameters of boreholes in the study area (Ng'ang'a et al., 2015)

	Name of Borehole	UTMX	UTMY	pH	Turbidity	Colour	EC	Iron	Flouride	Calcium	Nitratres	Yield
MK1	Jamia Mosque (A)	368779	9748818	6.85	12.5	12.5	16020	4.21	3.7	37.3	48.6	9.0
MK2	Jamia Mosque (B)	368785	9748822	6.91	16.0	7.5	12550	4.42	4.20	295.0	44.6	7.2
MK3	Sikh Temple Makindu (A)	368747	9748601	7.91	18	5.0	7625	4.52	5.1	286.0	65.5	8.1
MK4	Sikh Temple Makindu (B)	368789	9748604	7.01	15	7.5	7256	4.18	5.5	338.8	34.5	7.5
MK5	Makindu Hospital	369230	9747647	6.91	10	15	6900	5.35	5.1	32.8	24.76	6.9
MK6	Makindu Railway Station	369736	9759147	6.88	67	30	2310	5.34	6.5	21.9	8.73	5.8
MK7	Ministry of Water-Makindu	367735	9759158	7.01	22.5	15	6251	4.53	3.8	360.0	23.40	8.1
MK8	Makindu Mission 1	369589	9749384	7.30	10	7.5	14320	5.21	7.5	40.13	34.50	6.5
MK9	Makindu Mission 2	369589	9749383	7.35	1.0	7.5	14320	5.21	6.55	76.2	36.50	7.5
MK10	Makindu Sisters	368779	9749726	6.74	16	7.5	9520	5.37	8.2	40.8	14.22	8.5
MK11	Musimba 1	374289	9741666	7.16	27.5	15	4120	3.80	3.6	53.6	11.15	6.1
MK12	Musimba 2	374118	9742653	7.06	15.0	22.5	3200	2.90	1.9	121.0	56.32	6.8
MK13	Musimba 3	372840	9743415	7.00	17.5	18.5	1995	4.10	4.54	63.6	19.15	5.6
MK14	Musimba 4	71846	9751510	6.88	10	25	2600	5.12	2.60	129.0	46.32	5.9
MK15	Kisingo	374684	9744605	6.79	15	5	1150	4.75	5.70	16.5	35.5	12.5
MK16	Makilya Investment 1	366611	9751194	7.01	10	15	850	5.44	2.8	23.90	150	8.8
MK17	Makilya Investment 2	366620	9751199	7.02	12	15	1850	5.44	3.0	23.90	150	9.7
MK18	Makau Boniface	366637	9747604	7.08	15	12.5	1500	4.50	2.8	23.9	45	7.2
MK19	Ndivo and Company 1	366558	9747602	6.81	10	7.5	850	5.54	5.75	44.13	55.0	12.9
MK2O	Ndivo and Company 2	366565	9747601	6.92	18.5	7.5	2550	5.23	3.5	34.8	55.0	12.5
MK21	Experimental Farm	365451	9749046	7.09	2.5	5	3150	4.60	4.70	231.8	18.6	8.2
MK22	Kyeni	372397	9748748	6.91	17.5	5.0	8500	4.22	3.70	428.6	52.0	8.4
MK23	Kai	374008	9747935	7.07	10.5	7.5	1850	3.81	5.40	78.3	33.6	6.5
MK24	Katuluni	375288	9754345	6.69	20	2.5	5235	2.88	2.90	342.9	41.5	15.6
MK25	Mulili DWD	369285	9752125	7.17	15	5.0	8730	1.88	3.0	98.4	70.0	8.6
MK26	Kiltala/ Kibwezi	390658	9722227	6.84	22.5	7.5	6730	4.21	4.5	65.4	51.24	16.0
MK27	Kambo	395977	9713205	7.52	14.4	2.5	6320	5.56	2.8	556	22.0	12.5
MK28	Komboyoo project	389206	9712346	7.69	10	10.0	1680	4.80	3.60	8.0	22.05	15.2
MK29	Kibwezi 1	381363	9738438	7.68	15	17.5	494	1.72	2.43	25.2	35.5	2.9
MK30	Kibwezi 2	390789	9722224	7.06	7.5	15	484	1.72	1.79	25.2	35.5	0.42
MK31	Muthama	385466	9737171	7.54	15	7.5	4330	2.60	1.79	31.0	2.83	24.0
MK32	Kibwezi	386926	9734684	8.04	1.5	5.0	484	1.72	4.60	25.18	35.5	18.6
MK33	Masongaleni	399933	9738451	7.92	25.0	5.0	1905	4.70	4.5	133	12.8	2.7
MK34	Masongaleni	403602	9738454	6.58	25.0	5.0	1900	4.70	4.5	133	12.8	2.52
MK35	Teresia Ndunda	385954	9834852	8.10	10	7.5	655	5.12	1.79	286.4	65.0	1.5
MK36	Muli Ndambuki	385615	9806203	7.05	61	5.0	762	1.80	5.80	34.6	54.5	8.6
MK37	Kyalo Muteti	385026	9729371	6.84	5.0	5	4740	0.77	4.21	5.9	42.8	3.0
MK38	Kiboko Reaesrch	359111	9751244	7.20	15	12.5	2350	3.22	3.50	5.7	18.9	12.5
MK39	Kiboko Usungo	362773	9760534	6.93	7.5	2.5	3420	5.76	2.56	68.3	24.5	9.6
MK40	Kibwezi AA	386364	9742090	6.94	12.5	10	4350	4.21	4.31	23.9	18.96	10.6
KM41	Masongaleni A.A.	392535	9729196	6.92	30	15	2315	3.11	2.54	83.8	9.89	5.4
MK42	Kiboko	362773	9760534	7.02	17.5	17.5	1400	4.20	1.6	23.8	4.48	8.4
MK43	S.M..Mbova	370257	9722176	7.15	10	5.0	4592	5.88	4.80	135.6	23.5	4.8
MK44	Mtito Andei	403880	9738440	6.85	7.5	342.	1 480	4.42	2.48	29.8	24.8	3.8
Mk45	Mtito Andei	403701	9738430	6.89	10	25	1840	2.36	3.6	36.2	18.2	3.2

2.5.2 Distribution of pH As a Measure of Acidity or Alkalinity of Groundwater

The pH of 7 is termed as neutral and indicates that the groundwater has equal number of hydrogen (H^+) and hydronium (OH^-) ions. The pH of rain at 5.7 is slightly acidic and tends to evolve to neutral conditions in the environment. The pH controls many chemical reactions

involving groundwater and influences the presence or absence of iron, manganese, nitrogen and arsenic. Acidic groundwater is corrosive in nature while alkaline groundwater tends to be incrusting.

The pH of small depth wells (<20m) lies between a value of 6 to 7. This is due to the acidification influence of natural soil and atmospheric processes. Old ground waters mostly in confined aquifers, that are also deeper (>100 m) the pH lies between 7 and 8. Increased concentration of bicarbonates (HCO3-), a by-product of natural reduction reactions that take place in confined aquifers or in carbonate rich rock types like the ones found in the study area, cause the higher pH. For the pH of groundwater in Chyulu, the pH lies between 6.8 and 8.2 (Appendix III) which reflects the nature of recharge water, catchment geology and its evolutional history (Kithiia, 2009; Mbithi et al., 2017; Gevera et al., 2020).

2.5.3 Electrical Conductivity

Electrical conductivity is a measure of the capacity of groundwater to pass electrical conductivity. This ability is directly related to ions in the water that come from salts such as carbonates and chlorides (Clesceri et al., 1995). Electrical conductivity is widely used as an indicator of the dissolved salts in groundwater. High conductivity values in shallow wells are caused by a combination of overlying land uses and aquifer processes while conductivity of deeper groundwater reflects natural aquifer reactions.

2.5.4 Alkalinity

Alkalinity refers to the ability of a substance to neutralizer acids. The key elements that contribute to alkalinity are bicarbonates and carbonates. Sources of these elements are natural reactions between water and carbon dioxide. They also occur as by-products of naturally occurring reduction processes. According to Saggerson (1963), carbonaceous rocks in form of outcrops of limestone ($CaCO_3$) are a source of alkalinity and have an influence in groundwater chemistry in parts of the study area.

2.5.5 Calcium

Calcium was abundant in groundwater from the study area, for example the concentration of calcium at MK4 was 338.8 mg/L while that at MK7 was 360 mg/L and many other boreholes reported concentrations greater than the 75 mg/L which is the recommended limit by WHO standards. Calcium is removed from groundwater as it flows through the stratum due to cation exchange. This involves the exchange of calcium in the groundwater with magnesium or sodium on clay particles forming the aquifer.

2.5.6 Iron in Groundwater

Iron is the most abundant, natural element found in groundwater (Hem and Cropper, 1959). The presence of iron is influenced by the chemical composition of surrounding soil and bedrock. The presence of iron salt in the groundwater is attributed to the solution of rocks and minerals mainly oxides, carbonates, sulphides and silicates. In the study area it occurs in igneous rocks such as pyroxenes, amphiboles and ferromagnesian micas among other oxides. Iron often occur in aquifers even where groundwater may have little or no oxygen, and in areas where groundwater flows through soils rich in organic matter (Freeze and cherry, 1979; Donovan and Jacobsen, 1997). The concentration of iron in groundwater can fluctuate seasonally and vary with the depth and location of the well and the geology of an area. Groundwater contaminated with this metal tend to oxidize and precipitate in piping systems reducing their hydraulic capacities. Applin and Zhao (1989) described chemical clogging in wells and plumbing installations including tanks with iron compounds. This is best explained by the fact that rocks in the study area are mostly intermediate igneous rock as confirmed by several researchers among them Saggerson (1963) and Gaciri and Davies (1993).

2.5.7 Oxygenation of Ferrous Iron

Chemical oxidation of ferrous to ferric ions by oxygen and subsequent precipitation is a complex process and oxidation of dissolved iron (II) from the groundwater to iron (III) tends

to be gradual (Hem and Cropper. 1959; Abdel-lah et al., 2002). The ferrous ions are transferred into the heavier ferric ions substances in which precipitation occurs with the oxygen uptake depending on the area and duration of contact between water and air (Kiviloog and Fjall, 2001; Isaeva and Montes, 2011)

The overall process involves a variety of partially oxidized low-crystalline iron (II) to iron (III) intermediate species in aqueous solution. These Fe-intermediate recrystallize over time into a variety of stable iron hydro (oxide) end-product such as goethite (Yang et al., 2005).

The iron oxidation in the presence of dissolved oxygen, is expressed as:

$$Fe^{2+} + O_2 + 2\text{H} \rightleftarrows Fe^{3+} + 2OH^- \quad \text{…..……} \quad (2.1)$$

With the Fe^{3+} being immediately hydrolyzed

$$Fe^{3+} + 3H_2O \rightleftarrows \text{Fe } OH_3 + 3H^+ \quad \text{…..……} \quad (2.2)$$

The overall reaction that describes the formation of insoluble iron encrustation is given as:

$$4Fe^{2+} + O_2 + 10H_2O \rightleftarrows 4Fe\ (OH)_{3(s)} + 8H^+ \quad \text{…..……} \quad (2.3)$$

According to Majkic-Dursun et al (2015) the rate law of iron (II) oxidation for mildly acid to neutral water pH value between 6 to 8 was found to be first-order with respect to the concentrations of both Fe (II) and O_2 and second order with respect to OH. Other studies reported that the rate of oxygenation of ferrous iron in aquifer follow equation (2.4) and was influenced by pH, temperature, concentration of dissolved oxygen and presence of catalysts (Hem and Cropper 1959; Stumm and Lee, 1961).

According to Singer and Stumm (1969) the oxidation of iron (II) on or about neutral pH proceeds at a rate that was dependent upon the concentrations of iron (II), dissolved oxygen and OH - in accordance with the rate expression.

$$-dFedt=KFe2+pO2(OH)2 \quad \text{…..……} \quad (2.4)$$

where K = Rate constant and was function of pH.

Ferris, 2005 carried out studies on bacteriogenic iron oxides (BIOS) which were bacteria cells that were intermixed with variable amounts of poorly ordered hydrous ferric oxides minerals. These minerals form a response to chemical and or bacterial oxidation of Fe^{2+}, which gave rise to Fe^{3+}. These studies proposed the reaction rates shown in Table 2.3. Further studies by Majkic-Dursun et al., (2015) found that dissolved iron causes substantial growth of iron-oxidizing bacteria in anaerobic condition or in low amounts of dissolved oxygen (< 1.0 mg/L) conditions in the aquifer stratum.

Table 2.3 Rate of reaction for bacteriogenic iron oxides (James and Ferris, 2004)

Microcosm	Rate constant K (Min^{-1})	Half-life ($T^{½}$) (Min)	Oxidation Rate $MmolL^{-1}Min^{-1}$
Chemical control	0.024	28.9	0.0017
Sodium azide control	0.056	12.4	0.0022
BIOS	0.147	4.7	0.0086

Studies by Emerson and Moyer (1997), Majkic-Dursun et al., (2015), and Moser et al., (2021) found that in iron deposit large numbers of different bacteria are often found that are able to use iron for their metabolic activity. These studies also found that in low amounts of dissolved oxygen (0.1– 1.0 mg/L) environment dissolved iron can cause substantial bacteria growth. These bacteria include iron-oxidizing bacteria such as the stalked *Gallionella* and sheathed *Leptothrix.* It is believed that these bacteria accelerate iron oxidation.

When the pH is less than 4, iron as Fe (II) dominates and the oxidation rate is dependent on the pH value. In the pH range 5–8 the total amount of ferric iron that can remain in solution in the form of Fe^{3+}, Fe OH^{2+} and Fe $(OH)^{+2}$ is generally below 0.01 mg/L (Hem and Cropper, 1959, Abdel-Lah et al., 2002). However, if the pH is greater than 8 then the ferrous oxidation is not dependent on pH. Catalysts, especially copper, even in trace quantities as well as anions which form complexes of ferric iron (H_2PO_4) increase the reaction rate significantly while small amounts of Fe (III), Cl^- and SO_4^{2-} have no effect on reaction rate.

2.6 REMOVAL OF IRON USING AERATION AND FILTRATION

Several studies on reduction of concentration of iron and other related salts from groundwater using aeration and filtration method have been undertaken. Aeration refers to the addition of air to water to enhance oxygenation that more often than not is motorized. Abdel-lah et al., 2002 and Odell, 2001 noted that aeration and filtration reduced iron and manganese levels to below the allowable 0.3 mg/L and 0.1 mg/L respectively from a groundwater sample collected from groundwater in the Nile valley. Nik et al., 2013 carried out research on quality improvement by using aeration and filtration methods in Malaysia and noted that water-to-air method was more effective than air -to-water methods of aeration. In all these instances aeration was carried out using mechanized aerators, which would be expensive in a rural setup.

Types of Filters

According to Huisman and Wood (1974) filters can be categorized as pressure and gravity. Pressure filters require high degree of automation and is not an option in a rural set-up like Chyulu and the option is to explore use of gravity filters. Filters have a filter material which may be coarse sand, fine sand, glass feebles and any other inert material. Two categories of gravity filters exist; slow sand filters and rapid sand filters. According to Odell (2001) slow sand filters are normally bigger in size, and require human labour during their maintenance while rapid sand filters are much smaller and are machine cleaned. However, rapid sand filters are accompanied by chlorination but slow sand filters allow for growth of bacteria and are therefore biological. El-Naggar (2010) developed low technology for removal of iron and manganese from groundwater in Siwa oasis in Egypt and achieved 80% removal of iron. Odell, (2001) and Nik et al., (2013) also recorded such high percentage removal iron from the groundwater samples.

Groundwater treatment assumes that the water has no sediments which would dictate the use of rapid sand filtration. However, the composition of the groundwater from the study area

indicated high concentration of iron and oxidation occurred when the groundwater was exposed to oxygen. This led to formation of ferric compounds that precipitated and formed sediments.

2.7 MODELING DISPERSION OF IRON AND ITS DERIVATIVES IN THE CHYULU AQUIFER

Literature on development of a solute model that would be linked to groundwater modeling system (GMS) was reviewed. Such literature touched on general solute transport, and its processes such as advection, molecular diffusion, dispersion and the mass transport equation of iron as the parameter whose dispersion was the subject of this study. The development of the governing equations as well as their possible solutions were reviewed. The literature on groundwater modeling and related software was also reviewed. Finally, the writing of a sub-routing, its calibration and validation were reviewed.

2.7.1 Modeling Solute Transport

The transport of solutes such as iron ions that was the subject of this study occurs through cracks, fractures and pores in the stratum. Physical, chemical and biological processes as well as properties of the medium drive this transport (Anderson and Woessner, 1992; Vilhelmsen, 2012). Analytical solutions to the transportation of iron ions must be proceeded by an understanding of the processes that dictate flow in the aquifers. The major processes include advection, diffusion, dispersion, adsorption and decay/degradation. The ferrous ions are to some extent oxidized to ferrous ions in the presence of limited oxygen availability. The major processes that are likely to affect iron ions transportation in the aquifer are described briefly in the following sections.

2.7.2 Advection

Advection is defined as the movement of a solute with the flowing groundwater (Kumar, 2004). The mass flux of dissolved contaminant that is being transported depends on its concentration in groundwater and on the quantity of groundwater flowing. This flux is therefore a function

of velocity. For a one-dimensional flow normal to a cross-sectional area of porous media, this quantity of groundwater is the product of average linear velocity and the effective porosity. Therefore, for a one-dimensional flow, the mass flux, F_x is given by the following equation

$$Fx = Vx\eta eC \quad \text{..... (2.5)}$$

where V_x is the average linear velocity, η_e, is the effective porosity and C is the concentration of iron in mg/L.

The average linear velocity, V_x, is defined as the rate at which the flux of iron across unit cross sectional area of aquifer section under consideration flows. V_x will be estimated using equation (2.7).

The mass flux per unit cross-sectional area becomes:

$$f_{adv} = V_x \eta_e C dA \quad \text{..... (2.6)}$$

and

$$Vx = \frac{K}{\eta e}\frac{dh}{dL} \quad \text{..... (2.7)}$$

where K is the hydraulic conductivity of the aquifer and dh/dl is the hydraulic gradient.

The average linear velocity, V_x is thus equal to the Darcy's velocity divided by effective porosity associated with the porous medium through which solute can flow.

2.7.3 Fick's Law on Molecular Diffusion

Molecular diffusion in the aquifer describes the movement of a solute in the medium from an area of higher concentration to an area of lower concentration. In this study molecular diffusion is the movement of iron ions in the aquifer from an area of higher concentration to an area of lower concentration in the same aquifer. In this study flow was assumed to be from the South to the Northern part of the aquifer. Diffusion will take place as long as a concentration gradient exists, even if the fluid is not moving, causing spreading and random motion.

The mass of solute diffusing within the aquifer follows Fick's first law, which is given for one-dimensional flow by:

$$F = -D\frac{\delta C}{\delta x} \quad \text{…..…… (2.8)}$$

Where: F = the mass flux of solute per unit area,

D = the diffusion coefficient,

C = the iron concentration in the study area, and

δC / δx = the concentration gradient.

Values of D are specific for each salt and are among other parameters temperature dependent

When tortuosity (τ) is considered, F becomes:

$$F = \frac{\eta_e}{\tau}\left(D\frac{\delta C}{\delta x}\right) \quad \text{…..…… (2.9)}$$

Tortuosity is defined as the distance along a travel path that a molecule must follow between two points divided by the shortest distance between those two points. In porous medium the tortuosity is greater than one (>1). Typical diffusion coefficient for geological media range from about 10^{-11} to 10^{-10} m^2/s. The diffusion coefficient of ferric cations (Fe^{3+}) has been taken as - 6.07×10^{-10} m^2/s. Table 2.4 shows values of diffusion coefficient for different materials.

Table 2.4 Hydrodynamic dispersion (D) cm2/sec (Zhao et al., 2010)

Material	Dispersion Coefficient	Interstitial velocity
Medium sand	0.0017	0.086
	0.001	0.064
	0.0008	0.054
	0.0005	0.041
Silica	0.00016	0.035

2.7.4 Mechanical Dispersion

The other process that will affect transportation of iron ions in the aquifer is mechanical dispersion. Mechanical dispersion is the movement a solute resulting from minor differences in groundwater velocity as it flows through heterogeneous porous media. When solutes in the aquifer get into contact with water that does not contain a solute, mixing occurs along the flow path, resulting in a dilution of the solute at the advancing edge of flow. Mechanical dispersion can be broken down into two complementary dispersions (longitudinal dispersion) which is the

mixing that occurs along the direction of the flow path, and transverse dispersion, which is the mixing in directions normal to the flow path.

According to Fick's law for diffusion, mechanical dispersion is function of the average linear velocity and a coefficient of mechanical dispersion. This coefficient is defined by:

Coefficient of longitudinal dispersion $=\alpha_i V_i$ ……..…… (2.10)

where V_i is the average linear velocity in the principal direction of flow i and α_i is the dynamic dispersivity in the principal direction.

Hydrodynamic Dispersion

Hydrodynamic dispersion is a combination of diffusion and mechanical dispersion in flowing groundwater. If a hydrodynamic dispersion coefficient (D*) is introduced it would be defined as follows:

$D_L = \alpha_l V_i + D^*$ ……..…… (2.11)

$D_T = \alpha_T V_i + D^*$ ……..…… (2.12)

where: D_L = the longitudinal hydrodynamic dispersion coefficient,

D_T = the traverse dynamic dispersity coefficient,

α_L = the longitudinal dynamic dispersivity, and

α_T = the traverse dynamic dispersivity

Adsorption

The mathematical description of adsorption in x–direction (1D) is given by the relationship

$$\frac{\partial C_{ads}}{\partial t} = \frac{\rho b}{\eta e}\frac{\partial S}{\partial t}$$ ……..…… (2.13)

where ρb = bulk density of the porous material

S = fraction of the solute sorbed (or exchanged) on the porous material

The linear sorption exchange reaction considers that the concentration of solute sorbed to the porous medium, S, is directly proportional to the concentration of the solute in the pore fluid, C, according to the relation

$$S = KdC \quad \text{…..……} \quad (2.14)$$

where K_d = distribution coefficient.

The slope derivative of the sorbed concentration versus dissolved concentration curve, $\frac{dS}{dC}$ is equal to distribution coefficient K_d.

So, by including the linear sorption isotherm equation,

Then $$\frac{\partial S}{\partial t} = \frac{\partial S}{\partial C}\frac{\partial C}{\partial t} = Kd\frac{\partial C}{\partial t} \quad \text{…..……} \quad (2.15)$$

Therefore $$\frac{\partial C_{ads}}{\partial t} = \frac{\partial \ell bS}{\partial t} = \frac{\rho b}{\eta e} Kd\frac{\partial C}{\partial t} \quad \text{…..……} \quad (2.16)$$

2.7.5 Mass Transport Equation

The equation governing transport on groundwater is obtained from the derivation of the advection-dispersion equation. The derivation of the advection-dispersion equation is based on the law of conservation of mass of solute flux into and out of a small representative elementary volume of the porous media. In this derivation it is assumed that the porous medium is homogeneous, isotropic and saturated with fluid. Moreover, it further assumed that the flow is steady state, and that Darcy's law applies.

The solute is transported both by advection and hydrodynamic dispersion. In the x direction, the solute transport is given by:

Advection transport = $f_{adv} = V_x \eta_e C dA$ …..…… (2.17)

Dispersive transport = $f_{disp} = \eta_e D \ \frac{\delta c}{\delta x} dA$ …..…… (2.18)

where η_e is effective porosity, D is the hydrodynamic dispersion coefficient, C is the solute concentration and dA is the cross-sectional area of the element normal to the direction of flow. Assuming that the aquifer is homogeneous and that the porosity constant throughout the aquifer the total mass flux of iron cations transported per unit of cross-sectional area is given by:

$$F = f_{adv} + f_{disp} = V_x \eta_e C \delta A - \eta_e D \quad \frac{\delta c}{\delta x} \qquad \text{…..…… (2.19)}$$

$$F = \eta_e \delta A \ (V_x C - D \frac{\delta c}{\delta x}) \qquad \text{…..…… (2.20)}$$

The negative sign indicates that the dispersive flux is from areas of higher to areas of lower concentration.

The rate of mass change in the respective elementary volume is given as:

$$\eta_e \frac{\delta x}{\delta t} dx \qquad \text{…..…… (2.21)}$$

$$\left[Dx \frac{\delta^2 C}{\delta x^2}\right] - \left[Vx \frac{\delta C}{\delta x}\right] = \frac{\delta C}{\delta t} \qquad \text{…..…… (2.22)}$$

Equation (2.22) is the one-dimensional equation of mass transport for a conservative solute when the velocity in the aquifer is assumed to be steady and uniform.

2.8 DEVELOPMENT OF THE USER-DEFINED EXPRESSIONS

Boundary conditions refer to the interaction between the area under consideration and the environment. To obtain unique solution to a partial differential equation (PDE) such as equation (2.22) it is necessary to specify the initial and the boundary conditions. The initial conditions describe the values of the variables under consideration such as concentration of the solute at time, t, equal zero.

This type of equation can be solved using either analytical or a numerical method. Analytical method involves the solving the partial derivatives equations (PDE) using calculus based on the initial boundary conditions. They are limited to simple geometry and the aquifer being homogenous. Numerical methods also solve PDEs although they are prune to errors that show excess spreading of solute front (prunes). These errors include roundoff errors that occur during iterations that are dependent on one another and truncating error that occur when mathematical formula are expressed by approximation (Chapra, 2017).

2.8.1 Governing Equation

Equation (2.22) can be re-written as:

$$Dx\frac{d^2C}{dx^2} = \frac{dC}{dt} + V_x\frac{dC}{dx} \quad \text{…..…… (2.23)}$$

where: D_x = the dispersion coefficient

C = the concentration of ions in the solute.

V_x = the average velocity of the solute in the aquifer.

X = direction of flow

t = time in days

The one-dimensional solute transport equation, equation (2.23) can also be used to predict the transformation of ferrous to ferric ions along with their transport through the medium if first order kinetics are assumed.

As earlier indicated in section 2.5.7 dissolved iron causes substantial growth of iron oxidizing bacteria in anaerobic conditions or in low amount of oxygen (<1.0 mg/L) conditions in the aquifer stratum. The Chyulu aquifer particularly in and around Makindu is under such conditions of depressed amount of oxygen because the first Water Struck Level (WSL) is as low as 20 m. In addition, Majkic-Dursun et al. (2015) found that the rate law of iron (II) oxidation for mildly acid to neutral water of pH of between 6 and 8 process was first order with respect to the concentrations of both Fe (II) and O_2 and second order with respect to OH-.

If the general term ions in equation (2.23) is substituted with the specific ferrous ions and ferric ions that are the subject of this study then equation (2.23) becomes:

For the ferrous

$$Dx\frac{d^2[Fe(II)]}{dx^2} = \frac{d[Fe(II)]}{dt} + V_x\frac{d[Fe(II)]}{dx} \quad \text{…..…… (2.24)}$$

where: $[Fe(II)]$ = the concentration of ferrous ions.

For ferric

$$Dx\frac{d^2[Fe(III)]}{dx^2} = \frac{d[Fe(III)]}{dt} + V_x\frac{d[Fe(III)]}{dx} \quad \text{…..…… (2.25)}$$

where: $[Fe(III)]$ = the concentration of ferric ions.

2.8.2 Boundary Conditions

The initial condition and boundary conditions are at the highest points (1000 a.m.s.l) of the Makindu watershed which is in the Chyulu aquifer. In hydrogeocheminal studies the water table is an important boundary although its configuration is poorly known (Anderson and Woessner, 1992). The water table is controlled recharge and so recharge becomes one of the boundary conditions. In this study hydraulic conductivity, flow and depth are the other conditions. The coordinates of the watershed boundary are 9448071 and 388947 while the concentrations are as follows:-

For ferrous:

$$[Fe(II)]\,(x,0) = [Fe(II)]_0 \;\; for\; t \geq 0 \qquad [Fe(II)]\,(\infty,t) = 0\; for\; t \geq 0$$

For ferric:

$$[Fe(III)]\,(x,0) = [Fe(III)]_0 \;\; for\; t \geq 0 \qquad [Fe(III)]\,(\infty,t) = 0\; for\; t \geq 0$$

The advection-dispersion equation can be modified to take cognizance of iron reaction and sorption as the iron flow through the aquifer. This will be done to incorporate the possible reactions by the iron ions in the aquifer while assuming that this reaction is a first order reaction. Ferrous undergoes reduction with time by transforming to ferric which results in a loss given by equation (2.26).

The reduction for ferrous is given as:

$$\frac{d[Fe(II)]}{dt} = -k_2[Fe(II)] \quad \text{…..…… (2.26)}$$

where: k_2 = First order rate constant for the ferrous

Consequently, ferric undergoes addition with time when the ferrous transforms to the ferric, we add the gain to equation (2.225).

The addition for ferric is given as.

$$\frac{d[Fe(III)]}{dt} = k_3[Fe(II)] \quad \text{…..…… (2.27)}$$

Where: k_3 = First order rate constant for the ferric

When the loss, equation (2.24) for ferrous is added to equation (2.26), equation (2.26) becomes

$$\frac{d[Fe(II)]}{dt} = Dx\frac{d^2[Fe(II)]}{dx^2} - V_x\frac{d[Fe(II)]}{dx} - k_2[Fe(II)] \quad \text{…..…… (2.28)}$$

Again when the gain in equation (2.27) for ferric is added to equation (2.25), equation (2.25) becomes

$$\frac{d[Fe(III)]}{dt} = Dx\frac{d^2[Fe(III)]}{dx^2} - V_x\frac{d[Fe(III)]}{dx} + k_3[Fe(II)] \quad \text{…..…… (2.29)}$$

2.8.3 Effects of Mass Flux To The Advection And Dispersion

Considering reaction that can take place in the aquifer when the iron reacts with the medium a further mass flux is added to the advection-dispersion.

For the ferrous we have:

$$\frac{d[Fe(II)]}{dt} = Dx\frac{d^2[Fe(II)]}{dx^2} - V_x\frac{d[Fe(II)]}{dx} - k_2[Fe(II)] - \frac{d[Fe(II)]}{dt}\frac{\rho_b}{\eta_e}K_d \quad \text{…..…… (2.30)}$$

For the ferric we have

$$\frac{d[Fe(III)]}{dt} = Dx\frac{d^2[Fe(III)]}{dx^2} - V_x\frac{d[Fe(III)]}{dx} + k_3[Fe(II)] - \frac{d[Fe(III)]}{dt}\frac{\rho_b}{\eta_e}K_d \quad \text{…..…… (2.31)}$$

Where: ρ_b = bulk density of stratum and estimated from Appendix X.

η_e= porosity and

K_d = is the rate constant

As $[Fe(II)]$ decreases, $[Fe(III)]$ increases because the mass is being transferred from one phase to the other.

Rearranging equation (2.30)

$$\frac{d[Fe(II)]}{dt} + \frac{d[Fe(II)]}{dt}\frac{\rho_b}{\eta_e}K_d = Dx\frac{d^2[Fe(II)]}{dx^2} - V_x\frac{d[Fe(II)]}{dx} - k_2[Fe(II)] \quad \text{…..…… (2.32)}$$

Factoring out $\frac{d[Fe(II)]}{dt}$ equation (2.32) becomes:

$$\frac{d[Fe(II)]}{dt}\left(1+\frac{\rho_b}{\eta_e}K_d\right)=Dx\frac{d^2[Fe(II)]}{dx^2}-V_x\frac{d[Fe(II)]}{dx}-k_2[Fe(II)] \quad \text{…..……} (2.33)$$

2.8.4 Retardation Factor (R)

Now introducing retardation factor R_{II}, for ferrous and R_{III}, for ferric, then:

$$R=\left(1+\frac{\rho_b}{\eta_e}K_d\right) \quad \text{…..……} (2.34)$$

Therefore, a reorganized equation (2.32) for ferrous now becomes:

$$\frac{d[Fe(II)]}{dt}=\left(Dx\frac{d^2[Fe(II)]}{dx^2}-V_x\frac{d[Fe(II)]}{dx}-k_2[Fe(II)]\right)\frac{1}{R_{II}} \quad \text{…..……} (2.35)$$

Again a reorganized equation (2.33) for ferric now becomes:

$$\frac{d[Fe(III)]}{dt}=\left(Dx\frac{d^2[Fe(III)]}{dx^2}-V_x\frac{d[Fe(III)]}{dx}+k_3[Fe(II)]\right)\frac{1}{R_{III}} \quad \text{…..……} (2.36)$$

If we rearrange equation (2.35) and equation (2.36) by multiplying with the retardation factors throughout.

Equation (2.35) for ferrous now becomes:

$$R_{II}\frac{d[Fe(II)]}{dt}=Dx\frac{d^2[Fe(II)]}{dx^2}-V_x\frac{d[Fe(II)]}{dx}-k_2[Fe(II)] \quad \text{…..……} (2.37)$$

Equation (2.36) for ferric now becomes:

$$R_{III}\frac{d[Fe(III)]}{dt}=Dx\frac{d^2[Fe(III)]}{dx^2}-V_x\frac{d[Fe(III)]}{dx}+k_3[Fe(II)] \quad \text{…..……} (2.38)$$

Equation (2.37) and equation (2.38) are the advection-dispersion equations, the solute transport equations or the transport-dispersion equations.

For the ferrous equation (2.37), the first term on the right hand side represents the change in concentration of ferrous due to the hydrodynamic dispersion. The second term represents the effect of advective transport that is the movement of ferrous attributed to transport by flowing groundwater. The third term represents the contribution and removal of ferrous due to fluid sources and sinks and the transformation to the ferric.

For the ferric equation (2.38), the first term on the right hand side represents the change in concentration of ferric due to the hydrodynamic dispersion. The second term represents the

effect of advective transport, which is the movement of ferric attributed to transport by flowing Groundwater. The third term represents the contribution and removal of ferric due to fluid sources and sinks and the gain from the transformed ferric. The solution to these equations is presented in Section 3.9.2 of the methodology.

2.9 GROUNDWATER SIMULATING MODELS

Groundwater simulation models have been used to study groundwater flow patterns in order to help management decisions (Chiang, et al., 1998; Gorelick, 1983; Anderson and Woessner, 1992; Lin and Yang, 1991). Groundwater modeling entails use Finite Difference Method (FDM) or Finite Element Method (FEM). These methods obtain numerical solutions to differential equations that are defined by a finite grid (mesh) of points. Analysis of groundwater flow and flow of solutes in aquifers involves division of the stratum into a mesh and analysis using MODFLOW model that is widely used in groundwater studies (Ahmed et al., 2002). These models are a conceptual description that describe physical systems using mathematical equations (Anderson and Woessner, 1992). The models mathematically represent hydrogeochemical systems and through these systems various scenarios can be predicted, tested and compared (Spitz and Moreno, 1996; Zhao et al., 2010) In the development of these systems simplifying assumptions are made that involve direction of flow, geometry of aquifer, heterogeneity of sediments within the aquifer, contaminant transport mechanism and chemical reactions. Models are therefore approximations of the aquifer conditions despite the fact that they are a useful investigation tools in groundwater studies. Some of these models are applicable to hard rock zones such as at Chyulu. These include the groundwater modeling system (GMS).

2.9.1 Types of Groundwater Models

There are three types of groundwater models; Finite element models, Finite difference models and analytical element models. Finite element models include 3-D Finite-Element Model of

Flow and Transport through Saturated-Unsaturated Media (3DFEMFAT), 3-D Groundwater Flow and Contamination Transport Model (AQUA3D) and Finite Element Mass Transport Model (ChemFlux) among others. Finite difference models include MODFLOW, One-Dimensional Finite-Difference Vadose Zone Leaching Model (VLEACH) and Flow and Solute Transport in Variably-Saturated, Single-Phase Flow in Porous Media (VS2DT) among others. Analytical element models include Analytical Element Model with Conjunctive Surface Water and Groundwater Flow and a MODFLOW Model Extract Feature (GFLOW) (McDonald and Harbaugh, 1988.; Anderson and Woessner, 1992; Kumar, 2001). The decision on which model to use was dictated by the expected outcome. Softwares that allow use of combination of models exist. This include GMS and Groundwater Vistas (GV) among others. In GMS, one selects either finite element or finite difference method of analysis. Other packages/modules that enable solute transport and reactive transport are also incorporated in GMS. In this study the finite difference method was used because it allows for user defined reaction equations to be incorporated as a subroutine (Clement, 1997).

2.9.2 Groundwater Modeling System

The groundwater modeling system (GMS) is an interface that incorporates several numerical models as well as graphical tools that are geared towards generation and visualization of results (Herzorg, 2007). This software combines various tools referred to as modules and Models. The modules include Tins, Boreholes, Horizons, Meshes, Grids, Scatters points and Maps while Models include MODFLOW, MODPATH, MT3D, PHT3D, MT3DMS, and RT3D among many other models that deal with groundwater. The primary model is MODFLOW which is a three–dimensional, cell-centered finite difference saturated flow model. Many editions of GMS have been developed but in this study the 10.3 edition of July 2018 has been used. In this study only the models that have been used in the study have been discussed.

GMS is coded using the FORmula TRANsilation (FORTRAN) language, which is a general-purpose programming language for mathematical computations in science applications Herzog et al., (2007). The International Business Machines (IBM) developed the FORTRAN program that has been revised several times, with the latest edition being FORTRAN 95 series. The American National Standards Institute (ANIS) has standardized the program. The major advantages of FORTRAN language are that it is portable across computer platforms and runs on any computer that has a FORTRAN Compiler. However, the FORTRAN programs requires a compiler that is compatible with WINDOWS or UNIX operating systems. In this study the *Microsoft FORTRAN Power Station* compiler as incorporated in Microsoft Developer Studio software was used.

2.9.3 MODFLOW

The MODFLOW model is a computer model that was developed by the United State Geological Survey (U.S.G.S) to simulate three-dimensional groundwater flow through a porous medium such as aquifers. It uses the finite-difference method (McDonald and Harbaugh, 2000; Harbaugh et al, 2000; Wilson and Naff, 2004). The FORTRAN computing language was used in the development of the MODFLOW CODE that was designed to have a modular structure. It is a 3D, cell-centred, model that performs both steady state and transient analysis and has a wide variety of boundary conditions and input options.

2.9.4 MT3DMS

MT3DMS (Modular Transport, 3-Dimensional, Multi-Species model) is a modular three-dimensional transport model for the simulation of advection, dispersion and chemical reactions of dissolved constituents in groundwater system (Zheng, 1990). This model is used in conjunction with MODFLOW in a two-step flow and transport simulation. The reactive 3-dimensional multi species transport model (RT3D) is a special version of MT3DMS that has been customized to simulate reactive transport problems.

2.9.5 RT3D

RT3D is a multi-species reactive transport model developed by the Battelle Pacific Northwest National Laboratory (Clement, 1997; Zheng and Bennet, 2002). It is a numerical, modular three-dimensional transport model that simulates advection, dispersion, and chemical reactions of dissolved constituents in groundwater system.

RT3D as a software package simulates three-dimensional, multi-species, reactive transport of chemical compounds (solutes) in groundwater. It also provides an easy-to-use and flexible framework applicable to natural attenuation, accelerated bioremediation, or other reactive transport modeling scenarios. Predefined modules are available for common scenarios, but the software also allows the addition of any desired reaction kinetics that will represent multiple chemical species in aqueous and sorbed phases. Several graphical user interfaces to RT3D are available to organize the process of defining the required RT3D input information and to provide visualization capabilities for the RT3D output.

User-Defined / Custom Reaction Modules

A key feature of RT3D is the high degree of flexibility the user has in adding other reaction kinetics via the user-defined module. This facility allows one to make a sub-routine program using the same language as the GMS code and then uploading it into the GMS software (Clement, 1997). Testing is done using a Visual Fortran compiler where different versions exist. The Dynamic Link Library (DLL) option for the user-defined reaction module has been tested with Visual Fortran and Microsoft Fortran Power station v. 4.0 with positive results.

The information derived from the hydro-geochemical model is supplied to the MODFLOW through the grid approach or through the hydro-geologic model approach. The grid approach entails parameters being fed to a 3D grid on a cell by cell basis. On the other hand the hydro-geologic conceptual model approach involves entering parameters that are required for the simulation into the model using a graphical tool in the map module in GMS. These parameters are then used in the creation of the hydro-geochemical model by assigning areas, arcs, and

points with hydrological parameters. In the last stage of the model approach, the model is converted into a grid model by the software.

This software has been used to develop a Reactive Multi Species Transport in RT3D reaction module for simulating reactions of iron (Fe) and its derivatives in the Chyulu aquifers. RT3D supports a user-defined reaction packages created by a Dynamic Linked Library (DLL). The DLL entails compilation of a stand-alone code that is then copied to the (RT3D) directory of Microsoft visual studio that runs on Windows. The making of this code would entail the construction of a test kit to replicate the aquifer where the experimental studies for the rate of oxygenation of ferrous ions have been carried out.

2.9.6 Hydro-Geochemical Modelling Concept

In GMS the most efficient approach for building realistic complex models is the development of a hydro-geochemical model also referred to conceptual model. This approach is also the most critical step in hydro-geochemical modeling process and refers to construction, characterization and conceptualization of the problem and the relevant aquifer domain (Betancur, et al., 2014; Bredehoeft, 2005; Yihdego an Webb, 2015; Anderson and Woessner, 1992). According to Anderson and Woessner (1992) the outcome of this process is a pictorial representation of the groundwater flow through the strata which include hydraulic parameters, piezometric surfaces and groundwater flow conditions. This model forms the basis of the formulation of a numerical model and is a simplified representation of the groundwater flow system in the study area. It consists of sets of assumptions that reduce the real problem and real domain to simplified versions that are acceptable in view of the objectives of the modeling. It is a valid representation of the hydrogeological conditions with the nature of the conceptual model determining the dimensions of the numerical model and the design of the grids. According to Kahsay (2008) and Yihdego and Webb (2015) the purpose of developing a

conceptual model is to formulate a better understanding of site conditions, define the groundwater problem, develop a numerical model and finally select a suitable computer code.

2.10 CALIBRATION AND VALIDATION

Calibration is the process of adjustment of model parameters and forcing within the margins of the uncertainties to obtain a model representation of the processes of interest that satisfies pre-agreed criteria. According to Kitanidis, (1997), Rausch et al., (2005) and Lapworth et al., 2022 and two methods of calibration exist. These are the direct method and the inverse method. In the direct method parameters such as the initial conditions and boundary conditions are available while other parameters such head, flow or concentration are not available. On the other hand in inverse calibration parameters such head, flow and concentration are available but their distribution is unclear. The process of calibration entail comparison between the measured and the predicted data. Calibration process has four stages: Running of the model changing only one parameter at a time, documenting each of these runs, estimating of good fit by computing the mean square deviation (MSD) and finally by making a plot of $c_{calculated}$ against $c_{measured}$.

The mean square deviation (MSD) is given by the equation

$$MSD = \frac{1}{n}\sum_{i=1}^{n}(c_i^{observed} - c_i^{calculated})^2 \quad \text{..... (2.39)}$$

where MSD is the mean square deviation, n is the number of trial or data sets and c is the parameter in question.

The process of calibration is followed by the process of validation. Models are validated in order to demonstrate that the calibrated model is an adequate representation of the physical system. In this study it is an adequate representation of the chemical reactions in the aquifer. This gives greater confidence in the proposed model.

Calibration is achieved when the estimated error is ± 5% of the observed concentration. The confidence of 95 % is used which effectively allow an error of 5%. The calibration process is

depicted by Figure 2.1 that illustrates calibration target for borehole using inverse calibration process in GMS.

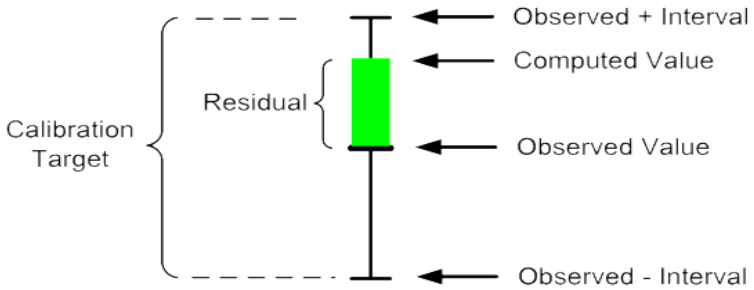

Figure 2.1 Expected calibration results for an observation well (Whelan and Castleton, 2006)

Calibration and Validation of the hydro-Geochemical Model

For a groundwater model to be used in any type of productive role it must be demonstrated that the model can successfully simulate observed aquifer behavior (La venue and Pickens, 1992; Kim et al., 1999; Harbaugh et al., 2000). The basic aquifer parameters are permeability and storage coefficient, land surface contour map, transmissivity maps, location of aquifers, precipitation, groundwater evapotranspiration, type of aquifer, percentage of infiltration, water table elevations from observation wells and observation flow rates in the stream (Mutreja, 1986; Harbaugh et al., 2000,). The model is being calibrated for use in arid region therefore, most of the flow in the stream will be assumed to be coming from groundwater. Hydraulic conductivity and well recharge values will be altered systematically and the model run until the computed solution match the field – observed values within an acceptable level.

2.11 SUMMARY ON LITERATURE REVIEW.

This chapter has presented relevant literature on generation of groundwater potential map, water quality index (WQI) and groundwater quality map using DRASTIC modeling technique. The salts that impact on the quality of groundwater generally and in particular of the Chyulu have been analysed. Chyullu has many salts that are above the upper limit for water for human

consumption. Literauture on possible intervention to reduce iron content in the water was presented.

The literature on concepts and equations that govern flow of solute in the stratum and aquifers was presented. These studies are carried out using groundwater modeling system among many other models, that reduces the work of exploration and analysis. Literature on solute studies in other aquifers was presented particularly on chlorides but modeling of iron flow in aquifers was not available yet understanding and modeling of iron in the study area would fill a gap that exists in solute transport studies. To fill this gap literature on derivation and development of equations that were used to program, calibrate, and validate a user defined RT3D FORTRAN sub- routine that was dynamically linked to GMS was presented.

CHAPTER 3: RESEARCH METHODOLOGY

In this chapter the geology, soils, rainfall, lineament, drainage, land use and vegetation of the study area was described. The research activities that were carried out in order to achieve the specific objectives were also described.

3.1 THE STUDY AREA

The study area is a confined aquifer, that measures 2879 km^2 is marked by the volcanic Chyulu Hills to the South, Athi River to the North East and Kiboko River to the West. The Mombasa–Nairobi highway traverses the study area from East to West while the Railway runs parallel to the Highway. The area, generally referred to as Chyulu, falls on the Arid and Semi-Arid segment of the Republic of Kenya. The landscape is dotted by outcrops such Mbiu Nzau that rise some 1500m a.m.s.l. Figure 3.1 shows the study area which is part of Makueni County in South Eastern Kenya.

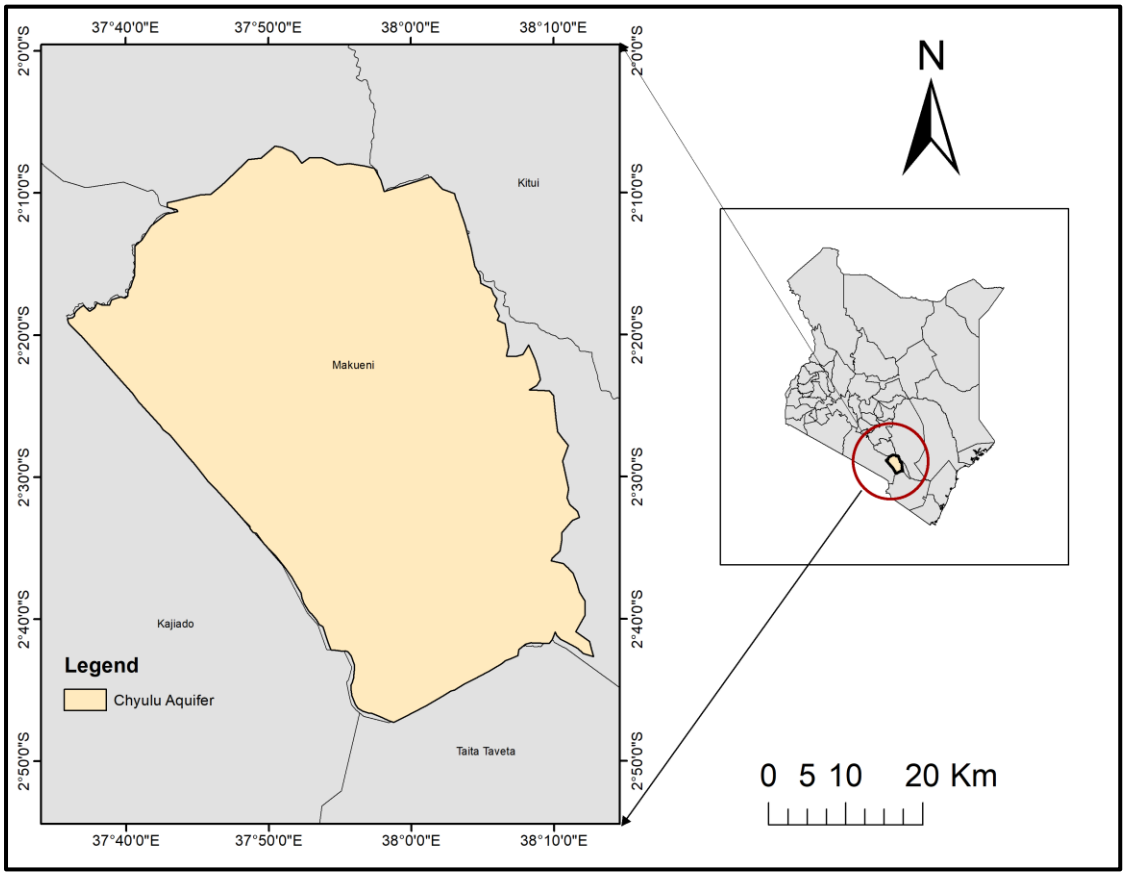

Figure 3.1 Location of the study area

3.1.1 Geology of the study area

Large areas of the eastern, northern and north-western parts of the Chyulu are underlain by crystalline Precambrian basement rocks of the Kasigau series that dominate south-eastern Kenya (Dodson, 1953; Michieka and Van Der Pour, 1977; Gaciri and Davies, 1993). According to Saggerson (1963), basement rocks of the semi-calcerous group underlie parts of the area while the Basement System of the middle, semi-pelitic group underlies other areas. Moreover, these Precambrian crystalline rocks are geologically complex with the spaces between their mineral crystals being microscopically small, few and generally unconnected. Thus, these metamorphic rocks are of low porosity and only permeable where they are fractured and their water yields are low but because they extend over large areas, large volumes of water are withdrawn from them. In areas dominated by the basement system the main water stuck levels (WSL) range from 15 to 25 m for the first aquifer, between 35 and 45 m for the second aquifer and from 85 to 140m for the third aquifer (Gaciri and Davies, 1993).

The Basement system dominates the northern section the study area while volcanic rocks dominate the southern part. These volcanic rocks have a wide range of chemical, mineralogic, structural, and hydraulic properties, due mostly to variations in rock type and the way the rock was ejected and deposited. Unaltered pyroclastic rocks have porosity and permeability similar to poorly sorted sediments while hot pyroclastic material became welded as it settled and is therefore almost impermeable (Dodson. 1953). Silicic lavas tended to be extruded as thick, dense flows, and have low permeability except where they are fractured. Basaltic lavas tended to be fluid and formed thin flow that has considerable pore space at the tops and bottoms of the flows. Figure 3.2 shows the geology of the study area. Numerous basalt flows commonly overlapped and the flows were separated by soil zones or alluvial material that formed permeable zones. Columnar joints developed in the central parts of basalt flows creating passages that allowed water to move vertically through the basalt. These Basaltic rocks are therefore characterized by very productive aquifers in volcanic rocks.

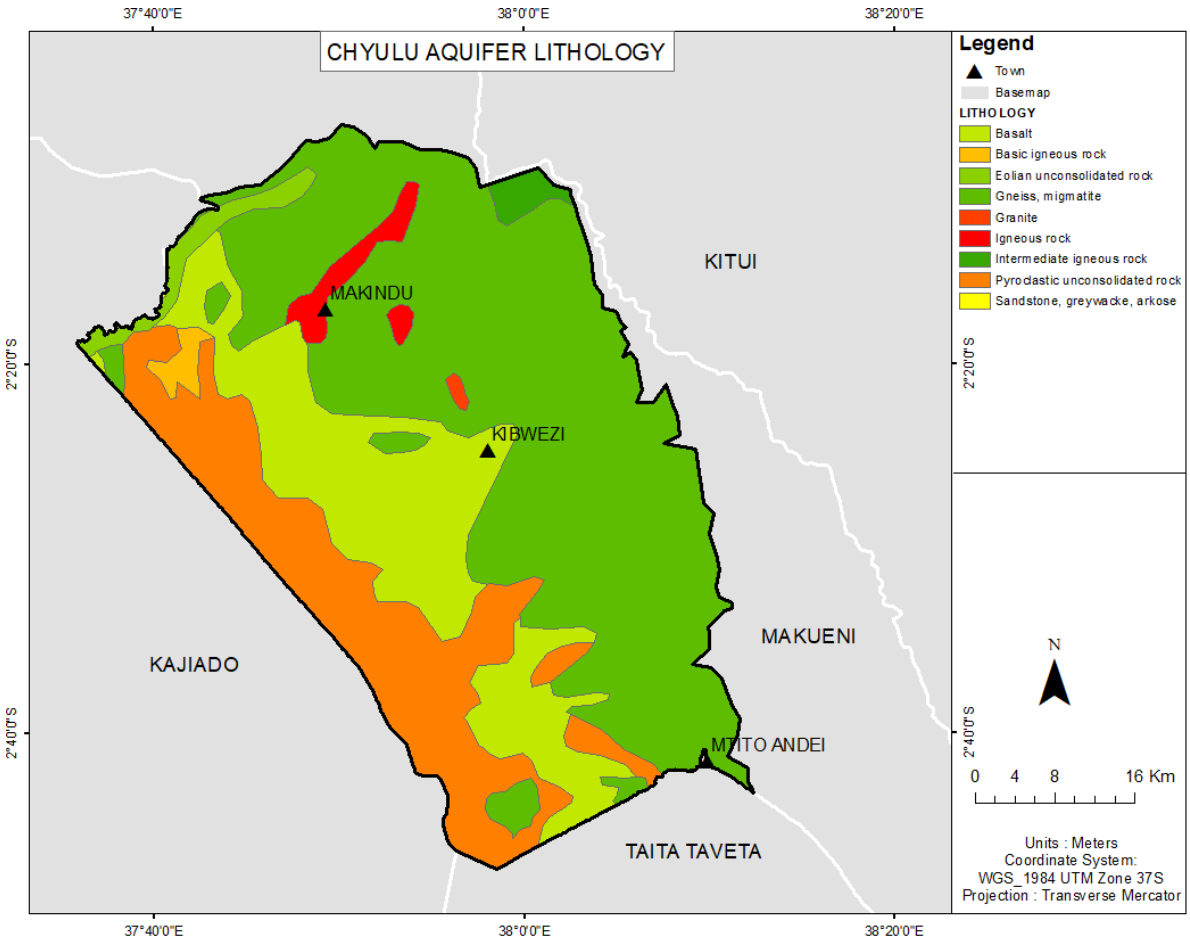

Figure 3.2 The geology of Chyulu generated using data from ILRI

The rocks in the study area have varying chemical composition depending on the age of formation and nature of formation. The area around Makindu has largely biotite-free hornblendic rock that is considered to be metamorphosised semi-calcareous. Table 3.1 shows results of analysis of a typical specimen from the study area that shows presence of silicates (44.68 %), aluminum oxide (15.79 %), magnesium oxide (15.74 %), calcium oxide (10%), ferrous oxide (5.50 %) while ferric oxide (hematite) was 3.9 %. Presence of sodium oxide, hydroxyl peroxide, manganese dioxide minerals were also recorded but these were in lower quantities.

Table 3.1 Results of analysis of a typical specimen collected on the North West of the study area (Saggerson, 1963)

S/No.	Name of chemical found	Chemical formula	Percentage (%) present
1	Silicon dioxide (silica)	SiO_2	44.68
2	Aluminium oxide	Al_2O_3	15.79
3	Magnesium oxide (Periclase)	MgO	15.74
4	Calcium oxide (Quick lime)	CaO	10.32
5	Ferrous oxide	FeO	5.50
6	Iron (III) oxide (Hematite), Ferric oxide	Fe_2O_3	3.90
7	Sodium oxide (Oxide Potassium)	Na_2O	1.22
8	Hydroxy peroxide	H_2O_4	0.96
9	Water	H_2O	0.80
10	Manganese dioxide	MnO	0.26
11	Potassium oxide	K_2O	0.13
12	Titanium dioxide (Titania)	TiO_2	0.11
13	Carbon monoxide	CO	0.10
14	Anhydrite phosphoric acid	P_2O_5	0.09
15	Chromium dioxide	Cr_2O_3	0.03

In other sections particularly those dominated by biotite-rich schistose gneiss, iron ore is an accessory. The other minerals that are rich in iron in the study area include magnetite, titano-magnetite and iron ore. These minerals and their derivatives are widespread in the study area. Titano-magnetite nodules measuring upto two (2) inches in length characterize the granitoid gneiss at Mbui Nzau found to the east of Makindu Town. These nodules represent iron-rich segregations in originally siliceous (sandy) deposits.

The southern part of this aquifer is dominated by volcanic Chyulu Hills, which are relatively young volcanic landscape which formed less than 10,000 years ago and is dominated by Basement rock system (Saggerson, 1963; Wright, 1982; Ritter and Kaspar, 1997). Recent volcanic activities may have occurred in the southern sector, where it created cinder cones and expansive lava cover. This lava is considered fresh, relatively unaltered vasicular porphyrisic and micro porphyritic rocks containing large amounts of phenocrysts of olive (Spath et al., 2001).

3.1.2 The Soils of the Study Area

A detailed study in the study area shows the rocks to be hornblende and gneiss in other areas. The soils are predominantly clayey silty SAND with those particularly around Makindu being described as ferrasols. Figure 3.3 show the soils of the study area.

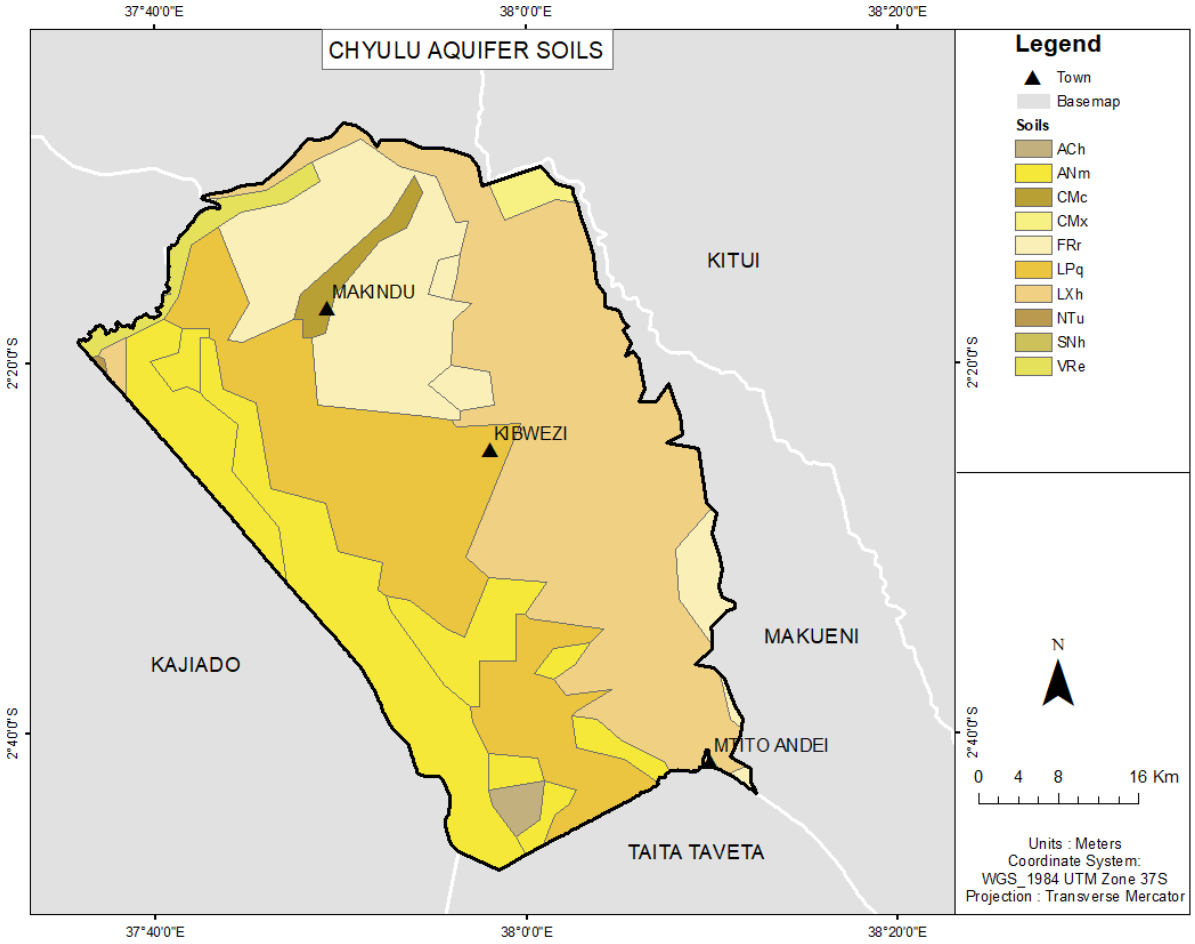

Figure 3.3 The soils of Chyulu generated using data from ILRI

The Soils of the Solute Flow Study Area

The soils of the solute flow study area were determined from the Chyulu soil map that was generated from the Kenya Soil Terrain Shapefile (KenSorter) which was obtained from the Kenya Soil Survey from which soils in Chyulu area were delineated using select layer by attribute tool in data management toolbox in ArcGIS (Mbithi et al., 2017). The soil was loam to the east of Kiumbi River while on the other of the other parts was sandy loam soil.

3.1.3 Rainfall Distribution in the study area

The rainfall data of the study area was obtained from Makindu Weather Station, a station of Kenya Meteorological Department and is fairly representative. The data availed covered a period of 36 years starting from 1980 to 2015. The rainfall data for Makindu Weather Station that is located in the aquifer is presented in Appendix I. The average monthly rainfall for the same period is shown in Table 3.2. The average annual rainfall for the period under review was 227 mm that is way below the documented value of 250 mm.

Table 3.2 Average monthly rainfall for Makindu

Month	Jan	Feb	Mar	Apr	May	Jun	Jul	Aug	Sept	Oct	Nov	Dec
Average Monthly Rainfall (mm)	17.0	18.22	31.14	36.33	14.98	1.62	0.12	1.09	1.78	13.05	51.08	41.72

There are two rainfall season in a year. The March-May that starts in Mid-March and continues to mid-May. The other season starts in mid-October, continues to the end of the year, and is more reliable (Kithiia, 2009). Figure 3.4 shows the annual rainfall for the Makindu weather station for thirty-six (36) while Figure 3.5 shows monthly rainfall for selected years. November was found to be the wettest month with an average monthly rainfall of 51.08 mm while the driest month was July with an average rainfall of 0.12 mm. The October-December season was generally wetter than the March-May season.

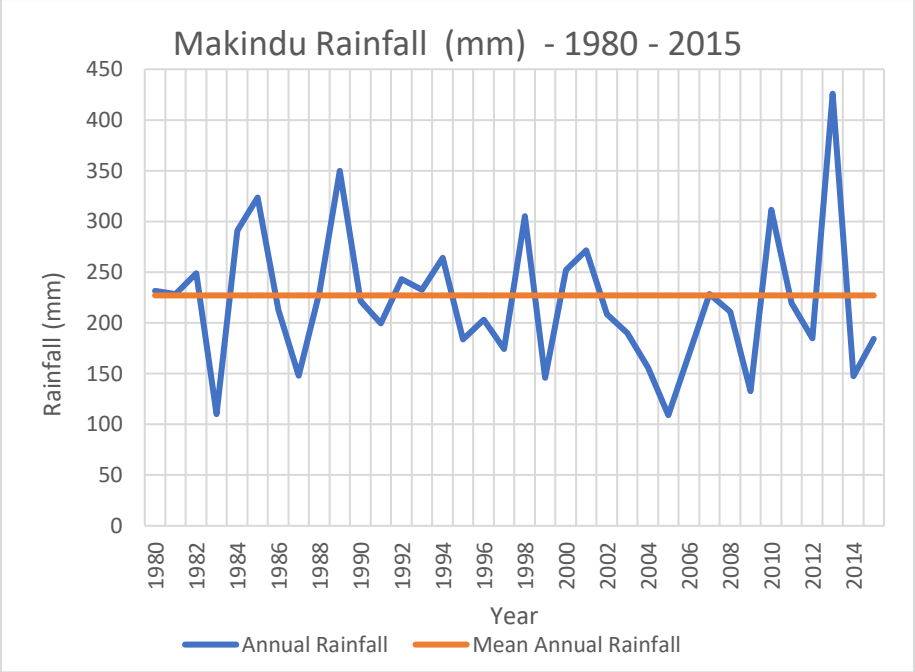

Figure 3.4 The Annual Rainfall for Makindu Weather Station in the Study Area (Courtesy: Kenya Meteorological Department)

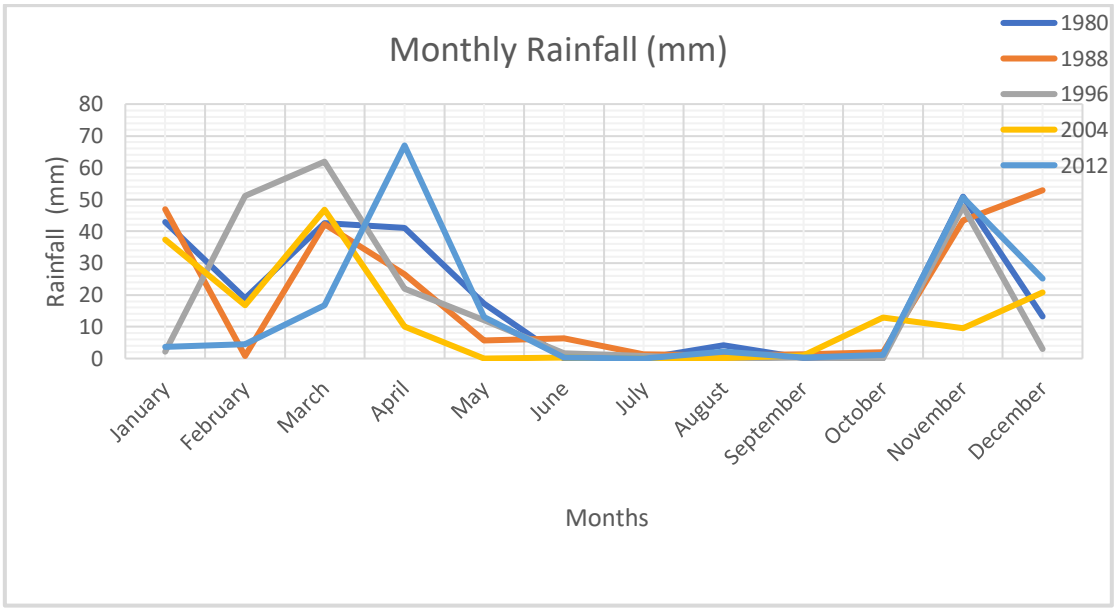

Figure 3.5 The Monthly Rainfall for Makueni

3.1.4 Lineament and Drainage

According to O'leary et al., (1976) lineament in groundwater exploration refers to linear features of a surface that differ in pattern from adjacent features that can justify presumption of a subsurface cause or change. In this study linear guide map has provided information on sites that have faults, fractures and cracks. These features indicate presence of groundwater because it is through them that recharge can take place (Koch and Mather, 1997). Lineament is given the highest weighting during the development of groundwater potential map. Figure 3.6 shows the lineament map of the study area.

3.1.5 Land Use and Vegetation

Land use is a major controlling factor in groundwater studies. Recharge is directly related to land cover. Rain that falls on rooftops and paved ground results in quick runoff and ultimately in low rate of infiltration.

3.1.6 Hydro stratigraphy

Hydro stratigraphic units comprise geologic units of similar hydrogeological properties. According to Anderson and Woessner (1992) several geologic formations may combine into a single hydro stratigraphic unit or a geologic formation may be sub-divided into aquifers and confining units. Based on available drilling records, VES data and geologic knowledge gained from previous studies the following hydro stratigraphic units are identified in the study area as Limestone-shale-marl intercalation and Limestone.

The main water bearing unit in the area is the limestone unit, but the weathered and fractured part of the dolorite also acts a conduit for occurrence and movement of groundwater. The groundwater in the area exists under confined to semi-confined conditions because of the interbedded fractured limestone and shale beds. Moreover, the reported storage coefficients for some of the wells are in the order of 10^{-4}, which suggests a confined aquifer system.

3.1.7 Hydro-geological Data

The boreholes in the study area were used to estimate the position of water table that is known to vary with rainfall such that the water table rises during the rainy season and lowers during the dry months. Information about hydraulic conductivity was obtained from reports by researchers from Kiboko Research Station that is just outside the study area (Saggerson, 1963; Kithiia, 2009; Mbithi et al., 2017).

3.2 THE RESEARCH ACTIVITIES

To achieve the specific objectives the following was undertaken:

1) Development of groundwater potential and water quality (WQI) maps of the study area using GIS and remote sensing techniques.
2) Development of a physical non-motorized aeration model for oxygenation of ferrous ions encountered in the Chyulu aquifer at Makindu.
3) Modeling of dispersion of iron and its derivatives in the Chyulu aquifer.

Table 3.3 shows the specific objectives and the corresponding research activity that helped in the realization of the objectives.

Table 3.3 Specific objectives and corresponding research activities

Objective	Proposed methodology	Supporting research activity
To develop groundwater potential and water quality (WQI) maps of the study area using GIS and remote sensing techniques.	DRASTIC modeling - Application of DRASTIC weighted overlay using weighted overlay tool in Arc map to generate the maps. (Use GIS and remote sensing techniques)	- Mapping of boreholes in the study area - Obtain DEM geologic, topographic, climatic data, soil data and drainage, - Stacking to obtain land cover. - Use GIS and Remote sensing techniques to make the groundwater potential maps for Chyulu aquifer. - Groundwater sampling and testing using standard method of water and wastewater analysis for pH, turbidity, Mn, Mg, Fe, Ca, Ec, TDS, K, F, and Na.
To develop a physical non-motorized aeration model for oxygenation of ferrous ions encountered in the Chyulu aquifer at Makindu	- Measurement of dissolved oxygen (DO) using DO meter - Water quality analysis using standard method for water and wastewater. - Methods used were volumetric analysis for TDS and spectrophotometry for metals among others.	- Design of non-motorized aeration and filtration unit for oxygenation of Iron - Determination of appropriate spacing of trays and rate of flow. - Fabrication and testing the design unit. - Collection of samples from the study area - Water quality testing of feed water and aerated/filtered water with emphasis on ferrous and ferric ions.
To model dispersion of iron and its derivatives in the Chyulu aquifer.	- Hydro-geochemical modeling using conceptual approach of GMS. - Batch/microcosm technique to determine the concentration of ferrous and ferric over time. -Writing, testing and debugging of sub-routine for simulation of ferrous and ferric reactions in the stratum using RT3D module in GMS.	- Calibrate and validate GMS. - Testing of feed and filtered water for ferrous and ferric ions. - Estimate the rate constant for oxygenation of ferrous ions in the aquifer. - Writing of a user-defined RT3D code for iron dispersion in Makindu aquifer. -Test and debug the subroutine. -Calibrate the sub-routine - Validate the sub-routine -Use the subroutine for scenario analysis

3.3 DEVELOPMENT OF GROUNDWATER POTENTIAL MAPS FOR THE STUDY AREA

Generation of groundwater potential maps for both quantity and quality (WQI) was achieved through sourcing of data that was required for these tasks. Generation of groundwater potential map for the study area entailed mapping of boreholes in the study area and sourcing of data

required for this generation. This was data on surface drainage density, lineament, soil type, slope steepness, rainfall distribution, land cover and topography. Generation of groundwater quality indexing on the other hand involved determination of water quality parameter from 45 boreholes that were identified in the study area.

3.3.1 Mapping of Boreholes in the Study Area

Mapping of all the boreholes in the aquifer was done using GPS and data that was collected from personnel from Ministry of Water and Irrigation as well as Water Resources Authority (WRA). The history of the boreholes was sought from the stakeholders to ascertain the performance of the boreholes in terms of yield. The boreholes were visited during the dry season as well as during the rainy season. The borehole's coordinates were recorded using GPS for inclusion on GIS platform. Where information was lacking, data was collected from the field.

Information on boreholes included an identity in form of a code, a name, location in form of coordinates, yield in m^3/day, depth (m) and altitude.

Data on water quality was also collected. In most cases data was missing in which case samples were collected and testing was carried out in JKUAT laboratories to obtain data on parameters such as pH, color, electrical conductivity, total dissolved solids (TDS), sulphates, chlorides, phosphorous, alkalinity, salinity, hardness, iron, flourides, magnesium, manganese, calcium, sodium, potassium etc.

3.3.2 Drastic Modelling For Groundwater Potential Map Generation

Generation of the groundwater potential map using DRASTIC Model entails sourcing and collection of data on factors that influence occurrence of groundwater as listed in section 2.2.1. Table 3.4 shows these factors and their respective sources.

Table 3.4 Groundwater potential mapping data and its source

S/No.	Data Type	Sources	Format	Output Layer
1	Surface Drainage	International Livestock Research Institute Database (ILRI)	Vector	Surface drainage
2.	Landsat 8 Satellite Imagery	USGS:http://earthexplorer.usgs.gov	Raster	Land cover classes
3	Borehole Data	Ministry of Water and Natural Resources, WRA, County office	Vector	Boreholes yield
4	Chyulu Digital Elevation Model (DEM)	Regional Centre for mapping and resource development (RCMRD)	Raster	Physiography
5	Rainfall Distribution	International Livestock Research Institute Database (ILRI)	Vector	Rainfall distribution
6	Kenya Soil Terrain Shape file (KenSoter)	Kenya Soil Survey	Vector	Soils
7	Lithology	International Livestock Research Institute Database (ILRI)	Vector	Lithology

3.3.3 Processing of Data for Groundwater Potential Mapping

Digital Elevation Model Map

The raster based 30m DEM datasets covering the area of interest were obtained from the Regional Centre for Mapping and Resource Development (RCMRD). The datasets covering the area of interest were first mosaicked using mosaic to new raster tool in the data management toolbox in ArcGIS. The area of interest was then extracted from the new raster using extraction by mask tool in spatial analyst toolbox to obtain the DEM for Chyulu area. A shaded relief from a surface raster was then created from the DEM using Hill shade tool in 3D analyst toolbox so as to produce the DEM map of Chyulu.

Study Area Slope Map

Using the 30m DEM extracted for Chyulu, the rate of maximum change in z-value from each cell was determined to obtain the slope. This was done using the slope tool in the spatial analyst toolbox in ArcGIS. For each cell the tool calculates the maximum rate of change in value

from that cell to its neighbours (Chepchumba et al., 2019).The slope was then classified into 5 classes using reclassify tool in spatial analyst toolbox in order to produce the study area slope.

Drainage Pattern Map

The drainage is well defined by rivers and streams. The drainage lines were generated using Arc Hydro tools in ArcGIS through a procedure that entailed generation of drainage lines that were defined by rivers and streams. These drainage lines were generated using the Arc Hydro Tools in ArcGIS. This entailed use of the fill sinks functions that modified the elevation value. This was followed by selection of terrain processing function that determines the flow direction. Terrain processing function was again used to determine the flow accumulation, stream definition and stream segmentation. The last stages in the generation of the DEM were catchment polygon processing and drainage line processing which were achieved through selection of the terrain processing function followed by picking of the corresponding process.

3.3.4 Lithology Map

Kenya Lithology shapefile was sourced from International Livestock Research Institute Database (ILRI) from which the Chyulu lithology was delineated using select layer by attribute tool in data management toolbox in ArcGIS. The lithology was classified into categories under symbology in layer properties in order to produce lithology map.

3.3.5 Soil Map

Kenya Soil Terrain Shapefile (KenSoter) which was obtained from the Kenya Soil Survey from which soils in Chyulu were delineated using select layer by attribute tool in data management toolbox in ArcGIS. The average permeability and infiltration values were used to classify soil into hydrologic groups. The soils were categorized into various types under symbology in the layer properties so as to produce the soil map.

3.3.6 Rainfall Distribution

Kenya rainfall distribution shapefile was obtained from the International Livestock Research Institute Database (ILRI) from which the Chyulu rainfall distribution was delineated using select layer by attribute tool in the data management toolbox. The rainfall was then categorized into distribution under symbology in the layer properties.

3.3.7 Land Cover Map

For this task, multi-temporal satellite data of Landsat 8 Operational Land Imager (OLI) were downloaded for the period for the year 2020 for the study area at 30 m spatial resolution.
The methodology used in the study involved the following steps:

Satellite image pre-processing

Cloud free Landsat imageries downloaded from the USGS website were subjected to atmospheric correction to enable the images to be comparable for change detection. Images were then projected to Google Mercator (EPSG: 3857). The images were clipped by study area. The individual bands were stacked and displayed as standard false colour (4-3-2 for TM and for 5-4-3 for OLI) composite which is good for urban and vegetation studies).

Satellite image classification

Satellite image classification involved training, choosing the classification algorithm, running the classification and accuracy assessment.
Training is the identification of a sample of pixels of known class membership gathered from reference data such as ground truth, existing maps and aerial photographs. In this study therefore, ground truth information was obtained using Google Earth. Furthermore, a pixel based supervised classification using Random Forest algorithm was used in the classification. Being a supervised classification, independent information was used to define training data which was then used to establish the classification categories. Therefore, the training data was converted into shapefiles which were overlain with each standard false colour composite maps i.e. for 2020, and then the nine LULC classes were digitalized on the computer screen.
In classification accuracy assessment, a sample of testing pixels was selected and their class identities compared on both the classified image and reference data. Thus, additional data collected for ground truthing in form of Google Earth imagery and open street maps was input

in QGIS under post processing procedures and used in accuracy assessment. The resultant error matrix was used in evaluation of the classification accuracy.

Classification Report

The final classified outputs were then filtered using majority filter to remove noise and enhance cartographic appearance. The image was classified into 9 classes: Forest, shrub, built up, grassland, wetlands, cropland, Baren, savana and water body.

Land sat 8 Satellite Imagery was sourced from USGS:http://earthexplorer.usgs.gov/. A total of four Landsat scenes which fully cover the area were stacked. A mosaic of bands 1-9 excluding band 8 of the four Landsat scenes covering the area was first made under ESRI ENVI platform. The stacked image was then subset to obtain the area of interest. The Region of Interest (ROI) were then picked using the spectral signature defined through "training". A shape file was created through the classification of a 30m resolution Chyulu Landsat 8 image with the classification being done on the ESRI ENVI platform. Supervised classification using the maximum likelihood classification method was carried out with the image being classified into six classes: Forest, shrub, woodland, bare land, cropland and water body.

3.3.8 Physiographic Map

Slope is a major factor in hydrogeology in that it defines the drainage characteristics of a water catchment. The projected 30m DEM for Chyulu was classified into 5 classes under symbology in layer properties based on the elevation in order to develop the physiographic map of the study area. The highest point lay at an altitude of 2138 m, while the lowest at a height of 259 m above sea level.

3.3.9 Surface Drainage Map

The surface drainage shapefile for Kenya was obtained from the International Livestock Research Institute (ILRI) Database from which the Chyulu surface drainage was delineated using select layer by attribute tool in the data management toolbox. The surface drainage was categorized into rapid, fast, slow and very slow drainage under symbology in the layer

properties. Surface drainage is strongly influenced by the slope, soil type and the land cover of the area.

3.3.10 Boreholes Map

The boreholes data for the study area were obtained from the Ministry of Water and Natural Resources in tabular format in an excel sheet. Other borehole data was obtained from the regional and sub-regional offices of WRA at Machakos and Kibwezi respectively and was added into the excel sheet. The excel data sheet was imported into the Arc map and added as a new layer. The added layer was exported as a new shapefile. The boreholes were categorized into yields under symbology in the layer properties so as to produce a map of boreholes yield.

3.3.11 Lineament Density

The detection of lineaments from satellite imagery was carried out using the automated processing tool; LINE from PCI Geomatica which used band 7 of Landsat 8 (OLI) in extraction of lineaments. Visual inspection of all the bands was carried out and the short-wave infrared band 7 was selected for use in the analysis. This band was stretched to an output of 0 to 255 and then an edge sharpening filter applied to it. The edge sharpened image was then used as an input for the Lineament Extraction tool, LINE, which applied edge detection, thresholding and curve extraction. Landsat 8 (OLI) was chosen because of its spectral discrimination of a variety of characteristics that are required for the study. A total of four Landsat scenes wholly cover the study area. Band 7; shortwave infrared, was useful in the extraction of geological formations and rock features. A mosaic of Band 7 of the four Landsat scenes covering the area was first made using ENVI 4.7. The automatic extraction involved using the LINE tool from Geomatica 2014. The tool extracts linear features from an image and records the polylines in a vector layer. The module was designed to extract lineaments from radar images; however, it can also be used on optical images to extract curve-linear features. The input in this case was

optical; the mosaicked Landsat 8 Band 7 scenes. The extracted lineaments were then saved as a shapefile and added in Arc Map.

3.4 GROUNDWATER POTENTIAL MAP

The various shape files (land cover, rainfall distribution, soil texture, lithology, lineament density, topography, slope) were reclassified. The methodology schema for the generation of the groundwater potential map is shown in Figure 3.6. Weights were applied in the DRASTIC-based overlay scheme using ‘weighted overlay’ tool in Arc map.

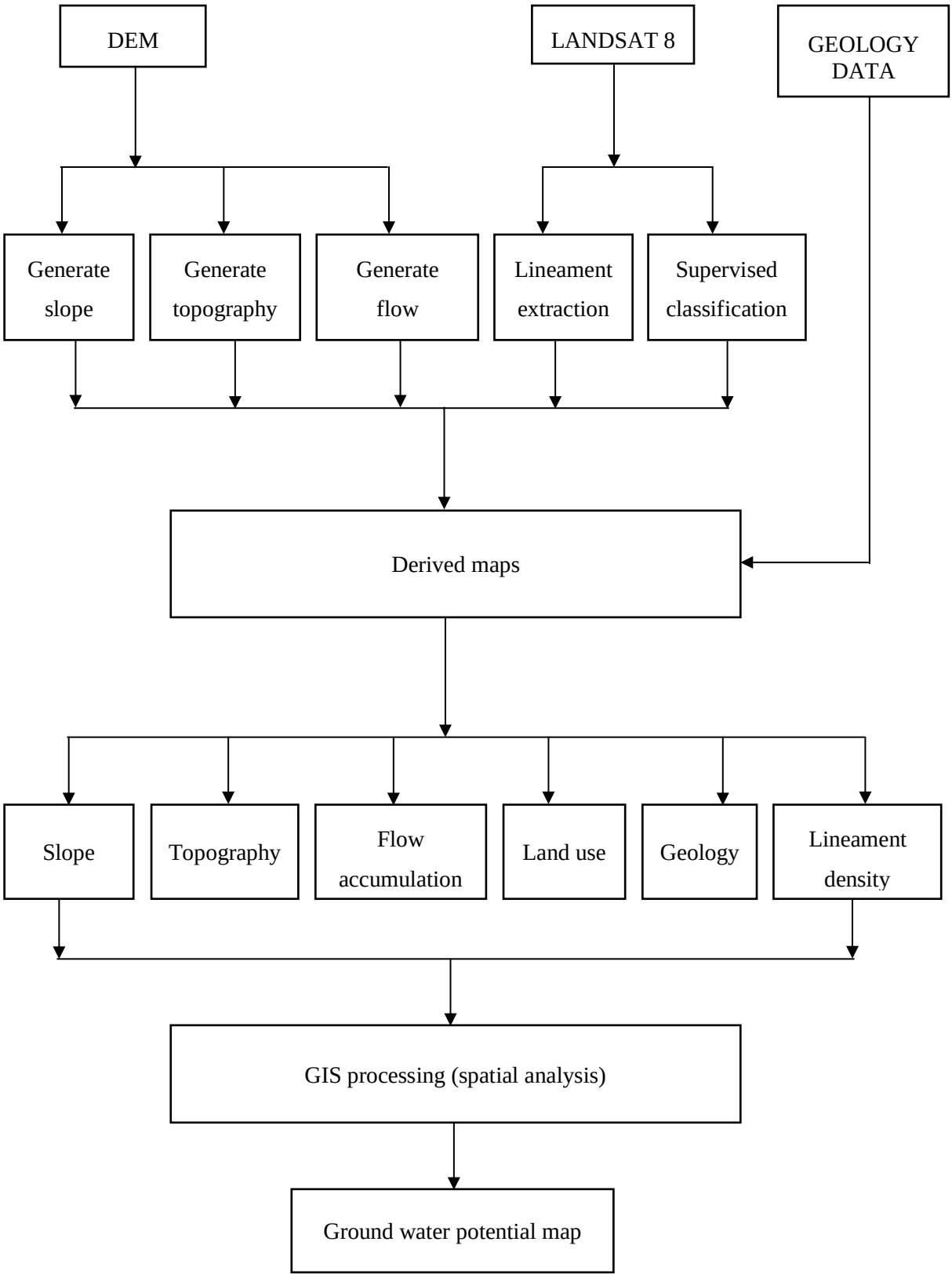

Figure 3.6 Ground water potential generation map flow chart (Kiplangat and Mutua, 2016)

The resulting groundwater potential map was classified into very low, low, moderate, high and very high groundwater potential areas. The existing boreholes were added in the map to check on the accuracy of the generation process. Table 3.5 shows the weights for the different parameters that contribute to groundwater potential.

Table 3.5 Weights applied the generation of potential maps using DRASTIC model

Feature	Classification	Rating	Drastic Weight	Total Weights	Weightage %
Lineament Density	0.126 – 0.528	1	5	5	23
	0.528 – 0.734	2		10	
	0.734 – 0.929	3		15	
	0.929 – 1.113	4		20	
	1.113 – 1.543	5		25	
Slope (%)	31.23 – 75.120	1	4	4	18
	17.68 – 31.23	2		8	
	9.43 – 17.68	3		12	
	3.83 – 9.43	4		16	
	0.00 – 3.83	5		20	
Topography (M. A.S.L.)	1467 – 2138	1	4	4	18
	1176 – 1467	2		8	
	961 – 1176	3		12	
	747 – 961	4		16	
	259 – 747	5		20	
Land cover	Bare land	1	3	3	17
	Cropland	2		6	
	Shrub	3		9	
	Forest	4		12	
	Woodland	4		12	
	Water	5		15	
Rainfall Distribution (mm)	200 – 400	1	2	2	9
	400 – 600	2		4	
	600 – 800	3		6	
	800 – 1200	4		8	
	1200 - 1600	5		10	
Lithology	Basalt, basalt igneous rock, granite, igneous rock, Intermediate igneous rock	1	2	2	9
	Sandstone, greywacke, arkose	2		4	
	Eolian unconsolidated rock, Pyroclastic unconsolidated rock	3		6	
	Fluvial	4		8	
	Acid metamorphic, Gneiss, magmatite, quartzite	5		10	
Soil texture	Clay	1	1	1	6
	Clay loam/ Silt loam	2		2	
	Loam	3		3	
	Clay loamy sand	4		4	
	Loamy Sand	5		5	

3.5 WATER QUALITY ASSESSMENT

A field survey was conducted and water samples were collected from 43 boreholes (Appendix 3). These water samples were analysed in the laboratory for different physical chemical parameters. The parameters include pH, colour, turbidity, electrical conductivity (EC), total dissolved solids (TDS), calcium (Ca), magnesium (mg), chloride, Iron (Fe), Manganese (Mn), fluoride (F), potassium (K), sodium, Na, sulphates (SO_4) and nitrates (NO_3).

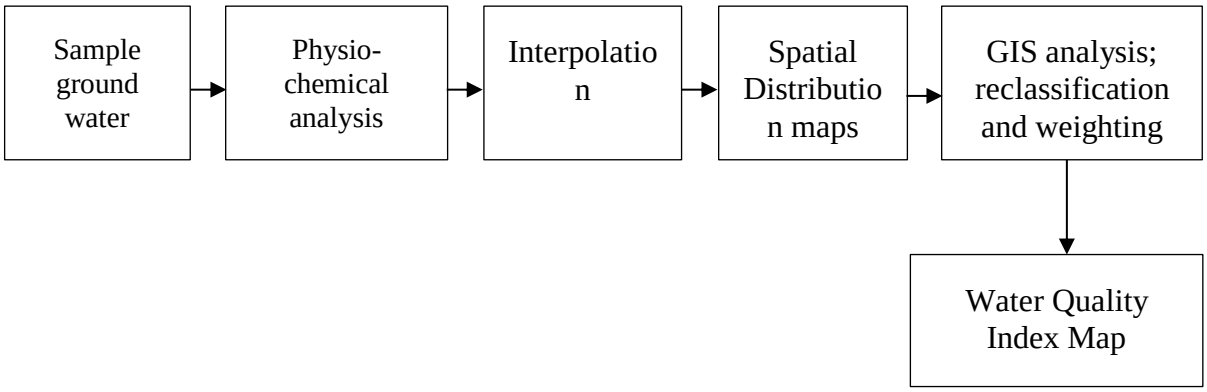

Figure 3.7 Water Quality Index flow chart (Kiplangat and Mutua, 2016)

3.5.1 Assessment of the Quality of Groundwater

The parameters were expressed as mg/L except for the pH, Electrical Conductivity (µs/cm), turbidity (NTU) and colour (TCU). Sampling, preservation, transportation and the analysis of the samples was carried out according to methods described in water and wastewater analysis (Clesceri et al., 1995). The high density polyethylene plastic sampling containers (20 litres) were rinsed with the groundwater being sampled and then completely filed up. The containers were then air-tightly capped. The samples for chemical analysis were preserved and analyzed within 48 hours. The Atomic Absorption Spectrophotometer (AAS) was used for in the analysis of heavy metals.

3.5.2 Water Quality Index (WQI)

To compute WQI, three steps were followed. In the first step, each of the 10 parameters; pH, turbidity, Ec, Mn, Mg, Ca, Fe, K, Na, and TDS were assigned a weight (wi) based on their perceived effects on primary health. The maximum weight of 5 was assigned to parameters like total dissolved solids, iron and electrical conductivity due to their major importance in water quality assessment. Manganese and potassium were assigned minimum weight of 1 as they play an insignificant role in water quality assessment. Other parameters were assigned a weight between 1 and 5 based on their importance in the overall quality of water for drinking purposes.

The second step, the relative weight (Wi) of each parameter was computed using the equation below.

$$\mathrm{Wi} = \frac{\mathrm{wi}}{\sum_{\mathrm{i}=1}^{\mathrm{n}} \mathrm{wi}} \qquad \text{…..…… (3.1)}$$

where, W_i is the relative weight, w_i is the weight(value) of each parameter, and n is the number of parameters.

In the third step, quality rating scale (qi) was calculated for each parameter using the equation below.

$$q_i = \left(\frac{C_i}{S_i}\right) \times 100 \qquad \text{…..…… (3.2)}$$

where, q_i is the quality rating, C_i is the concentration of each chemical parameter in each water sample in mg/L and S_i is the standard value of each parameter in mg/L.

To compute the WQI, the S_i is first determined for each chemical parameter using the equation below.

$$S_i = W_i * \mathrm{qi} \qquad \text{…..…… (3.3)}$$

where, S_i is the sub-index of ith parameter, q_i is the rating based on concentration of i parameter and n is the number of parameters.

WQI was then computed using the equation below:

$$WQI = \sum SIi \quad \text{…..…… (3.4)}$$

The various maps of pH, Turbidity, Ec, TDS, Mn, Mg, Fe, K, Na, and F as developed were weighted and the weights applied in the DRASTIC-based overlay scheme using the IDW (Geostatisical Analyst) tool in Arc Map to generate groundwater quality index (WQI) map. Table 3.6 shows the parameters used in the development of WQI and their corresponding weighting.

Table 3.6 Parameters used in developing WQI and their corresponding weighting

Chemical Parameters	Weight (wi)	WHO Standard	Relative weight (wi)
Fe	5	0.3	0.16129
TDS	5	1000	0.16129
EC	5	500	0.16129
Turbidity	4	5	0.129032
F	3	1.5	0.096774
pH	3	8.5	0.096774
Mg	2	50	0.064516
SO_4	2	75	0.064516
Mn	1	0.1	0.032258
K	1	12	0.032258
	31		1

3.6 DEVELOPMENT OF PHYSICAL MODEL FOR THE REMOVAL OF IRON THROUGH NATURAL AERATION

This was the second specific objective of this study: To develop a physical non-motorized aeration model for oxygenation of ferrous ions encountered in the Chyulu aquifer at Makindu. To achieve this objective a physical model was developed using the system operation concept that followed the block diagram in Figure 3.7. Water from a 50 litre raised tank falls through three sets of trough/tanks that have ¾-inch (19.1mm) coarse aggregate before falling into the pre-filtration chamber. To determine the filtration rate of the filter bed a review of literature

was undertaken. These studies included studies by Das (2007), Barlokova and Ilavsky (2009), Ling (2011), Nik et al., (2013) and Siwila et al., (2017).

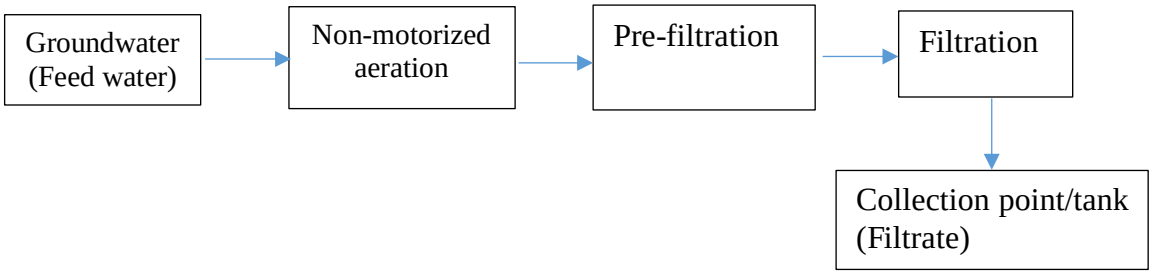

Figure 3.8 Parameters used in developing WQI and their corresponding weighting

3.6.1 The Non-Motorized Aeration and Filtration Stages

This prototype was a three-stage non-motorized aeration filtration system with a flow rate of 30 l/day. Only non-corrosive materials such UPVC pipes, and plastic buckets were used in the fabrication. However, galvanized materials were used only where plastic alternatives were not readily available. The designed filtration unit was used as a test unit for determination of rate constant for the oxygenation of ferrous iron (K_3) in the study area. The effectiveness of designed unit to positively change the other parameters in water sample was also investigated through performance of standard tests. Groundwater samples were collected from twelve boreholes within the Chyulu aquifer. Physical chemical tests were then carried out on these samples before the water was passed through the aeration filter. The water quality parameters were determined using the standard procedure mentioned in section 3.5.2 while the test results are shown in Section 4.3.1.

3.6.2 Aeration of Water Samples

The percentage increase in aeration was determined and the dissolved oxygen measured using trays spaced at 50 cm from top of stand. This spacing was the most ideal for optimal number of trays used, and for prevention of water splashing and erosion of aggregates.

3.6.3 Design of the Aerator

The aerator was made such that the feed (raw) water was put into a 50 litre plastic container that had ½ inch (13 mm) diameter outlet pipe and a gate valve that controlled the rate of flow. The rate of flow having been determined in terms of the degree of turn of the gate valve.

In this instance, the rate of flow was set at 30 l/day and the water layer on the tray taken as 1.5 cm (0.015m). The height from one tray to the next was 50 cm and the width of tray was 25 cm. The total drop from the top tray to the top of the tetrahedron shaped filter was 1.50 m - the space between trays and the number (n) of space. That is 50 × 3 =150 cm = 1.5 m. The plastic container was hoisted on top of a timber platform and the total height of the platform was 2m. The platform was placed on a low table as seen in Plate 3.1 that showed the non-motorized aeration and filtration setup as per designed components in figure brought forward from end of section 3.6.4.

Plate 3.1 The experimental setup of non-motorized aeration test

3.6.4 Design of Filter

Filtration process was carried out using sand in the filtration media. The effective diameter of the sand d_{20} ensured a good quality effluent while at the same time preventing penetration of clogging matters to such a depth that it could not be removed by surface scrapping. The effective diameter usually lies in the range of 0.15-0.35 mm and is determined by experiment. Both finer and coarser materials have been found to work satisfactorily in practice and the final selection will usually depend on the locally available materials.

The minimum depth was determined using the Hudson formula, equation (3.4) to avoid breakthrough to floc.

$$\frac{Qd^3h}{L} = B_i \times 29323 \qquad \text{…..…… (3.5)}$$

where: Q = Filtration rate ($M^3/m^2/h$)

L= depth of filter bed (m)

h = Terminal head loss (m)

d = Sand size (mm)

B_i = Breakthrough index is a dimensionless constant whose value ranges between 0.0004 to 0.006 depending on response to pre-treatment in the filter unit.

The value of B_i is taken as 0.0004 for poor response to filtration and the average degree of pretreatment.

Filter capacity

The flow from the aeration arrangement is the flow that enter the filtration chamber, therefore $Q_{in} = Q_{out}$ = 30 l/day = 3.472×10^{-3} m^3/s. The rate of flow is also given by Darcy's equation.

That is Q = KiA where K= hydraulic conductivity, i = hydraulic gradient and A is area of filter.

Hydraulic conductivity

The value Hydraulic conductivity, k, was taken as 5.00×10^{-3} m/s. This is the value of hydraulic conductivity for sand size ranging from medium and coarse (Freeze and Cherry,

1979). The hydraulic conductivity is divided by a factor of safety of 3, due to possibility of clogging. $K_{ave} = (5 \times 10^{-3})/3 = 1.67 \times 10^{-3}$ m/s.

The filter area

Using Darcy's equation and a filter area of 0.326 m^2, the flow rate of the filter is calculated as 0.000544 m^3/s. This flow rate is smaller than the flow rate in the inlet section where aeration takes place. The size of the filter is adequate and delivers the same amount as the water it receives from the aeration section.

Filtration component head loss calculations

Darcy's law was then used to calculate the head loss in the filter. $Q = kiA$ and $i = \Delta h / \Delta l$

$$\Delta h = (Q \times \Delta l) / (k \times A) \quad \text{…..…… (3.6)}$$

For design purposes and simplicity, the calculations were based on filter consisting of one layer and sand with grain size of 0.20mm, and where:

$A = 0.326\ m^2$; $Q = 0.000544\ m^3/s$; $K = 1.67 \times 10^{-3}$ m/s; Length = 0.38 m.

Therefore, the head loss is 0.38m. The designed components are shown in Figure 3.8 while the designed components are shown in Table 3.7.

Table 3.7 The designed components

Parameter	**Value**
Rate of flow (M^3/s)	3.472×10^{-3}
Sand size (mm)	0.2
Area (m^2)	0.326
Hydraulic conductivity (m/s)	1.67×10^{-3}
Break through index	0.004
Total drop (m)	1.50
Tray spacing (m)	0.50

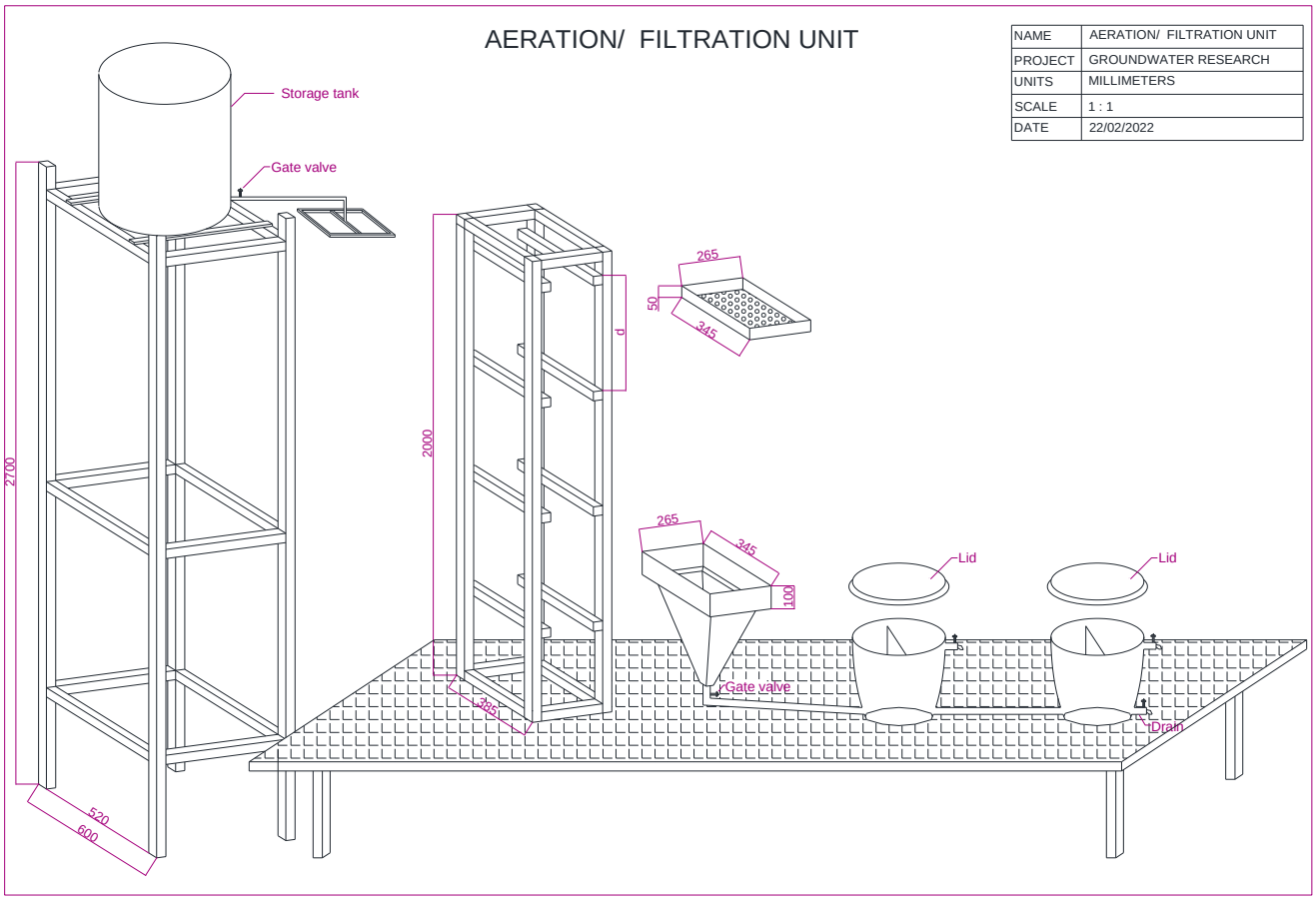

Figure 3.9 The non- motorized aeration and filtration setup

3.7 TESTING FOR FERROUS IRON (II) AND FERRIC IRON (III)

3.7.1 Laboratory Testing of Iron (II)

Determination of ferrous iron in a groundwater water sample was achieved using potassium permanganate, which is a strong electrolyte when dissolved in groundwater. 50 ml of groundwater sample was placed in 125 ml Erlenmeyer flask to which 50 ml of sulphuric acid was added. The flask was then swirled until complete mixing was achieved. The concentrate was then titrated using potassium permanganate solution until the calorimetric end point was reached.

3.7.2 Testing For Ferric Iron (III)

An aliquot of 0.25 M ferric solution was taken into a 250 ml conical flask to which 20 ml of 0.05 % solochrome Azurine B.S. indicator is added. The pH was then adjusted to 3 using

sodium hydroxide. The solution was then warmed to 45^0 C and then titrated with 0.01 MEDTA solution until the colour changes from dark blue to brown or light violet. The dye reacts with Fe (III) by giving a very sharp endpoint. The key advantage of using solochrome azurine B.S indicator is that most ions do not interfere with this reaction. The only ions that interfere are Cu^{2+}, Zn^{2+}, $C_2O_4^{2-}$ and CH_3COO - which interfere even when in traces.

The results of aeration/filtration tests obtained from this test set up are presented in section 4.3.

3.8 MODELING DISPERSION OF IRON AND ITS DERIVATIVES IN THE STUDY AQUIFER

The third specific objective was the modeling of iron and its derivatives in the Chyulu aquifer. To achieve this specific objective the following steps were taken:

1) Selection and generation of a hydro- geophysical model in the study area.
2) Selection of packages and incorporation of aquifer properties in the hydro-geophysical model.
3) Running of MODFLOW, MT3DMS and RT3D modules.
4) Calibration of the hydro-geochemical model (inverse method).
5) Writing and testing of user-defined (Sub-routine) RT3D code for iron reaction in the aquifer.
6) Calibration and validation of the user-defined RT3D Subroutine code.
7) Validation of the user-defined RT3D subroutine code.
8) Application of the user-defined code in prediction of ferrous and ferric concentration in the Chyulu aquifer.

The flow chart shown in Figure 3.9 shows the interaction between the various steps been undertaken to achieve this objective.

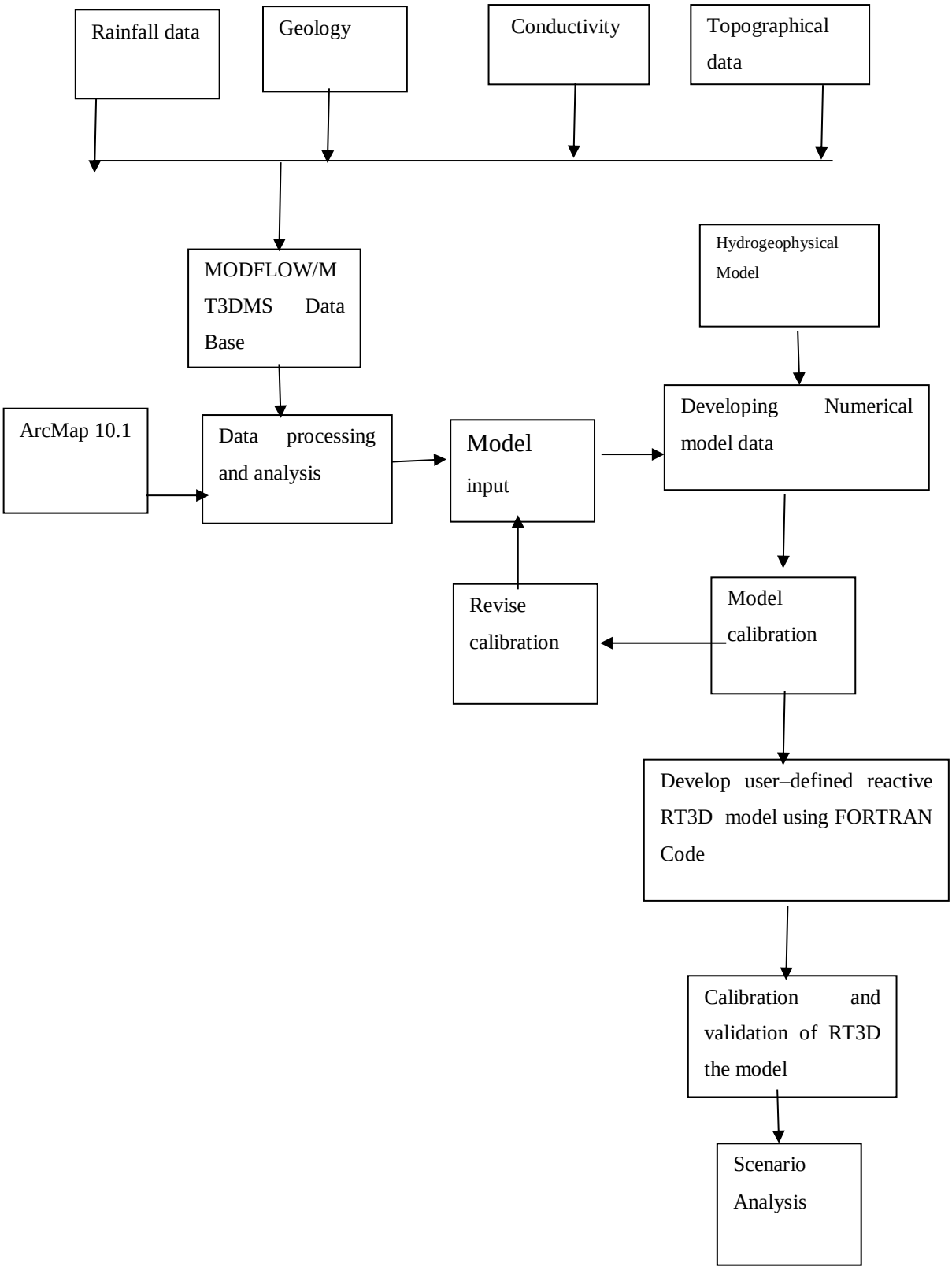

Figure 3.10 Flow chart of activities involved in user defined RT3D modeling of iron

3.8.1 Selection and Generation of the Hydro-Geophysical Model

The selected section for the detailed solute flow study was Makindu watershed as shown in Figure 3.10. The highest point in the watershed is at an altitude of 1000 a.m.s.l. The Makindu River drains the watershed and has Kiumbi, Wayona and Kikumbulyu as its three main tributaries, with Kilingoni as a sub-tributary to Wayona. The watershed has many boreholes that are close to one another. Many institutions such as hospitals, schools, religious institutions, hotels alongside many businesses and farms are also situated in the area.

In this study the delineated section was converted into a grid model by the GMS software. The GMS, a comprehensive Graphical User Environment for performing groundwater simulations, has many modules but only the two modules, MT3DMS and RT3D, were activated in this study. As discussed in section 2.9.2, both modules operate on the primary groundwater model, MODFLOW.

The watershed boundary that has been curved out using the create arc tool in GMS software

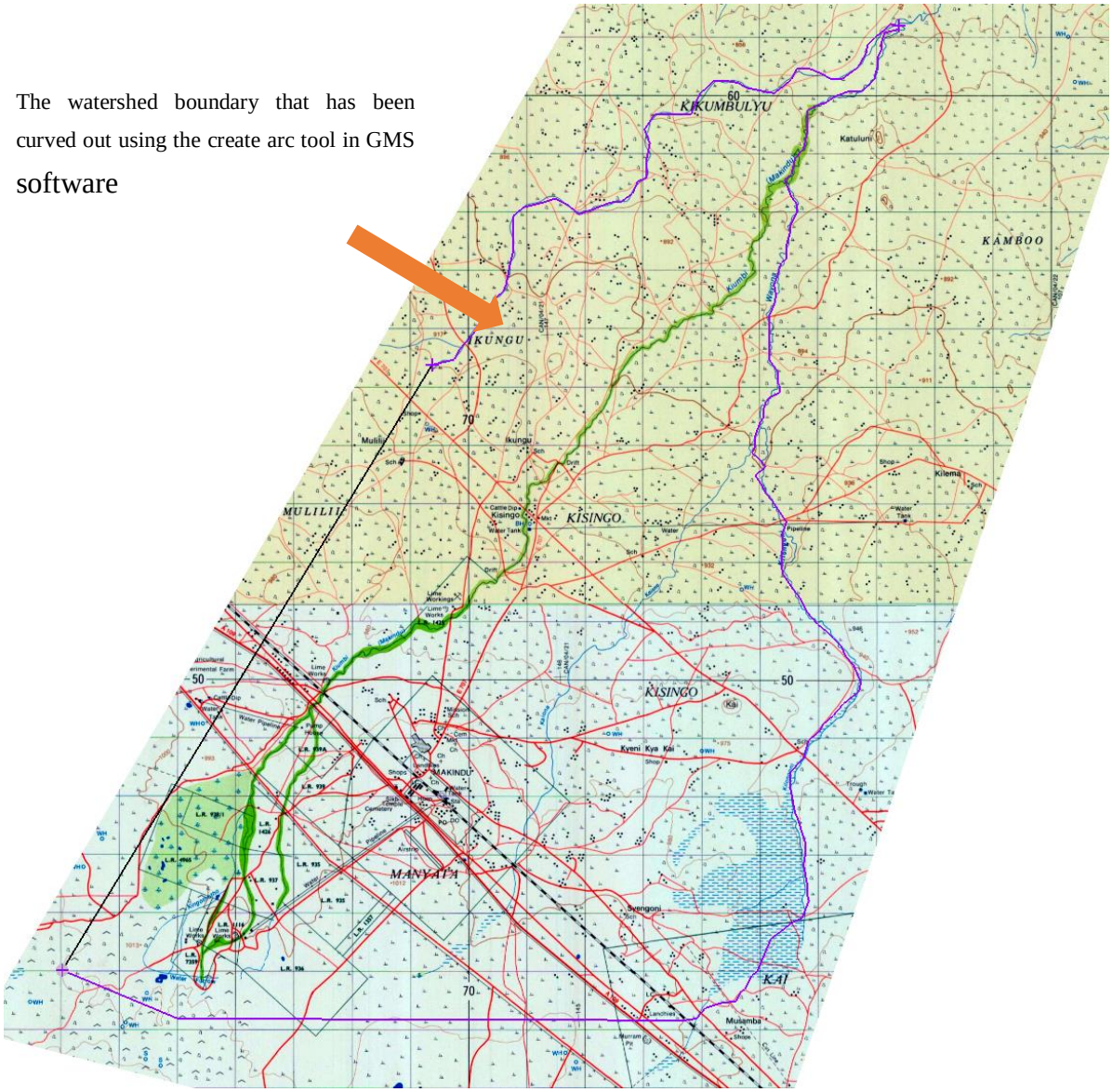

Figure 3.11 Georeferenced map of Makindu Watershed (Courtesy: Survey of Kenya topographical sheet number 174/4 (Kibwezi) and 174/2 (Ikoyo).

Twenty-five (25) boreholes from the watershed were selected and their characteristics input into the hydro-geological model. The data that was input included yield, depth, water struck level (WSL) and boreholes log data. Representative borehole logs are shown in Appendix XI. Table 3.8 lists the code, name and coordinates of the 25 boreholes selected and used in the solute study.

Table 3.8 Boreholes used in hydro-geochemical modeling of flow of iron ions through the aquifer

ID. No.	Name of Borehole	UTM Coordinates		Yield	Depth	Altitude
		X	Y	(m^3/day)	(m)	(AMSL)
MK1	Jamia Mosque A	368779	9748818	9.0	120	1007
MK2	Jamia mosque B	368789	9748822	7.2	135	999
MK3	Sikh Temple A	368747	9748601	8.1	91	1006
MK4	Sikh Temple B	368789	9748604	7.5	83	1005
MK5	Makindu Hospital	369230	9747647	6.86	110	990
MK6	Makindu Railway	369736	9759147	5.8	65	990
MK7	Makindu Water	367735	9759158	8.1	78	996
MK8	Makindu Mission 1	369589	9749384	6.5	84	1004
MK9	Makindu Mission 2	369589	9749383	7.5	51	1002
MK10	Makindu Sisters	369579	9749726	8.5	66	1003
MK11	Musimba 1	374289	9741666	6.1	150	1010
MK12	Musimba 2	374118	9742653	6.8	120	993
MK13	Musimba 3	372840	9743415	5.6	89	988
MK14	Musimba 4	371846	9751510	5.9	224	970
MK15	Kisingo	374684	9744605	12.5	98	1036
MK16	Makilya Invest 1	366611	9751194	8.8	120	990
MK17	Makilya Invest 2	366611	9751194	9.65	64	985
MK18	Makau Boniface	366637	9747604	7.2	56	935
MK19	Ndivo Invest 1	366558	9747601	12.9	34	986
MK20	Ndivo Invest 2	366565	9747602	12.5	37	970
MK21	Experiment Farm	365451	9749046	8.2	47	1025
MK22	Kyeni	372397	9748748	8.4	56	992
MK23	Kai	374008	9747935	6.5	98	982
MK24	Katuluni	375288	9754345	15.6	56	985
MK25	Mulili	369285	9752125	8.6	85	947

3.8.2 Selection of Packages and Incorporation of Aquifer Properties in the Hydro-Geophysical Model

As indicated in section 3.8.1, the GMS software modules that were activated in this study are MT3DMS and RT3D. MT3DMS module simulates advection, dispersion and chemical reactions of dissolved constituents in the groundwater system while RT3D simulates multi-

species reactive transport of salts in an aquifer. In this study RT3D reaction module has been activated to simulate reactions of iron (Fe) and its derivatives in the aquifers.

The "selected area" model developed in section 3.8.1 was imported to the GMS software which was followed by definition of units, stress periods, specification of output controls that specify the time step in days.

The packages that were selected are advection, dispersion, sources/sink mixing package and transport observation package. This was followed by inputting of porosity, dispersion coefficient and recharge of the study area. These parameters are assigned using the Map to MT3DMS command. The value of porosity is taken as 0.3 while the longitudinal dispersivity is taken as 0.000016 read from Appendix IX. The value of recharge is input using the recharge coverage process. The assumptions that were made in this study are that the weathered and fractured gneiss formed a single aquifer system and that both Darcy's and Fick's laws apply.

3.8.3 Calibration of the Hydro-Geologic Model of Makindu Area of the Chyulu Aquifer

The hydro geophysical model that had now been generated was calibrated using an inverse process as per operation manual for GMS. The process of calibration and validation of the selected area was done to ensure that it predicted parameters that were used in the sub- routine accurately.

The map in Figure 3.9 was imported into GMS software. It consisted of model boundary, specific head boundary, streams and boreholes, recharge zones and hydraulic conductivity coverage. After the importation of the model, observation boreholes as seen in Table 3.8 were positioned using the "create point" tool that enables the positioning of boreholes using the X and Y coordinates. These boreholes were selected close to one another and are on the eastern side of Makindu River that was considered as a drain because it is a seasonal river. The

respective data of these boreholes was used to estimate depth of water table, recharge, hydraulic conductivity as well as other data that was required as input in the calibration exercise.

This was followed by the specification of the corresponding heads for boreholes as well as the confidence value (95%) which represents the confidence in the error estimate, which is also the observation head confidence.

The observation stream flows were assigned directly in the source/sink coverage of the model. MODFLOW determines the computed flow from the aquifer to the steam. The streams in the study area are seasonal therefore; the stream flow that is measured at the site is the total flow from the aquifer to the stream outlet at the top of the model.

Recharge in the study area

The form of groundwater recharge that dominate in watersheds ASAL environments such as Makindu, in the Chyulu is focused recharge. As indicated the section 2.1.2 the major factors that contribute to groundwater recharge of an area are mainly rainfall, evapotranspiration and soil type. Groundwater recharge in this watershed could take place by direct percolation through the vadose zone in excess of moisture deficits after a downpour and evapotranspiration or indirect recharge from the ephemeral streams such as Makindu River and its tributaries; Kiumbi, Wayona and Kikumbulyu. Recharge is a function of rainfall and is taken to be between 5 and 10 % of rainfall. In the study area, the average annual rainfall is 227 mm as per section 3.1.3 and taking recharge as 5% for this arid environment the average daily recharge was 0.000032 m/day. This was the amount of recharge that was used in the calibration exercise.

Running of MODFLOW, MT3DMS and RT3D modules

To demonstrate that the hydro-geologic model simulated the observed aquifer behavior the model was run repeatedly using recharge and hydraulic conductivity values, which were systematically altered, until the computed solution matched the field/observed values within an acceptable level accuracy. The eight boreholes used in this exercise are shown Table 3.9 and the computed solutions were then imported into groundwater modeling system, which was

followed by a plot of flux residual errors. These errors were plotted on a set of calibration targets to show the overall calibration statistics. The results of this calibration exercise are shown in section 4.3.

Table 3.9 The observation boreholes

S/No	Identification of borehole	x	y	Head (amsl)
1	Jamia Mosque (B) (MK3)	368779	9748818	999
2	Sikh temple (A) (MK3)	368747	9748601	1006
3	Makindu Mission 1 (MK8)	369589	9749384	1004
4	Makindu Sisters (MK10)	368779	9749726	1002
5	Kisingo (MK15)	374684	9751510	1016
6	Makilya Investment 1(MK16)	366611	9751194	990
7	Makau Boniface (MK18)	366637	9748604	935
8	Ndivo and co. 1 (MK19)	366558	9747601	985

3.9 DEVELOPMENT OF SUB-ROUTINE TO SIMULATE IRON REACTION IN CHYULU AQUIFER AT MAKINDU

The development of this sub-routine entailed writing the sub-routine in FORTRAN 90 and then linking it into a RT3D code version 2.5 (RT3Dv2.5). This version incorporated changes introduced into version 3.5 of the modular three-dimensional multi species transport model (MT3DMS), a module of the groundwater modeling system (GMS). User-defined reaction package was created as a dynamic linked library (DLL) which enabled the sub-routine to be created as a stand-alone FORTRAN 90 code. Then this code was compiled using the *Microsoft Fortran Power Station* compiler incorporated in the Microsoft Developer Studio software. The output of the compilation was a DLL file specifically named as rxns.dll that was then copied to the RT3D directory under the GMS installation folder.

The DLL file was then launched by the RT3D as part of the Modular Three Dimensional Multi Species Transport model (MT3DMS) that could simulate advection, dispersion and chemical reactions of dissolved constituents in the groundwater system of the study area.

The specific equations that the sub- routine sought to solve are developed in the following sections.

The code sought to simulate the flow of ferrous salts and the continuous oxidation of ferrous to ferric salts under the condition of limited availability of oxygen. In the presence of limited amounts of oxygen equation (2.37) and equation (2.38) may be modified to take into consideration the complexes that form.

3.9.1 Catalytic Effect of Fluoride in the Study Area Aquifer

According to Hem and Cropper (1959) and Stumm and Lee (1961) among other researchers both ferrous and ferric iron are powerful formers of complexes. For example ferric can form complexes with many different inorganic anions. In the Chyulu aquifer, the ferric present is likely to form complexes with fluoride because of its relatively high concentration as can be seen in Table 2.2. Therefore, this study considers the catalytic effect of fluoride ions in the ferrous and ferric reactions in the Chyulu aquifer in the limited availability of oxygen. The catalytic effect of Fluoride was tested through the running of the batch reactor code (Appendix XII) with concentration of Fluoride and running of the same code without the Fluoride and then comparing the confidence level of the two runs. The results of this test are shown section 4.4.1 If this assumption is taken into consideration, the ferrous equation (2.37) (section 2.8.4) becomes

$$R_{II}\frac{d[Fe(II)]}{dt} = D_x\frac{d^2[Fe(II)]}{dx^2} - V_x\frac{d[Fe(II)]}{dx} - k_2[Fe(II)][O_2][F] \quad \text{…..…… (3.7)}$$

Therefore, for ferric, equation (2.38) (section 2.9.4) becomes

$$R_{III}\frac{d[Fe(III)]}{dt} = D_x\frac{d^2[Fe(III)]}{dx^2} - V_x\frac{d[Fe(III)]}{dx} + k_3[Fe(II)][O_2] \quad \text{…..…… (3.8)}$$

Where: $[O_2]$ = the concentration of oxygen

$[F]$ = the concentration of fluoride.

D_x = the dispersion coefficient

V_x = the average velocity of the solute in the aquifer.

X = direction of flow

t = time in days

$[Fe(II)]$ = the concentration of ferrous ions

$[Fe(III)]$ = the concentration of ferric ions

k_2 = First order rate constant for the ferrous

k_3 = First order rate constant for the ferric

R_{II} = Retardation factor for the ferrous

R_{III} = Retardation factor for the ferric

The results of this test are reported in section 4.4.2.

3.9.2 Application of the Operator-Split Strategy

To solve equations (3.7) and (3.8) that are non-linear and reactive relation is a challenge. The operator–split strategy is applied which entails splitting the original equation into two parts over a time step (Valoucchi and Malmstead, 1992; Zysset et al., 1994; Zengh and Bennet, 2002; Simpson and Landman, 2007) This is followed by separate computation of a solution for each part followed by combination of the two solutions to form a solution to the original problem. The split, however, comes at the expense of a truncation error, which comprises an error component due to boundary condition and an error component which occurs within the domain. If the concentration of iron (Fe) in the stratum is assumed to be constant, then the dispersion and advection components become negligible.

$\frac{d[Fe(II)]}{dx} \approx 0 \qquad \frac{d[Fe(III)]}{dx} \approx 0$

Upon application of the operator – split strategy to equation (3.7), part of the relationship that can be used to describe the oxidation of ferrous ions is equation (3.9).

$$R_{II}\frac{d[Fe(II)]}{dt} = -k_2[Fe(II)][O_2][F] \qquad \text{…..……} \quad (3.9)$$

This relationship represents the rate expression of the oxidation of Fe (II) in the neutral pH-range. When this relationship is customized to fit the conditions in the study area of Chyulu aquifer at Makindu and upon division of equation (3.9) by RII we get the modified relationship in equation (3.10) which is suggested and tested.

$$\frac{d[Fe(II)]}{dt} = \frac{-k_2[Fe(II)][O_2][F]}{R_{II}} \quad \text{..... (3.10)}$$

Similar relationship had been suggested in the kinetics of oxygenation of ferrous iron studies by Sung and Morgan (1980) where copper was taken as the catalyst.

The first order rate constant for ferrous, k_2, is a variable that depends on pH. (Ghosh et al., 1966). According, to Singer and Stumm (1969) and Stumm and Lee (1961) the rate constant for ferrous vary substantially as the pH increases on or about neutral (6.5 - 8.5). For example the rate constant varied from 0.0085 min^{-1} for a pH of 6.5 to 0.0337 min^{-1} for a pH of 8.5 as read from Table 3.10. The value of k_2, the rate constant was obtained using the relationship shown in equation (3.11) with the corresponding values being read from Table 3.10.

$$k_2 = \frac{(k_{pH8.5}+k_{pH6.5})(pHvalue-6.5)}{2} \quad \text{..... (3.11)}$$

where: k_2 = the first order constant of Fe (II) (ferrous)

$k_{pH8.5}$ = the first order constant of Fe (II) (ferrous) at a pH of 8.5

$k_{pH6.5}$ = the first order constant of Fe (II) (ferrous) at a pH of 6.5

pH value = the specific pH value of the aquifer

When the operator split strategy, as discussed in section 2.8.3, is applied to equation (3.9), equation (3.12) is arrived at.

$$R_{III}\frac{\partial[Fe(III)]}{\partial t} = k_3[Fe(II)][O_2] \quad \text{..... (3.12)}$$

Upon division by R_{III} we have

$$\frac{d[Fe(III)]}{dt} = \frac{k_3[Fe(II)][O_2]}{R_{III}} \quad \text{..... (3.13)}$$

Where

k_3 - is the first order rate constant of $Fe(III)$ (ferric)

$[Fe(III)]$ - is the concentration of $Fe(III)$ (ferric)

$[Fe(II)]$ - is the concentration of $Fe(II)$ (ferrous)

$[O_2]$ - is the concentration of O_2 (oxygen)

The above equation is a coupled differential equation that describe the kinetics of iron III. The first order rate constant, K_3 Fe (III) is estimated using equation (3.14). Equation (3.10) and equation (3.13) represent the relationship of the kinetics of oxygenation of ferrous iron and ferric ions respectively.

Table 3.10 Design matrix and experimental results for the iron oxidation first order rate constants, k (min^{-1}) after Stumm and Lee (1961)

Expt. No.	Composition of synthetic water	Factors				Reaction rate (k) constants (min^{-1})	r^2
		pH Unit (A)	DOM CONC. (B)	PO_4^{3-} Conc. (C)	Chlorine Conc. (D)		
1.	Fe (II) + O_2	6.5	0 mg/L	0 mg/L	0 mg/L	0.0085	0.99
2.	Fe (II) + O_2	8.5	0 mg/L	0 mg/L	0 mg/L	0.0337	0.99
3.	Fe (II) + O_2 + DOM	6.5	2.85 mg/L	0 mg/L	0 mg/L	0.0097	0.99
4.	Fe (II) + O_2 + DOM	8.5	2.85 mg/L	0 mg/L	0 mg/L	0.016	0.98
5.	Fe (II) + O_2 + PO_4^{3-}	6.5	0 mg/L	1.5 mg/L	0 mg/L	0.0046	0.98
6.	Fe (II) + O_2 + PO_4^{3-}	8.5	0 mg/L	1.5 mg/L	0 mg/L	0.0018	0.97
7.	Fe(II) + O_2 + DOM + PO_4^{3-}	6.5	2.85 mg/L	1.5 mg/L	0 mg/L	0.0056	0.98
8.	Fe(II) + O_2 + DOM + PO_4^{3-}	8.5	2.85 mg/L	1.5 mg/L	0 mg/L	0.014	0.97
9.	Fe(II) + O_2 + CI_2	6.5	0 mg/L	0 mg/L	2.2 mg/L	0.0087	0.98
10.	Fe(II) + O_2 + CI_2	8.5	0 mg/L	0 mg/L	2.2 mg/L	0.0329	0.94
11.	Fe(II) + O_2 + DOM + CI_2	6.5	2.85 mg/L	0 mg/L	2.2 mg/L	0.0102	0.98
12.	Fe(II) + O_2 + DOM + CI_2	8.5	2.85 mg/L	0 mg/L	2.2 mg/L	0.0298	0.97
13.	Fe(II) + O_2 + PO_4^{3-} + CI_2	6.5	0 mg/L	1.5 mg/L	2.2 mg/L	0.0048	0.94
14.	Fe(II) + O_2 + PO_4^{3-} + CI_2	8.5	0 mg/L	1.5 mg/L	2.2 mg/L	0.0203	0.99
15.	Fe(II) + O_2 + DOM + PO_4^{3-} + CI_2	6.5	2.85 mg/L	1.5 mg/L	2.2 mg/L	0.0085	0.97
16.	Fe(II) + O_2 + DOM + PO_4^{3-} + CI_2	8.5	2.85 mg/L	1.5 mg/L	2.2 mg/L	0.0148	0.95

3.9.3 The Estimation of Rate Constants K_2 and K_3

The aeration filtration unit designed in section 3.6.2 to 3.6.5 was used in the test for determination of the rate constant. Geologic sample from Makindu was put in the filter and

compacted. Groundwater samples from the 8 boreholes tabulated in Table 3.10 were passed through the filter at a rate of 30 l/day. After a sample was run through the filter, deionized water was passed through the filtration unit to avoid contamination.

The filtrate was collected from the outlet of the filter set up every 6 hours for 42 hours. The concentration of ferrous iron (II) and ferric Iron (III) were determined using the procedure outlined in sections 3.7.1 and 3.7.2 respectively. The first order reaction rate for ferrous K_2, is a function of pH and was calculated using equation (3.11) while the first order reaction rate constant for ferric, K_3, was calculated using these concentrations as input to equation (3.14) and depends on the concentrations of dissolved oxygen, ferrous ions and ferric ions.

According Stumm and Lee (1961) the rate constant, K_3, Fe (III) is estimated using equation (3.14)

$$k_3 = \frac{\left[\frac{2.303}{(a-2b)}\right]\log\left[\frac{2b(a-x)}{\{a(2b-x)\}}\right]}{t} \qquad \text{..……..…….. (3.14)}$$

where:

a = the initial concentration of ferrous iron, Fe (II), in $\mathrm{mg/L}$,

b = the initial concentration of oxygen (O_2) in $\mathrm{mg/L}$,

t = the time in days,

x = the concentration of iron (III) (ferric) in $\mathrm{mg/L}$ in time t.

3.9.4 Compiling and Testing of the Sub-Routine

The new user defined reaction module was incorporated into the GMS through a dynamic link library (DLL) file. The reaction expressions were coded inside a FORTRAN file, which was compiled into a DLL. The DLL file was used to exchange the user defined reaction expressions and parameter values between GMS and the user defined reaction module.

To compile the code that had been written the following steps were undertaken:

1) The Microsoft Developer Studio software (which had FORTRAN code editor and compiler) was launched.

2) A new project workspace was created specifically for dynamic Link Library (DLL). It was saved as rxns_1.
3) The user defined FORTRAN code subroutine that had a name rxns_1.f was copied into the project folder C:\MSDEV\Project\rxns_1. The FORTRAN file was then imported into the project using the File ⟶ Insert facility of the Microsoft Developer Studio software.
4) The file was opened in the project workspace that showed the code source which could now be compiled.
5) Compiling involved the compile option under the build facility of the Microsoft Developer Studio. The output of the compiling process was a dynamic link library (rxns1.DLL) file that was placed under the folder C:\MSDEV\Projects\rxns_1\Debug.

3.9.5 Verification of the User-Defined Reaction Package

The user defined reaction package was tested to gauge its response in a batch mode using the BATCHRXN utility in the GMS model. Whenever BATCHRXN was run, it searched for RXNS.DLL file in the same directory. Therefore, the rxns_1.DLL was renamed into rxns.dll and copied in the same folder as batchrxn.exe provided by GMS located at C:\Program Files\GMS 10.4 64-bit\models\rt3d.

After copying the rxns.dll file in the given GMS directory, a CMD window was opened and batchrxn.exe was run from the same directory. The utility queries for the following data:

i) The number of species under test, which were two, Fe (II) and Fe (III).
ii) The total number of time steps to run the test, which were seven (42/6).
iii) The time interval between the steps in days, which was 0.25 days representing six hours.
iv) Initial concentration of the species corresponding to each test run.
v) The rate reaction parameter for Fe (III) corresponding to each test run.

After providing all the data the batchrxn.exe runs and outputs the simulated change in concentrations of the species in the define time interval. The output file was named as BATCHRXN.out which was a white spaced separated ASCII data in column format (written using the format statement 21E15.5). For this test three columns are output, time, Specie-1(Fe (II)) and Specie-2(Fe (III)).

Excel software was used to plot the output data for verification of the user defined reaction expressions and parameters with the aerated water samples. The batch reactor was a test rig that generated the field conditions and provided data that was compared to the theoretical data. The oxygenation test was carried out using the non- motorized filtration system. This experimental system gave results of the concentration of ferrous iron (Fe II) and Ferric (Fe III) iron after every 6 hours.

The experiment was carried out for a total of 42 hours and a total of seven samples were collected. The groundwater samples that were introduced into the filtration rig were of known oxygen concentration and this was maintained throughout the experiment. To achieve greater accuracy the experiment was repeated three times. The test results were compared to the results generated by the model.

3.9.6 Calibration of the Proposed Equations/Models

To calibrate the ferrous and ferric models that were proposed to estimate the chemical reactions in the stratum groundwater samples from six (6) boreholes with different flouride and oxygen levels from the adjoining areas to Chyulu/Makindu aquifer at Makindu were passed through the non-motorized filtration unit for 42 hours. A sample was collected from the filter every six (6) hours and tested for both ferrous and ferric ion concentrations. The concentrations so obtained were compared with results generated by the model and run through GMS software.

The steps followed in the calibration were:

1) Input of data - Initial concentration of both ferrous ferric as well as K_3.

2) Parameter variation – Introduction of fluoride and dissolved oxygen in the sub-routine
3) Simulation of concentrations – Running the Batch reactor/microcosm sub-routine (Appendix XII)
4) Comparison of experimental/observed (batch reactor results) and calculated data which is the sub-routine output - Graphs of experimental/observed concentration vs calculated concentration with fluoride and without fluoride.
5) Check of level of confidence.

Table 3.11 The boreholes used in calibration of the sub-routine

S/No	Identification of borehole	x	y	Concentration of fluoride (F)	Concentration of dissolved oxygen (O_2)
1	Musimba 1(MK11)	374289	9741666	2.0	2.0
2	Musimba 3 (MK13	374289	9743415	2.0	0.9
3	Makilya (MK16)	366612	9751194	2.5	2.1
4	Ndivo & Co. (MK20)	366565	9747602	3.5	1.8
5	Kyeni (MK22)	366637	9748604	3.0	1.0
6	Mulili (MK25)	369285	9752125	4.6	1.5

Table 3.11 shows the boreholes from where samples were collected for the concentration of fluoride and the corresponding dissolved oxygen. Samples from these boreholes were passed through the non - motorized aeration and filtration unit and the results of this testing exercise were used in the calibration exercise. The results of the calibration are shown in chapter 4.

3.9.7 Relationship Between Experimental And Simulated Values Of Concentration; Validation

The code that was used in the validation of the proposed sub-routine was the same as the one in Appendix XII but the parameters were declared spatially variable as seen in Appendix XIV. The main difference is highlighted in blocks 4 and block 5 of the code.

- Block 4 the reaction parameter initialization block has no parameters because there are no spatially constant variables.

- Block 5 is used to both transfer variables into meaningful names for clarity purposes and providing values for the spatially variable user defined reaction parameters.

The ability of the proposed sub-routine, to be used as a tool for estimating the concentration of ferrous ions or ferric ions in the Chyulu aquifer was determined by the relationship between the simulated concentration of ferrous and ferric ions and the results of testing for the ions from the samples collected from the boreholes.

This relationship was determined as the coefficient of correlation also referred to as coefficient of determination and depicted as R^2. If the value of R^2 is greater or equal to 0.5 ($R^2 \geq 0.5$) then the proposed equation or relationship is considered to be good. If the value of R^2 is greater or equal to 0.7($R^2 \geq 0.7$) then proposed equation or relationship is considered to be very good (Anatolyev, 2020).

The concentration of ferrous and ferric ions iron in the aquifer was tested every six months from January 2016 to December 2019. Samples were collected from Jamia Mosque A (MK1) borehole, Sikh temple B (MK4) borehole, Makindu Hospital (MK5) borehole, Railway (MK6) borehole and Makindu Mission 1(MK8) borehole which were 10m (taken as starting point), 250m, 350m, 700m and 1050m respectively from the Nairobi-Mombasa Highway. The Highway is adjacent to the most southerly of the boreholes selected for the detailed study; the Jamia Mosque A (MK1).

3.9.8 The Application of the User Defined RT3D Sub-Routine (Scenario Analysis)

The proposed code (Appendix XIV) was used to estimate the time it would take for iron ions to flow from one borehole to the adjacent one. This was useful information in selecting positions where to place boreholes in the study area. This simulation was achieved when GMS software was launched followed by the execution of the user defined reaction package in the rxns.dll file by rt3dv25.exe (RT3D) module. In this way, the reaction equations were transferred from the user defined package to the GMS software for simulation.

Then the simulation was run using the data from the five (5) boreholes that were approximately in line, that is, MK1, MK4, MK5, MK6 and MK8. The corresponding data for each of the boreholes was entered in the GMS software and results produced when the GMS was run. The data that was required to run the simulation were rate of flow, concentration of fluoride, initial ferrous concentration, initial ferric concentration, among other data. However, the rest of the aquifer was assumed to have the same concentration of the parameters under consideration which was also specified.

The output was concentration of ferrous (iron II) and concentration of ferric ions (iron III) for the specified time (every 3 months or 91.25 days). The results were obtained for four (4) years that is 1460 days.

CHAPTER 4: RESULTS AND DISCUSSION

The results of this study are presented under sub-topics that follow the specific objectives. The results so presented are then followed by a discussion.

4.1 GENERATION OF GROUNDWATER POTENTIAL MAP AND WATER QUALITY INDEX (WQI) MAP

The generation of these maps of the study area involve generation of maps of the parameters that are then overlain to produce the groundwater potential maps as per methodology in section 3.3 for groundwater potential and section 3.4 for the water quality index (WQI). The results for land cover, physiography, soil texture, lineament and drainage are hereunder.

4.1.1 Generation of Land Cover Shapefile

Overall, the land use land cover classification of the study area in the 9 classes were done with high accuracy (Table 4.1). The overall land cover classification was found to be 99.05 with a Kappa coefficient of 0.99 as seen in Table 4.1. These suggest that the classified land cover mimics the reality on the grand and is representative.

Table 4.1 Image classification assessment

	Water	**Savanna**	**Forest**	**Grassland**	**Wetland**	**Cropland**	**Shrubland**	**Built up**	**Barren**
Water	1003	0	0	0	0	0	0	0	0
Savanna	0	1004	0	0	0	0	0	0	0
Forest	0	0	1199	0	0	0	26	0	0
Grassland	0	0	0	1003	0	0	0	0	0
Wetland	0	0	0	0	1001	0	0	0	0
Cropland	0	0	0	0	0	1085	25	0	0
Shrubland	1	0	27	2	2	10	1767	1	0
Built up	0	0	0	0	0	0	3	1005	0
Barren	0	0	0	0	0	0	0	0	1002
Overall accuracy = 99.04583907						**Kappa coefficient = 0.989198037**			

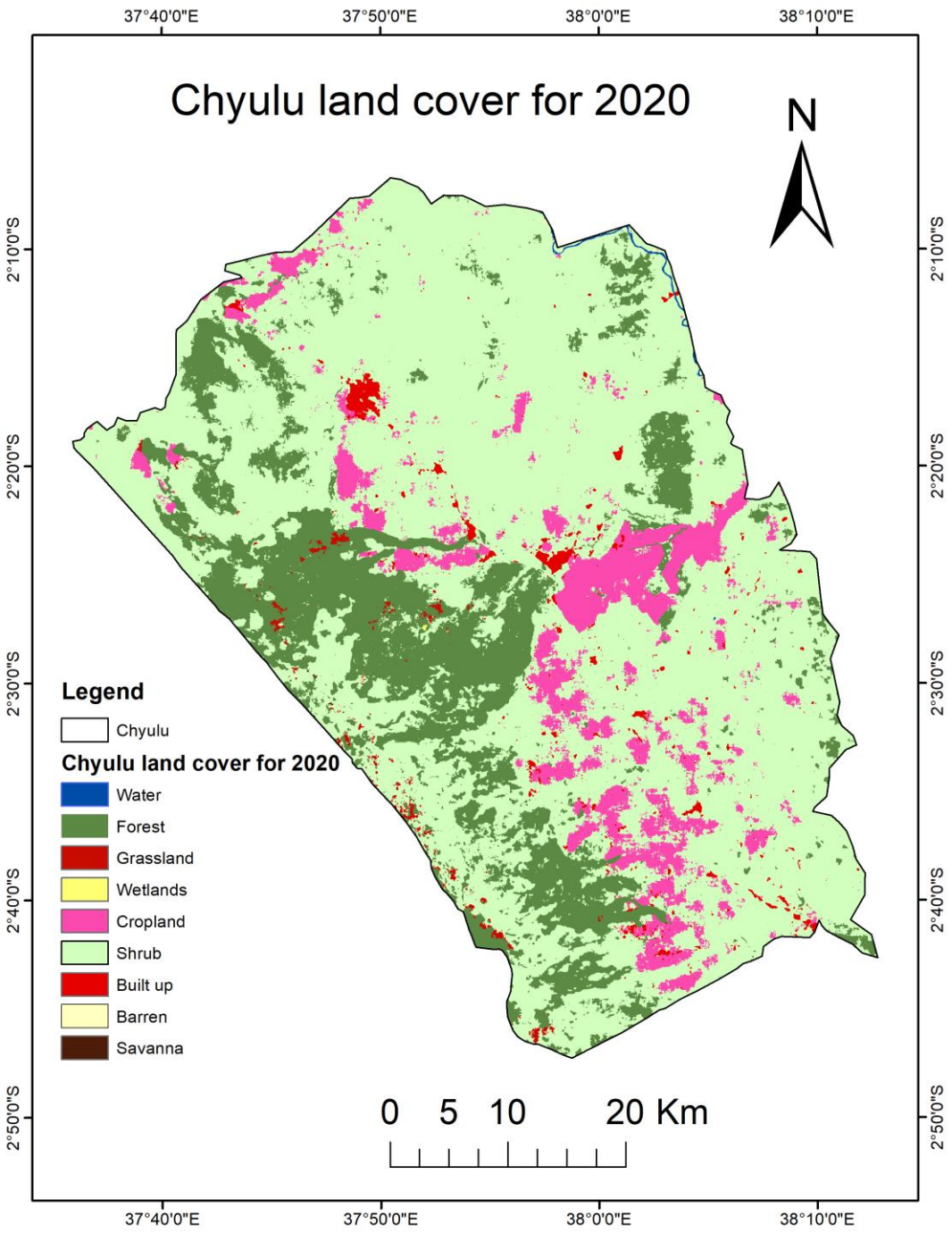

Figure 4.1 Chyulu land cover for 2020

Figure 4.1 shows the land cover map of the study area generated as per procedure indicated in section 3.3.7.

4.1.2 Physiography

Slope is a major factor in hydrogeology in that it defines the drainage characteristics of a water catchment. STRM data of the area was used to derive the DEM and then using 3D analyst tool

the slope of the area was derived. The ratings specified in Table 4.1 were used to make the suitability map. The Northern side of Chyulu is gently sloping but as one moves southwards, the angle of slope increases. This is as a result of residual hills on the Southern and southwestern parts of the map. The hills are oriented in an almost East-West direction conforming to the strike direction. The highest point lies at an altitude of 2138 m. while the lowest at a height of 259 m above sea level. Greater rates of infiltration are common in areas of gentler slopes than those with steep slopes. Physiography (ground elevation) is significant due to piezometric head of boreholes if drilled. The areas having elevation values ranging between 259–747 m are gently sloping while elevations ranging between 1592-2138 m represent areas with very steep slopes. Figure 4.5 shows the topographical map while Figure 4.6 represents the slope map of the study area.

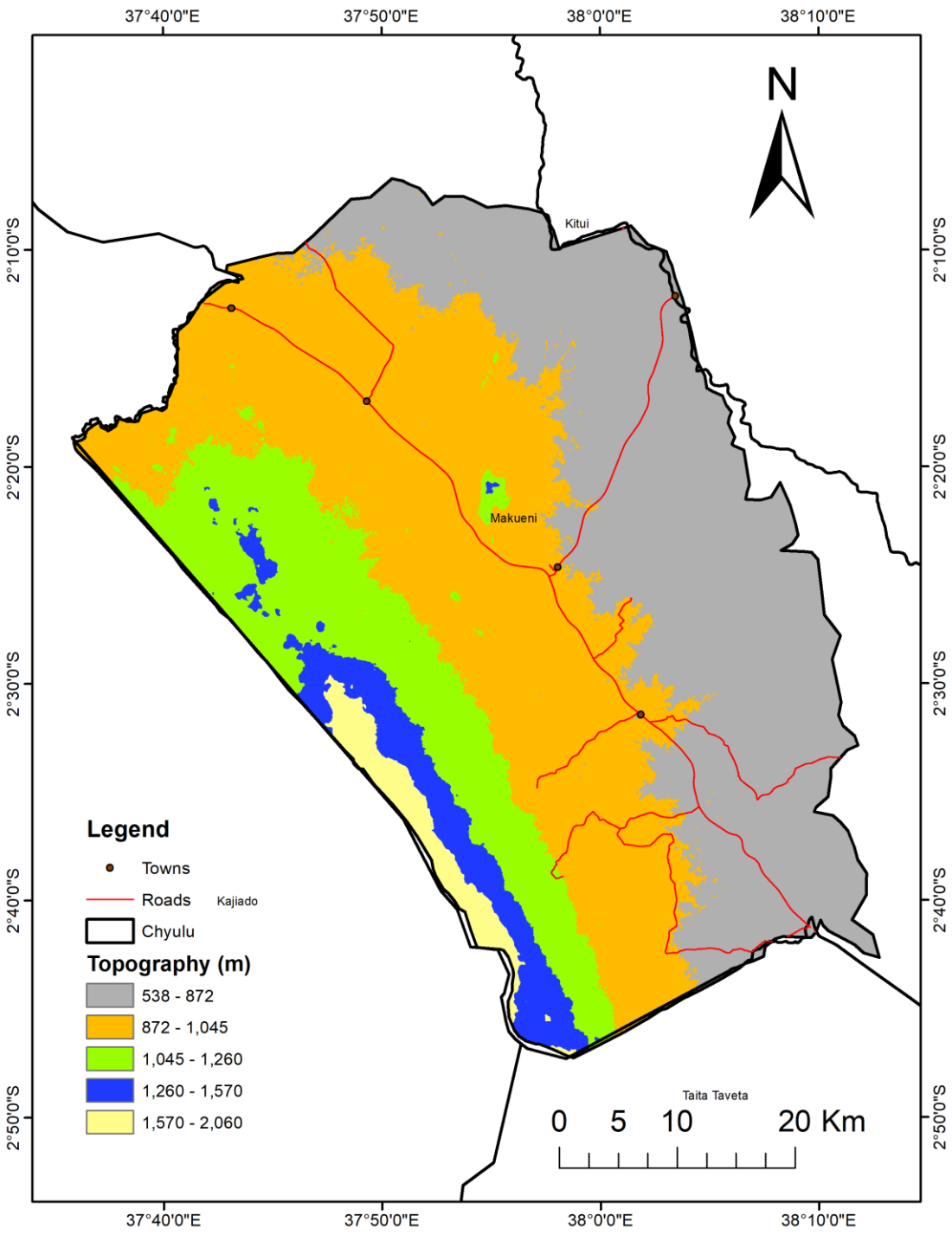

Figure 4.2 Topography map of study area

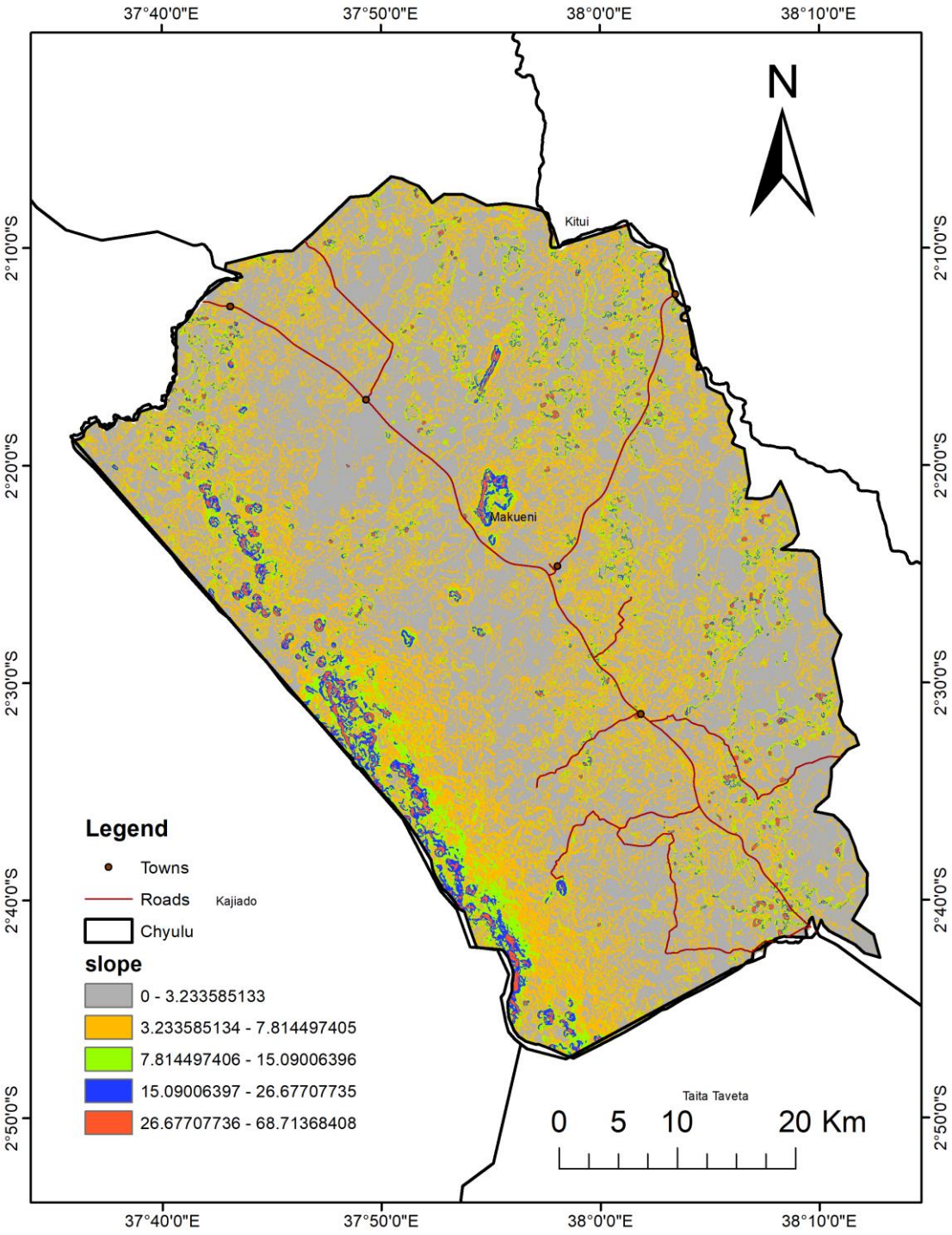

Figure 4.3 Slope map of study area

4.1.3 Soil Texture

This represents the top soil layer extending only a few meters from the surface. It is generally a weathered zone and has a significant impact in the movement of recharge water, which infiltrates deeper into the aquifer (Gupta, 2014). On a scale of 1 to 5 the soils in Chyulu were

classified as clay with a rating of 1 and clayey sand rated 5 in light of infiltration capacity. The DRASTIC weight of soil texture was 6 as shown in Table 3.5.

4.1.4 Lineament and Drainage

As indicated in section 3.1.4 lineament and drainage are key features in groundwater recharge. In this study lineament density map has provided information on sites that have faults, fractures and cracks. These features indicate presence of groundwater because it is through them that groundwater recharge can take place (Koch and Mather, 1997). Lineament was given the highest weighting at 23 in the development of groundwater potential map. Figure 4.7 shows the lineament density map of the study area.

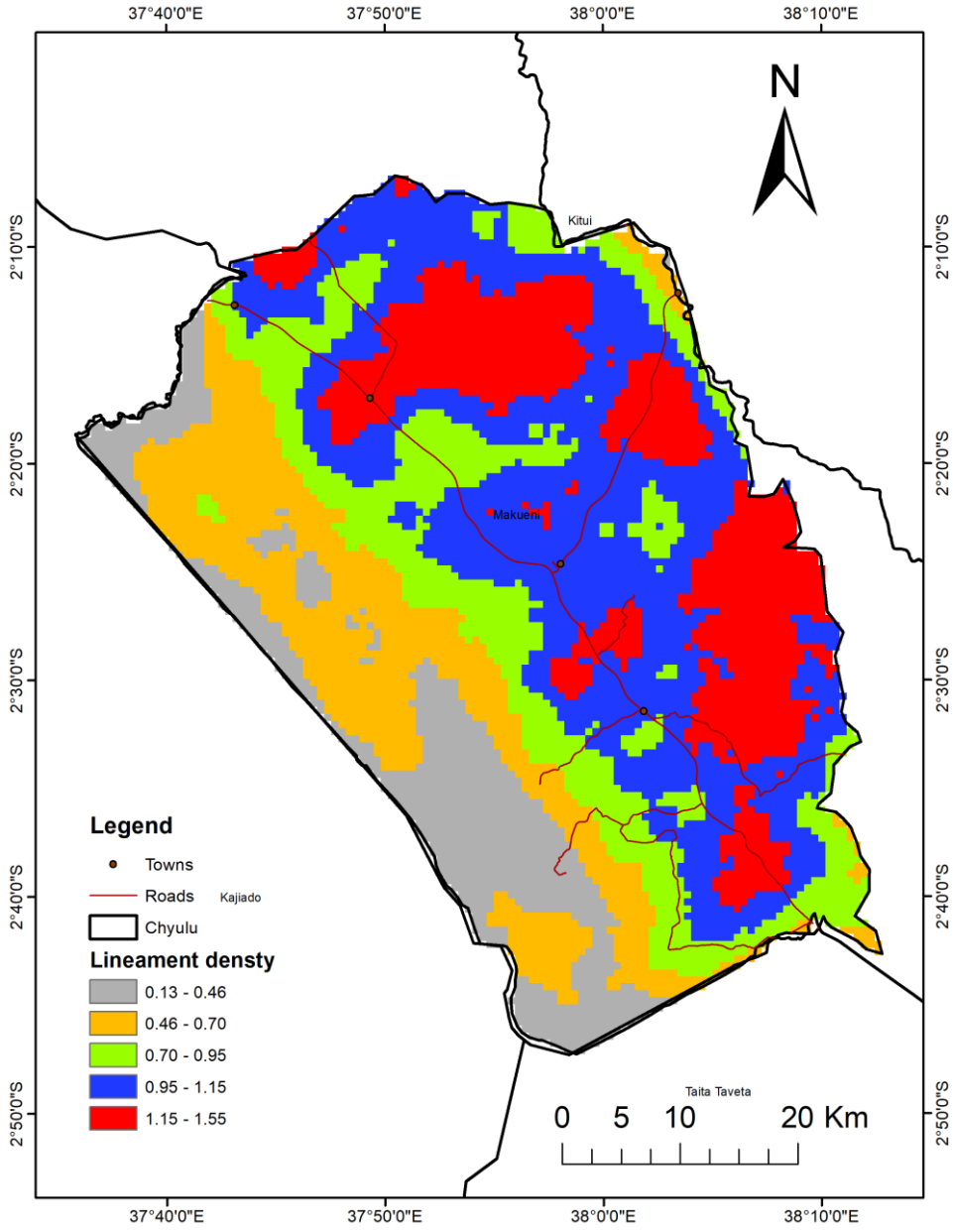

Figure 4.4 Lineament density map

4.1.5 Groundwater Potential Map

The integration of thematic maps resulted in the production of groundwater potential map of the study area as shown in Figure 4.8. As shown in the map the area with high groundwater potential constituted about 36.95 % of the study area while 54.78 % of study area fell in the moderate groundwater potential area. 8.27 % was found to be in low groundwater potential. Towns near rivers both all season and seasonal have relatively high yielding boreholes.

Boreholes that had moderate to high yield of between 6.1 m^3/hr and 12 m^3/hr were located in areas with moderate to high potential as can be seen in Figure 4.5. For example, Makindu, Kibwezi and Mtito Andei have moderate to high yielding boreholes in their vicinity and are in high yielding localities in the groundwater potential map. Although the aquifer is the same the rocks in the aquifer may not be the same in every location in the same aquifer. The water strike level (WSL) will vary from location to location in the same aquifer because the ground level may vary from point to point because of the respective heights above sea level.

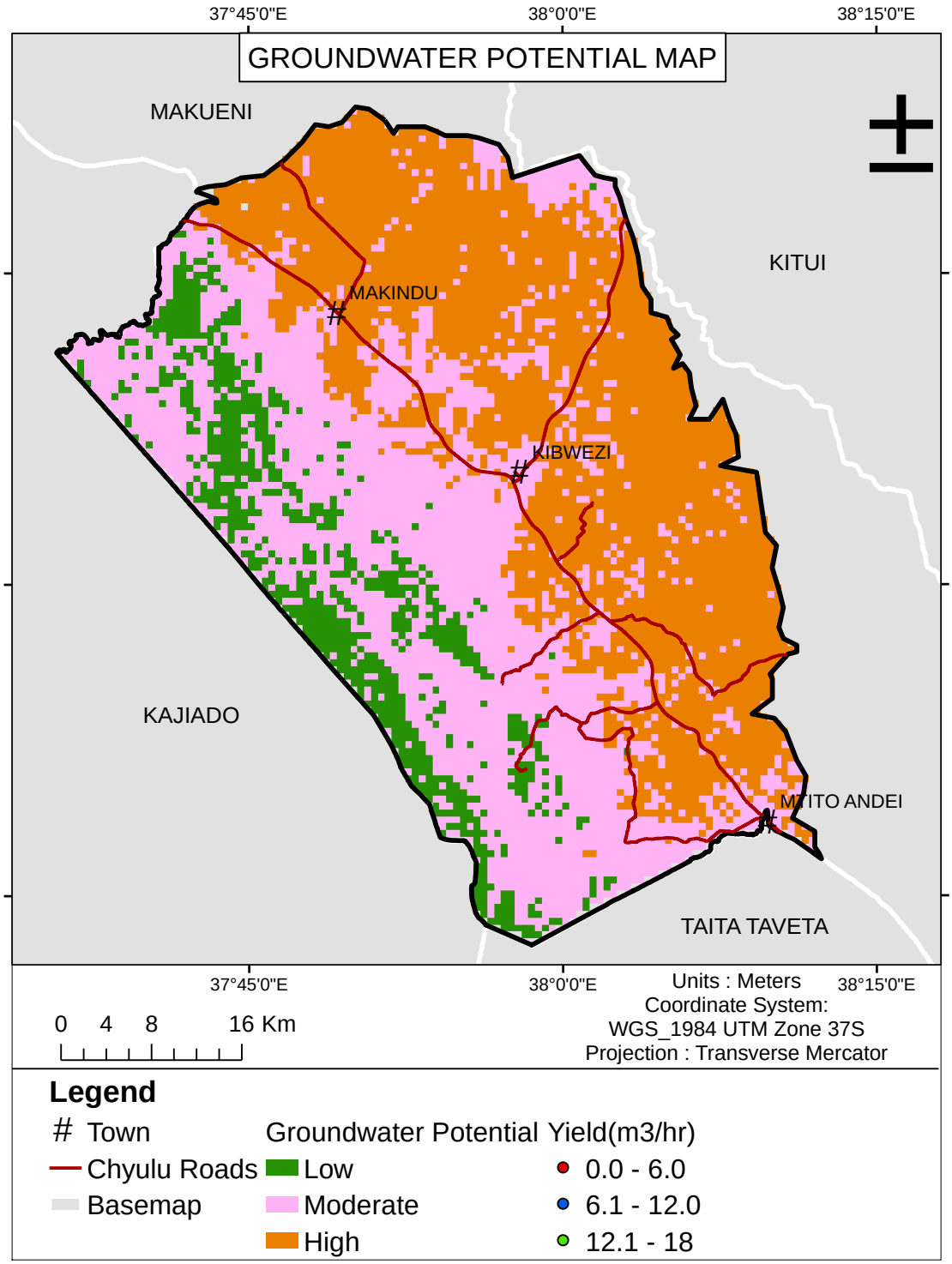

Figure 4.5 Groundwater potential map of the study area

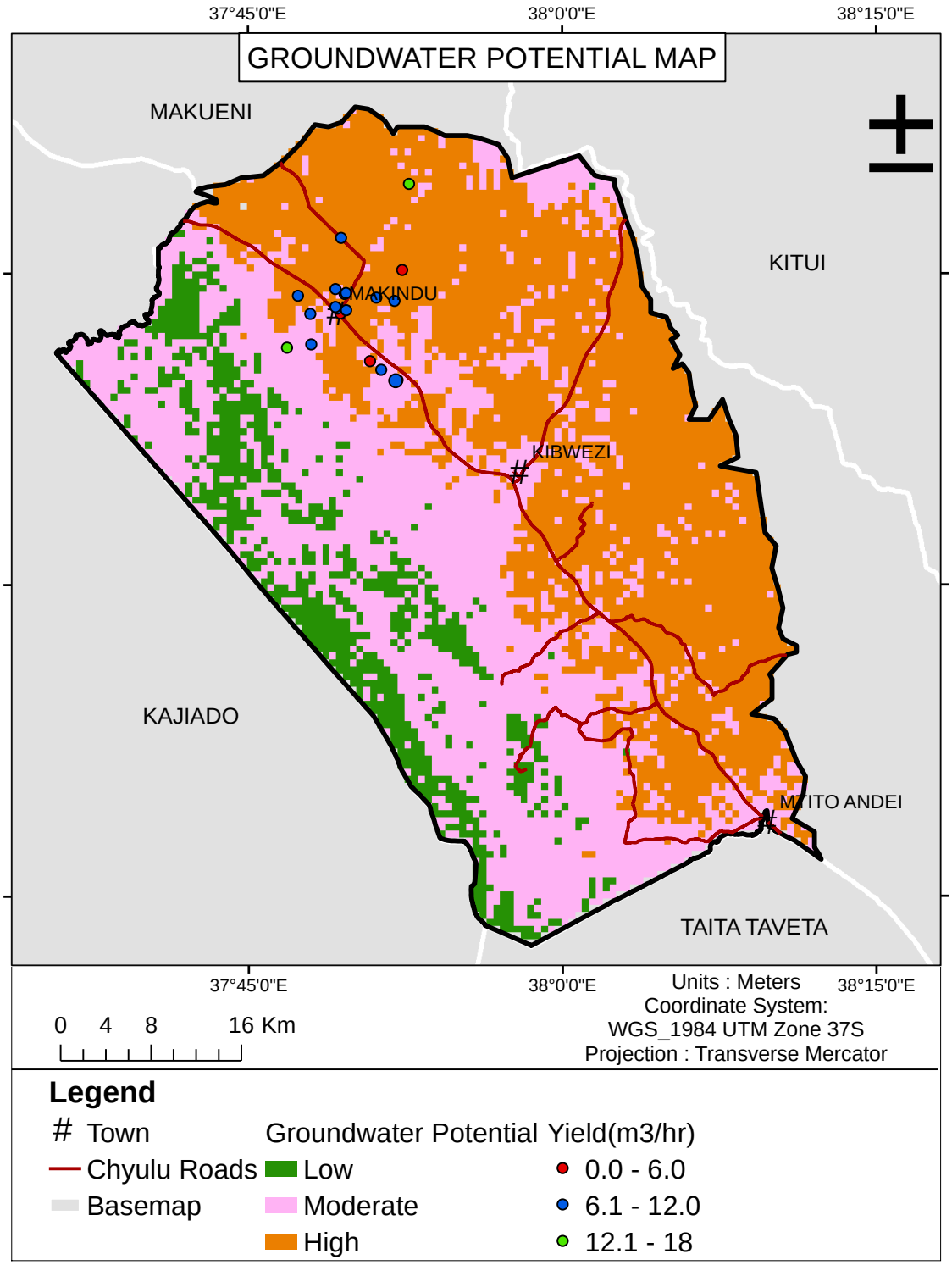

Figure 4.6 The groundwater potential map of the study area with existing boreholes

4.1.6 Results Validation/ Ground Truthing

The incorporation of boreholes into the groundwater potential map, as shown in Figure 4.9, was used in assessing the accuracy of the map. The area on the Kajiado border is characterized by green colour representing areas with low groundwater potential. This area is actually the Chyulu Hills which is effectively an area not good for placing of boreholes. In order to validate the classification of the study area into different groundwater potential zones (high, moderate and low) borehole yield data from Ministry of Water, Water Resources Authority (WRA) and Ministry of Water at County level in Wote were collected and evaluated. The data revealed that boreholes from the study area can be categorized into high yield (> 12.1 m^3/hr) moderate (6.1 – 12.0 m^3/hr) and low yield < 6.0 m^3/hr. The yield of the boreholes range between 1.42 – 16 m^3/hr. The depth on the other hand range from 22 m to 224 m (Appendix II). The yield varies in the same aquifer because the rainfall, topography, drainage, soils, land cover among other factors vary from location to the other.

4.1.7 Groundwater Discharge and Groundwater Flow System

Generally, mechanism of groundwater discharge in an aquifer system is discharge to streams and well abstractions. The groundwater discharge from this aquifer is expressed in form of borehole abstractions in different parts of the watershed. The only springs worthy noting are gravity springs found where the volcanic system joins the basement system of rocks. Water from these springs contributes to the groundwater recharge is also piped into Makindu and Kibwezi towns.

According to Kahsay (2008) and Gebregziabher (2003), a groundwater flow system is a set of flow paths with common recharge and discharge areas. This knowledge on conceptualization of how and where water originates from or leaves in the groundwater flow system is critical to the development of an accurate model. As pointed out by Saggerson (1963) and Kithiia (2009), groundwater flow in Chyulu is mainly controlled by extensive faults and fractures that are

characteristic of the basement system. The local flow system is also controlled by the topography, geology and the degree of fracturing.

To construct groundwater flow direction, hydraulic head information is required. Head measurements are also needed to establish initial conditions for the numerical groundwater modeling and for model calibration. The static water level records from wells in the study area was found to range between 5 and 40 meters.

4.2 GENERATION OF GROUNDWATER QUALITY INDEX (WQI)

The second part of the first specific objective was the generation of the water quality index map. The parameters considered were the water quality test results for key salts in the groundwater samples.

4.2.1 Results of Physical Chemical Tests

The results of physical chemical tests carried on samples of boreholes that were processed in the generation of WQI are shown in Appendix III. The pH value is a measure of ions in the sample and the lowest pH was 6.58 recorded at MK35 while the highest pH was 8.20 recorded at MK33. All water from boreholes in the study area had pH values that fall within the WHO and KEBS permissible range of between 6.5 and 8.5 for drinking water. This range of pH is slightly acidic to moderately high alkaline as reported by the British Geological Survey (BGS) (2000) for groundwater quality in the region. Appendix IV shows the pH and turbidity maps of the study area. Turbidity values varied from a low value of 1 NTU to a high value of 110 NTU recorded from borehole MK6 at Makindu Railway Station. Several other boreholes had values greater than 5 NTU which is the upper limit for domestic water. Boreholes such as MK36 (61 NTU), MK11 (27.3 NTU), MK24 (20 NTU) and MK33 (25 NTU) all show that their water is highly turbid. Thus, some of these boreholes are only used during prolonged drought due to their high turbidity.

High electrical conductivity or total dissolved solids concentrations in water are objectionable and offensive to taste (Onyancha & Getenga, 2013). Total dissolved solids represents inorganic substances: salts and minerals in groundwater, which explains why groundwater in ASALs has been described as saline (Krhoda, 1989; Mailu, 1997; Kithiia, 2009). Values greater than 200 mg/L causes scale deposition in pipes and tanks. The high values of hardness recorded are likely to form scum in the process of cleaning and washing.

Electrical conductivity (EC) was highest in areas around Makindu and was lowest in areas around Kibwezi. Thus, borehole MK1 had an EC value of 16020 µS/cm while the EC value for borehole MK29 was 494 µS/cm. Maps for electrical conductivity and the total dissolved solids of the study area shown in Appendix IV.

Calcium and magnesium compounds in water cause it to be hard. Among other salts, magnesium sulphate (Epson salt), calcium sulphate, magnesium hydrogen carbonate and calcium hydrogen carbonate cause both permanent and temporary hardness in water. Boiling of water removes temporary hardness but permanent hardness cannot be removed by boiling. Equation (4.1) shows the chemical reaction when aqueous calcium hydrogen carbonate is boiled, thereby making water soft.

$$Ca(HCO_3)_{2\,(aq)} = CaCO_{3(s)} + H2O + CO2_{\,(gas)} \quad \ldots\ldots\ldots\ldots\ldots (4.1)$$

Groundwater is generally harder than surface water due to presence of both calcium and sodium carbonate that in the groundwater (Hove, 1973). The total hardness of groundwater for over 60% of the borehole exceeded the allowable 500 mg/ $CaCO_3$/l as shown in Appendix III. Thus, groundwater for most of boreholes in Chyulu is hard as presented in the hardness map of Chyulu in Appendix IV. In this respect, the alkalinity that is a measure of the capacity of the water to neutralize acidity was also high.

The amount of calcium and carbonates ions in solution controls the ability of water to act as a buffer. Localities like Makindu that have limestone are likely to contain high levels of Ca^{++} and CO_3^{2-} ions and consequently elevated hardness as well as high alkalinity. Moreover, highly alkaline ions react with cations in water resulting in a precipitate that corrode pipes and other accessories in water distribution systems.

4.2.2 Results of Iron and Flouride Concentrations in the AQUIFER

Tests of groundwater samples from boreholes from this aquifer reported concentration of iron far greater than the allowable 0.3 mg/L. For example, all boreholes in Table 2.2 had iron concentration ≥ 1.72 mg/L. Higher concentrations of 5.44 mg/L, 5.54 mg/L and 5.88 mg/L for MK16, MK19 and MK43 respectively were reported as can be seen in Appendix III. The turbidity of MK6 borehole increased upon storage in a tank leading to rapid deterioration of the tank. This was attributed to oxidation of ferrous ions (Fe^{2+}) to ferric ions (Fe^{3+}). Similar behaviour was reported in other localities where the groundwater had high iron content. Iron data had not been reported in published water quality investigations and iron was assumed not to represent serious water problems but high concentrations >4 mg/L were causing rusting of steel storage tanks as well as syringes in health facilities in the study area (Mbithi et al., 2017). Excess iron may cause conjunctivitis, choroiditis and retinis if it remained in body tissues for long while chronic inhalation of high concentrations of iron oxide fumes or dusts results in development of benign pneumoconiosis. It also enhances the risk of lung cancer development in workers exposed to pulmonary carcinogens.

The flouride concentration in all the boreholes whose concentration has been reported in Chyulu was found to be higher than the allowable 1.5 mg/L. For example, the average concentration of fluoride from samples from borehole identified as MK10 was found to be 8.2 mg/L. Groundwater from boreholes located near Kibwezi had relatively high values of

fluoride too. The variation of fluoride concentration at different points in the aquifer is dictated by the chemical composition of the rocks in a given location in the aquifer.

A study by Mbithi et al., (2017) in Makindu area reported values > 4.2 mg/L, which has precipitated a crisis in dental health care. According to Gaciri and Davies (1993) fluorine is the most electronegative of all known elements with an electronegativity of 4. It is also the most reactive element and rarely occurs free in nature. It combines chemically to form flourides and occurs as fluoride ion (F-). Flourides ions in drinking water increase skeletal abnormalities and dental fluorosis (Shupel et al., 1979; Chaturvedi et al., 1988; Gaciri and Davies, 1993; Mbithi et al., 2017) conditions that are common in the study area. The prevalence of dental caries and dental fluorosis in the study area have been attributed to the amount of flourides consumed from borehole water. According to Maina (1982), Nanyaro et al., (1984) and Gaciri and Davies (1993) the major source of fluoride and other compounds in groundwater particularly in the volcanic Chyulu hills is traced to volcanic activity, chemical weathering of the volcanic rocks and carbonic rich sedimentary rocks. Figure 4.7 is the generated iron map for the study area.

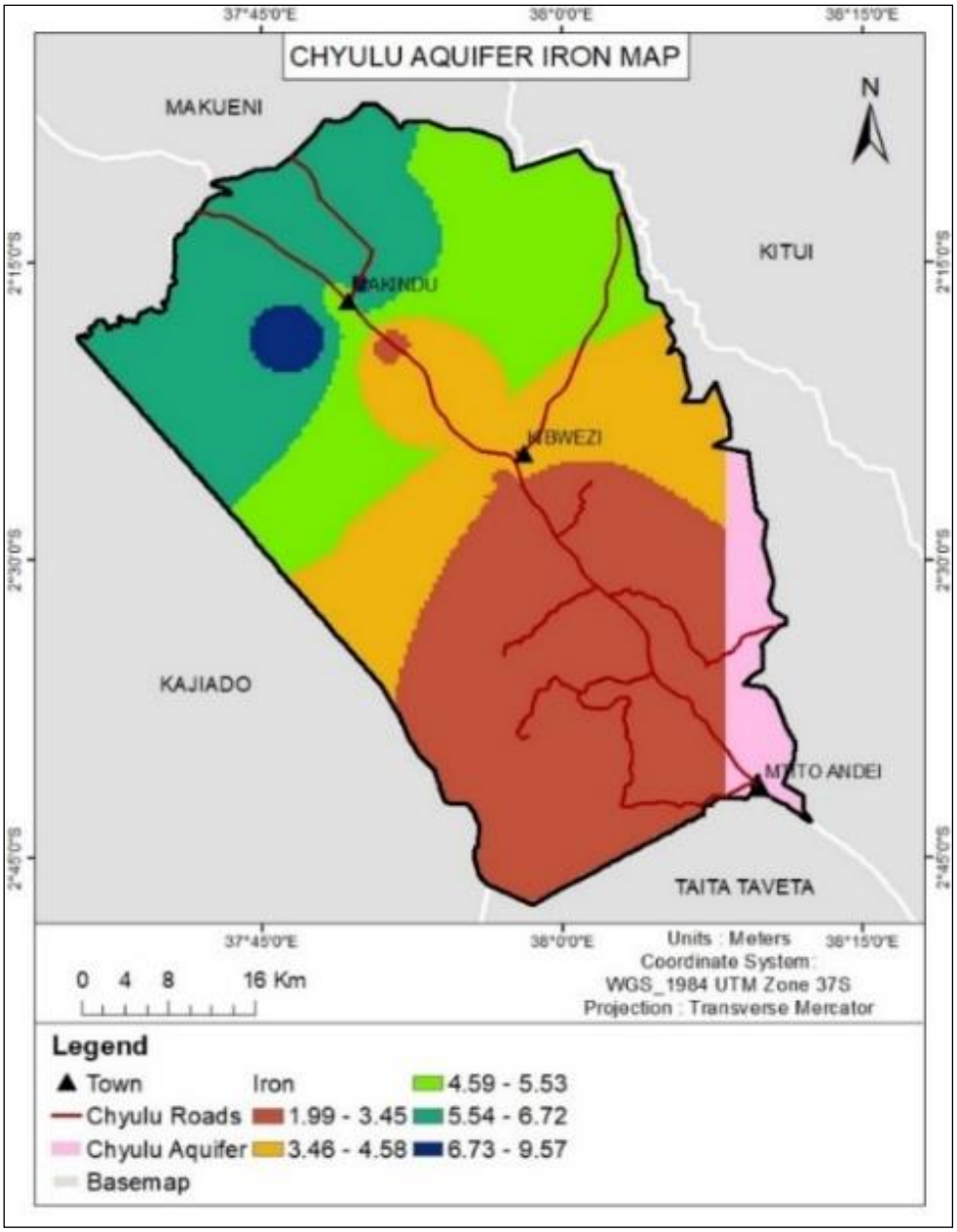

Figure 4.7 The iron map of the study area

The overall water quality of the study is represented by the WQI of the study area is shown in Figure 4.8. The higher the value of WQI the better the water quality. As can be seen from Figure 4.8 only a small section of the study area has good quality. Most of the boreholes in the study are located in areas that have low quality water as can be seen in Figure 4.9. Therefore, groundwater from boreholes in the Chyullu must be treated before it is consumed by humans and animals. Makindu Town, a major settlement on the Nairobi-Mombasa highway has a WQI

that falls in an area that is ‘frequently’ impaired. Makindu has many documented boreholes, which have adequate amount of water, but the quality is wanting. The fluoride concentration in the Makindu Hospital borehole, for instance, is 5.1 mg/L while that of a borehole at the nearby Catholic Mission is 7.3 mg/L. The high level of fluoride concentration in these areas are due to the proximity of the volcanic Chyulu hills that are several kilometres to the South of Makindu Hospital. Other important locations such as Kibwezi and Mtito Andei also show that groundwater in Chyulu is of low quality. For example, at Kambo borehole (MK27) the chloride value is 324.2 mg/L, which is way above the permissible value of 250 mg/L (WHO, 1994).

Groundwater in some areas is fresh depending on the chemical composition of the host rock and the retention time of the water in the aquifer. Spread throughout the study area are seasonal langas that are filled with recent alluvium deposits comprising of sand and soil. These langas are shallow and unconfined and their yields depend on recharge. The water quality in the langas which comprise of alluvium deposits is good where the aquifer lies between lava flow episodes but may be hard where the aquifer is along the contact zone of the basement system or along ancient river valleys which were by carbonaceous rocks (Saggerson, 1963).

As was discussed in section 1.3 methods of water treatment exist but they are relatively expensive and a method that can reduce all parameters to the allowable levels is untenable in ASAL environments. Results of aeration/filtration method of reduction of iron and other parametes are presented in section 4.3.

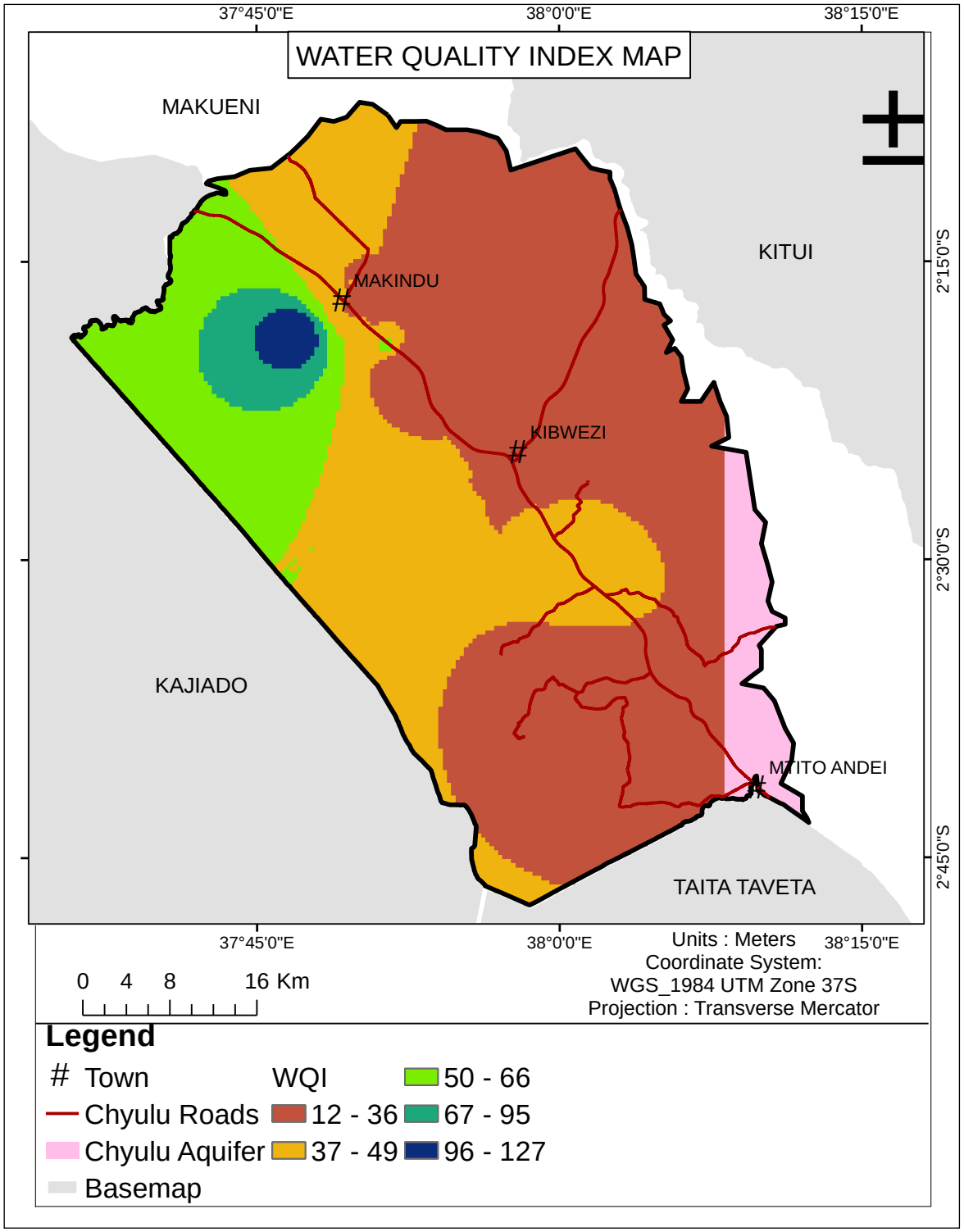

Figure 4.8 The water quality index (WQI) map of the study area

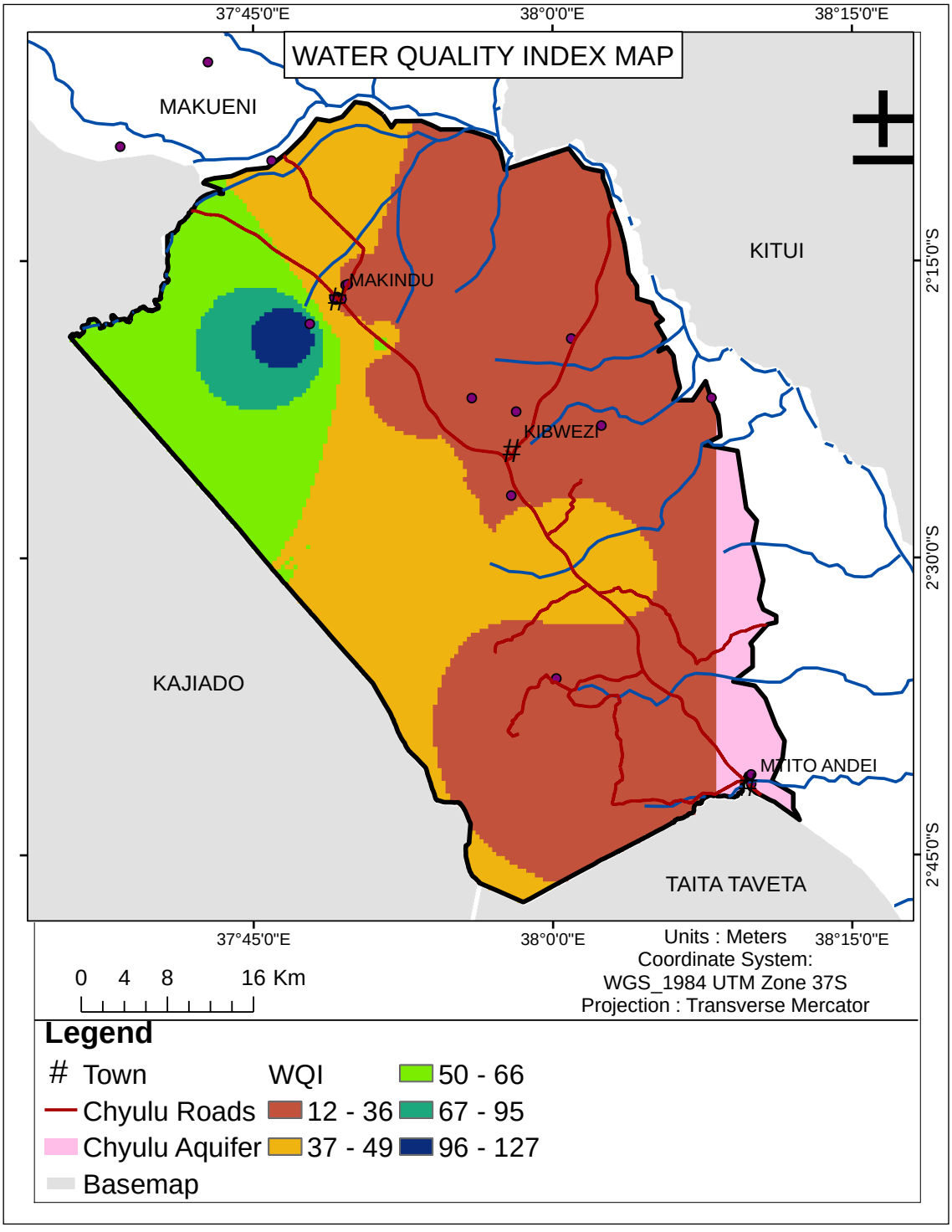

Figure 4.9 The water quality index (WQI) map and boreholes of the study area

4.3 DEVELOPMENT OF PHYSICAL MODEL FOR THE REMOVAL OF IRON THROUGH NATURAL AERATION

4.3.1 Results of Aeration Trials

Tables 4.2 and 4.3 show the results of these aeration trials. The percentage increase of dissolved oxygen when the trays had aggregates was found to be 41.3 % as can be seen in Table 4.2 while the corresponding increase when the trays had no aggregates was found to be 39.8 as shown in Table 4.3.

Table 4.2 Results of test to determine amount of aeration (tray with aggregates)

Position of tray	Temperature ^{o}C	Dissolved Oxygen mg/L	Average	Percentage increase	Overall percentage increase
Tray on Top of stand	20.6	1.25			
	19.8	1.24	1.25		
	20.4	1.26			
Tray 50 cm from top	19.8	1.39			
	19.8	1.41	1.40	12	41.3
	20.0	1.41			
Tray 100 cm from top	19.7	1.62			
	20.6	1.59	1.61	15	
	19.7	1.63			
Tray 150 cm from top	19.4	1.82			
	19.6	1.85	1.84	14.3	
	19.6	1.84			

Table 4.3 Results of test to determine amount of aeration (tray with no aggregates)

Position of tray	Temperature ^{o}C	Dissolved Oxygen mg/L	Average	Percentage increase	Overall Percentage increase
Tray on Top of stand	21.2	1.52			
	21.4	1.50	1.51		
	21.2	1.50			
Tray 50 cm from top	20.6	1.76			
	20.4	1.82	1.79	18.5	39.8
	21.4	1.78			
Tray 100 cm from top	21.4	1.92			
	20.5	1.94	1.94	8.4	
	21.2	1.96			
Tray 150 cm from top	20.8	2.17			
	21.2	2.19	2.19	12.9	
	20.4	2.21			

Tray with aggregates reported slightly higher rate of aeration and use of aggregates was therefore recommended. The aggregate sizes that were used were 25 mm diameter and 37.5 mm that were mixed equally.

4.3.2 Iron Reduction

The feed water flowed through the aeration/filtration setup at a rate of 30 l/day. Nonetheless, the water sample collected after aeration was more turbid than that at the start of the process. This is illustrated in Plate 4.1 where the feed water, beaker 1 was clearer (less turbid) than the water after aeration represented by beaker 2. After filtration the water became clear and the turbidity was 5 NTU or slightly above 5 NTU. After 24 hours, the water became even clearer with turbidity values of less than 5 NTU in all the cases as can be seen in beaker 3.

All the values of the feed water samples in all the runs had Electrical Conductivity (EC) values as well as total dissolved solids (TDS) greater than the allowable; 1000 mg/L for EC and 600 mg/L for TDS. After filtration, the values of EC and TDS reduce drastically. However, the values of EC surpass 1000 mg/L in some cases but, on the whole, the EC reduces to an average of 1145 mg/L for MK6 and 1504 mg/L for MK10.

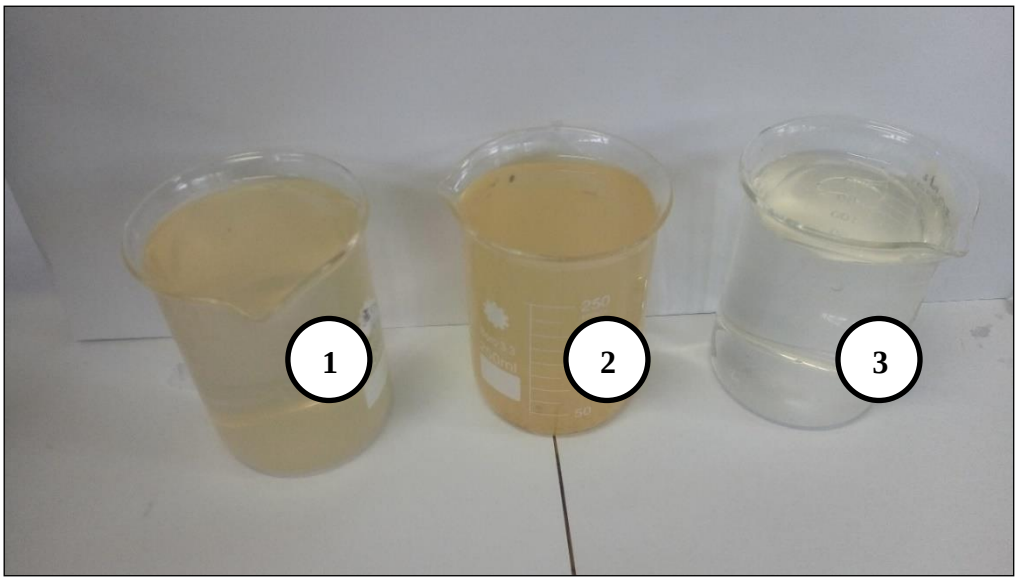

Plate 4.1 Changes in turbidity as the water passes through the different filtration stages

The change in concentration of various parameters after the groundwater samples from boreholes MK6 and MK10 passed through the aeration/filtration set up are shown in Table 4.4 and Table 4.5. Additionally, Appendix V shows the average values of eight (8) runs for various parameters and salts of the feed water and the corresponding values (filtrate) after aeration and filtration process. The standard error (SE) was shown in all the cases.

Table 4.4 Results of the tests of feed water and filtrate for MK6

Parameter	Feed water		Filtrate	
	Average Conc.	Standard error (± SE)	Average Conc.	Standard error (± SE)
pH	7.62	0.26	7.54	0.23
Ec ((μS/cm)	1812.4	182.1	1145.13	368.51
TDS (mg/L)	1194.63	93.8	666	311.9
Turbidity (NTU)	71.05	12.5	5.19	0.79
Colour (TCU)	123	12.5	19	3.17
Total Hardness (mg/L)	792.25	67.89	781.25	69.82
Alkalinity (mg/L)	861.88	52.10	823.50	52.40
Iron (mg/L)	5.9	0.725	2.34	0.48
Manganese (mg/L)	0.75	0.07	0.44	0.10
Magnesium (mg/L)	73.81	2.06	70.30	2.85
Calcium (mg/L)	402.53	18.13	308.97	75.95
Potassium (mg/L)	314.16	11.10	285.47	49.34
Sodium (mg/L)	185.09	15.34	187.06	12.32
Flouride (mg/L)	7.04	1.07	6.04	0.87
Sulphate (mg/L)	177.64	14.02	180.49	15.14
Nitrate (mg/L)	9.65	1.62	8.82	1.23

The aeration /filtration unit was meant to oxidize ferrous ions to ferric ions. Appendixes V show summaries of results of aeration/filtration tests. The results show iron (Fe) concentrations of the feed water (water that is fed into the unit), iron (Fe) concentration after aeration and iron (Fe) concentration after filtration. The percentage decrease in amount of iron (Fe) in the water is greater than 54 % in all the runs with the average being 60.17 %, 59.25 %, 59.83 %, and 62.12 % for MK1, MK2, MK10 and MK27 respectively. A value of 62.12 % reduction in concentration of iron (Fe) is high. However, high percentage (>85%) have been attained but

this could be attributed to the fact that the aeration was not mechanized (Sarikeya, 1990; Ahmed et al., 2002; Nik et al., 2013).

Table 4.5 Water and the filtrate for MK10. Also shown is the standard error (SE)

Parameter	Feed water		Filtrate	
	Average Conc.	Standard error (± SE)	Average Conc.	Standard error (± E)
pH	7.08	0.27	7.22	0.24
Ec ((µS/cm)	3192.75	884.52	1504.5	233.55
TDS (mg/L)	1886.63	507.14	997.75	65.97
Turbidity (NTU)	35	24.03	5	1.25
Colour (TCU)	36.5	7.30	20	3.16
Total Hardness (mg/L)	732.63	50.56	730.63	48.46
Alkalinity (mg/L)	545.38	88.24	517.61	82.83
Iron (mg/L)	5.72	0.52	2.81	0.24
Manganese (mg/L)	0.29	0.541	0.238	0.017
Magnesium (mg/L)	2.50	0.541	2.47	0.502
Calcium (mg/L)	65.63	4.413	60.56	2.69
Potassium (mg/L)	14.18	0.67	14.43	0.68
Sodium (mg/L)	358.18	30.60	335.83	4.69
Flouride (mg/L)	7.35	0.699	6.46	1.06
Sulphate (mg/L)	131.49	30.34	127.93	39.28
Nitrate (mg/L)	12.91	1.96	11.22	2.13

Figure 4.10 and Figure 4.11 show the concentration of iron and its corresponding reduction after the aeration/filtration process over eight runs for the two boreholes MK1 and MK2 at Jamia Mosque compound in Makindu. Graphs for the other boreholes are shown in Appendix VI.

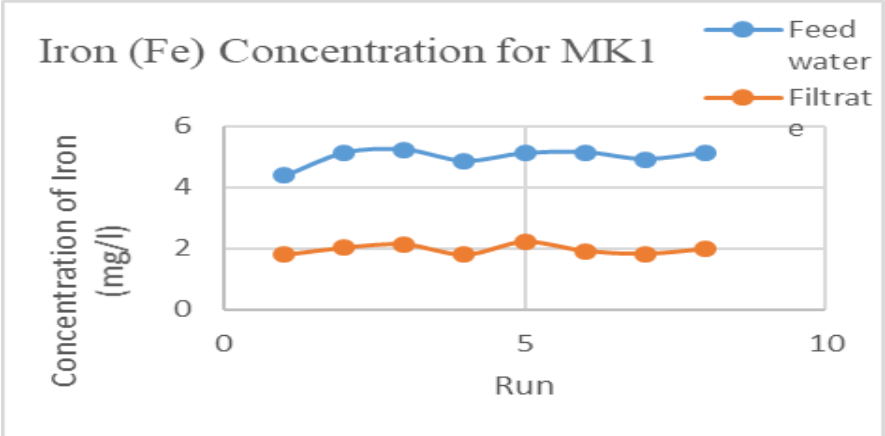

Figure 4.10 Concentration of iron for the eight runs for Jamia Mosque (A) (MK1)

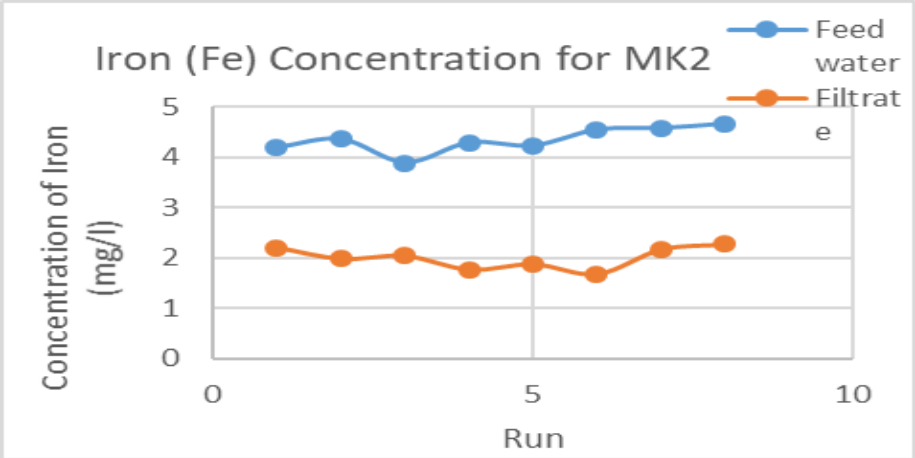

Figure 4.11 Concentration of iron for the eight runs for Jamia Mosque (B) (MK2)

4.4 THE RESULTS OF DEVELOPMENT OF SOLUTE TRANSPORT MODEL FOR PREDICTING DISPERSION OF IRON AND ITS DERIVATIVES IN THE STUDY AQUIFER

The results and discussion presented in this section relate to the third specific objective on the development of a solute transport model that predicts the dispersion of ferrous and ferric ions in the Chyulu aquifer at Makindu. More results towards achievement of this objective are presented in sections 4.4.1 and 4.6.

4.4.1 Results of Georeferencing, Generation of Grid and Calibration of Hydro-Geophysical Model

Figure 4.12 is one of the products of the GMS model and shows the location of seasonal rivers in the Chyulu aquifer at Makindu. The rivers are marked by the pink and green colors. The yellow spots in the figure marks the twenty-five (25) boreholes considered in this study. The yields, depths.

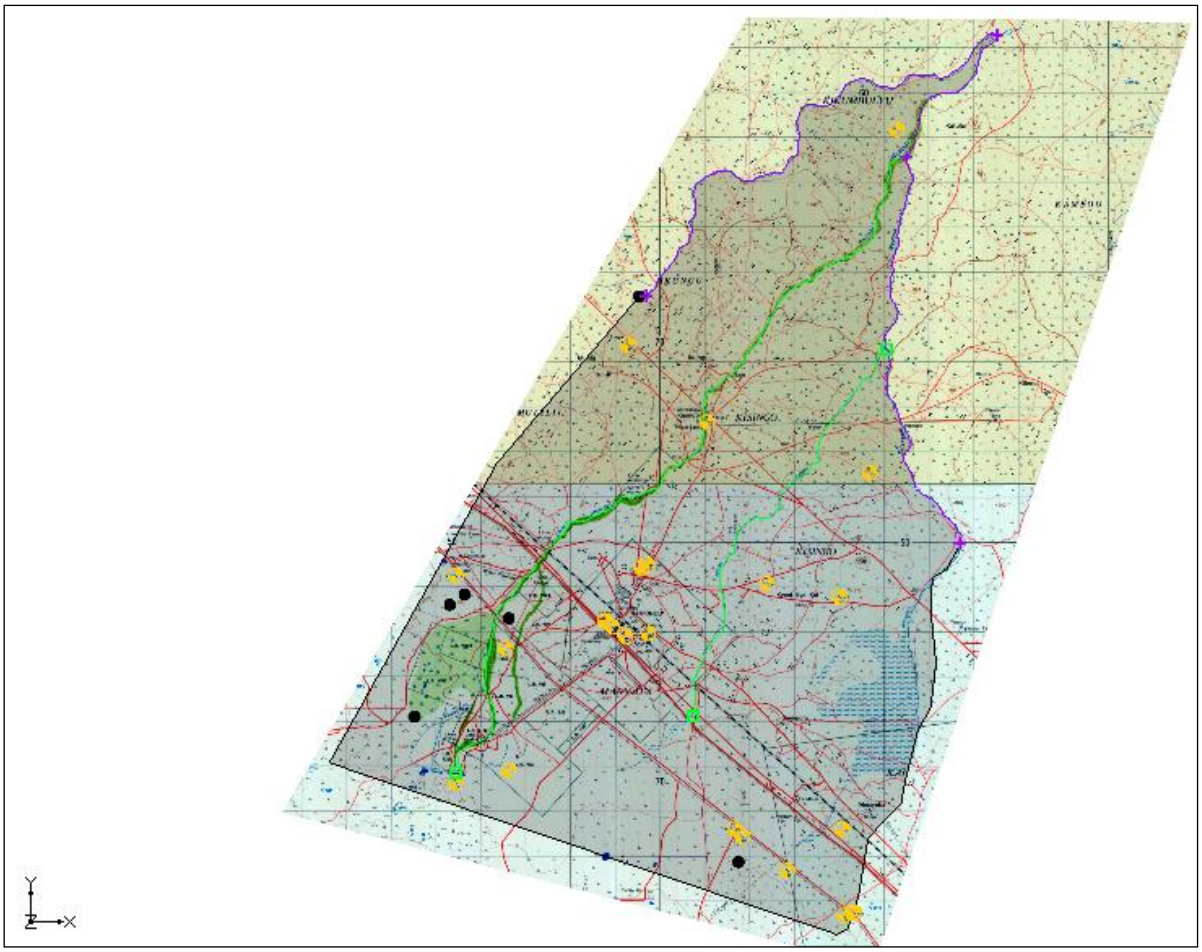

Figure 4.12 Makindu Watershed and the locations of the boreholes used in the solute study

Further results in generation of grids by the GMS model for the Chyulu aquifer at Makindu are presented as Figure 4.13, Figure 4.14 and Figure 4.15. Zooming on the grid in the software resulted in the opening up of grids as the scale increased. After generation of the grid, the mapped area was marked out through generation of a frame by the software to delimit the area. The very prominent dark blocks in Figure 4.13 represent the positions with a high concentration of grids due to overlap caused by the closeness of boreholes in the study area. The grids were 100m × 100 m while the boreholes that were in this 289 km^2 watershed were 25. The names, codes, coordinates, yields, depths and average height above sea level are as shown on Table 3.8. The borehole with the highest yield was Katuluni (MK24) with an average yield of 15.6

m^3/day at a depth of 56m. the lowest yield was from Musimba 3(MK13) with a yield of 5.6 m^3/day at depth of 89m.

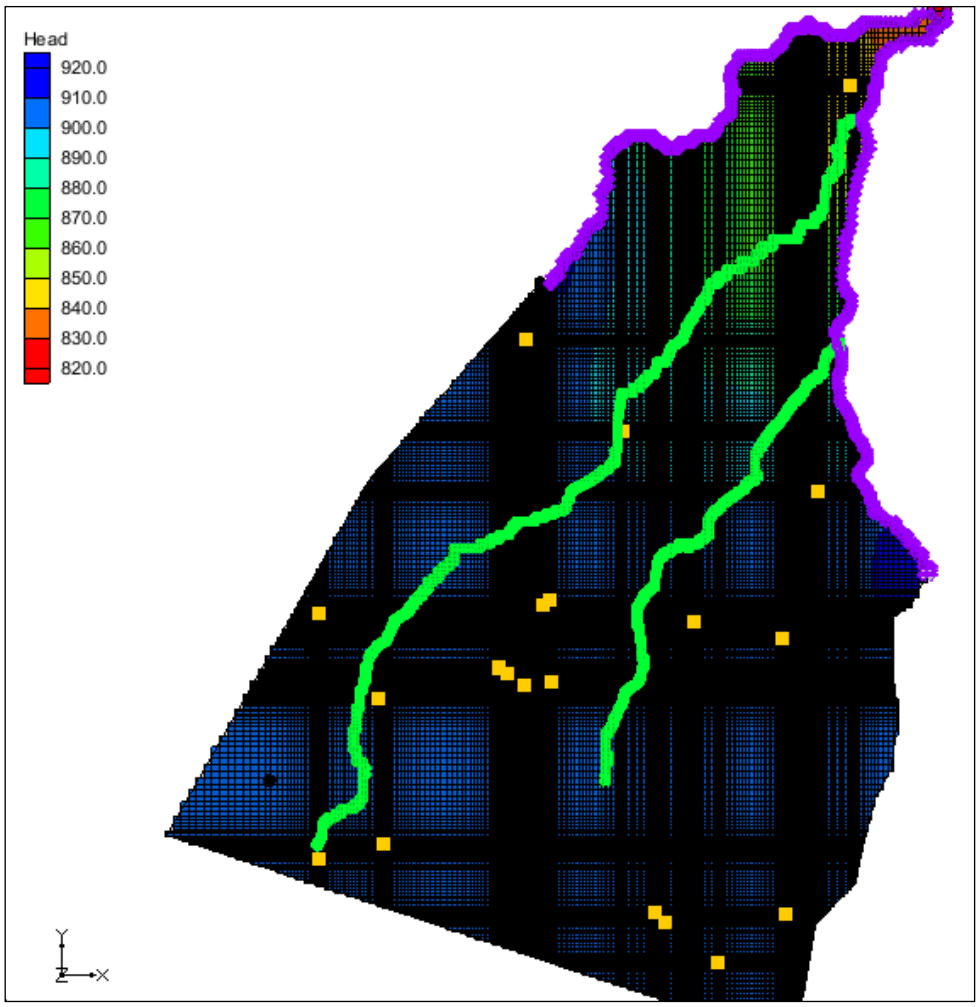

Figure 4.13 Grids of solute flow of the study area

The green marks represent the boreholes drained by the same seasonal Makindu River that were selected for the calibration of the GMS model. These boreholes are shown in Table 3.11. The green bar next to all observation boreholes indicated that the model was successfully calibrated. The results of calibration of the GMS model are shown in Figure 4.15.

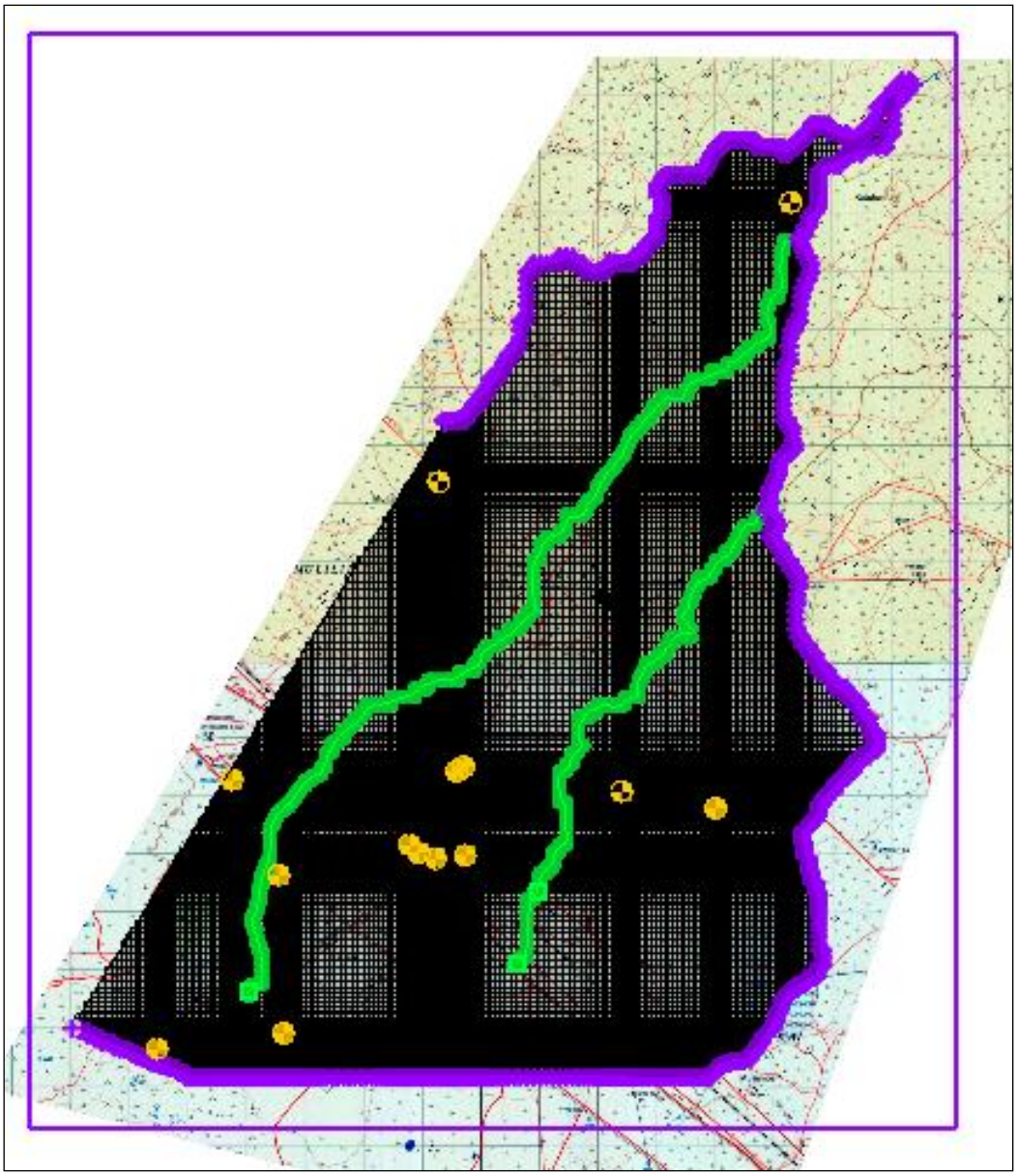

Figure 4.14 Grid frame of solute flow study area

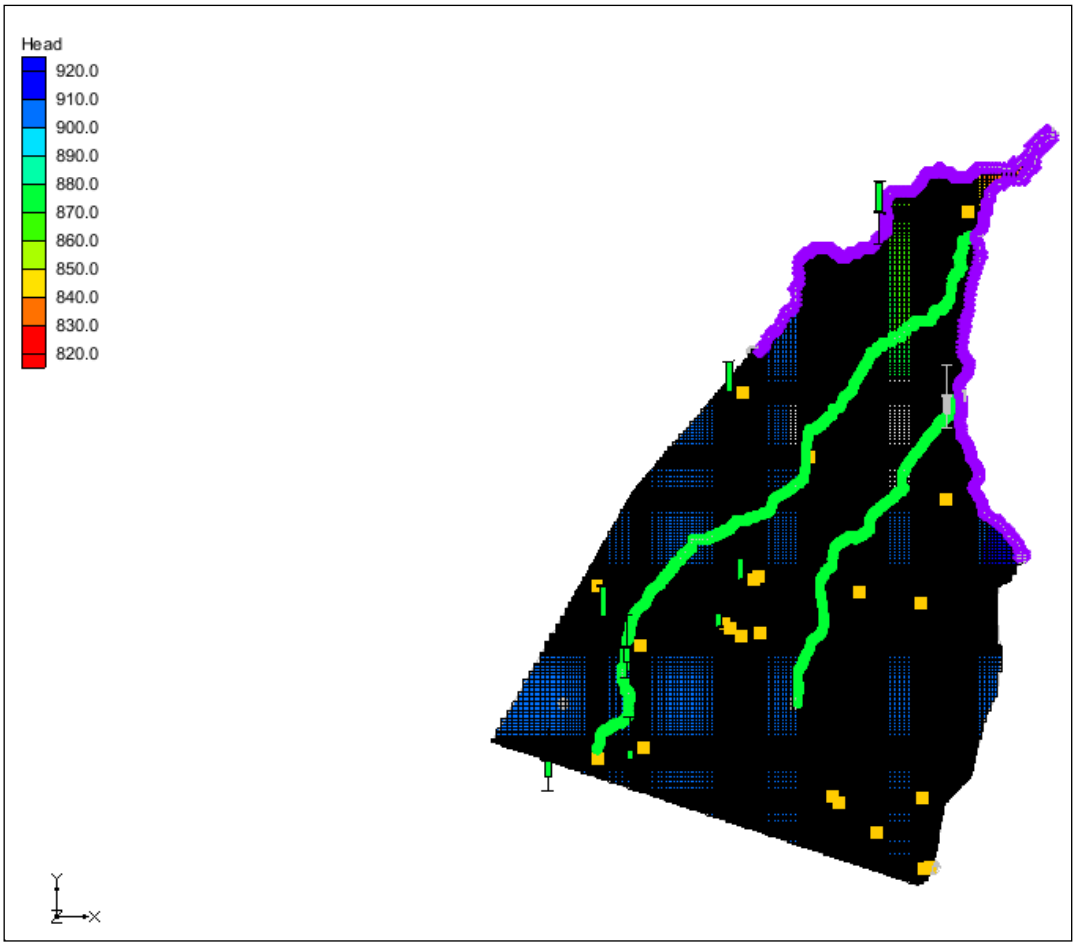

Figure 4.15 Calibration results of the GMS model and observation wells

Figure 4.16 is a plot of the computed verses the observed values of head. The observation points are near the diagonal line, which is an indication of a low error. Points that are far from the diagonal represent a larger error. The calibrated hydro-geophysical model of Chyulu aquifer at Makindu was therefore used in the subsequent stages in the solute modeling process.

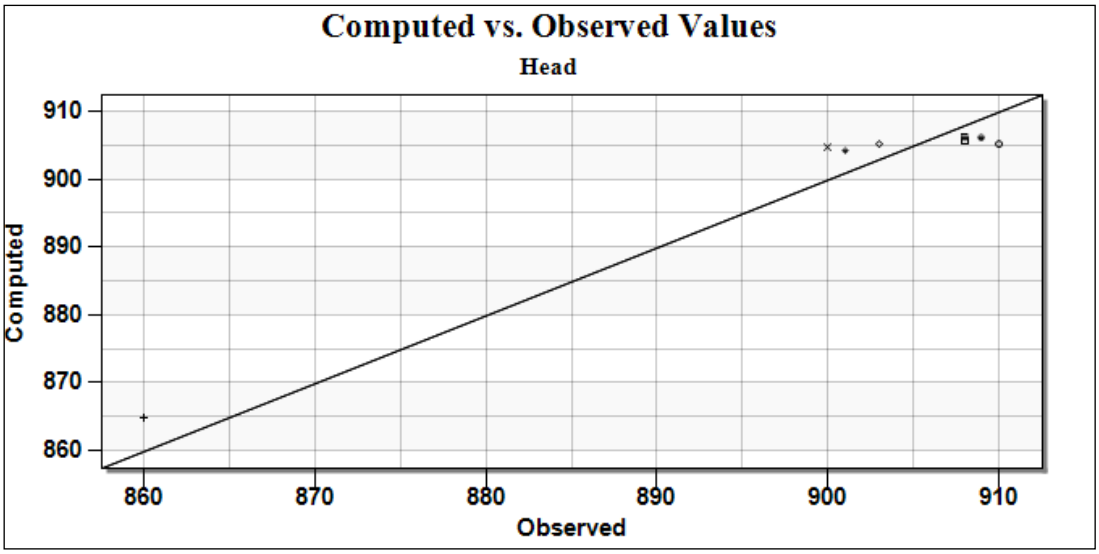

Figure 4.16 Graph of computed against observed values of head of the observation wells

4.5 USER DEFINED SUB-ROUTINE RESULTS

4.5.1 Flouride as a Catalyst

The results of the catalytic effect of fluoride ions in the reaction in the Chyulu aquifer in limited availability of oxygen are shown in Figure 4.17.

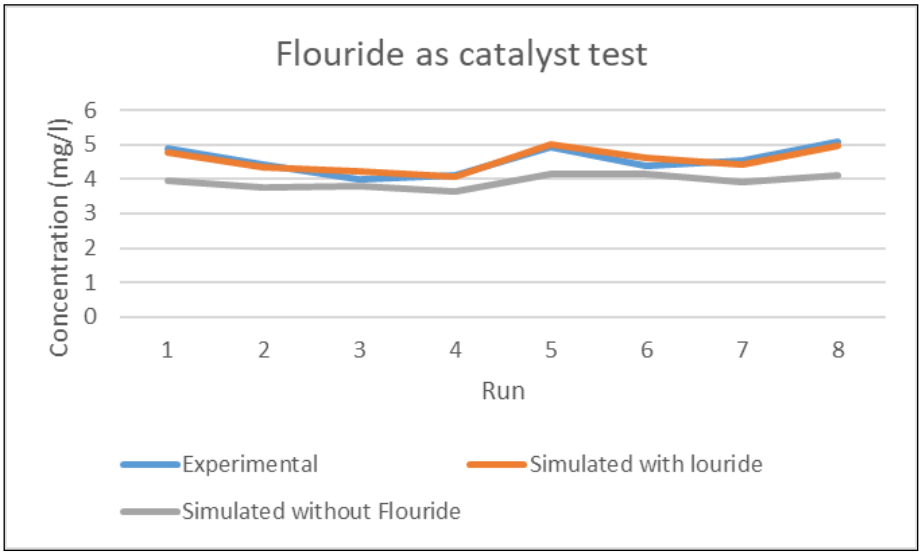

Figure 4.17 Graph of experimental iron concentration against simulated iron concentration (with and without fluoride).

The coefficient of correlation (R^2) for the experimental and the simulated concentration of iron in the aquifer while assuming the concentration of fluoride was >4.0 mg/L was 0.85 while the coefficient of correlation (R^2) between the experimental and the simulated of iron in the aquifer while assuming the concentration of fluoride is negligible was 0.45. The results show that equation (3.7) that has fluoride as one of the inputs estimates the concentration of ferrous as well as ferric ions in the stratum better than when fluoride concentration is not an input.

4.5.2 Batch Reaction Data

The results of nine (9) boreholes are presented in Appendix XII while the graphs of concentration of ferrous ions and ferric ions against a time of 42 hours are shown in Appendix XIII. The boreholes were all in the same locality and were roughly along the same line. The geology, soils and the topography were similar. The Jamia Mosque A (MK1) and Sikh Temple A (MK3) boreholes are almost the same distance from the Nairobi-Mombasa Highway and were taken as the datum. Both the Jamia Mosque B (MK2) and Sikh Temple B (MK4) boreholes were 250 m from the same highway while the Hospital (MK5) and Railway (MK6) boreholes were 350 m and 700 m from the highway respectively. The other three boreholes, namely Makindu Mission 1 (MK8), Makindu Mission 2 (MK9) and Makindu Sisters (MK10), were located within the Makindu Catholic Mission compound situated 1050 m from the highway.

The results obtained through direct testing using the procedure described in section 3.7.1 for concentration of ferrous ions and section 3.7.2 for the concentration of ferric ions were compared to the results obtained through simulation of the code (Appendix XIII) using the batchrxn.exe program provided by RT3D (section 3.9.4). The corresponding coefficient of correlation, R^2, for the two sets of data were determined and the value shown in Table 4.4. Also shown are the corresponding values of the rate constant K_3 for Fe (III). The values obtained for the ferrous ions (Fe (II)) for Makindu Hospital borehole had a coefficient of correction of 0.94

while the values obtained for ferric ions for the same borehole had a coefficient of correction of 0.97.

Table 4.6 Summary of results obtained using the code

S/N	Identification of borehole	Rate constant for Fe (III)	Coefficient of correlation (R^2) for Ferrous	Coefficient of correlation (R^2) for Ferric
1	Jamia Mosque (A) (MK1)	0.10	0.95	0.98
2	Jamia Mosque (B) (MK2)	0.07	0.92	0.92
3	Sikh temple (A) (MK3)	0.097	0.95	0.97
4	Sikh temple (A) (MK 4)	0.09	0.94	0.95
5	Makindu Hospital (MK5)	0.11	0.94	0.97
6	Makindu Railway (MK6)	0.06	0.96	0.93
7	Makindu Water (MK7)	0.063	0.95	0.97
8	Makindu Mission 1 (MK8)	0.060	0.92	0.97
9	Makindu Sisters (MK10)	0.070	0.88	0.91

Figure 4.18 to Figure 4.20 are graphs presenting results of ferrous Fe (II) ion concentration obtained for a period of 42 hours and results generated through the proposed code for Makindu Hospital borehole. The correlation is 0.94 for the three runs for the ferrous concentration and 0.983, 0.963 and 0.958 for the three runs respectively for the ferric ions as seen in Figure 4.21 to Figure 4.23. The graphs for the other boreholes are shown in the appendix XIII.

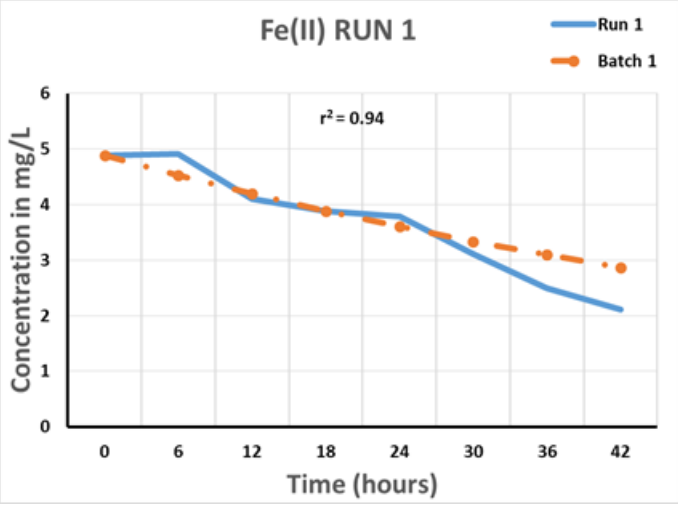

Figure 4.18 Makindu Hospital Data Fe (II) RUN 1

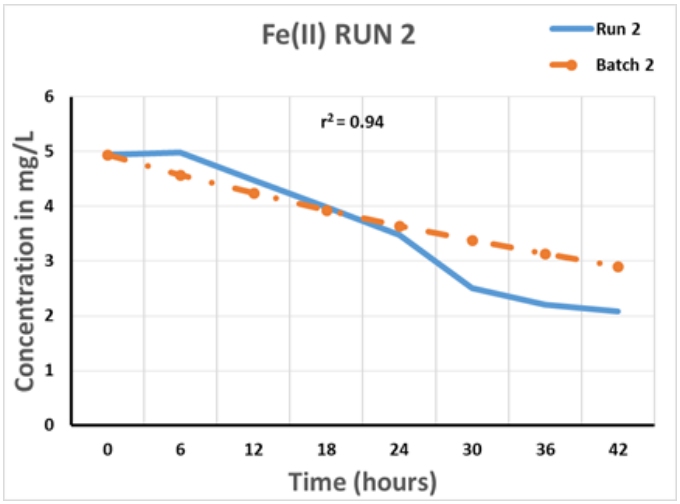

Figure 4.19 Makindu Hospital Data Fe (II) RUN 2

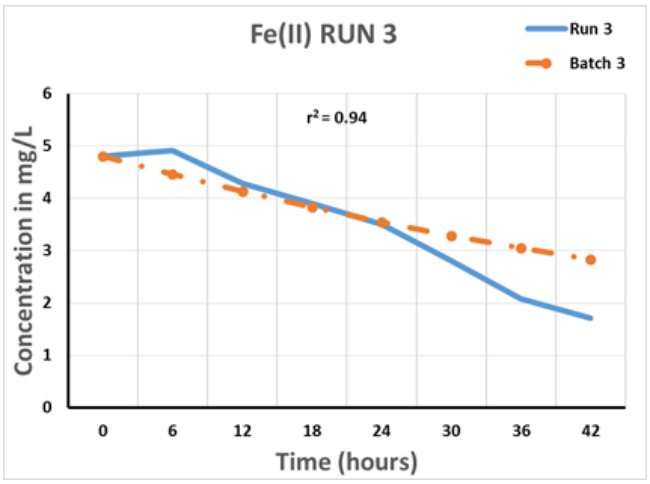

Figure 4.20 Makindu Hospital data Fe (II) RUN 3

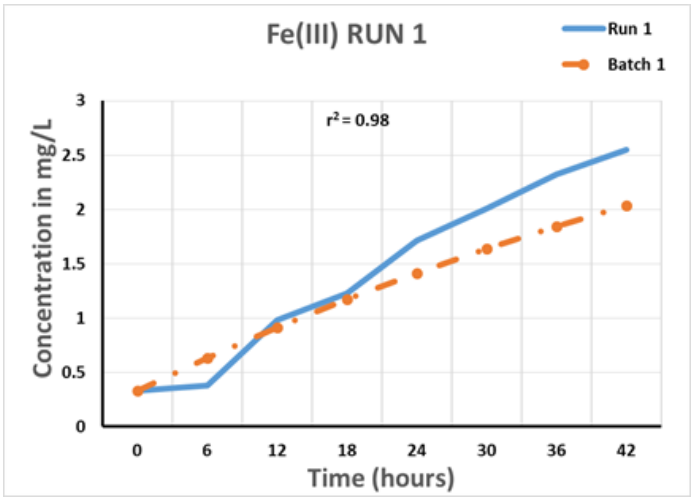

Figure 4.21 Makindu Hospital Data Fe (III) RUN 1

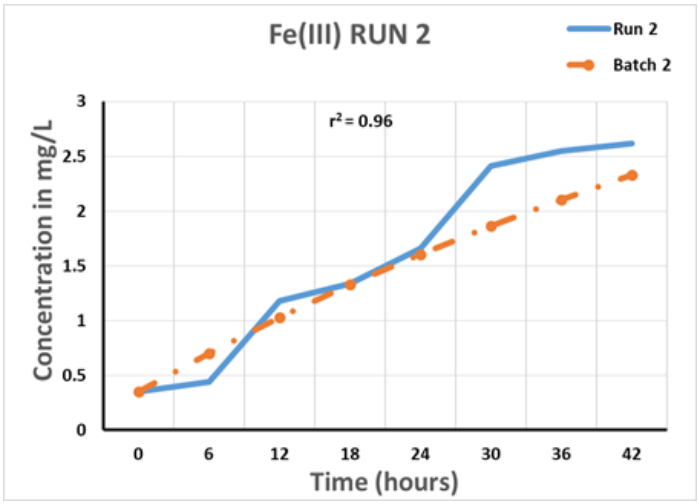

Figure 4.22 Makindu Hospital Data Fe (III) RUN 2

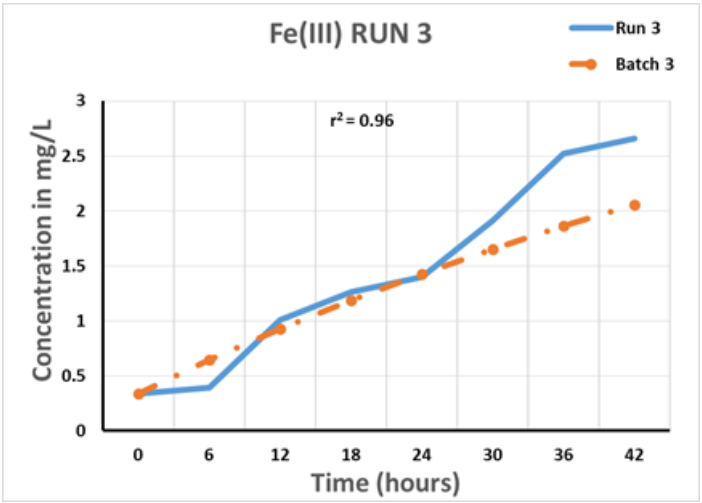

Figure 4.23 Makindu Hospital Data Fe (III) RUN 3

4.5.3 Results of the Calibration of the Sub-routine

The results of the calibration of the proposed user-defined RT3D sub-routine (Appendix XIV) are summarized in Table 4.5. Results of tests on six (6) boreholes for the concentration of ferrous ions and those for the concentration of ferric ions are presented.

Table 4.7 The mean standard deviation of the calibration exercise

S No	Identification of borehole	Mean standard deviation	
		Ferrous	Ferric
1	Musimba 1 (MK11)	0.0437	0.00211
2	Musimba 3 (MK13)	0.6873	0.0040
3	Makilya 2 (MK20)	0.0795	0.1230
4	Ndivo & Co. 1 (MK16)	0.0137	0.0110
5	Kyeni (22)	0.0555	0.0215
6	Mulili (25)	0.2384	0.0210

The mean standard deviation for all the test boreholes for ferrous ion concentration for the experimental was low. It was 0.6875 for Musimba 3 (MK13) borehole and was much lower for Mulili borehole which was 0.2384. The Mean Standard deviation (MSD) for the Ndivo and Company borehole was even lower at 0.0137. It means that the proposed user–defined RT3D model predicted the concentration of iron (II) accurately. The same boreholes had values of ferric ions of 0.0044, 0.0210 and 0.0110 for Musimba 3 (MK13), Mulili (MK25) and Ndivo and Co. 2(MK20). Figure 4.24 a is a graph of experimental data against simulated data for ferrous concentration for the Musimba 3 borehole while the graph for ferric ions for the same borehole is shown in Figure 4.25. The graphs of the other boreholes are presented in Appendix XV.

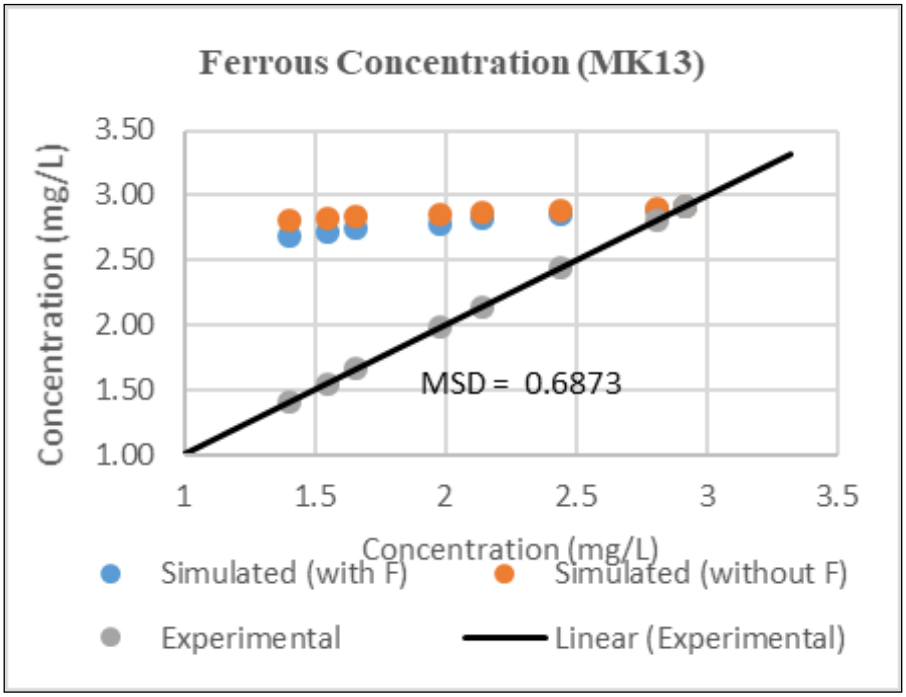

Figure 4.24 The experiment against simulated data for ferrous ions for Musimba 3 borehole (MK13)

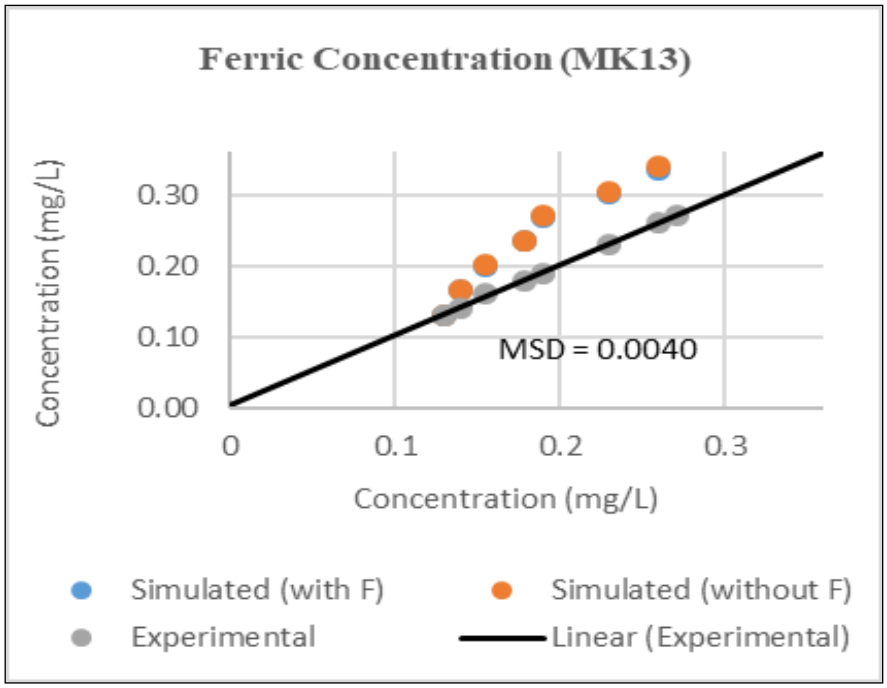

Figure 4.25 The experiment against simulated data for ferric ions for Musimba 3 borehole (MK13)

4.5.4 Relationship between Simulated and Tested Values of Concentration; Validation

The ability of the developed code that has been proposed in this study (Appendix XIV), to estimate the concentration of ferrous ions or ferric ions in the Chyulu aquifer was determined by the relationship between the simulated concentration of ferrous and ferric ions and the results of testing for the ions in the samples collected from the boreholes.

This relationship is determined as the coefficient of correlation also referred to as coefficient of determination and depicted as R^2. If the value of R^2 is greater or equal to 0.5 ($R^2 \geq 0.5$) then the proposed equation or relationship is considered to be good. If the value of R^2 is greater or equal to 0.7 ($R^2 \geq 0.7$) then proposed equation or relationship is considered to be very good. The concentration of ferrous and ferric ions iron in the aquifer was tested every six months from January 2016 to December 2019. Samples were collected from Jamia Mosque A (MK1) borehole, Sikh temple B (MK4) borehole, Makindu Hospital (MK5) borehole, Railway (MK6) borehole and Makindu Mission 1(MK8) borehole which were 10m (taken as starting point),

250m, 350m, 700m and 1050m respectively from the Nairobi-Mombasa Highway. The Highway is adjacent to the most southerly of the boreholes selected for the detailed study; the Jamia Mosque A (MK1).

4.5.5 Relationship between Simulated and Tested Values of Concentration of Ferrous Ions

The simulated results for ferrous ions that were obtained using the user-defined reaction code and run in the GMS/RT3D software are shown Table 4.6. The table shows the simulated results for the five (5) boreholes. The results were recorded every 3 months although a result could be obtained for any specified duration including even in seconds but the data generated would be too huge.

The value of ferrous ions for the Jamia Mosque A (MK1) was higher than the values of the other boreholes. The value shows a general reduction of the concentration of ferrous ions in the boreholes and consequently in the aquifer. The concentration of ferrous in March 2016 for Jamia Mosque was 1.559 mg/L while the concentration was 0.905 mg/L at Makindu Mission I (MK8) which is 1.05 km away.

Table 4.8 Simulated change in ferrous ions over time for 5 borehole in 1.05 km of aquifer

Time (Days)	Concentration of Ferrous ions (mg/L)				
	Jamia (MK1)	Sikh B (MK4)	Hospital (MK5)	Railway (MK6)	Makindu Mission 1 (MK8)
91.25	1.559	1.247	1.064	0.864	0.905
182.5	1.505	1.197	1.015	0.830	0.878
273.75	1.462	1.151	0.967	0.784	0.827
365.0 (1year)	1.427	1.114	0.924	0.744	0.785
456.25	1.439	1.129	0.934	0.768	0.813
547.50	1.431	1.1205	0.916	0.760	0.805
638.75	1.435	1.127	0.914	0.775	0.822
730.0 (2 years)	1.424	1.111	0.890	0.760	0.800
821.25	1.422	1.111	0.88	0.753	0.799
912.50	1.435	1.127	0.888	0.777	0.825
1003.75	1.419	1.109	0.863	0.751	0.797
1095.0 (3 years)	1.398	1.086	0.837	0.724	0.766
1186.25	1.419	1.1095	0.854	0.754	0.800
1277.50	1.413	1.106	0.848	0.750	0.799
1368.75	1.420	1.117	0.855	0.768	0.816
1460.0 (4 years)	1.410	1.106	0.870	0.750	0.795

As shown in Table 4.6, the simulated concentration at the Jamia Mosque A (MK1) reduced gradually over the period of 4 years. For example, it was 1.427 mg /l after 1 year, 1.424 mg/L after 2 years and 1.398 after 3 years. At the Railway (MK6) borehole the concentration was 0.744 mg/L after 1 year and 0.724 mg/L after 3 years. The concentration also dropped from 0.905 mg/L in March 2016 to 0.795 mg/L in December 2019 at the Makindu Mission 1(MK8). The percentage reduction in the concentration of ferrous ions for Jamia Mosque A (MK1) was 10.6 % while that for Makindu Mission 1 (MK8) was 13.8%. Appendix XVI shows the results of comparison between the simulated concentration of ferrous ions and the tested concentration of ferrous ions for a period of four (4) years.

The simulated concentration is decreasing over the four years while the tested concentrations are also decreasing for example for the Sikh temple B (MK4) the experimental concentration was 1.505 mg/L in June 2016 and reduced to 1.410 mg/L in December 2019. The tested concentrations also decreased from 1.60 mg/L to 1.39 mg/L over the same period.

Figures 4.26 to 4.30 are plots for both simulated and experimental values of ferrous ions concentration for the five boreholes in a period of four (4) years. In all the cases the coefficient of correlation has been calculated. The values of the coefficient of correlation (R^2) for the Jamia Mosques A (MK1), Sikh Temple B (MK4), Makindu Hospital (MK5), Makindu Railways (MK6) and Makindu Mission (1)(MK8) boreholes were 0.9, 0.76, 0.88, 0.70 and 0.75 respectively. In all these cases the value of R^2 was equal to or greater than ($\geq$) 0.7. Thus, the simulated and tested data sets were very close. This also means that the proposed code estimated the concentration of ferrous ions in the stratum very accurately.

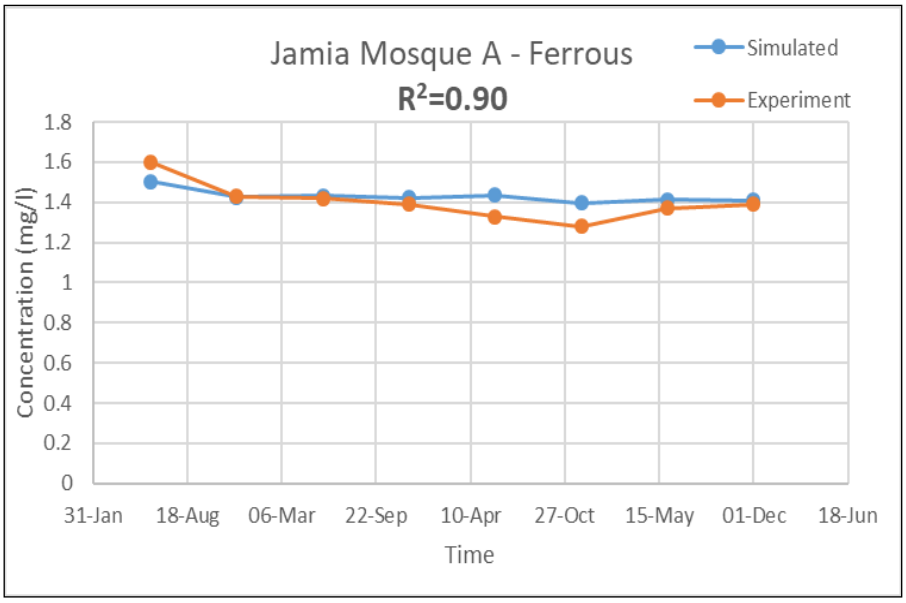

Figure 4.26 Concentration of ferrous ions for Jamia Mosque A (MK1) in four (4) years

The change of concentration of ferrous ions over the four (4) years in the Makindu Mission 1 (MK8) borehole as seen in Appendix XVI over the four (4) years, the simulated and the tested concentrations of the borehole have been decreasing just as is the case with the other boreholes.

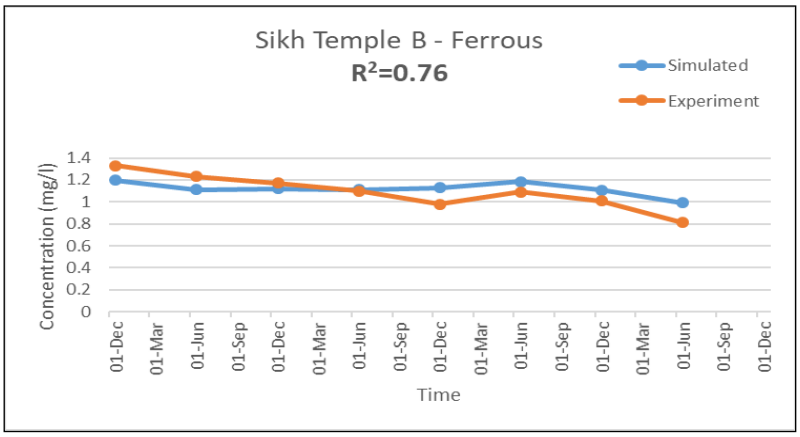

Figure 4.27 Concentration of ferrous ions for Sikh Temple B (MK4) in four (4) years

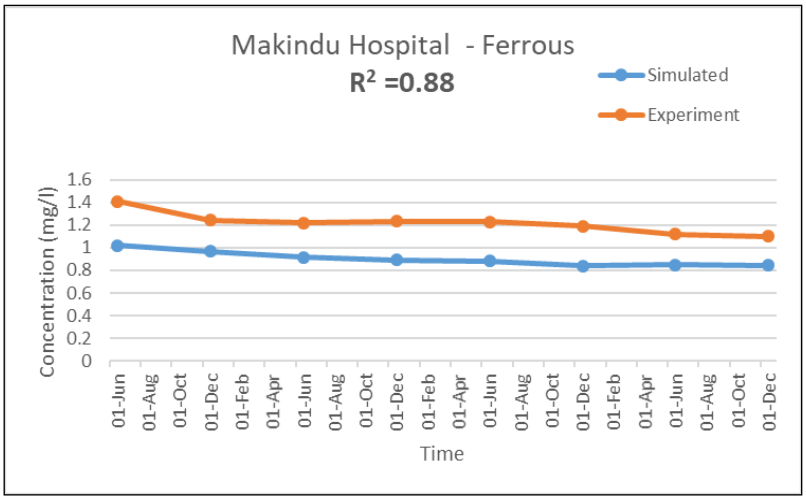

Figure 4.28 Concentration of ferrous ions for Makindu Hospital (MK5) in four (4) years

The simulated concentration was 0.878 mg/L in June 2016 and 0.795 mg/L in December 2019, a 10% decrease while the tested concentration was 0.902 mg/Lin June 2016 reducing to 0.77 mg/L in December 2019, a decrease of 17%.

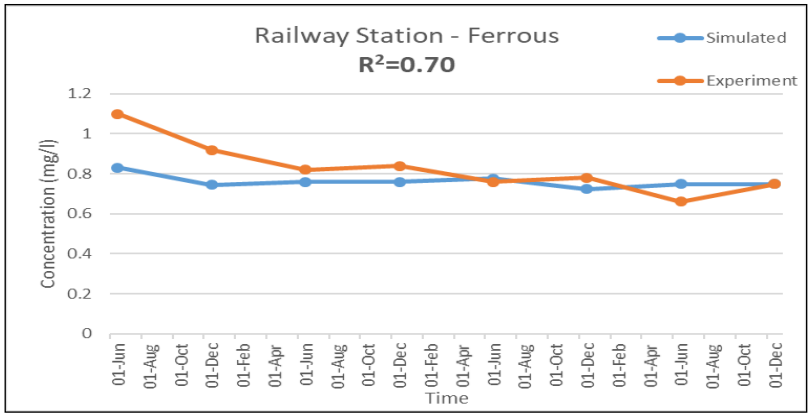

Figure 4.29 Concentration of ferrous ions for Makindu Railway (MK6) in four (4) years

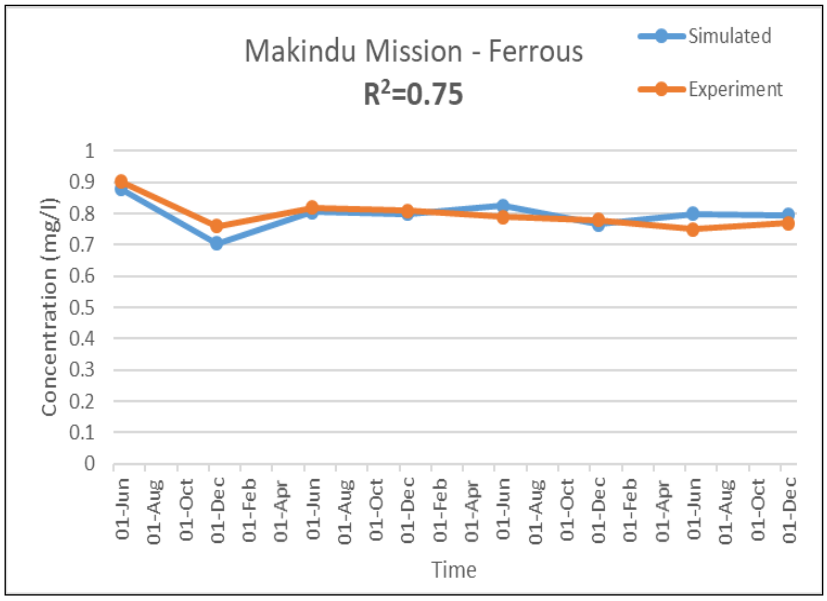

Figure 4.30 Concentration of ferrous ions for Makindu Mission 1 (MK8) in four (4) years

4.5.6 Relationship between Simulated and Tested Values of Concentration of Ferric Ions

The simulated results for ferric ions for the user-defined reaction code and run in the GMS/RT3D software were also obtained on similar duration as in the ferrous case and are shown Table 4.9.

Table 4.9 Simulated change in ferric ions for 5 boreholes in 1.05 km of aquifer over time

	Concentration of Ferric ions (mg/L)				
Time (Days)	**Jamia A**	**Sikh B**	**Hospital**	**Railway**	**Mission 1**
91.25	3.926	2.478	2.715	2.2467	2.200
182.5	4.058	2.494	2.7366	2.254	2.191
273.75	4.144	2.518	2.7691	2.274	2.183
365.0 (1year)	4.207	2.540	2.807	2.390	2.15203
456.25	4.200	2.525	2.817	2.277	2.176
547.50	4.218	2.529	2.8536	2.380	2.1499
638.75	4.216	2.523	2.881	2.273	2.153
730.0 (2 years)	4.235	2.532	2.927	2.292	2.161
821.25	4.24	2.532	2.96	2.283	2.1542
912.50	4.224	2.520	2.984	2.281	2.201
1003.75	4.247	2.533	3.018	2.283	2.1554
1095.0 (3 years)	4.275	2.549	3.057	2.296	2.152
1186.25	4.248	2.532	3.0587	2.282	2.155
1277.50	4.252	2.534	3.10	2.283	2.456
1368.75	4.241	2.526	3.081	2.276	2.1503
1460.0 (4 years)	4.252	2.534	3.48	2.40	2.1501

The values of ferric ions for the Jamia Mosque A (MK1) were higher than the values of the other boreholes. The values show a general increase in the concentration of ferric ions in the boreholes and consequently in the aquifer. The concentration of ferric in June 2016 for Jamia Mosque was 3.926 mg/L while the concentration was 2.20 mg/L at Makindu Mission I (MK8) which is 1.05 km away. The simulated concentration at the Jamia Mosque A (MK1) increased over the period of 4 years. For example, it was 4.207 mg /l after 1 year, 4.235 mg/L after 2 years and 4.275 after 3 years. At the Hospital borehole (MK5), the concentration was 2.807 mg/L after 1 year and 3.48 after 4 years. The concentration also increased from 2.390 mg/L in December 2016 to 2.40 mg/L in December 2019 at the Makindu Mission 1 (MK8). The percentage increase in the concentration of ferric ions for Jamia Mosque A (MK1) was 8.3% while that for Makindu Railway (MK6) was 6.8%.

Appendix XVI shows the results of comparison between the simulated concentration of ferric ions and the tested concentration of ferric ions for a period of four (4) years.

The simulated concentration is increasing over the four years while the tested concentrations are also increasing for example for the Sikh temple B (MK4) the simulated concentration was 2.494 mg/L in June 2016 and increased to 2.534 mg/L in December 2019. The tested concentrations also increased from 2.44 mg/L to 2.54 mg/L over the same period.

Figures 4.31 to 4.34 are plots of the concentration of ferric ions for the four (4) years for the five boreholes for both simulated and experimental values. In all the cases the coefficient of correlation has been calculated. The values of the coefficient of correlation (R^2) for the Jamia Mosques A (MK1), Sikh Temple (B)(MK4), Makindu Hospital (MK5), Makindu Railways (MK6) and Makindu Mission 1(MK8) boreholes were 0.91, 0.70, 0.94, 0.72 and 0.83 respectively. In all these cases the value of R^2 was equal or greater than 0.7. This means that the two sets of data, simulated and tested, were very close. It means that the proposed code estimated the concentration of ferric ions in the stratum very accurately.

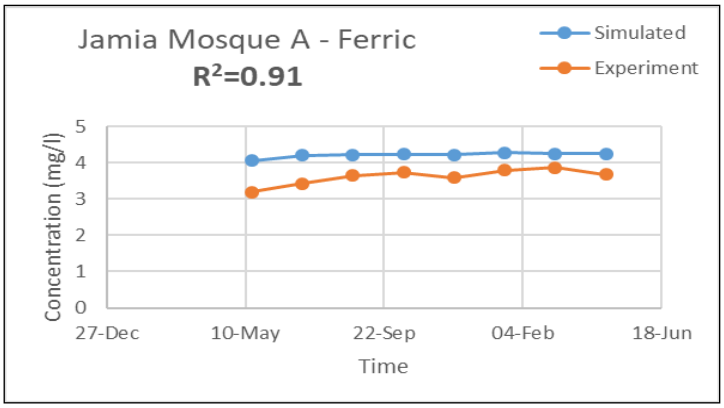

Figure 4.31 Concentration of ferric ions for Jamia Mosque A (MK1) in four (4) years

Over the four (4) years, the simulated and the tested concentrations of the borehole have been increasing just as is the case with the other boreholes. The simulated concentration was 2.118 in June 2016 and 2.157 December 2019, a 2.0 % increase while the tested concentration was 2.51 mg/L in June 2016 increasing to 3.25 mg/L in December 2019, an increase of 29.6 %.

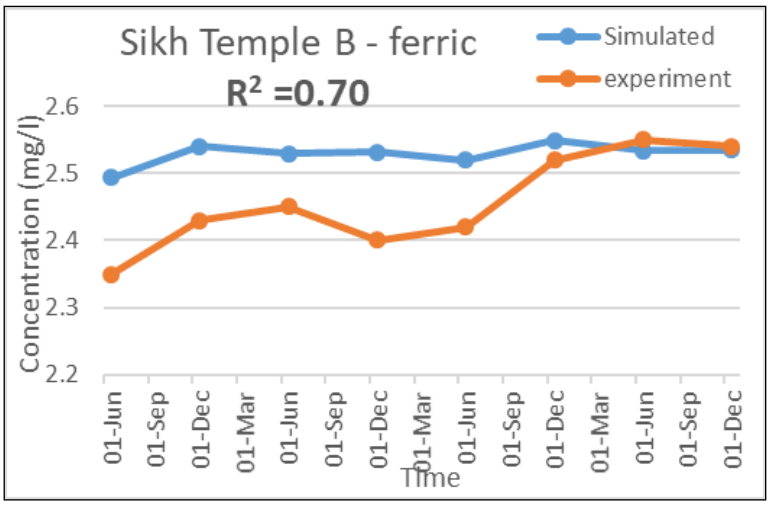

Figure 4.32 Concentration of ferric ions for Sikh Temple (MK4) in four (4) years

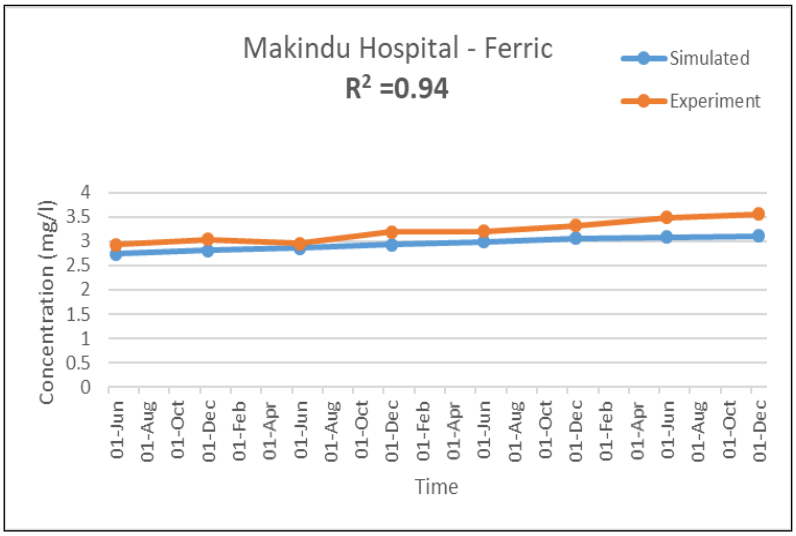

Figure 4.33 Concentration of ferric ions for Makindu Hospital (MK5) in four (4) years

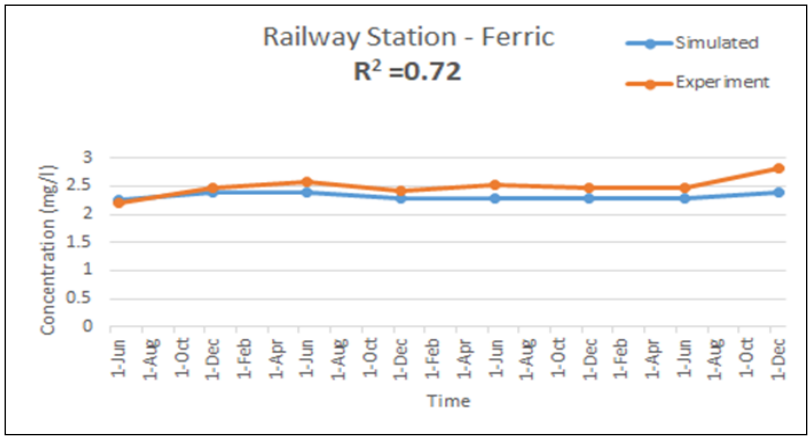

Figure 4.34 Concentration of ferric ions for Makindu Railways (MK6) in four (4) years

Figure 4.35 is the graph of concentration of ferric ions against time from January 2016 to December 2019, a period of four (4) years. The simulated data is plotted as well as the experimental data.

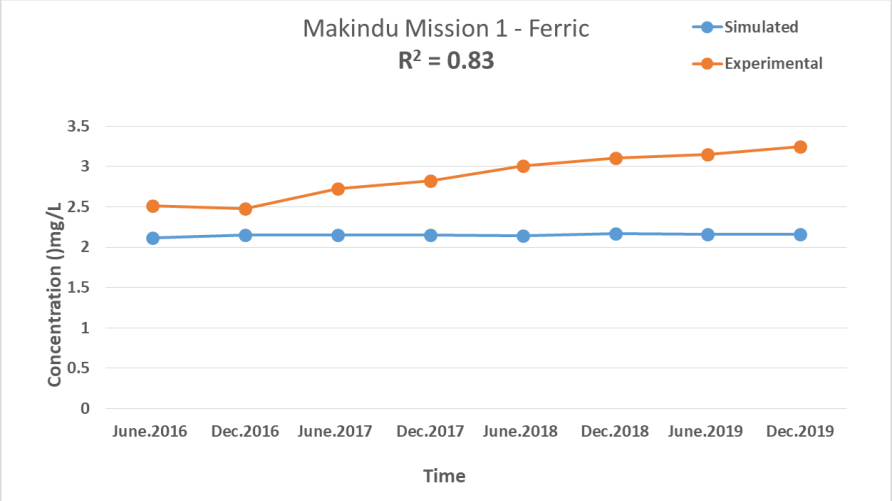

Figure 4.35 Concentration of ferric ions for Makindu Mission 1 (MK8) in four (4) years

The coefficient of correlation (R^2) for the two sets of data was found to be 0.83 for the Makindu Mission 1 (MK8). This means that the two sets of data, the simulated and tested data were very close.

4.5.7 Summary of Simulation and Test Concentration of Ferrous and Ferric Ions

The calibrated stratum model is represented by equations (4.2) and (4.3) thus:

$$R_{II}\frac{d[Fe(II)]}{dt} = -4.6k_2[Fe(II)][O_2] \quad \text{..... (4.2)}$$

$$\frac{d[Fe(III)]}{dt} = \frac{k_3[Fe(II)][O_2]}{R_{III}} \quad \text{..... (4.3)}$$

These calibrated expressions were able to predict the concentration of ferrous and ferric ions in the stratum with 90% of the values of the coefficient of correlation (R^2) being greater than 0.70 as seen in Table 4.8. The average coefficient of correlation for ferrous ion reactions is 80% while that for ferric ion reaction is 82%. This means that these relationships can be used to predict the chemical reactions in the aquifer well since the simulated values matched the values obtained through testing. The time and resources spent in sampling and testing will therefore be saved.

Table 4.10 Average coefficients of correlation for simulated and tested values of concentration of ferrous and ferric ions

S/No	Borehole Identification	Coefficient of correlation (R^2) for Ferrous	Coefficient of correlation (R^2) for Ferric
1	Jamia Mosque (A) (MK1)	0.90	0.91
2	Sikh temple (A) (MK 4)	0.76	0.70
3	Makindu Hospital (MK5)	0.88	0.94
4	Makindu Railway (MK6)	0.70	0.72
5	Makindu Mission 1 (MK8)	0.75	0.83
Average R^2 correlation coefficient		0.80	0.82

4.6 Proposed Expressions and Sub-routine

The third objective of this study ought to develop a user-defined solute transport model that is dynamically linked to the GMS to be used to predict dispersion that would be used to accurately generate ferrous oxygenation reactions in the Chyulu aquifer at Makindu. The proposed relationships, one that would predict ferrous oxygenation and the other ferric oxygenation under low dissolved oxygen environment are presented hereunder for:

i) Ferrous estimation

$$\frac{d[Fe(II)]}{dt} = \frac{-k_2[Fe(II)][O_2][F]}{R_{II}}$$

ii) Ferric estimation

$$\frac{d[Fe(III)]}{dt} = \frac{k_3[Fe(II)][O_2]}{R_{III}}$$

The proposed equation (4.2) quantitatively predicts the concentration of ferrous ions in the Chyulu aquifer. The corresponding values of fluoride ions concentration in the stratum and the corresponding first order rate constant for ferrous (k_2) will be input into the equation. To predict the ferric concentration in the aquifer equation (4.3) will be used with the corresponding parameter, first order rate constant of ferric (k_3).

4.7 APPLICATION OF PROPOSED SUB-ROUTINE

The code that has been proposed (Appendix XIV) was linked with the GMS software and run to simulate the flow of ferrous ions in the aquifer at Makindu in the Chyulu aquifer. Figure 4.36 shows the status of the flow of the ferrous ions under conditions of low dissolved oxygen (<0.5 mg/L) after one year. After that one year, the ferrous ions will have spread to a distance of 50m in the direction of flow. Figure 4.37 show the extent of the ferrous ion movement after 2 years.

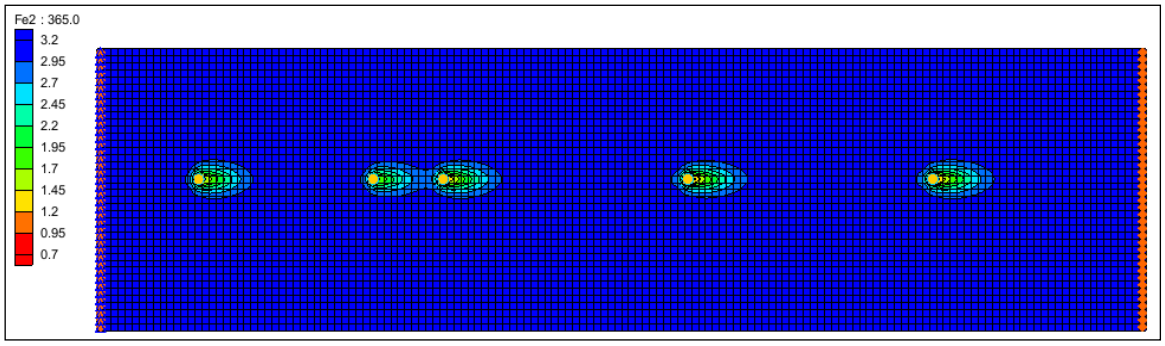

Figure 4.36 The extent of movement of ferrous ions in the aquifer at Makindu in the Chyulu aquifer after one year

From Figure 4.37 it is seen that the groundwater that had been aerated from borehole MK4 reaches borehole MK5 after two years of transport. Therefore, the concentration of ferrous at borehole MK5 is because of aeration at MK5 itself at that instant and the aeration at borehole MK4.

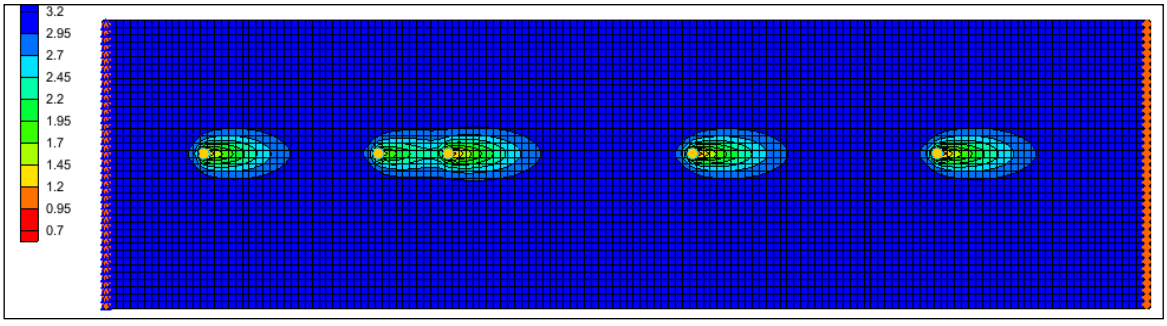

Figure 4.37 The extent of movement of ferrous ions in the aquifer after two years

In Figure 4.38, after three years of transport, more aerated water from borehole MK4 reaches borahole MK5. Therefore the concentration of ferrous at borehole MK5 not only depends on aeration at borehole MK5 itself but significantly on the water that had been aerated at borehole MK4 during the previous three years. Even after the three years the concentration ferrous at boreholes MK1, MK4, MK6 and MK8 is not affected by the neighbouring boreholes. This is because of much greater distance that separates them.

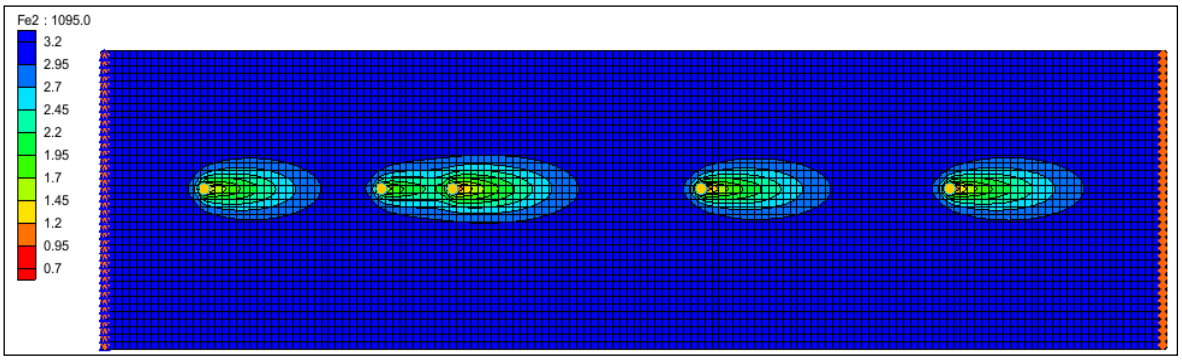

Figure 4.38 The extent of spread of ferrous ions in the aquifer after three years

In Figure 4.39, the aerated water with ferrous ions from borehole MK1 reaches borehole MK4 after four years of transport. Therefore the concentration of ferrous ions at borehole MK4 depends on both the aeration at borehole MK4 itself and much less on aeration at borehole MK1 because now small amout of ferrous ions from borehole MK1 now reach borehole MK4 after the four years.

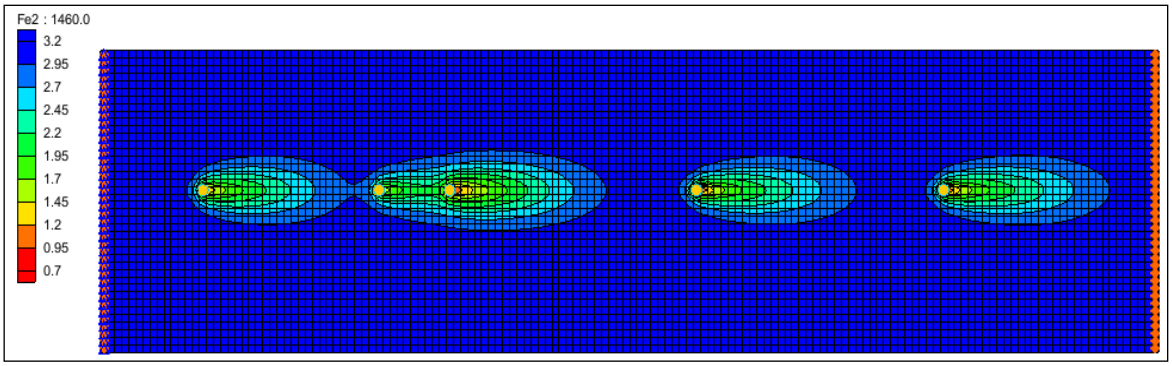

Figure 4.39 The spread of ferrous ions in the aquifer after four years

Concentration of ferrous at borehole MK5 depends greatly on aeration at borehole MK4 after four years because large most of aerated water from borehole MK4 reaches borehole MK5. Even after four years, the concentration of ferrous at borehole MK6 and MK8 is not affected by the water from neighbouring boreholes because of the distance that separate them.

Figure 4.40 shows the status of the flow of the ferric ions under conditions of low dissolved oxygen (0.5 mg/L) after one year. After that one year, the ferric ions will have spread to a distance of 40m in the direction of flow.

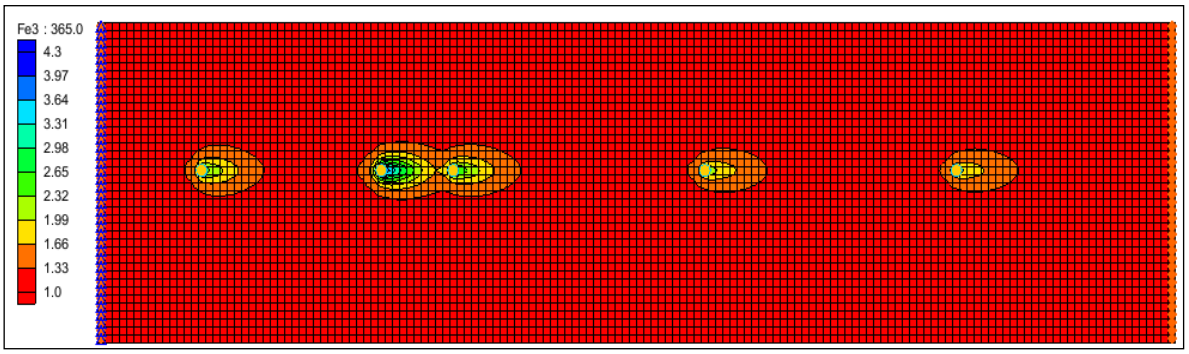

Figure 4.40 The extent of movement of ferric ions in the aquifer after one year

Figure 4.41 show the extent of the ferric ion movement after 2 years. This figure demonstrates that the aerated water from borehole MK4 reaches borehole MK5 after two years of transport. Therefore, the concentration of ferric at borehole MK5 is slightly enhanced by aeration from MK4.

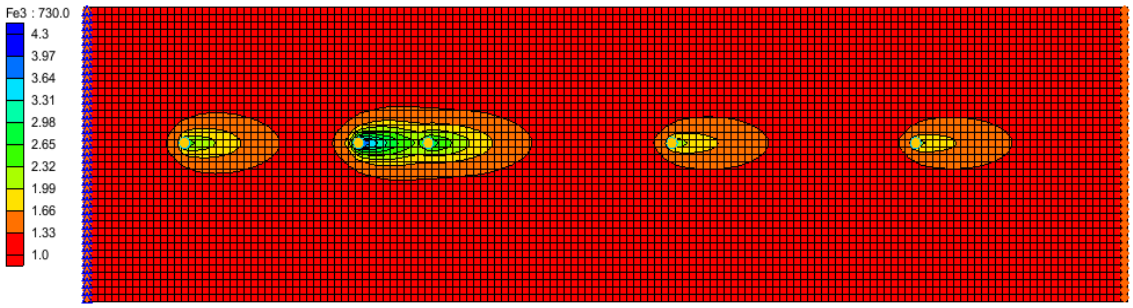

Figure 4.41 The extent of movement of ferric ions in the aquifer after two years

In Figure 4.42, after three years of transport, more aerated water from borehole MK4 reaches borehole MK5. Therefore, the concentration of ferric at borehole MK5 not only depends on aeration at borehole MK5 itself but also on the solute that had been aerated at borehole MK4 in the previous three years. Even after the three years, the concentration ferric at boreholes MK1, MK4, MK6 and MK8 is not affected by their neighboring boreholes. This is because of much distance that separates these boreholes.

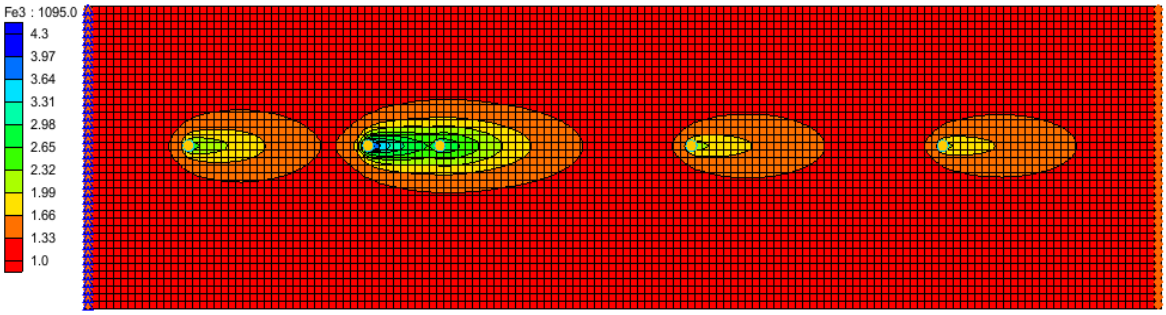

Figure 4.42 The extent of movement of ferric ions in the aquifer after three years

In Figure 4.43, the aerated water with ferric ions from borehole MK1 reaches borehole MK4 after four years of transport. Therefore, the concentration of ferric at borehole MK4 depends on both the aeration at borehole MK4 itself and on aeration at borehole MK1. Concentration of ferric at borehole MK5 depends on its aeration and on aeration at borehole MK4. Even after four years, the concentration of ferric ions at borehole MK6 and MK8 is not affected by the water from neighboring boreholes because of the distance that separates them.

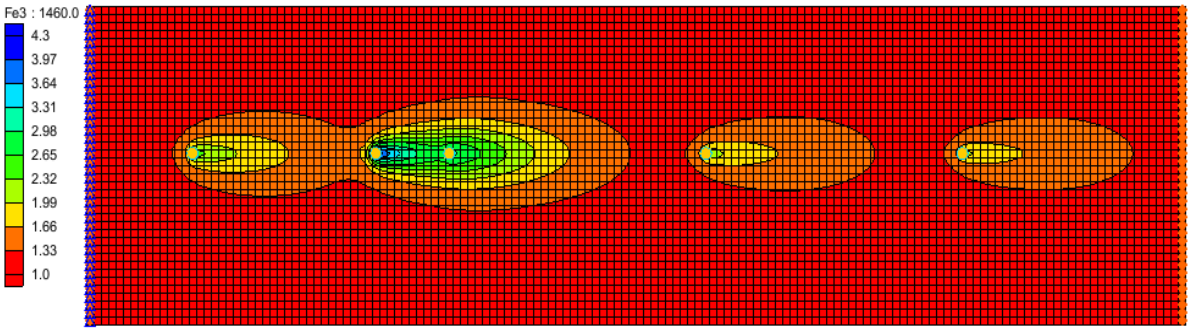

Figure 4.43 The extent of movement of Ferric ions in the aquifer at Makindu in the Chyulu aquifer after four years

CHAPTER 5: CONCLUSIONS AND RECOMMENDATIONS.

5.1 INTRODUCTION TO CONCLUSION AND RECOMMENDATION

The objective of this study was to develop tools for groundwater assessment and transport characterization of iron and its derivatives for use in aquifers. The results of this study were the significant development and testing of relationship describing the dispersion of iron in the stratum. Significant also was the acceptable performance of non-motorized aeration/filtration unit that reduced iron concentration in groundwater by 58.3 %. 86 .5 % of the boreholes in the study area had either medium to high potential but only 10 % of the Chyulu aquifer has acceptable water quality.

5.2 CONCLUSIONS

This study drew the following conclusions:

1) The main consideration in deciding the site of a borehole in the study area should be the water quality because according to the water quality index map where only 10% of the study area had water that is fit for human consumption while according groundwater potential map, 92% of the study area has either high (> 12m^3/day) or moderate (6 – 12m^3/day) yield.
2) The cost of treating water to reduce iron concentration from borehole water using a non-motorized aeration filtration unit is worth investment since such unit reduced iron concentration from groundwater by 58.3%
3) The user-defined Fortran sub-routine (code) of RT3D of Groundwater Modeling System (GMS) that incorporated the proposed equations of $\frac{d[Fe(II)]}{dt} = \frac{-k_2[Fe(II)][O_2][F]}{R_{II}}$ and $\frac{\partial[Fe(III)]}{\partial t} = \frac{k_3[Fe(II)][O_2]}{R_{III}}$ accurately predicted the concentration of both ferrous and ferric ions respectively in the Chyulu aquifer at Makindu.

5.3 RECOMMENDATIONS

These studies recommends that:

1) The user-defined RT3D FORTRAN sub routine that has been modelled in the study be tested and calibrated for use in other aquifers.
2) The chemical compounds such as calcium carbonate exist in the Chyulu aquifer be studied. Such study will investigate how calcium and its derivatives flows in the Chyulu aquifer. This will broaden the knowledge on the groundwater situation in the Chyulu and adjoining areas.

REFERENCES

Abdel-Lah, A. A., Mohamoud, M. S. and Abadai, S. A., 2002. "Efficiency of Iron and Manganese Removal from Groundwater, using Aeration Tower in Nile Valley, Egypt" 3rd Middle East Regional Conference on Civil Engineering Technology and 3rd International Symposium on Environmental Hydrology. American Society of Civil Engineers- Egypt Section (ASCE-EGS). Cairo Egypt.

Ahmed, S. S., Mazumber, Q. H., Jahan, C. S. and Ahmed, A., 2002. "Hydrochemistry and Classification of Groundwater, Rajshahi City Corporation Area, Bangladesh". Journal of the Geological Society of India, 60(4), 411-418.

Ahsen 2020. "A GIS–based DRASTIC Model and Adjusted DRASTICA Model for Groundwater Susceptibility Assessment along China–Pakistan Economic Corridor (CPEC) route" International Journal of Geo-information (ISPRS), 9.

Aller, L., Bennet, T., Lehr, J., Petty, R. and Hackett, G., 1987. "DRASTIC: Standardized System for Evaluating Groundwater Pollution Using Hydrogeologic Settings". National Water Well Association- EPA 600/2-87-035.

Allison, G.B., Gee, G. W. and Tyler, S. W., 1994. "Vadose–Zone techniques for Estimating groundwater Recharge in Arid and Semi-Arid Regions" Journal of Soil Science, 58, 6-14.

Amadi, A. N., Tukur Aminu, Okunlola, I. A., Olasehinde, P. I, Jimoh, M. O., 2015. "Lithologic Influence on the Hydrogeochemical Characteristics of groundwater in Zango, North-West Nigeria". Journal of Natural Resources and Conservation, .3(1), 11-18.

Anatolyev, S. 2020. "A Ridge to Homogeneity for Linear Models". Journal of Statistical Computation and Simulation, 90, 2455-2472.

Anderson, M. P. and Woessner, W. W., 1992. "Applied Groundwater Modelling". 381. San Diego (Academic Press).

Applin, K. R. and Zhao, N., 1989. "The kinetics of ferrous oxidation and well screen encrustation" Journal of Groundwater, 27(2), 168-174.

Barlokova, D. and Ilavsky, J., 2009. "Removal of Iron and Manganese from Water using Filtration by Natural Materials". Polish Journal of Environment, 19(6), 1117-1122.

Betancur, T. V., Palasio, C. A. T. and Escobar, J. F., 2014. "Conceptual Models in Hydrogeology, Methodology and Results".

Breaban, I. G. and Paiu, D. G., 2012. "Determination of Water Quality Index of Jijia and Miletin Ponds, Romania". Journal of Agriculture, UASVM, 69(2).

Bredehoeft. J. D. 2005. “The Conceptual Model Problem” Journal of Hydrology, Vol. 13, 37-46.

BSG - British Geological Survey (2000)

Burke, J. J. and Moench, M.H., 2000. “ Groundwater and Siciety; resources, tensions and Opportunities “. New York: United nations Publication ST/ESA/205.

Chapelle, F. H., McMahon, P. B., Dubrovsky, B., Fujii, R. F., Oaksford, E. T. and Vroblesky, D., 1995. “Deducing the Distribution of Terminal Electron Accepting Processing in Hydrologically Diverse Groundwater Systems”. Water Resources Research 31. No. 2, 359-371.

Chapman, P. J., Kay, P., Mitchel G. N. 2013. “Surface Water Quality. Water Resources; An Integrated Approach”. Water Rose Research Online. AC. Uk.

Chapra, S.C. 2017. ”Applied Numerical Methods with MATLAB for Engineers and Scientists” MCGraw Hill. 2017

Chaturvedi, A., A. K. Pathak, K. C. and Singh, V. N., 1988. “Flouride Removal from Water by Adsorption on China Clay”. Applied Clay Science, 3(4), 337 -346.

Chepchumba, M. C., Raude, J. M. and Sang J. K., 2019. “Geospatial Delineation and Mapping of Groundwater Potential in Embu County, Kenya”. Italian Journal of Groundwater. AS -369

Chiang, W. H., Kinzelbach, W. and Rausch. R., 1998. “Aquifer Simulation Model for Windows. Groundwater Flow and Transport Modeling. An Integrated Program”.

Chilton, P.J. and Foster, S. S. D., 1995. ”Hydrogeological characterization and water-supply potential of basement aquifers in tropical Africa”. Journal of Hydrogeological. 3, 36-49.

Clement, T. P., 1997, “RT3D: A Modular Computer Code for Simulating Reaction Multi – Species Transport in 3 – Dimensional Groundwater Aquifers”. PNNL – SA 28967.

Clesceri, L. S., Eaton, D. A., and Greenberg, A. E., 1995. “Standard Methods for the Examination of Water and Wastewater”. American Public Health Association, Washington, DC USA. 19th edition.

Coetsiers, M., Kilonzo, F. and Walraevens, K., 2008. “Hydro chemistry and source of high fluoride in groundwater of the Nairobi are, Kenya” Journal of Hydrological Sciences, 53(6), 1230 – 1240.

Das, J. K., 2007. “Design of Rapid Gravity Filter using AUTOCAD and C Programming”. 2007.

Dodson, R. G., 1953. “Geology of South–East Machakos Area”. Geological Survey of Kenya, 25.

Domenico, P.A. and Schwarz, F. W., 1997. “Physical and Chemical Hydrogeology”, 506. New York (Wiley and Sons, INC)

Donovan, J. J. and Jacobsen, J. S., 2001. ”Iron and Iron Bacteria in Montana Groundwater”Montana State University. Water Resources Management (Water Quality).

Ebrahimi, R and Bhatla, S. C., 2011. “Effect of Sodium Chloride Levels on Growth, Water Status, Uptake, Transport and Accumulation Pattern of Sodium and Chloride ions in Young Sunflower Plants” Communications in Soil Science and Plant Analysis, 2(7).

Emerson, D and Moyer, G. C., 1997. “Isolation and Characterization of Novel Iron-Oxidizing Bacteria that Grow at Circumneutral pH.” Journal of Applied and Environmental Microbiology, 63(12), 4784 -4792.

El-Naggar, H. M., 2010. “Development of Low Technology for the Removal of Iron and Manganese”

Ferris, 2005. “Biogeochemical Properties of Bacteriogenic Iron Oxides”. Journal of Geomicrobiology, 22(4), 79-85.

Foster, S.S.D. & Chilton P.J. 2003. “Groundwater: The Process and Global Significance of Aquifer Degradation” British Geological Survey, Wallingford, Oxford shire OX10 8BB, UK.

Foster, S.S.D., Lawrence, A.R. & Morris, B.L., 1997. Groundwater in Urban Development: Assessing management needs and formulating policy strategies. World Bank Technical Paper 390.

Freeze, R. A. and cherry, J. A., 1979. “Groundwater”. Prentice Hall Inc. New Jersey.

Gaciri, S. J. and Davies, T. C., 1993. “The Occurrence and Geochemistry of Flouride in Some Natural Waters of Kenya”. Journal of Hydraulics, 143, 395 -412.

Ganapuram, S., Kumar, G. T. V., Krishna, I. V. M., Ercan, K., Demirel, M. C., 2009. “Mapping of Groundwater Potential Zones in the Musi Basin Using Remote Sensing Data and GIS”. Advances in Engineering Software, 40(7), 506 – 518.

Gebregziabher, B., 2003. “Integrtaed Geophysical Methods to investigate the geological Structures and Hydrostratigraphic Unit of the Aynalem South East Mekele”. MSc Thesis, Addis Ababa University.

Gevera, P. K., Cave, M., Dowling, K., Gikuma-Njuru, P. and Mouri, H., 2020. “Naturally Occurring Potentially Harmful Elements in Groundwater in Makueni County. South – Eastern Kenya: Effect on Drinking Water Quality and Agriculture”. Geosciences, 10(2).

Ghosh, M. M., O’connor, J. T and Engelbrecht, R. T., 1966. “Rate of Precipitation of Iron in Aerated Groundwaters” Journal of Sanitation Engineering Division, A. M. Society of Civil Engineering, 92.

Gorelick, S. M., 1983. “A Review of Distributed Parameter Groundwater Management Modeling Methods”. Water Resources Research, 19(2), 305-319.

Gupta, N. 2014.“Groundwater Vulnerability Assessment Using DRASTIC Method in Jabalpur District of Nadhya Pradesh”. International Journal of Recent Technology and Engineering (IJRTE), 3(3), 2277-2288.

Hansel, C. M., Benner, S. G., Fendorf, S., 2005. “Competing Fe (II) Induced Mineralization Pathways of Ferrihydrite”. Journal of Environmental Science and Technology, 39, 7147-7153.

Harbaugh, A. W. Banta, E. R., Hill, M. C., Michael, G. and McDonald, M. G., 2000. “MODFLOW -2000” The U.S. Geological Survey Modular Groundwater Model- User Guide to modularization Concepts and groundwater Flow Process. USGS Report 00-92. Reston, Virginia. .

Harbaugh, A. W., 2005. “MODFLOW (2005): The U.S. Geological Survey Modular Groundwater Model- the Groundwater Flow Process”. USGS Techniques and Methods 6-A16. Reston, Virginia.

Hardwick, T. J., 1956. “The Rate Constant of the Reaction between Ferrous ions and Hydrogen Peroxide in Acid Solution”. Canadian Journal of Chemistry. No. 427.

Hem, J. D., and Cropper, W. H., 1959. “Chemical Equilibria and Redox Potential; Chemistry of Iron in Natural Waters”. Geological Survey. Water Supply Paper 1459-A

Herzog, S. D., Person, Kvashnina K. and Kritzberg, S. 2007. “Organic Iron Complexes that Enhance Iron Transport Capacity along Estuaries Salinity Gradients of Baltic Estuaries”. Journal of Biogeosciences, 17, 331- 344.

House, M. A. and Newsome D. H., 1989. “Water Quality Indices for the Management of Surface Water Quality”. Water Science Technology. 21, 1137-1148.

Hove, A., 1973. “Sectorial Study and National Programming for Community and Rural Water Supply”. Sewerage and Water Pollution Control.

Hugo, B. F., 1968. “Dispersion Coefficients in the Natural Streams with Applications to Lower Reaches of the Green and Duwamish River- Washington”. U.S.G.S. Geological Survey Professional Paper number 582-A

Huisman, L. and Wood, W. E, 1974. “Slow Sand Filtration” World Health Organization (WHO), Geneva.

Isaeva, M and Montes Castro, N., 2011. “Water Treatment for the Removal of Iron and Manganese”

Jakeman, A. J., Burreteau, O., Hunt, R. J., Rinaudo, J. and Ross A., 2016. "Integrated Groundwater, Concepts, Approaches and Challenges". Springer International Publishing. A.G. Switzerland.

James, R. E. and Ferries, F. G., 2004 "Evidence for Micribial-mediated iron oxidation at a neutrophibic groundwater spring" Geo chemistry journal. 212, 301-311.

Kahsay, G. H., 2008. "Groundwater Assessment through Distributed Steady State Flow Modeling, Aynelem Wellfield, Mekele, Ethiopia". MSc. Thesis Submitted to the International Institute for Geo-information Sciences and Earth Observation. Enschede. The Netherlands.

Kaluli, W. and Gathenya, M., 2004. "Water Supply and Sanitation in Makueni District. Paper Presented at the 17th WAITRO International Conference held in Nairobi, Kenya from 6th –11th of September 2004.

Kamaraju, M. V., Bhattacharya, A., Reddy, G. S., Rao, G. C., Murthy, G. S. and Rao, T. C. M., 1996. "Groundwater Potential Evaluation of West Godavari District, Andhra Pradesh State, India, A GIS approach". Groundwater, 34 (2), 318–325.

Kapulu, M., Lusambo, E. Haankuku, C., 2013. "Iron Removal in Borehole Water: A case Study of Luapula Province, Zambia".https:www.Researchgate.net Publication/ 28142029.

Kenya Bureau of Standards (KEBS), 1996. Kenya Standard Specification for Drinking Water. Part 1. Kenya Bureau of Standards. Nairobi, Kenya.

Ketata-Mouna, R., Gueddari, M., and Bouhlila, R., 2011. "Use of Geographical Information System and Water Quality Index to Assess Groundwater Quality in El Khairat Deep Aquifer, Enfidha, Tunisian Sahel". Iranica Journal of Energy & Environment, 2(2), 133-144.

Khan, M. A., Pieffer, S. 2003. "Prospecting Groundwater Resources Using Remote Sensing and GIS: Case Study of Arid Western Rajasthan, India. Journal of Indian Society of Remote Sensing, 34(2)

Kim, K., Anderson, M. P. and Bowser, C. J., 1999. "Model Calibration with Multiple Targets: A Case Study. Groundwater". 37 (3), 345–351.

Kiplangat, C. N. and Mutua, F., 2016. "Ground Water Quality Assessment Using GIS and Remote Sensing: A Case Study of Juja Location, Kenya". American Journal of Geographic Information System, 5(2), 12-23.

Kitanidis, P.K., 1997. "Introduction to Geostatistics". Cambridge University Press.

Kithiia, S. M., 2009. "Integrated Surface Water and Groundwater Resources Management in Makueni District, Kenya. Improving Integrated Surface and Groundwater Resources Management in a Vulnerable and Changing World". Proceeding of JS. 3 at the Joint IAHS and IAH Convention. Hyderabad, India, 362-367.

Kiviloog, J, and Fjall, R., 2001. “The Oxygenation Ability of the Ejector Aerator, A Theoretical and Practical Study of Oxygenation for Iron and Manganese Oxidation. Goteborg Chalmers Institute of Technology. Sweden.

Koch, M. and Mather, P. M., 1997. “Lineament Mapping of Groundwater Resources Assessment. A Comparison of Digital Synthetic Aperture Radar (SAR) Imagery and Stereoscopic Lange Formac Camera (LFC) Photographs in the Red Sea Hills”. Sudan International Journal of Remote Sensing, 4471 – 4493.

Krhoda, O. G., 1989. “Groundwater Assessment in Sedimentary Basins of Eastern Kenya, Africa. Regional Characterization of Water Quality”. Proceedings of the Baltimore Symposium.

Kumar, C.P., 2001. Common ground water modelling errors and remediation. *Journal of Indian Water Resources Society*, *21*(4), pp.149-156.

Kumar, M., 2004. “An integrated hydrogeochemical and isotopic Study of NCR-Delhi, India”. Mphil, Jawaharlal Nehru University, India

Kuria, D. N., Gachari, M. K., Macharia, M. W., Mungai, E., 2012. “Mapping Groundwater Potential in Kitui District, Kenya Using Geospatial Technologies”. International Journal of Water Resources and Environmental Engineering, 4(1), 15-22.

La Venue, A. M., and Pickens, J. F., 1992. “Application of a Coupled Adjoints Sensitivity and Kriging Approach to Calibrate a Groundwater Flow Model”, Water Resources Research, 28(6), 1543– 569.

Lapworth, D. P., Boving, T. B., Kreamer, D.K., Kebede, S. and Smedley, P. L., 2022. “Groundwater threats, Opportunities and Realising the Potential of Groundwater”. Journal of Science of Total Environment, 811.

Lee, S., Song, K., Park, I., 2015 “Groundwater Potential Mapping Productivity Potential Mapping Using a Geographic Information System (GIS) based Artificial Neutral Network Saro”. Journal of hydrogeology , 1511-1527.

Lin, X and Yang, Y., 1991. “The Optimization of Groundwater Supply Systems in Shijiaz-Huang City, China”. Water Science Journal, 24(11), 71-76

Ling, E. J., 2011. “Household Water Quality Program: Iron and Manganese in Household Water”. College of Agriculture and Life Sciences, Virginia Polytechnic Institute and State University.

Liou, S., Lo, S. and Wang, S., 2004. “A Generalized Water Quality Index for Taiwan”. Environmental Monitoring Assessment, 96, 35-42.

Llamas, M. R. and Custodio, E., 2002. “Intensive Use of Groundwater: a new Situation which demand Proactive action”. In Intensive Use Groundwater, 13-31. Lisse the Netherlands: Balkema

Luo, W. Gao, X. Ziang, X. 2018 “Geochemical Processes Controlling the Groundwater Chemistry and Fluoride Contamination in the Yuoncheng Basin, China. An Area With Complex Hydrogeochemical Conditions. PLoSONE 13(7)ne.0199082.”

Mailu, G. M., 1997. “The Impact of Urbanization on Groundwater Quality in Wajir Town, Kenya. Freshwater Contamination”. Proceedings of Rabat Symposium S4, IAHS Publ. no. 243.

Mailu, G. M., 1994. “The Influence of Precambrian Metamorphic Rocks on Groundwater in the Chyulu Area, Kenya.”. Journal of applied Hydrogeology, 2, 26-32.

Mailu, G. M. 1983. “The Hydrogeology of the Athi Basin”. M.Sc. Thesis. University of Nairobi.

Maina, J. W., 1982. “Groundwater Chemistry of the Area to the Immediate North of Nairobi Conservation Area’’. M.Sc. Thesis. University of Nairobi.

Majkic-Dursun, B., Petkovic, A. and Dimkic, M., 2015. “The Effect of Iron Oxidation the Groundwater of the Alluvial Aquifer in the Velika Morava River, Serbia, on the Clogging of Water Supply Wells”. Journal of the Serbian Chemical Society, 947-957.

Mbithi, F.M. Patrick, C.K. and Peter, G. N., 2017. “Assessment of the Impact of Groundwater Flouride on Human Health: Case Study of Makindu District in Kenya”. Journal of Earth Science and Climate Change, 8

McDonald, M.G. and Harbaugh, A.W., 1988. A modular three-dimensional finite-difference ground-water flow model. US Geological Survey.

McDonald, M. G. and Harbaugh A. W., 2000. “MODFLOW Code and Manual, U.S. Geological Survey Modular Ground-Water Model”

Michieka, D. O. and Van der Pour, 1977. “Soils and Vegetation of the Kiboko Range Research Station”. Semi-Detailed Soil Survey Report Number 53. Kenya Soil Survey, Nairobi.

Mohamad, B. A. M., 2013. “Knowledge and Data Driven Approach to GIS Modelling Techniques for Groundwater Potential Mapping at the Upper Langat Basin, Malaysia”, Ph.D Thesis presented to the University of Putra, Malaysia.

Mohesn, S., Abess, O. and Hamed, M., 2009. “Development of Groundwater Quality Index”. Environment Monitoring and Assessment, 163, 337-335.

Morris, B. L, Lawrence, A. R., Chilton, P.J., Adams, B., Caylow, R. C. and Clinck, B. A., 2003. “Groundwater and its Susceptibility to Degradation: a Global Assessment of the Problem and

Options of Management."UNEP Early warning and Assessment report series RS. 03-3 Nairobi -Kenya

Moser, B., Bekhazarova, M., Whiley, H., Keerthirathne, T. P., Harrington, N., Degraris, K. and Wallis, I., 2021. "Investigation into the cause of Iron-Related Clogging of Groundwater bores in Viticulture in the Limestone Coast, South Australia"

Mullaney, J. R., Lorenz, D. L. and Arritson, A. D., 2009. "Chloride in Groundwater and Surface Water in Areas Underlain by the Glacial Aquifer System. Northern United States". USGS Scientific Investigations Report 2009-5086.

Murphy, K. S. R., 2000. "Groundwater Potential in a Semi-Arid Region of Andhra Pradesh: a Geographical Information System Approach". International. Journal of Remote Sensing, 2(9), 1867-1884.

Mutreja K. N., 1986. "Applied Hydrology" Tata Mcgraw-hill publishing Company limited first edition, Page 661.

Mwango, F. K., Muhang'u, B. C., Juma, C. O. and Githae, I. T., 2002. "Groundwater Resources in Kenya". Proceedings of the International Workshop on Managing Shared Aquifer Resources in Africa, 93–100.

Nair, K. R., Manji, F and Gitonga, J. N., 1984. "The Occurrence and Distribution of Flouride in Groundwater in Kenya" East African Medical Journal, 61(7), 503–512.

Nanyaro, J. T., Aswathanarayana, U. and Mungure, J. S., 1984. "A Geochemical Model for the Abnormal Flouride Concentration in Waters in Parts of Northern Tanzania". Journal of African Earth Science, 2(2), 129-140.

Neukum, C. and Azzam, R., 2008. "Quantitative Assessment of Intrinsic Groundwater Vulnerability to Contamination Using Numerical Simulations". Science of the environment, 5, 799–812.

Nik, N., Nik, D., Nur. H., Izehar, B. Y., Thamer, A. M., and Ahsan, A., 2013. "Groundwater Quality Improvement by Using Aeration and Filtration Methods". World Academy of Science, Engineering and Technology. 7.

Nyaberi, D., Baswet, E., Barongo, J., Ogendi, G and Kariuki, P., 2019. "Mapping of groundwater through Integration of Remote Sensing and Vertical Sounding in ASALs: A Case Study of Turkana South Sub-County, Kenya". Journal of Geoscience and Environmental Protection, 7, 229-243.

Odel, L., 2001. "High Rate Iron and Manganese Removal for Small Systems", AWWA Annual Conference proceedings, Washington D.C. USA.

Ochungo, E.A., Ouma, G.O. Obiero, J.P.O. and Odero, N. A., 2019. “Water Quality Index for assessment of Portability of Groundwater Resource in Langata Sub-County, Nairobi-Kenya”. American Journal of Water Resources, 7(2), 62-75.

O’Leary, D. W., Friedman, J. D. and Pohn, H. A., 1976. “Lineament, Lineation; Standards for Geological Society”. Amer Bull 87, 1463–1469.

Onyancha, C. and Getenga, Z., 2013. “Geochemistry of Groundwater in the Volcanic Rocks of Nairobi City”. Global Journal of Science Frontier Research Environment & Earth Science, 13(3).

Patil, S. B. and Chore, H. S., 2014. “Contaminant Transport through Porous Media: An Overview of Experimental and Numerical Studies”. Advances in Environmental Research, 3(1), 45-69

Priya, U., Iqbal, M.A., Salam M.A., Nur-E-Alam, Md., Uddin, M.F., Abu Reza Md., Islam, T., Sarkar, S.K., Imran, S.I., Rak, A.E. 2022. "Sustainable Groundwater Potential Zoning with Integrating GIS, Remote Sensing, and AHP Model: A Case from North-Central Bangladesh," Sustainability, MDPI, vol. 14(9), pages 1-24, May.

Rahmati, O., Samani, A. N., Mahdavi, M., Pourghasemi, H. R., and Zeinivand, H. (2015). Groundwater potential mapping at Kurdistan region of Iran using analytic hierarchy process and GIS. Arabian Journal of Geosciences, 8(9), 7059-7071.

Raju, N., 2006. “Iron Contamination in Groundwater in Tirupata-Tirupata Environments”. Nigerian Bureau of Standards.

Rao, P. J., Harikrishna, P., Srivastav, S.K., Satyanarayana, P. V. and Rao, B. B. D., 2009. “Selection of Groundwater Potential Zones in and Around Madhurwada Dome, Visakhapatnam District: A GIS approach”. Journal Indian Geophysics, 13(4), 191–200.

Rausch, R., Schafer, W., Therrian, R. Wagner, C., 2005. “Solute Transport Modeling: An Introduction to Models and Solution Strategies”. 205.

Rusiniak, P., Sekula, K., Sracek, O. and Stopa, P., 2021. “Flouride ions in Groundwater of the Turkana County, Kenya, East Africa”. Journal of Geochemistry, 40(6), 945-960.

Ritter, J. R. R. and Kaspar, T., 1997. “A Tomography of the Chyulu Hills, Kenya”.

Saggerson, E. P., 1963. “Geology of the Simba–Kibwezi Area”. Report Number 58. Geological Survey of Kenya. Government of Kenya.

Sander, P., Chesley, M. M., Minor, T. B., 1996. “Groundwater Assessment using Remote Sensing and GIS in a rural Groundwater Project in Ghana: Lessons Learned”. Journal of hydrogeology, 4, 40-44.

Sarikeya, H. Z., 1990. “Contact Aeration for Iron Removal – A Theoretical Assessment”. Water Research, 24(3), 329-331.

Saxena, V.K and Ahmed S. 2003. “Inferring the Chemical Parameters for the Dissolution of Flouride in groundwater”. Environmental Geology. Vol. 43. Pg. 731-736.

Sener, E., Davraz, A. and Ozcelik, M., 2005. “An Integration of GIS and Remote Sensing in Groundwater Investigations: A Case Study in Burdur, Turkey”. Hydrogeol. J., 13, 826-834.

Shahid, S., Nath, S. K. and Roy, J., 2000. “Groundwater Potential Modelling in a Soft Rock Area using GIS”. International Journal of Remote Sensing, 21(9), 1919-1924.

Shiklomanov, I. A., 1998. “World Water Resources: A new appraisal and assessment for the 21st Century”. UNESCO-IHP Publication.

Shupel, J. L., Olson, A. E. and Sharma, R., 1979. “Effect of Fluorides in Domestic and Wild Animals”. Toxicity of Heavy Metals in the Environment, Part 2.

Simmers, I., 1997. “Recharge of Phreatic Aquifers in Semi-Arid Areas”. Journal of Hydrogeology, 19. 27.

Simpson, M. J. and Landman, K. A., 2007. “Analysis of Split Operator Methods Applied to Reactive Transport with Monod Kinetics”. Advances in Water Resources, 30(9), 2026–2033.

Singer, P. C. and Stumm, W., 1969. “Oxygenation of Ferrous Iron: The Rate – Determining Steps in the Formation of Acidic Mine Drainage”. Federal Water Pollution Control, U.S.D.I.

Singh, D. F., 1992. “Studies on the Water Quality Index of Some Major Rivers of Pune, Maharashtra”. Proceedings of the Academy of Environ. Biol. 1(1), 61-66.

Singh, P. and Khan, I. A., 2011. “Groundwater Quality Assessment of Dhankawadi Ward of Pune using GIS”. International Journal of Geomatics and Geosciences, 2(2), 688-703.

Siwila, S., Chota, C., Yambani, K., Sampa, D., Siangalichi, A., Ndawa, N. and Tambwe, G., 2017. “Design of Small Scale Iron and Manganese Removal System for Copper University Borehole Water, Journal of Environmental Geology, 1(1).

Spath, A., Anton, P., and Norbert, O. P., 2001. “Plume-lithosphere Interaction and the Origin of Continental Rift-Related Alkaline Volcanism; the Chyulu Hills Volcanic Province, Southern Kenya”. Journal of Petrology, 42(4), 765-787.

Spitz, K. and Moreno, J., 1996. “A Practical Guide to Groundwater and Transport Modeling”. New York, John Wiley and Sons Inc.

Stumm, W. and Lee, G. F., 1961. Journal of Hydraulics. 22.

Sung, W. and Morgan, J. J., 1980. “Kinetics and Product of Ferrous Oxygenation in Aqueous System “. Journal of Environmental Science and Technology, 14(5), 561-568.

SunpriyaAchary, G., 2014. “Studies on Groundwater Pollution due to Iron Content in Bhubaneswar, Odisha, India”. International Journal of Current Engineering and Technology. Vol. 4. Issue 1.

Syazwan, M. F., Mohd Renny Rozainy, M. A. Z. and Jamil, R., 2020. “Removing Iron and Manganese by Using Cascade Aerator and Limestone Horizontal Roughing Filters”. 2nd Joint Conference on Green Engineering Technology and Applied Computing. Material Science and Engineering.

Todd, D.K., 1980. “Groundwater Hydrology”. Wiley, New York. 2nd edition, 556

Valoucchi, A. J. and Malmstead A., 1992. “Accuracy of Operator Splitting for Advection – Dispersion Reaction Problems” Water Resources, 28, 1471-1476.

Vilhelmsen, T. N., 2012. “Groundwater Flow in Geological Complex Areas Using Local Grid Refinement, Combined Parameterization Methods and Joint Inversion”. A Thesis Submitted in Partial Fulfilment of the Requirement of the Ph. D. Department of Geosciences, Aarhus University, Denmark.

Volodymyr, O., Osadchyy, V., Nabyvanats, B., Linnik. P. Osadcha, N and Nabyvanets, Y. 2016. “Processes of Determining Surface Water Chemistry”. Springer International Publishing, Switzerland.

Whelan, G and Castleton, K. J., 2006. “Groundwater Modeling System Linkages with the Framework of Risk Analysis in Multimedia Environmental Systems”. Pacific Northwast National Laboratory, United States Department of Energy.

WHO, 1994, Water Quality Standards. Published by World Health Organization. Geneva, Switzerland.

Wilson, J. D. and Naff, R. L., 2004. “MODFLOW 2000: The U S Geological Survey Modular Groundwater Model – GMG Linear Equation Solver Package Documentation”. U. S. Geological Survey, Denver. Colorado.

Wright, E. P., 1982. “Groundwater Resources of the Chyulu Hills”. Institute of Geological Science, Wallingford.

Yang, L., Steefel, C. I., Marcus, R. K., Dong, H., Shelobolina, E. S., Zhang, J., Kim, J., 2005. “Effects of Redox Cycling of Iron in Nontronite on Reduction of Technetion”. Chem. Geol. 291, 206-216.

Yihdego, Y. and webb. J. A. 2015. “Use of a Conceptual hydrogeological Model and a Time Variant Water Budget Analysis to Determine Controls on Salinity in Lake Burrumbeet in Southeast Australia”. Journal of Enviromental Earth Sciences, 73, 1587-1600.

Yogendra and Puittaiah, 2008. “Determination of Water Quality Index and Suitability of an Urban Waterbody in Shimoga Town, Karnataka”. Proceedings of the 12th World Lake Conference, 342-346.

Zhao, Z., Jing, L. and Neretieks, I., 2010. “Evaluation of Hydrodynamic Dispersion Parameters in Fractured Rocks”. Journal of Rock Mechanics and Geotechnical Engineering, 2(3), 243-254

Zengh, C., 1990. “MT3D; A Modular Three Dimensional Transport Model for Simulation of Advection, Dispersion and Chemical Reactions of Contaminants in Groundwater Systems”. USA

Zengh, C. and Bennet G. D, 2002. “Applied Contaminant Transport Modeling” second edition, Singapore John Wiley and Sons.

Zysset, A. Stauffer F. and Dracos T., 1994. “Modeling of Chemically Reactive Groundwater Transport: Water Resources, 30, 2217-2228.

APPENDICES

APPENDIX A

Appendix I : Monthly Rainfall

Table A.1 Monthly rainfall for Makindu Weather Station Courtesy of Meteorological department of Kenya

Year	24 hour and Annual Rainfall (mm)																
Month	1980	1981	1982	1983	1984	1985	1986	1987	1988	1989	1990	1991	1992	1993	1994	1995	1996
January	42.5	0	1	0.3	27.7	3.1	15	7.5	4.7	48.5	29.2	17.5	20.5	36.3	0.3	2.7	2.2
February	18.9	0	0	25.1	0	18	0.1	0	0.8	1.2	53.7	0.3	0	53.5	38.3	40	51.2
March	42.5	29.5	6.9	1.8	5.6	16.8	15.6	13.1	42.3	39.8	30.5	15.2	8	16.7	49.6	56.4	61.9
April	41	98.3	43.2	18.2	65.4	22	45.4	24.2	26.4	90.7	20.8	29.6	40.5	0.6	70.1	6.7	22
May	17.3	25.3	27.7	6.9	0	6.8	11.9	32.3	5.6	32.3	7	9.8	22.8	1.2	4.8	6.4	12.1
June	0	0	0.3	0.1	0	0.2	5.7	12.2	6.3	0.2	0	2	0	0.5	0	0	1.7
July	0	0	1.6	0.5	0.8	1	0	0.9	1.3	0	0	1.4	0	0	0.2	0.3	0.8
August	4.1	0.4	1	0	0	0	3	0.7	0.9	0.7	0	13.3	0	1.9	0	0.2	0
September	0.1	2.4	6.1	2.3	0.2	0.8	0	0	1.4	0.3	0.2	0	2.4	0	0.3	0	0.3
October	0.6	18.9	28.9	0.3	27.3	30.1	11.4	0.5	2	53	4.6	0.2	71.7	58.5	7	29.9	0
November	50.9	10.9	94.7	9	81.3	44.4	49.5	47.0	43.4	37.5	38.3	91.9	43.6	28.4	59.2	18	47.8
December	13.3	42.9	37.4	45.7	82.6	180.2	55	9.6	52.9	45.4	37.2	18.3	33.4	35	34.1	23.3	3
Annual Rainfall	231.6	228.6	248.8	110.2	290.9	323.4	212.6	148	230.3	349.6	221.5	199.5	242.9	232.6	263.9	183.9	203

Table A.2 Courtesy of Meteorological department of Kenya(Contd.)Courtesy of Meteorological department of Kenya (continued)

Year / Month	24 Hour and Annual Rainfall (mm)																
	1997	1998	1999	2000	2001	2002	2003	2004	2005	2006	2007	2008	2009	2010	2011	2012	2013
January	0.2	58.1	4	3.4	0.1	10.6	0.3	37.4	3.1	1.3	64.9	36.9	14.5	10.2	10.5	3.7	17
February	0	101.9	0	0	0.9	2.7	34.6	16.7	0	0.2	4.9	5.2	7.9	85.6	34.8	4.5	0
March	8.1	26.4	25.4	11.8	36.8	54.7	58.5	46.8	18.4	21.5	18.5	92.2	1.1	82.8	50.8	16.7	19
April	59.1	30.5	18.6	67.1	45.6	18.2	24.2	10.1	17.4	48.7	39.2	4.8	17.1	24.7	1.2	67	62
May	20.5	31.5	1.3	1.8	0.1	23.7	14.3	0	24.2	25.5	2.7	1	11	11.2	3.3	13.1	15.4
June	3.1	15	0.5	1.8	0.8	0.4	0	0.3	0	3.1	1	0	0.3	0	0	0.3	0
July	0	4.8	0	0.7	0	0	0	0	0.4	0	0.3	0	0	0	0	0	0
August	0	0	0.8	3.4	0	3.1	0	0.2	2.2	0	0	0	0	0	0.1	2.1	0
September	0	1.1	0	3.4	0	16.1	0.5	1	1.6	0	0	1.3	0	0.8	0.3	0.3	0
October	7	0.4	0.2	0	0.5	12.1	0	12.9	5.8	7	5	13	17.3	2.6	24	1.2	3
November	44.8	30.8	73.5	43.6	0	30.9	16.6	9.6	12.3	44.8	28.7	53	15.6	57.6	33	50.7	268.3
December	31.4	4.6	21.5	114.9	130	35.7	40.9	20.8	2.8	17.5	63	3.5	47.8	36.2	61.2	25.1	41.5
Annual Rainfall	174.2	305.1	146	251.9	271.5	208.2	189.9	155.8	109	169.6	228.2	210.9	132.6	311.7	219.2	184.7	425.9

Table A.3 Monthly rainfall for Makindu Weather Station (Contd.) Courtesy of Meteorological department of Kenya (continued)

Year	24 Hour and Annual Rainfall (mm)	
Month	2014	2015
January	0	0
February	19	45.2
March	17.2	21.7
April	27.8	23.1
May	5	45.4
June	0	1
July	0	1.2
August	0	0
September	30	0
October	0	0.1
November	21.8	26.7
December	26.7	19.8
Annual Rainfall	147.5	184.2

Appendix II : The Boreholes Used in the Chyulu Aquifer Study

Table A.4 The boreholes used in the chyulu aquifer

ID. No.	Name of Borehole	UTM Coordinates X	UTM Coordinates Y	Yield (m^3/day)	Depth (m)	Altitude (AMSL)
MK1	Jamia Mosque A	368779	9748818	9.00	120	1007
MK2	Jamia mosque B	368789	9748822	7.20	135	999
MK3	Sikh Temple A	368747	9747601	8.10	91	1006
MK4	Sikh Temple B	368789	9747604	7.52	85	1005
MK5	Makindu Hospital	369230	9747647	6.86	110	990
MK6	Makindu Railway	369736	9759147	5.80	65	990
MK7	Makindu Water	367735	9759158	8.10	78	996
MK8	Makindu Mission 1	360589	9749384	6.52	84	1004
MK9	Makindu Mission 2	369589	9749383	7.50	51	1002
MK10	Makindu Sisters	368779	9741726	8.55	66	1003
MK11	Musimba 1	374289	9741666	6.12	150	1010
MK12	Musimba 2	374118	9742653	6.80	120	993
MK13	Musimba 3	372840	9743415	5.60	89	988
MK14	Musimba 4	371846	9751510	5.90	224	970
MK15	Kisingo	374684	9744605	12.5	98	1036
MK16	Makilya Invest	366612	9751194	8.80	120	990
MK17	Makilya Invest	366611	9751193	9.65	64	985
MK18	Makau Boniface	366637	9747604	7.20	56	935
MK19	Ndivo Invest 1	366558	9747601	12.9	34	986
MK20	Ndivo Invest 2	366565	9747602	12.5	37	970
MK21	Experiment Farm	365451	9749046	8.20	47	985
MK22	Kyeni	372397	9748748	8.42	56	935
MK23	Kai	374008	9747935	6.52	98	986
MK24	Katuluni	375288	9754345	15.6	56	970
MK25	Mulili	369285	9752125	8.6	86	1025
MK26	Kitala	390658	9722227	16.0	56	992
MK27	Kambo	395977	9713205	12.5	98	982
MK28	Komboyoo	389206	9712346	5.22	56	947
MK29	DWD, Kibwezi 1	381363	9738438	2.88	107	840
MK30	DWD, Kibwezi 2	390789	9722224	0.42	136	940
MK31	Muthama	385466	9737171	7.10	70	986
MK32	DWD, Kibwezi 3	386926	9734684	6.50	119	859
MK33	Masongaleni 1	399933	9738451	2.72	25	875
MK34	Masongaleni 2	403602	9738454	2.52	26	875
MK35	Teresia Sol. Ndunda	385954	9834852	1.50	130	893
MK36	Muli Ndambuki	385615	9806203	4.80	75	896
MK37	Boni. Kyalo	385026	9729371	3.00	100	890
MK38	Kiboko Research	359111	9751244	12.52	101	1015
MK39	Kiboko Usungo	362773	9760534	9.6	92	1005
MK40	Kibwezi Action Aid	386364	9742090	10.6	94	960
MK41	Masongaleni 3	392535	9729196	6.4	56	838
MK42	Kiboko	362773	9760534	8.4	86	854
MK43	S.M.Mbova	370257	9722176	4.8	119	1070

Appendix III : Results of Tests of Physical-Chemical Parameters

Table A.5 Results of tests of physical-chemical parameters of groundwater from representative boreholes in June 2015 (dry season)

	Name of Borehole	UTMX	UTMY	Water Quality Parameters						
				pH	Turbidity (NTU)	Ec µS/cm	TDS (mg/L)	Colour (TCU)	Fe	Mn
MK1	Jamia Mosque (A)	368779	9748618	6.95	3.0	16020	10252.8	7.5	4.21	0.206
MK2	Jamia Mosque (B)	368785	9748622	6.98	16	12550	7808.3	12.5	4.42	0.1311
MK3	Sikh Temple (A)	368747	9748601	7.12	7.12	7650	4413.5	5.0	4.52	1.65
MK4	Sikh Temple (B)	368789	9748604	6.95	6.95	7256	4329.1	5.0	4.18	2.07
MK5	Makindu Hosp.	369230	9747647	6.89	10	6900	4416	15	5.35	32.86
MK6	Makindu railway	369736	9759147	6.84	110	2310	1420	25	5.34	0.15
MK7	Water Makindu	367735	9759158	7.05	22.5	6251	4421.20	15	4.53	5.45
MK8	Makindu Mission 1	369589	9749384	7.40	1.0	14320	9164.8	7.5	5.21	0.15
MK9	Makindu Mission 2	369589	9749383	7.40	1.0	14320	9170.8	7.5	5.21	0.15
MK10	Makindu Sisters	368779	9749726	6.75	16	9520	6093	7.5	5.37	15.20
MK11	Musimba 1	374289	9741666	7.19	27.3	4120	2636.8	15	1.802	0.350
MK12	Musimba 2	374118	9742653	7.1	15.1	3200	2100	12.5	1.90	0.6
MK13	Musimba 3	372840	9743415	7.05	5.5	1995	120	7.5	4.1	0.95
MK14	Musimba 4	371846	9751510	6.91	10	2600	1675	5	5.12	1.50
MK15	Kisingo	374684	9744605	6.85	15	1150	670	5	4.75	2.50
MK16	Makilya Invest 1	366611	9751194	7.05	10	850	550	15	5.44	0.95
MK17	Makilya Invest 2	366620	9751199	7.05	12	1850	1180	15	5.44	0.95
MK18	Makau Boniface	366637	9747604	7.13	15	1500	1235	12.5	4.50	0.88
MK19	Ndivo and Co	366558	9747602	7.05	10	850	540	7.5	5.54	0.75
MK20	Ndivo and Co	366565	9747601	6.85	18.5	2550	1641	7.5	5.23	0.95
MK21	Experimental Farm	365451	9749046	6.99	2.5	3150	2010	5	4.6	1.01
MK22	Kyeni	372397	9748748	7.15	17.5	8500	5420	5.0	4.22	2.4
MK23	Kai	374008	9747935	6.96	10.5	1850	1165	1	3.81	1.5
MK24	Katuluni	375288	9754345	7.11	20	5235	3345	2.5	2.88	1.41
MK25	Mulili DWD	369285	9752125	6.75	15	8730	5590	5.0	1.88	3.5
MK26	Kitala	390658	9722227	7.21	2.5	6730	4708	7.5	4.21	0.25
MK27	Kambo	395977	9713205	6.88	14.4	6320	4044.8	2.5	5.56	0.53.
MK28	Komboyoo Water	389206	9712346	7.56	10	1680	1075	5.3	4.8	33.6
MK29	Kibwezi 1	381363	9738438	7.75	5	494	310	5.0	1.72	0.05
MK30	Kibwezi 2	390789	9722224	7.75	5	484	315	5.0	1.72	0.05
MK31	Muthama	385466	9737171	7.10	15	4330	2270	7.5	2.6	0.28
MK32	Kibwezi	386926	9734684	7.60	1.5	484	306	5.0	1.72	0.05
MK33	Masongaleni	399933	9738451	8.20	25.0	1905	1140	5.0	4.7	0.45
MK34	Masongaleni	403602	9738454	8.00	25.0	1900	1140	5.0	4.7	0.4
MK35	Teresia Ndunda	385954	9834852	6.58	1	655	419.2	7.5	5.12	1.3
MK36	Muli Ndambuki	385615	9806203	8.1	61	762	487.68	5.0	1.8	2.67
MK37	Kyalo Muteti	385026	9729371	7.12	2.5	4740	3048	5	1.77	0.010
MK38	Kiboko Reaesrch	359111	9751244	6.88	5	2350	1880	12.5	3.22	0.76
MK39	Kiboko Usungo	362773	9760534	7.32	1.5	3420	2480	2.5	5.76	0.43
MK40	Kibwezi A. Aid	386364	9742090	6.99	2.5	4350	3418	10	4.21	0.23
KM41	Masongaleni Aid	392535	9729196	6.98	30	2315	1895	15	3.11	0.90
MK42	Kiboko	362773	9760534	7.05	5	1400	1241	17.5	4.20	0.19
MK43	S.M..Mbova	370257	9722176	7.20	1	4592	2750	5.0	5.88	0.525

Table A.6 Results of tests of physical-chemical parameters of groundwater from representative boreholes in June 2015 (dry season) continued

Code	Borehole Identity	Water Quality Parameters									
		Mg	Ca	Na	K	Flou ride	Chlor ide	SO^{-}_{4}	NO_3^-	Alkali nity	Hardness
MK1	Jamia Mosque (A)	1.97	37.33	148.5	5.25	3.7	52.65	201	48.6	152	178.6
MK2	Jamia Mosque (B)	2.55	295.00	125.9	4.54	4.20	47.5	240.2	44.6	182	202.6
MK3	Sikh Temple (A)	2.54	286.0	135.6	18.45	5.1	36.54	212.0	65.5	320	936.4
MK4	Sikh Temple (B)	1.95	338.8	154.2	26.24	5.5	45.21	235.0	34.5	384	500.0
MK5	Makindu Hosp.	1.93	32.84	362.0	4.60	5.1	41.25	121.3	24.8	324	1180
MK6	Railway station	1.78	21.88	211.9	5.25	6.5	51.15	187.1	8.73	325	880
MK7	Min.Water- Makindu	2.76	360.0	402.0	4.84	3.8	45.75	75.15	23.4	392	304
MK8	Makindu Mission 1	1.94	40.13	395.6	18.35	7.5	48.50	110.0	34.5	140	1180
MK9	Makindu Mission 2	2.92	76.18	346.4	18.99	6.55	58.50	231.0	36.5	132	1010
MK10	Makindu Sisters	1.85	40.75	399.5	16.99	8.2	42.87	119.0	14.2	404	835.4
MK11	Musimba 1	1.93	53.6	351.0	3.60	3.6	4.55	88.56	11.2	114	354.6
MK12	Musimba 2	1.12	121.0	289.0	6.85	1.9	45.65	254.6	56.3	421.3	624.5
MK13	Musimba 3	1.69	63.60	324.8	3.87	4.54	24.54	82.56	19.2	243	364.3
MK14	Musimba 4	2.12	129	254.0	10.85	2.60	41.65	187.6	46.3	461.8	639.5
MK15	Kisingo	15.7	16.5	125.0	23.8	5.70	56.0	88.55	35.5	159	545.0
MK16	Makilya Investment	27.5	23.90	56.45	12.5	2.8	15.5	85.5	150	170	675.0
MK17	Makilya Investment	25.1	23.90	56.45	12.5	3.0	45.2	85.5	150	170	675.0
MK18	Makau Boniface	5.55	23.9	56.45	12.5	2.8	15.5	92.5	45	185	343.7
MK19	Ndivo and Co	7.54	44.13	55.22	12.6	5.75	6.8	96.55	55.0	239	453
MK20	Ndivo and Co	18.5	34.8	56.5	12.6	3.5	6.8	96.55	55.0	239	453
MK21	Experimental Farm	42.5	231.8	246.1	8.9	4.70	18.9	64.5	18.6	454	360
MK22	Kyeni	24.6	428.6	135	12.56	3.70	34.60	36.4	52.0	346	432
MK23	Kai	46.9	78.3	196	9	5.40	21.5	28.4	33.6	132	724.5
MK24	Katuluni	12.6	342.9	153.6	28.5	2.90	23.8	48.9	41.5	208	635.5
MK25	Mulili DWD	8.75	98.4	65.4	17.4	3.0	10.8	86.5	70.0	261	510
MK26	Kitala	1.96	65.4	148.0	3.64	4.5	120.55	210.1	51.2	154	345.4
MK27	Kambo	4.96	556	295.5	4.20	2.8	125.0	248	22.0	131	305
MK28	Komboyoo	50.4	0.8	144.2	8.2	3.60	3.063	123.7	22.1	172	501
MK29	Kibwezi	70.0	25.18	30.31	75.4	2.43	0.56	128	35.5	94	80
MK30	Kibwezi	1.70	25.18	30.31	83.23	1.79	0.56	128	35.5	94	56
MK31	Muthama	8.76	31.02	29.0	83.23	1.79	56.43	47	2.83	350	1060
MK32	Kibwezi	64.2	25.18	30.31	7.6	4.60	23.9	128	35.5	94	8
MK33	Masongaleni	100	133	10.20	83.23	4.5	108.4	88.0	12.8	112	690
MK34	Masongaleni	90.6	133	10.20	15	4.5	167	88.0	12.8	112	690
MK35	Teresia Ndunda	83.0	286.4	95.90	15	1.79	180	135.6	65.0	192	585
MK36	Muli Ndambuki	24.8	34.60	94.50	2-	5.80	19.60	54.8	54.5	345	560
MK38	Kyalo Muteti	56.8	5.868	48.50	42.0	4.21	34.96	64.8	42.8	412	512
MK39	Kiboko Reaesrch	42.6	5.68	24.20	8.4	3.50	25.6	24.5	18.9	421	586
MK40	Kiboko USU	2.40	68.3	18.0	29	2.56	43.8	48	24.5	285	544
KM41	Kibwezi action Aid	1.89	23.90	143.0	9.45	4.31	128.0	84.6	19.0	276	60
MK42	Masongaleni A. Aid	2.64	83.8	55.6	4.66	2.54	34.90	93	9.89	368	514
MK42	Kiboko	16.8	23.76	69.3	42.7	1.6	21.85	86.5	4.48	348	398
MK43	S. Mbova	54.0	135.6	34.8	25.6	4.80	45.90	128	23.5	342	564

Table A.7 Results of tests of physical-chemical parameters of groundwater from representative boreholes during the wet season in November 2015 (wet season)

Code	Name of Borehole	UTMX	UTMY	Water Quality Parameters						
				pH	Turbidity (NTU)	Ec µS/cm	TDS (mg/L)	Colour (TCU)	Fe	Mn
MK1	Jamia Mosque (A)	368779	9748818	6.89	5	11239	7580	12.5	4.19	0.35
MK2	Jamia Mosque (B)	368785	9748822	7.10	17.5	12004	7612	10	4.38	0.66
MK3	Sikh Temple (A)	368747	9748601	7.16	15	7520	4495	15	4.73	1.5
MK4	Sikh Temple (B)	368789	9748604	7.02	12	6930	4398	5	4.83	1.45
MK5	Makindu Hosp.	369230	9747647	6.95	10	6530	4221	5	5.41	3.86
MK6	Railway station	369736	9759147	7.01	88	2510	1477	25	5.25	0.15
MK7	Min. Water Makindu	367735	9759158	7.11	20	6331	4462	5	4.86	5.48
MK8	Makindu Mission 1	369589	9749384	7.46	2.5	12208	7812	5	4.99	0.45
MK9	Makindu Mission 2	369589	9749383	7.18	12.5	11668	7601	5	4.96	0.86
MK10	Makindu Sisters	368779	9749726	7.22	5.0	8815	4539	5	4.64	5.20
MK11	Musimba 1	374289	9741666	7.08	10	8725	4508	15	4.11	0.35
MK12	Musimba 2	374118	9742653	6.92	25	7810	4354	15	4.36	1.20
MK13	Musimba 3	372840	9743415	7.10	17.5	7816	4358	10	4.56	1.05
MK14	Musimba 4	371846	9751510	6.95	15.0	7516	4426	5	4.66	0.95
MK15	Kisingo	374684	9744605	6.82	5	1250	720	2.5	5.12	1.22
MK16	Makilya Investment 1	366611	9751194	7.01	15.0	1015	655	25	4.92	0.85
MK17	Makilya Investment 2	366620	9751199	6.95	12.5	1135	711	1	4.88	1.20
MK18	Makau Boniface	366637	9747604	7.12	10	2150	1331	15	4.92	1.33
MK19	Ndivo and Co	366558	9747602	7.08	2.5	2770	1536	5	4.11	0.40
MK20	Ndivo and Co	366565	9747601	6.95	10	1650	1080	15	5.12	2.3
MK21	Experimental Farm	365451	9749046	7.15	20	2955	1652	17.5	4.61	0.53
MK22	Kyeni	372397	9748748	7.05	15	6550	4496	15	4.19	1.33
MK23	Kai	374008	9747935	6.96	12.5	1850	1712	1	4.33	1.15
MK24	Katuluni	375288	9754345	7.05	10	4850	3140	5	4.12	4.32
MK25	Mulili WD	369285	9752125	6.95	5.0	7440	4326	2.5	4.59	1.33
MK26	Kitala	390658	9722227	6.85	5.0	6500	4491	1.0	4.83	1.49
MK27	Kambo	395977	9713205	6.91	17.5	6650	4510	2.5	5.62	0.80
MK28	Komboyoo	389206	9712346	7.69	10.0	2536	1410	1.0	4.92	0.90
MK29	Kibwezi 1	381363	9738438	7.21	1	2450	1406	2.5	4.81	1.10
MK30	Kibwezi 2	390789	9722224	7.05	12.5	2100	1286	1.0	4.92	1.20
MK31	Muthama	385466	9737171	7.26	5.0	2836	1640	2.5	4.79	1.42
MK32	Kibwezi	386926	9734684	7.11	5.0	2618	1510	2.5	4.18	0.99
MK33	Masongaleni	399933	9738451	6.98	2.5	1990	1180	1.0	6.90	0.80
MK34	Masongaleni	403602	9738454	7.49	5.0	2105	1350	5.0	4.65	1.30
MK35	Teresia Ndunda	385954	9834852	6.60	22.5	1850	1121	1.0	4.46	1.70
MK36	Muli Ndambuki	385615	9806203	7.90	50	891	624	5.0	4.18	0.6
MK37	Kyalo Muteti	385026	9729371	7.50	5	4610	3018	20.0	3.92	0.28
MK38	Kiboko Reaesrch	359111	9751244	6.98	25	2880	1628	1.0	4.25	0.10
MK39	Kiboko Usungo	362773	9760534	7.10	10	3550	2020	20	5.10	1.20
MK40	Kibwezi action Aid	386364	9742090	7.80	2.5	3620	2148	5	4.58	0.42
KM41	Masongaleni A. Aid	392535	9729196	7.54	22.5	2134	1680	7.5	4.11	0.80
MK42	Kiboko	362773	9760534	7.18	5	1350	780	5	4.31	0.71
MK43	S.M..Mbova	370257	9722176	7.21	5	3100	2989	1	5.61	1.02

Table A.8 Physical-chemical parameters of groundwater from representative boreholes during the wet season in November 2015 (continued)

Code	Borehole Identity	Water Quality Parameters									
		Mg	Ca	Na	K	F	Cl	SO^{-}_{4}	NO_3^-	Alkalinity	Hardness
MK1	Jamia Mosque (A)	1.80	138.2	146	11.4	5.31	40.2	196	38.2	328	512
MK2	Jamia Mosque (B)	1.94	266.0	66	7.4	3.8	44.3	243	31.8	164	151
MK3	Sikh Temple (A)	1.84	296.2	196	9.88	5.9	38.4	201.3	27.8	37.2	960
MK4	Sikh Temple (B)	2.32	339.26	166	15.4	5.3	38.2	218.0	55.8	312	880
MK5	Makindu Hospital	2.41	36.24	340	5.80	5.2	38.9	112	48.8	308	178
MK6	Railway station	1.66	32.68	216	6.2	5.2	48.6	164	10.8	344	712
MK7	Min.Water- Makindu	1.94	340.2	389	7.2	4.2	45.5	76.0	27.4	289	280
MK8	Makindu Mission 1	1.88	50.23	174.5	71.1	5.59	152	20.15	17.8	40.12	1080
MK9	Makindu Mission 2	1.43	62.36	268	18.35	7.21	148	176.2	14.2	160	480
MK10	Makindu Sisters	1.66	43.18	309	24.9	6.9	66.0	114.0	4.82	156	218
MK11	Musimba 1	1.29	54.1	348	36.2	4.0	55.22	126	5.24	224	165
MK12	Musimba 2	1.25	126.4	289	36.64	7.3	49.14	151	14.4	166.2	311
MK13	Musimba 3	2.37	74.26	36.5	28.9	5.70	52.82	146.2	16.9	128.4	492
MK14	Musimba 4	1.89	108.2	166	24.4	4.80	46.8	164	27.4	169.8	428
MK15	Kisingo	2.31	26.32	136	18.9	3.69	52.2	117	6.94	242.4	511
MK16	Makilya Investment	1.66	33.22	412	20.8	2.43	36.4	189	4.8	188.4	526
MK17	Makilya Investment	2.84	36.40	516	39.86	1.56	39.2	166	5.51	166.4	316
MK18	Makau Boniface	2.19	56.24	18.93	47.18	2.62	61.2	118	4.12	144.2	384
MK19	Ndivo and Co	1.99	34.18	389	32.54	2.30	29.4	148	6.60	188.2	372
MK20	Ndivo and Co	2.32	36.28	576	39	1.92	36.1	114	4.89	381.56	324
MK21	Experimental Farm	4.21	218.2	22.9	36.9	2.61	18.2	194	3.42	381.8	359
MK22	Kyeni	5.56	386.50	136	46.9	5.28	19.2	179	1.88	148.6	589
MK23	Kai	1.86	89.2	246	126	1.81	16.8	136.2	1.99	381.54	512
MK24	Katuluni	2.83	292.2	418	212	2.24	144	196	7.9	148.3	338
MK25	Mulili DWD	2.69	108.60	340	12.6	3.01	136	202.6	4.81	162.8	362
MK26	Kitala	1.38	92.4	189	16.8	2.94	126	198	54.2	180.2	169.4
MK27	Kambo	1.42	4.82	248	446.7	4.92	34.2	174	3.82	368.4	514.2
MK28	Komboyoo	2.33	18.2	129	33.2	2.99	56.0	170.7	5.89	84.64	539
MK29	Kibwezi 1	4.55	26.92	275	367	2.41	52.2	136.4	5.64	168.8	402
MK30	Kibwezi 2	1.23	23.94	512	29	4.12	37.6	185	0.18	350.4	382
MK31	Muthama	2.86	33.6	150	7.6	2.44	56.2	359	2.83	310.2	1060
MK32	Kibwezi 3	3.60	28.96	29	42.6	3.12	47.1	304.2	3.64	585.6	585
MK33	Masongaleni	2.41	136.21	8.10	16.6	4.81	36.8	262.8	2.88	412.42	216.8
MK34	Masongaleni	1.88	123.2	146	80.12	2.92	148.8	124.8	12.4	928.8	526
MK35	Teresia Ndunda	1.70	254.26	120	71.02	1.96	175	129.4	6.82	186.4	584
MK36	Muli Ndambuki	1.38	39.2	28.30	92.04	1.79	22.8	48.4	5.91	326.12	534
MK37	Kyalo Muteti	2.56	8.23	92.1	56.34	2.60	24.2	86.3	4.33	196.42	416
MK38	Kiboko Reaesrch	2.10	7.64	160	44.4	3.20	26.4	126	3.89	126.00	104
MK39	Kiboko USU	1.10	56.9	374	116	0.89	46.2	118.4	7.10	154	49.4
KM40	Kibwezi Action Aid	2.40	32.90	224	48	4.12	148.0	126.8	8.20	86.2	68.2
MK41	Masongaleni A. Aid	1.88	72.81	164	122	2.84	38.90	58.8	4.40	314	154
MK42	Kiboko	1.92	28.20	294	26.8	3.24	26.24	162.7	3.60	186.4	116
MK43	S. Mbova	2.42	118.21	266	17.3	1.79	48.90	158.4	4.48	196	156

Appendix IV : Water Quality Maps That are Used for Generation Of Groundwater Quality Map

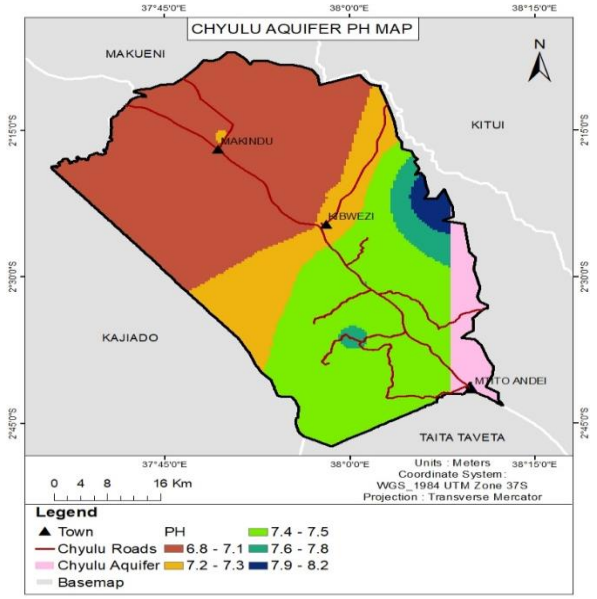

Figure A.1 The pH map of the study area

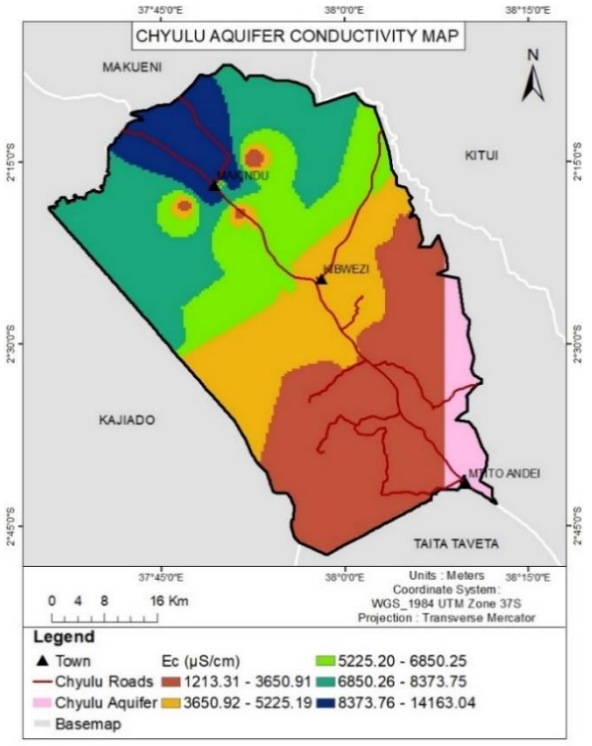

Figure A.2 The electrical conductivity map of the study area

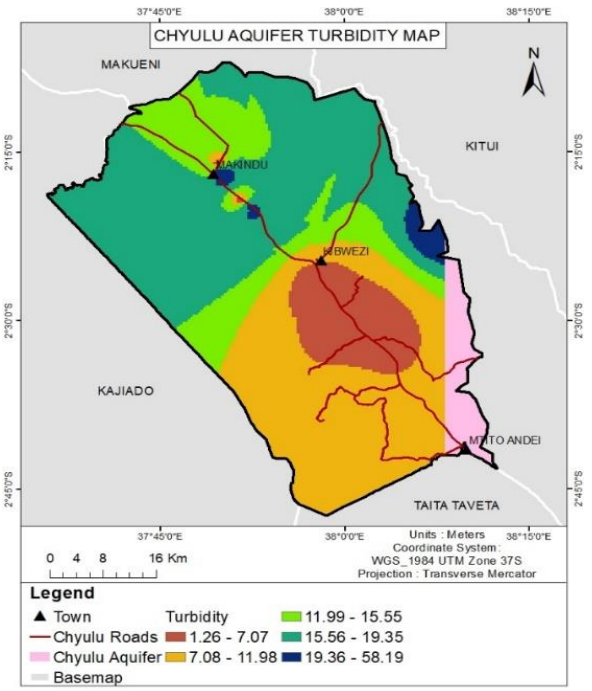

Figure A.3 The turbidity map of the study Area

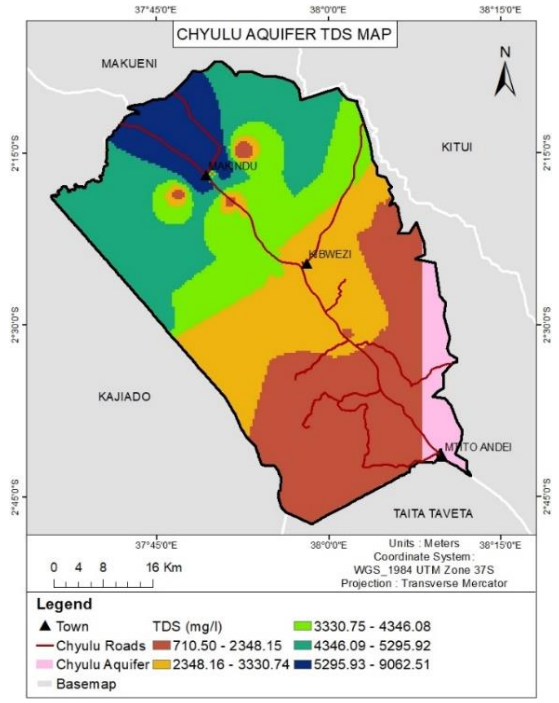

Figure A.4 The total dissolved solids map of the study area

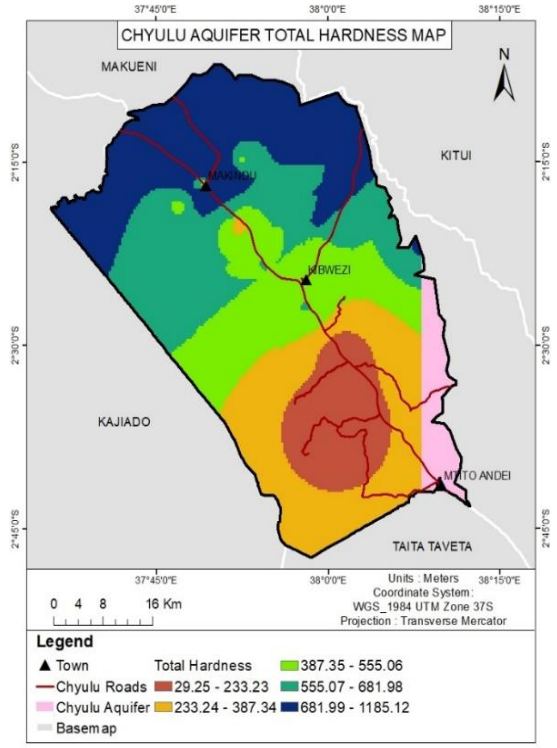

Figure A.5 The total hardness map of the study area

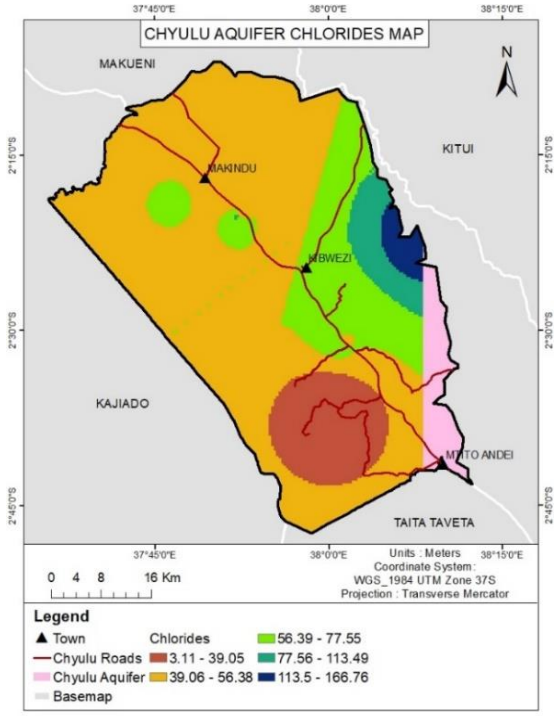

Figure A.6 The chloride map of the study area

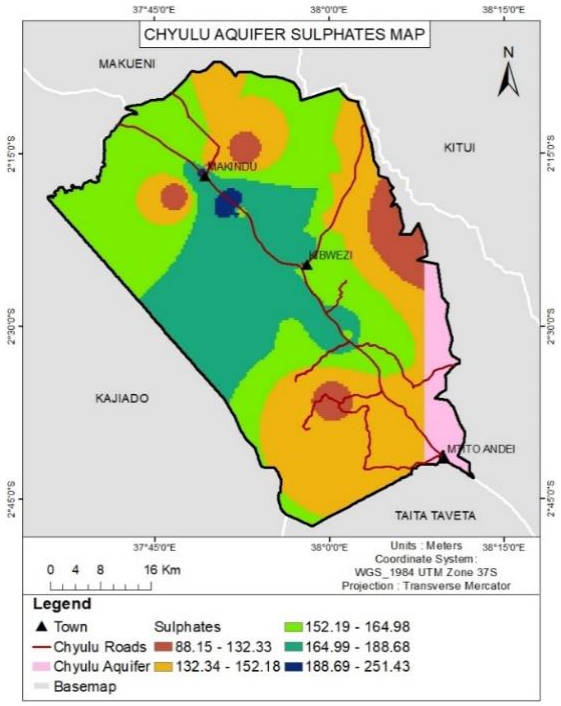

Figure A.7 The sulphate map of the of the study area

Appendix V : Results of Iron (Fe) Concentration for Various Boreholes

Table A.9 Results of iron (Fe) concentration test at Jamia Mosque A&B for Boreholes MK1&MK2

Site	Jamia Mosque (A) borehole (MK1)					Jamia Mosque (B) borehole (MK2)				
	Iron Concentration mg/L			Percentage decrease (%)		Iron Concentration mg/L			Percentage decrease (%)	
Run	Feed water	After aeration	After Filtration	Per Run	Average	Feed water	After aeration	After Filtration	Per Run	Average
1	4.37	5.31	1.78	59.95		4.19	4.56	2.21	47.26	
2	5.11	5.56	2.01	60.67		4.36	4.87	1.98	54.59	
3	5.21	5.75	2.11	59.50	**60.17**	3.89	4.49	2.04	47.56	**54.01**
4	4.85	5.12	1.72	63.09		4.29	4.86	1.76	58.94	
5	5.10	5.43	2.19	57.06		4.23	4.76	1.87	55.79	
6	5.13	5.16	1.91	60.04		4.55	5.01	1.67	63.30	
7	4.91	5.22	1.82	62.93		4.58	5.06	2.17	52.52	
8	5.11	5.53	1.97	58.32		4.67	4.93	2.27	51.39	

Table A.9 Results of iron (Fe) concentration test at Sikh Temple A (MK3) and Sikh Temple B (MK4) boreholes

Site	Sikh Temple(A) borehole (MK3)					Sikh Temple (B) borehole (MK4)				
	Iron Concentration mg/L			Percentage decrease (%)		Iron Concentration mg/L			Percentage decrease (%)	
Run	Feed water	After aeration	After Filtration	Per Run	Average	Feed water	After aeration	After Filtration	Per Run	Average
1	4.23	4.59	1.65	60.99		4.25	4.52	1.81	57.41	
2	3.83	4.53	1.55	56.92		3.76	5.61	1.60	57.45	
3	4.33	5.01	2.02	53.35		4.75	6.75	1.94	59.16	
4	4.98	6.01	1.45	70.88	**60.40**	3.71	6.93	1.45	60.92	**61.03**
5	4.12	4.44	1.79	56.55		4.80	7.15	1.86	61.25	
6	3.56	4.23	1.56	56.18		4.13	4.95	1.45	64.89	
7	4.54	5.32	1.48	67.40		4.44	4.95	1.75	60.59	
8	4.08	4.52	1.71	58.09		4.15	5.36	1.40	66.27	

Table A.10 Results of iron concentration test for Makindu Hospital (MK5) and Makindu Railway (MK6) boreholes

Site	Makindu Hospital (MK5) borehole					Makindu Railway (MK6) borehole				
	Iron Concentration mg/L			Percentage decrease (%)		Iron Concentration mg/L			Percentage decrease (%)	
Run	Feed water	After aeration	After Filtration	Per Run	Average	Feed water	After aeration	After Filtration	Per Run	Average
1	4.52	6.54	2.06	58.85		4.79	5.07	2.21	53.86	
2	4.33	5.76	2.12	59.82		4.66	5.10	1.98	57.51	
3	5.33	5.42	2.50	60.04		5.35	4.98	2.34	56.26	
4	5.98	5.45	2.11	64.72	**59.25**	4.29	5.51	1.76	58.97	**59.66**
5	5.12	5.51	2.13	58.40		5.36	7.65	2.25	58.02	
6	4.56	4.84	2.01	58.11		4.55	5.24	1.67	63.30	
7	4.29	5.89	1.88	56.18		4.78	4.83	1.71	64.23	
8	5.08	4.71	2.14	57.87		4.67	5.66	1.59	65.95	

Table A.11 Results of iron (Fe) concentration test for Makindu Water (MK7) and Makindu Mission (MK8) boreholes

Site	Makindu Water (MK7) borehole					Makindu Mission 1 (MK8) borehole				
	Iron Concentration mg/L			Percentage decrease (%)		Iron Concentration mg/L			Percentage decrease (%)	
Run	Feed water	After aeration	After Filtration	Per Run	Average	Feed water	After aeration	After Filtration	Per Run	Average
1	4.47	5.07	2.13	52.35		5.65	6.08	2.21	60.88	
2	4.65	5.10	1.98	57.42		4.21	5.19	1.80	57.24	
3	4.48	4.98	2.04	54.46		5.22	5.75	2.44	53.26	
4	4.29	5.51	1.76	58.97	**56.54**	4.75	4.62	2.18	54.11	**56.05**
5	4.23	5.65	1.87	55.79		5.32	6.65	2.50	53.01	
6	4.55	5.24	1.67	63.30		4.76	5.14	2.17	54.41	
7	4.58	4.83	2.17	52.62		4.12	5.55	1.71	58.50	
8	4.67	5.16	1.99	57.39		3.71	5.12	1.85	57.27	

Table A.12 Results of iron (Fe) concentration test for Makindu Sisters (MK10) and Musimba1 (MK11) boreholes

Site	Makindu Sisters (MK10) borehole					Musimba 1 (MK11) borehole				
	Iron Concentration mg/L			Percentage decrease (%)		Iron Concentration mg/L			Percentage decrease (%)	
Run	Feed water	After aeration	After Filtration	Per Run	Average	Feed water	After aeration	After Filtration	Per Run	Average
1	5.78	7.02	2.24	61.25		4.24	5.07	2.06	51.42	
2	5.93	7.95	2.35	60.37		4.53	5.10	2.12	53.20	
3	6.13	8.25	2.51	59.05		4.33	4.98	2.50	42.26	
4	6.23	8.43	2.70	56.66	**59.83**	4.98	5.51	2.11	57.63	**54.35**
5	5.73	8.05	2.21	61.43		5.12	7.65	2.13	58.40	
6	6.34	8.50	2.56	59.62		4.56	5.24	2.01	55.92	
7	4.90	5.45	2.10	57.14		4.29	4.83	1.88	56.18	
8	5.76	5.86	2.13	63.02		5.08	5.66	2.14	57.87	

Table A.13 Results of iron (Fe) concentration test for Kitala (MK26) and Kambo (MK27) boreholes

Site	Kitala (MK26) borehole					Kambo (MK27) borehole				
	Iron Concentration mg/L			Percentage decrease (%)		Iron Concentration mg/L			Percentage decrease (%)	
Run	Feed water	After aeration	After Filtration	Per Run	Average	Feed water	After aeration	After Filtration	Per Run	Average
1	4.42	5.02	1.75	60.41		5.68	7.16	2.067	63.6	
2	5.11	6.11	2.01	60.67		5.97	7.47	2.68	55.11	
3	5.21	7.25	2.11	59.50		5.48	7.27	1.83	66.61	
4	4.85	7.43	1.72	64.64	**60.98**	6.23	7.55	2.11	6613	**62.12**
5	5.10	7.65	2.19	57.06		5.98	7.26	1.77	70.40	
6	5.13	5.45	1.91	62.77		6.53	7.53	3.15	60.03	
7	4.91	5.45	1.82	62.93		7.19	7.84	2.73	62.05	
8	5.76	5.86	2.13	63.02		5.08	6.56	2.40	52.8	

Appendix VI : Concentration of Iron After Flow Through the Aeration/ Filtration Filter

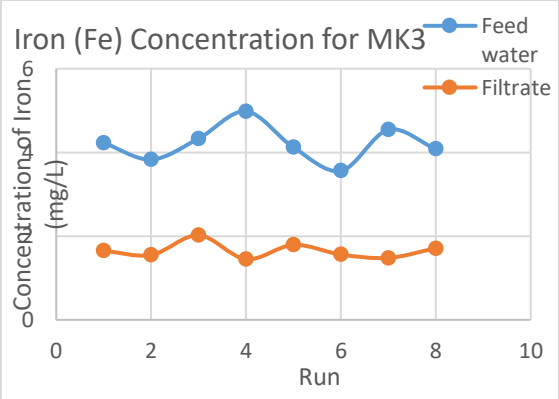

Figure A.8 Concentration of iron for the eight runs for MK3

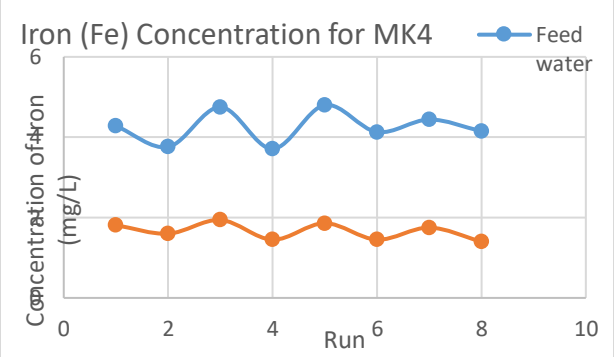

Figure A.9 Concentration of iron for the eight runs for MK4

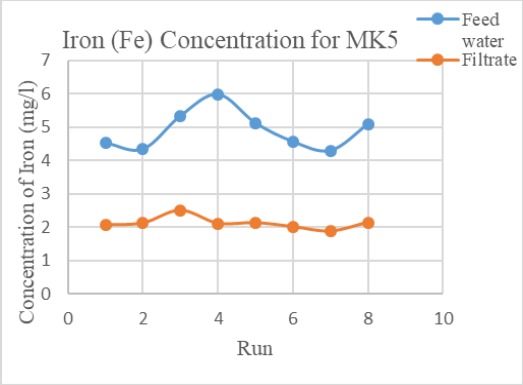

Figure A.10 Concentration of iron for the eight runs for MK5

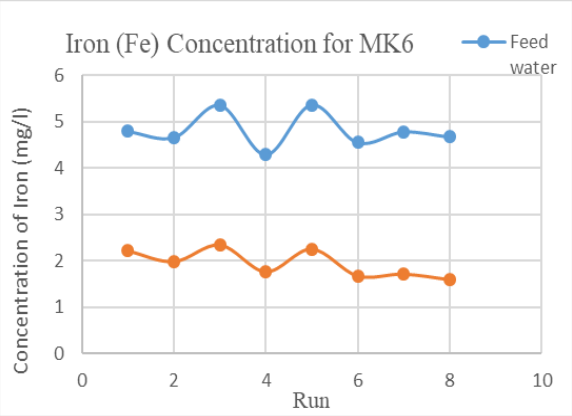

Figure A.10 Concentration of iron for the eight runs for MK6

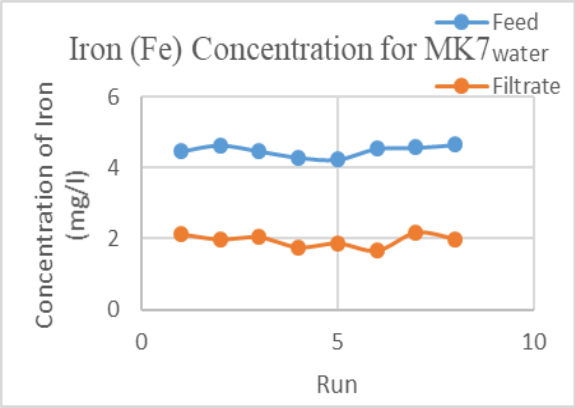

Figure A.11 Concentration of iron for the eight runs for MK7

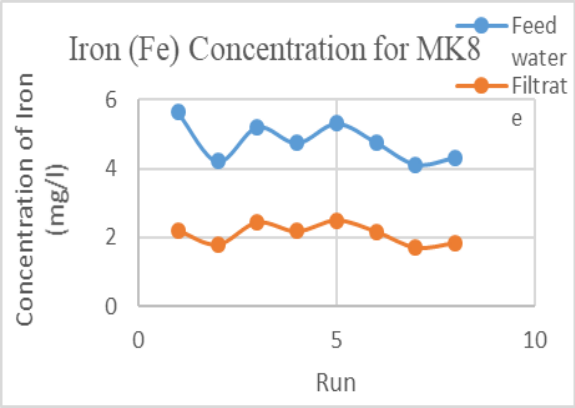

Figure A.13 Concentration of iron for the eight runs for MK8

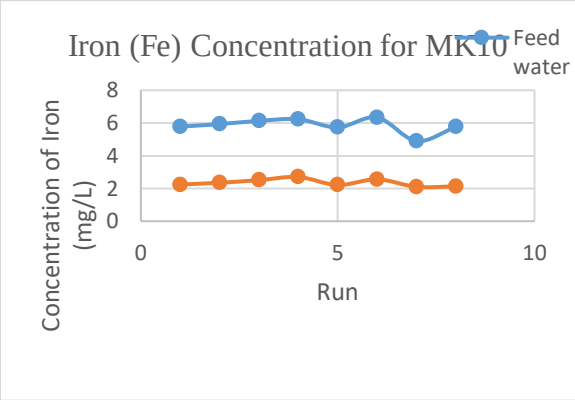

Figure A.14 Concentration of iron for the eight runs for MK10

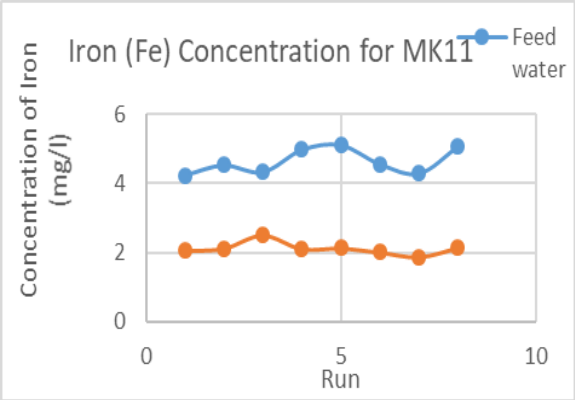

Figure A.12 Concentration of iron for the eight runs for MK11

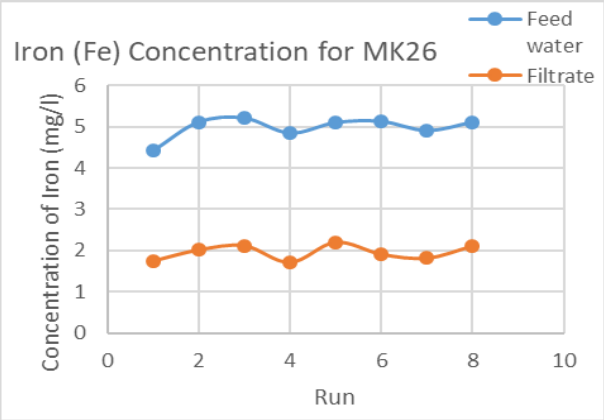

Figure A.13 Concentration of iron for the eight runs for MK26

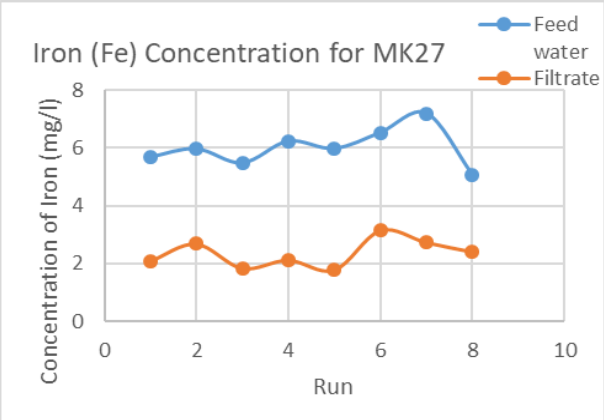

Figure A.14 Concentration of iron for the eight runs for MK27

Appendix VII : Boreholes Used in Hydro-Geochemical Modeling Of Flow Of Iron Ions Through The Aquifer

Table A.14 Table of boreholes used in hydro-geochemical modeling of flow of iron ions through the aquifer

ID. No.	Name of Borehole	UTM Coordinates		Yield (m^3/day)	Depth (m)	Altitude (AMSL)
		X	Y			
MK1	Jamia Mosque A	368779	9748818	9.0	120	1007
MK2	Jamia mosque B	368789	9748822	7.2	135	999
MK3	Sikh Temple A	368747	9748601	8.1	91	1006
MK4	Sikh Temple B	368789	9748604	7.5	83	1005
MK5	Makindu Hospital	369230	9747647	6.86	110	990
MK6	Makindu Railway	369736	9759147	5.8	65	990
MK7	Makindu Water	367735	9759158	8.1	78	996
MK8	Makindu Mission 1	369589	9749384	6.5	84	1004
MK9	Makindu Mission 2	369589	9749383	7.5	51	1002
MK10	Makindu Sisters	369579	9749726	8.5	66	1003
MK11	Musimba 1	374289	9741666	6.1	150	1010
MK12	Musimba 2	374118	9742653	6.8	120	993
MK13	Musamba 3	372840	9743415	5.6	89	988
MK14	Musamba 4	371846	9751510	5.9	224	970
MK15	Kisingo	374684	9744605	12.5	98	1036
MK16	Makilya Invest	366611	9751194	8.8	120	990
MK17	Makilya Invest	366611	9751194	9.65	64	985
MK18	Makau Boniface	366637	9747604	7.2	56	935
MK19	Ndivo Invest	366558	9747601	12.9	34	986
MK20	Ndivo Invest	366565	9747602	12.5	37	970
MK21	Experiment Farm	365451	9749046	8.2	47	1025
MK22	Kyeni	372397	9748748	8.4	56	992
MK23	Kai	374008	9747935	6.5	98	982
MK24	Katuluni	375288	9754345	15.6	56	985
MK25	Mulili	369285	9752125	8.6	85	947

Appendix VIII : Relationship Between the Coefficient Of Dispersion And Velocity (Hugo, 1968)

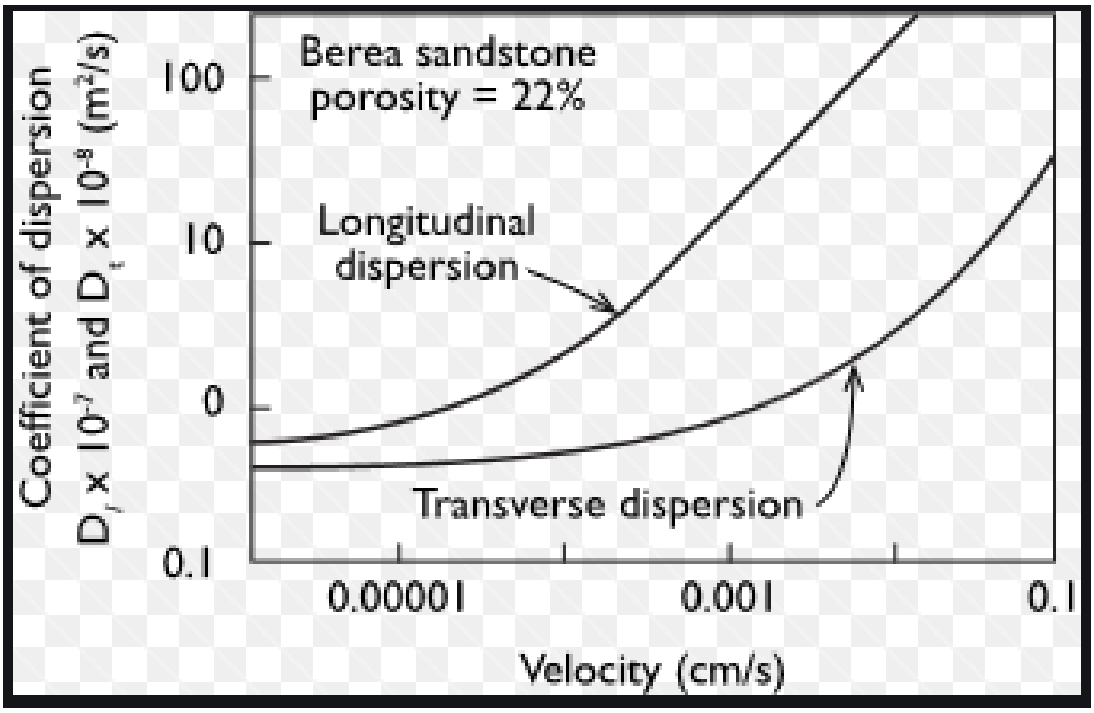

Figure A.15 Relationship between the coefficient of dispersion and velocity (HUGO, 1968)

Appendix IX : Values Of Bulk Density, Total Porosity And Effective Porosity Of Selected Soils

Table A.15 Values of bulk density, total porosity and effective porosity of selected soils

Aquifer Matrix	Dry Bulk Density (g/cm^3)	Total Porosity	Effective Porosity
Clay	1.00 - 2.40	0.34 - 0.60	0.01 - 0.2
Peat	--	--	0.3 - 0.5
Glacial sediments	1.15 - 2.10	--	0.05 - 0.2
Sandy Clay	--	--	0.03 - 0.2
Silt	--	0.34 - 0.61	0.01 - 0.3
Loess	0.75 - 1.60	--	0.15 - 0.35
Fine Sand	1.37 - 1.81	0.26 - 0.53	0.10 - 0.3
Medium Sand	1.37 - 1.81	--	0.15 - 0.3
Coarse Sand	1.37 - 1.81	0.31 - 0.46	0.2 - 0.35
Gravely sand	1.37 - 1.81	--	0.1 - 0.35
Fine Gravel	1.36 - 2.19	0.25 - 0.38	0.2 - 0.35
Medium Gravel	1.36 - 2.19	--	0.15 - 0.25
Coarse gravel	1.36 - 2.19	0.24 - 0.36	0.1 - 0.25
Sandstone	1.60 - 2.68	0.05 - 0.36	0.1 - 0.4
Siltstone	-	0.21 - 0.41	0.01 - 0.35
Shale	1.54 - 3.17	0.0 - 0.10	--
Limestone	1.74 - 2.79	0.0 - 50.0	0.01 - 0.02
Granite	2.24 - 2.46	--	--
Basalt	2.00 - 2.70	0.03 – 0.35	--
Volcanic Tuff	-	--	0.02 - 0.35

Appendix X : Borehole Logs for Selected Borehole in the Study Area

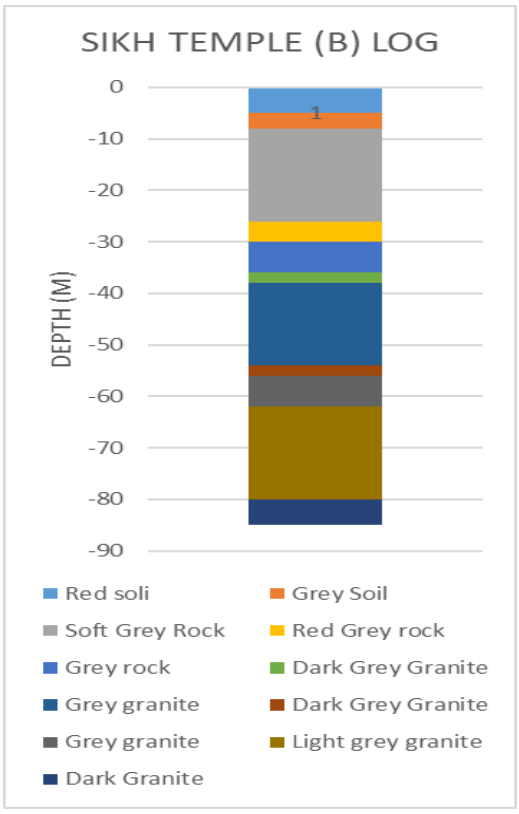

Figure A.16 Sikh Temple (B) Log

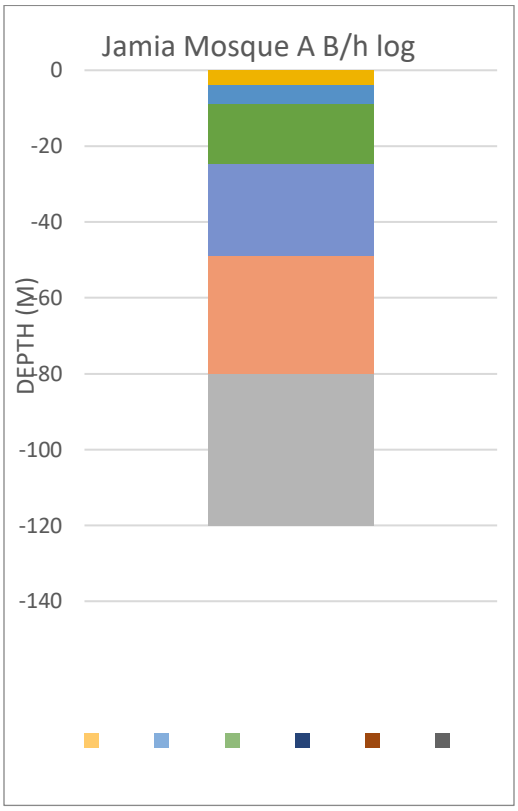

Figure A.17 Jamia Mosque A B/h Log

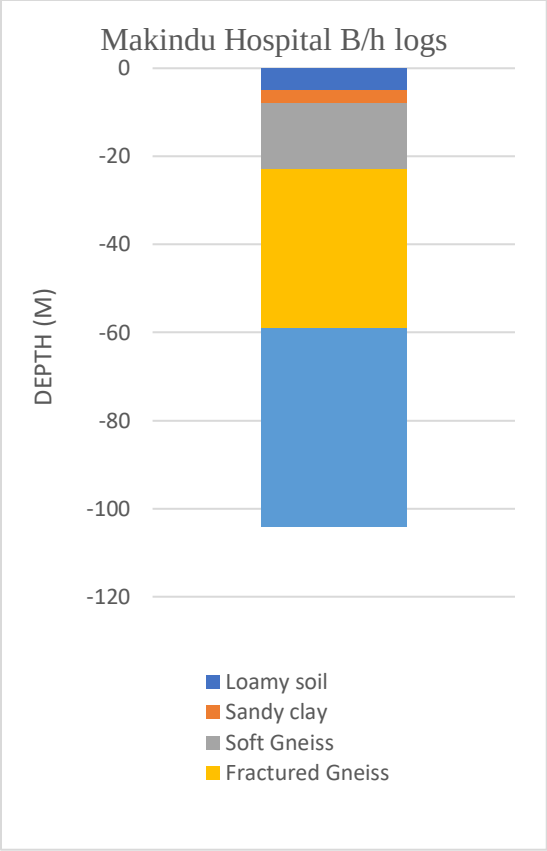

Figure A.18 Makindu Hospital B/h Log

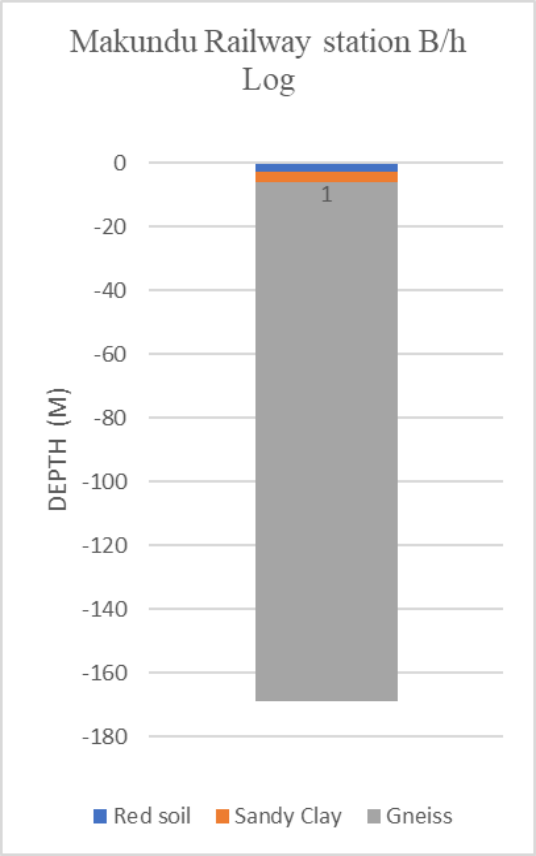

Figure A.19 Makindu Railway station B/h Log

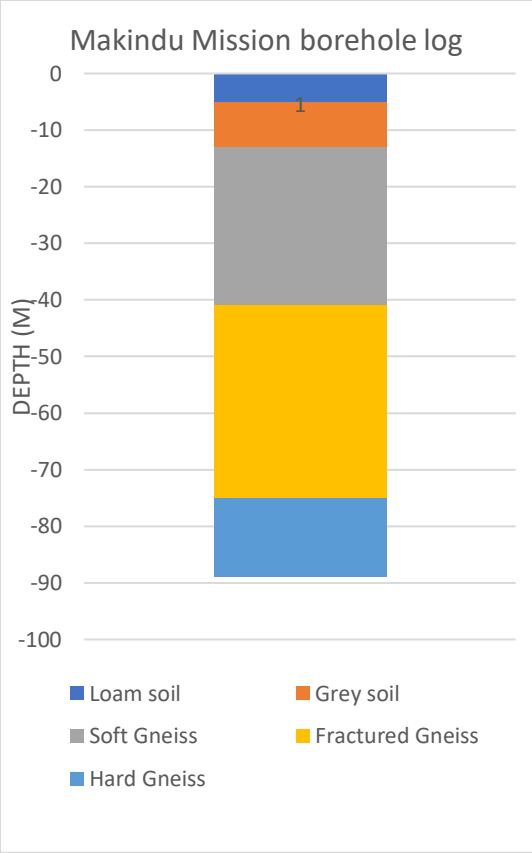

Figure A.20 Makindu Mission borehole Log

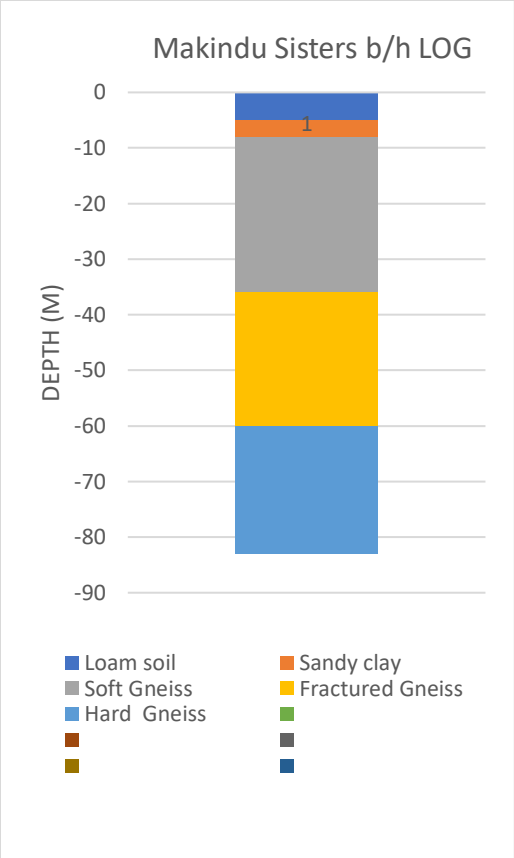

Figure A.21 Makindu Sisters b/h Log

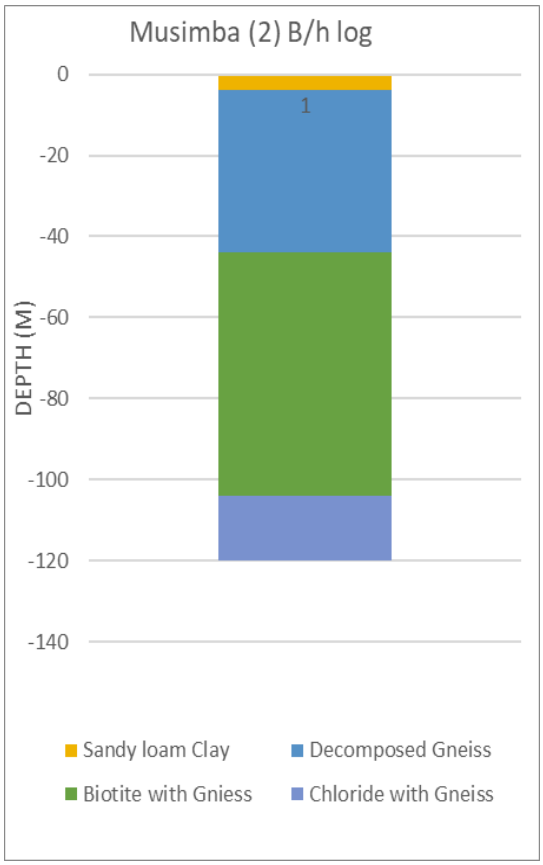

Figure A.22 Musimba (2) Log

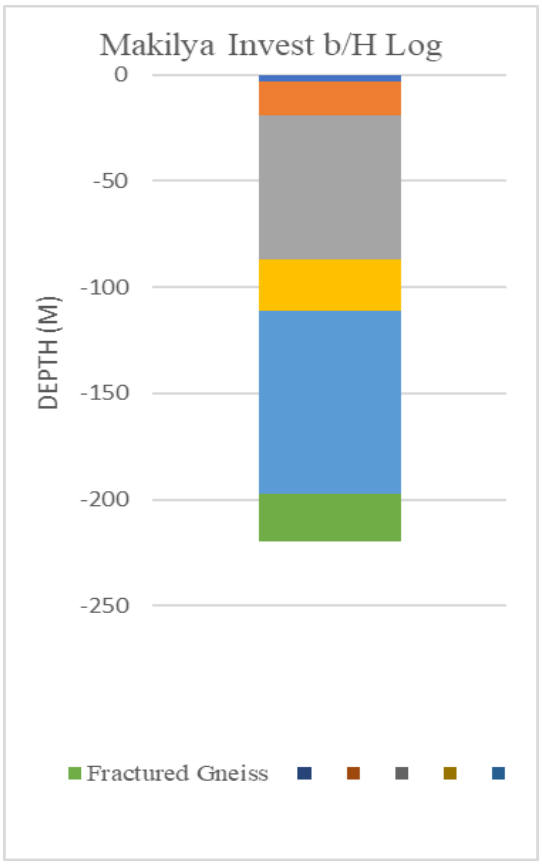

Figure A.23 Makilya Invest b/H Log

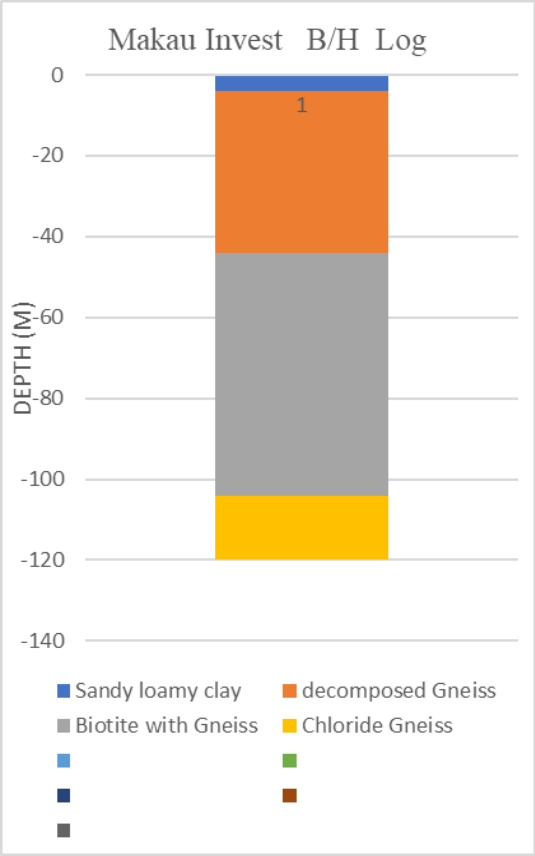

Figure A.24 Makau Invest B/H Log

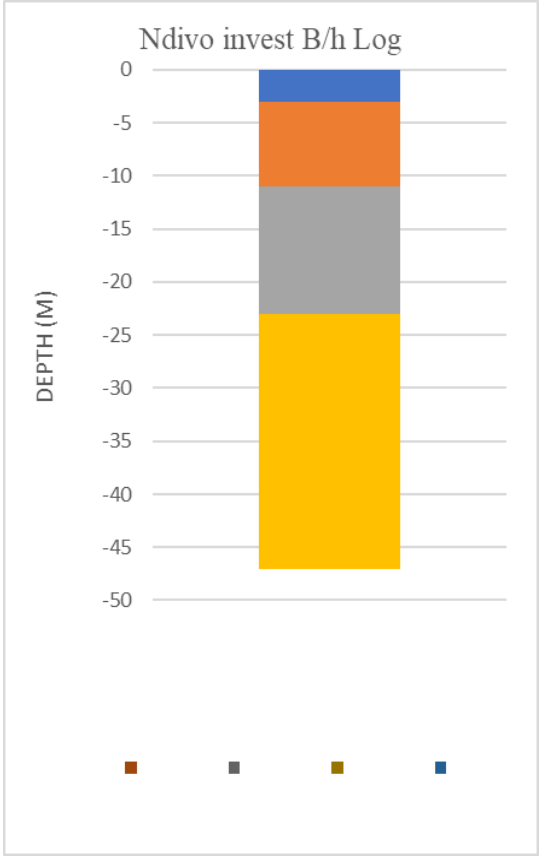

Figure A.25 Ndivo Invest B/h Log

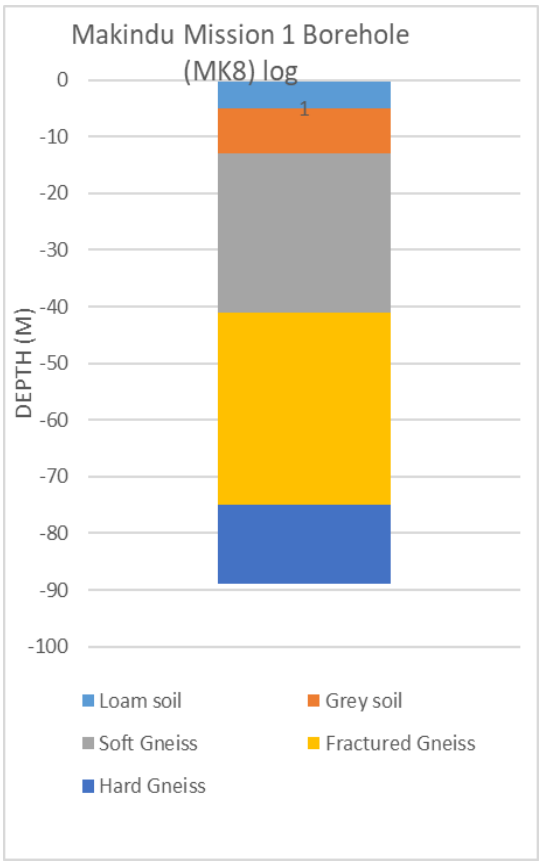

Figure A.26 Makindu Mission 1 Borehole (MK8) Log

Appendix XI : Data for the Batch Reactor Experiments

A. Description of the batch reactor Code

The Code had six blocks

Block 1, the comments block that contains definitions of all the variables that were passed into the RXNS routine from the RT3D main program/ Code.

Block 2, the interfacing block that contains FORTRAN statements that define the type of variables.

Block 3, the subroutine specific variables block where variables that are used exclusively in this specific subroutine are defined.

Block 4, the reaction parameter initialization block where all values of reactions parameters are specified.

Block 5 was used to transfer variables into meaningful names for clarity purposes.

Block 6 was the differential equations block that describes the ferrous oxidation reaction equations in FORTRAN language.

The following was the source code in FORTRAN used in RT3D for simulating reactions for degradation kinetics for ferrous salts under conditions of limited availability of oxygen.

B. The Subroutine Code for Expressions and Parameters Verification.

```
1    SUBROUTINE rxns (ncomp,nvrxndata,j,i,k,y,dydt,
2    &        poros, rhob,reta,rc,nlay,nrow,ncol,vrc)
3    c ***** Block 1: Comments block *******
```

```
4  c234567890123456789012345678901234567890123456789012345678901234567890123456789012
5  c ncomp - Total number of components
6  c nvrxndata - Total number of variable reaction parameters to be input via RCT file
7  c J, I, K - node location (used if reaction parameters are spatially variable)
8  c y - Concentration value of all component at the node [array variable y(ncomp)]
9  c dydt - Computed RHS of your differential equation [array variable dydt(ncomp)]
10 c poros - porosity of the node
11 c reta - Retardation factor [array variable reta (mcomp)]
12 c rhob - bulk density of the node
13 c rc - Stores spatially constant reaction parameters (up to 100 values)
14 c nlay, nrow, ncol - Grid size (used only for dimensioning purposes)
15 c vrc - Array variable that stores spatially variable reaction parameters
16 c ***** End of Block 1 *******
17 c *** Block 2: Standard interface block ***
18 !MS$ATTRIBUTES DLLEXPORT :: rxns
19 IMPLICIT NONE
20 INTEGER ncol,nrow,nlay
21 INTEGER ncomp,nvrxndata,j,i,k
22 INTEGER First_time
```

23 DATA First_time/1/

24 DOUBLE PRECISION y,dydt,poros,rhob,reta

25 DOUBLE PRECISION rc,vrc

26 DIMENSION y(ncomp),dydt(ncomp),rc(50)

27 DIMENSION vrc(ncol,nrow,nlay,nvrxndata),reta(50)

28 C **** End of block 2 *******

29 C * Block 3: Declare your problem-specific new variables here ***

30 C INTEGER

31 DOUBLE PRECISION FE2,FE3,kFE2,kFE3

32 DOUBLE PRECISION O2,FL

33 C *** End of Block 3 ******

34 C * Block 4: Initilize reaction parameters here, if required ***

35 IF (First_time .EQ. 1) THEN

36 kFE2 = 0.026375 !FE2 first-order degradation rate

37 kFE3 = rc(1) !FE3 first-order degradation rate

1. O_2= 2.5 ! the concentration of O2
2. FL = 4.6 1 The concentration of F

38 First_time = 0 !reset First_time to skip this block later

39 END IF

40 C *** End of Block 4 ******

41 C * Block 5: Definition of other variable names ***

42 FE2 = y(1)

43 FE3 = y(2)

44 C *** End of Block 5 ******

45 c * Block 6: Definition of Differential Equations ***

46 c *** concentration of Fe2 was assumed to be constant throughout the aquifer ***

47 IF (FE2 .GT. 1.0E-11) THEN

i. dydt(1) = ((-kFE_2*FE_2*O_2*FL)) /reta(1) ! from equation (3.12)

2. ELSE

i. dydt(1) = 0

48 END IF

49 dydt(2) = ((kFE_3*FE_2*O_2))/reta(2) ! from equation (3.13)

50 C *** End of Block 6 ******

51 RETURN

52 END

C. Data produced by the batch reactor code

Table A.16 Jamia Mosque (A) (MK1)

Time (Hrs)	Concentration of iron after aeration (mg/L)			Concentration of ferrous ions (mg/L)						Concentration of ferric ions (mg/L)								
	Run 1	Run 2	Run 3	Run 1	Batch 1	Run 2	Batch 2	Run 3	Batch 3	Run 1	Batch 1	K_3	Run 2	Batch 2	K_3	Run 3	Batch 3	K_3
0	4.95	5.12	4.84	4.58	4.58	4.67	4.67	4.50	4.50	0.25	0.25		0.41	0.41		0.25	0.25	
6	5.81	5.90	5.54	4.44	4.25	4.98	4.33	4.35	4.17	0.31	0.53	0.06	0.44	0.71	0.08	0.30	0.50	0.06
12	5.77	5.81	5.36	3.92	3.94	4.31	4.01	3.89	3.87	0.92	0.78	0.10	0.99	0.98	0.11	0.89	0.74	0.10
18	4.85	5.66	5.18	3.55	3.65	3.80	3.72	3.60	3.58	1.24	1.02	0.10	1.29	1.24	0.10	1.20	0.96	0.10
24	4.78	5.16	5.01	3.35	3.38	3.45	3.45	3.30	3.32	1.39	1.24	0.09	1.49	1.48	0.09	1.32	1.16	0.08
30	4.79	4.81	4.61	2.37	3.13	2.53	3.20	2.31	3.08	1.89	1.44	0.11	1.99	1.70	0.12	1.71	1.35	0.10
36	4.53	4.66	4.52	2.16	2.91	2.21	2.96	2.06	2.86	2.18	1.63	0.12	2.24	1.90	0.12	2.14	1.52	0.12
42	4.33	4.52	4.18	1.79	2.69	1.81	2.75	1.73	2.65	2.52	1.80	0.13	2.50	2.09	0.13	2.34	1.69	0.12
R^2 = coefficient of correlation				0.96		0.93		0.95		0.98			0.98			0.98		
Average values of K_3												0.10			0.11			0.09

Concentration of raw sample was 4.42 mg/L, 4.54 mg/L, and 4.38 mg/L for runs 1, 2 and 3 respectively.

Table A.18 Jamia Mosque (B) (MK2)

Time (Hrs)	Concentration of iron after aeration (mg/L)			Concentration of ferrous ions (mg/L)						Concentration of ferric ions (mg/L)								
	Run 1	Run 2	Run 3	Run 1	Batch 1	Run 2	Batch 2	Run 3	Batch 3	Run 1	Batch 1	K_3	Run 2	Batch 2	K_3	Run 3	Batch 3	K_3
0	4.95	5.12	4.84	4.58	4.58	4.67	4.67	4.50	4.50	0.25	0.25		0.41	0.41		0.25	0.25	
6	5.81	5.90	5.54	4.44	4.25	4.98	4.33	4.35	4.17	0.31	0.53	0.06	0.44	0.71	0.08	0.30	0.50	0.06
12	5.77	5.81	5.36	3.92	3.94	4.31	4.01	3.89	3.87	0.92	0.78	0.10	0.99	0.98	0.11	0.89	0.74	0.10
18	4.85	5.66	5.18	3.55	3.65	3.80	3.72	3.60	3.58	1.24	1.02	0.10	1.29	1.24	0.10	1.20	0.96	0.10
24	4.78	5.16	5.01	3.35	3.38	3.45	3.45	3.30	3.32	1.39	1.24	0.09	1.49	1.48	0.09	1.32	1.16	0.08
30	4.79	4.81	4.61	2.37	3.13	2.53	3.20	2.31	3.08	1.89	1.44	0.11	1.99	1.70	0.12	1.71	1.35	0.10
36	4.53	4.66	4.52	2.16	2.91	2.21	2.96	2.06	2.86	2.18	1.63	0.12	2.24	1.90	0.12	2.14	1.52	0.12
42	4.33	4.52	4.18	1.79	2.69	1.81	2.75	1.73	2.65	2.52	1.80	0.13	2.50	2.09	0.13	2.34	1.69	0.12
R^2 = coefficient of correlation				0.96		0.93		0.95		0.98			0.98			0.98		
Average values of K_3												0.10			0.11			0.09

Concentration of raw sample was 4.42 mg/L, 4.54 mg/L, and 4.38 mg/L for runs 1, 2 and 3 respectively.

Table A.19 Makindu Sikh temple (A) (MK3)

Time (Hrs)	Concentration of iron after aeration (mg/L)			Concentration of ferrous ions (mg/L)						Concentration of ferric ions (mg/L)								
	Run 1	Run 2	Run 3	Run 1	Batch 1	Run 2	Batch 2	Run 3	Batch 3	Run 1	Batch 1	K_3	Run 2	Batch 2	K_3	Run 3	Batch 3	K_3
0	5.07	5.14	4.91	4.42	4.42	4.61	4.61	4.11	4.11	0.24	0.24		0.31	0.31		0.19	0.19	
6	5.10	5.18	5.01	4.53	4.10	4.77	4.27	4.23	3.81	0.26	0.49	0.05	0.36	0.61	0.07	0.22	0.41	0.05
12	4.98	5.06	4.92	4.11	3.80	4.05	3.96	3.84	3.53	0.74	0.72	0.08	0.96	0.89	0.10	0.66	0.60	0.08
18	4.75	4.82	4.60	3.38	3.52	3.48	3.67	3.21	3.27	1.01	0.93	0.08	1.18	1.15	0.09	0.91	0.79	0.07
24	4.65	4.66	4.32	2.91	3.26	3.01	3.40	2.72	3.03	1.56	1.13	0.11	1.78	1.38	0.12	1.35	0.96	0.09
30	4.28	4.45	4.15	2.46	3.03	2.31	3.16	2.31	2.81	1.80	1.31	0.11	2.08	1.60	0.13	1.69	1.12	0.11
36	4.06	4.29	3.75	1.89	2.80	2.03	2.92	1.71	2.61	2.13	1.48	0.12	2.25	1.81	0.12	1.85	1.27	0.10
42	3.76	3.07	3.52	1.45	2.60	1.65	2.71	1.32	2.42	2.27	1.64	0.11	2.41	2.00	0.12	2.11	1.40	0.11
R^2 = coefficient of correlation				0.95		0.96		0.95		0.97			0.97			0.98		
Average values of K_3												0.09			0.11			0.09

Concentrations of raw samples were 4.52 Mg/L, 4.66 Mg/L, and 4.33 Mg/L for runs 1, 2 and 3 respectively.

Table A.17 Sikh temple (B) (MK4)

Time (Hrs)	Concentration of iron after aeration (mg/L)			Concentration of ferrous ions (mg/L)						Concentration of ferric ions (mg/L)								
	Run 1	Run 2	Run 3	Run 1	Batch 1	Run 2	Batch 2	Run 3	Batch 3	Run 1	Batch 1	K_3	Run 2	Batch 2	K_3	Run 3	Batch 3	K_3
0	4.60	4.42	4.38	4.30	4.30	4.21	4.21	4.01	4.01	0.25	0.25		0.23	0.23		0.23	0.23	
6	4.84	4.57	4.49	4.42	3.99	4.26	3.90	4.17	3.72	0.31	0.60	0.09	0.28	0.52	0.06	0.25	0.39	0.05
12	4.77	4.51	4.41	4.15	3.69	4.12	3.62	3.84	3.45	0.60	0.92	0.09	0.51	0.79	0.05	0.44	0.53	0.05
18	4.62	4.34	4.21	3.24	3.43	3.18	3.35	3.04	3.19	1.04	1.22	0.12	0.92	1.03	0.07	0.65	0.67	0.05
24	4.45	4.22	4.05	3.01	3.18	2.69	3.11	2.51	2.96	1.39	1.49	0.13	1.22	1.27	0.08	0.93	0.79	0.06
30	4.26	3.99	3.76	2.42	2.94	2.01	2.88	1.97	2.74	1.81	1.75	0.16	1.64	1.48	0.10	1.24	0.91	0.07
36	4.15	3.69	3.52	1.94	2.73	1.84	2.67	1.54	2.54	2.18	1.99	0.18	1.82	1.68	0.10	1.65	1.02	0.09
42	3.76	3.52	3.01	1.50	2.53	1.39	2.48	1.18	2.36	2.22	2.21	0.16	2.01	1.86	0.10	1.78	1.11	0.08
R^2 = coefficient of correlation				0.94		0.94		0.94		0.97			0.97			0.94		
Average values of K_3												0.13			0.08			0.06

Concentrations of raw samples were 4.33 mg/L, 4.18 mg/L, and 4.07 mg/L for runs 1, 2 and 3 respectively.

Table A.18 Makindu Hospital (MK5)

Time (Hrs)	Concentration of iron after aeration (mg/L)			Concentration of ferrous ions (mg/L)						Concentration of ferric ions (mg/L								
	Run 1	Run 2	Run 3	Run 1	Batch 1	Run 2	Batch 2	Run 3	Batch 3	Run 1	Batch 1	K_3	Run 2	Batch 2	K_3	Run 3	Batch 3	K_3
0	5.34	5.45	5.26	4.88	4.88	4.94	4.94	4.81	4.81	0.33	0.33		0.35	0.35		0.34	0.34	
6	5.76	5.89	5.39	4.91	4.52	4.99	4.58	4.92	4.46	0.38	0.63	0.07	0.44	0.70	0.08	0.39	0.64	0.07
12	5.76	5.81	5.33	4.11	4.19	4.48	4.24	4.29	4.13	0.98	0.91	0.10	1.18	1.03	0.13	1.01	0.93	0.11
18	5.44	5.45	5.20	3.88	3.89	3.99	3.93	3.90	3.83	1.23	1.17	0.09	1.34	1.33	0.10	1.26	1.19	0.09
24	5.55	5.22	4.98	3.79	3.60	3.48	3.65	3.51	3.55	1.71	1.41	0.11	1.66	1.61	0.10	1.40	1.43	0.08
30	5.13	4.96	4.83	3.11	3.34	2.51	3.38	2.81	3.29	2.01	1.64	0.11	2.41	1.87	0.15	1.91	1.65	0.10
36	4.89	4.86	4.67	2.49	3.10	2.21	3.13	2.08	3.05	2.32	1.84	0.12	2.55	2.11	0.14	2.52	1.86	0.14
42	4.71	4.75	4.42	2.11	2.87	2.08	2.91	1.71	2.83	2.55	2.04	0.12	2.62	2.33	0.13	2.66	2.05	0.14
R^2 = coefficient of correlation				0.94		0.95		0.94		0.98			0.96			0.96		
Average values of K_3												0.10			0.12			0.11

Concentrations of raw samples were 5.25 mg/L, 5.36 mg/L, and 4.95 mg/L for runs 1, 2 and 3 respectively.

Table A.19 Makindu Railway station (MK6)

Time (Hrs)	Concentration of iron after aeration (mg/L)			Concentration of ferrous ions (mg/L)						Concentration of ferric ions (mg/L)								
	Run 1	Run 2	Run 3	Run 1	Batch 1	Run 2	Batch 2	Run 3	Batch 3	Run 1	Batch 1	K_3	Run 2	Batch 2	K_3	Run 3	Batch 3	K_3
0	6.07	5.86	5.64	5.48	5.48	5.31	5.31	5.18	5.18	0.35	0.35		0.30	0.30		0.26	0.26	
6	6.40	6.12	5.90	5.51	5.08	5.39	4.92	5.24	4.80	0.31	0.61	0.05	0.34	0.49	0.05	0.31	0.43	0.05
12	6.10	5.90	5.76	4.93	4.71	4.85	4.56	4.65	4.45	0.92	0.85	0.08	0.90	0.66	0.08	0.84	0.58	0.08
18	5.57	5.21	5.15	4.18	4.37	4.05	4.23	3.95	4.13	1.34	1.08	0.09	1.09	0.83	0.07	1.01	0.73	0.06
24	5.12	4.60	4.40	3.39	4.05	3.25	3.92	3.12	3.82	1.69	1.28	0.09	1.21	0.98	0.06	1.11	0.86	0.05
30	4.35	4.18	4.10	2.53	3.75	2.84	3.63	2.78	3.55	1.79	1.48	0.08	1.33	1.11	0.05	1.19	0.99	0.05
36	3.91	3.90	3.82	1.88	3.48	2.10	3.37	2.01	3.29	1.98	1.65	0.08	1.39	1.24	0.05	1.22	1.10	0.04
42	3.62	3.20	3.12	1.58	3.22	1.52	3.12	1.49	3.05	2.32	1.82	0.09	1.44	1.36	0.04	1.29	1.21	0.04
R^2 = coefficient of correlation				0.96		0.96		0.96		0.97			0.92			0.90		
Average values of K_3												0.08			0.06			0.05

Concentrations of raw samples were 5.53 mg/L, 5.34 mg/L, and 5.22 mg/L for runs 1, 2 and 3 respectively.

Table A.20 Ministry of Water, Makindu (MK7)

Time (Hrs)	Concentration of iron after aeration (mg/L)			Concentration of ferrous ions (mg/L)						Concentration of ferric ions (mg/L)								
	Run 1	Run 2	Run 3	Run 1	Batch 1	Run 2	Batch 2	Run 3	Batch 3	Run 1	Batch 1	K_3	Run 2	Batch 2	K_3	Run 3	Batch 3	K_3
0	4.95	4.76	4.66	4.55	4.55	4.72	4.72	4.43	4.43	0.22	0.22		0.21	0.21		0.18	0.18	
6	5.16	5.02	4.73	4.71	4.22	4.78	4.38	4.45	4.11	0.31	0.40	0.06	0.29	0.37	0.05	0.26	0.34	0.05
12	5.01	4.79	4.65	4.25	3.91	4.01	4.06	4.03	3.81	0.64	0.56	0.07	0.53	0.51	0.05	0.59	0.49	0.06
18	4.89	4.65	4.34	3.91	3.62	3.74	3.76	3.51	3.53	0.95	0.72	0.07	0.84	0.65	0.06	0.79	0.63	0.06
24	4.65	4.46	4.25	3.49	3.36	3.44	3.49	3.25	3.27	1.14	0.86	0.07	1.01	0.77	0.05	0.95	0.76	0.05
30	4.52	4.35	4.15	3.24	3.11	3.15	3.23	3.01	3.03	1.27	0.99	0.06	1.19	0.89	0.05	1.13	0.88	0.05
36	4.41	4.21	4.11	2.84	2.89	2.67	2.99	2.45	2.81	1.54	1.11	0.07	1.38	0.99	0.05	1.65	0.99	0.08
42	4.28	4.01	3.95	2.45	2.68	2.21	2.78	1.89	2.61	1.75	1.22	0.07	1.75	1.09	0.07	1.84	1.10	0.08
R^2 = coefficient of correlation				0.95		0.96		0.95		0.99			0.97			0.95		
Average values of K_3												0.07			0.06			0.06

Concentrations of raw samples were 4.67 mg/L, 4.53 mg/L, and 4.46 mg/L for runs 1, 2 and 3 respectively.

Table A.21 Makindu mission 1 (MK8)

Time (Hrs)	Concentration of iron after aeration (mg/L)			Concentration of ferrous ions (mg/L)						Concentration of ferric ions (mg/L)								
	Run 1	Run 2	Run 3	Run 1	Batch 1	Run 2	Batch 2	Run 3	Batch 3	Run 1	Batch 1	K_3	Run 2	Batch 2	K_3	Run 3	Batch 3	K_3
0	5.38	5.46	5.57	5.08	5.08	5.12	5.12	4.94	4.94	0.27	0.27		0.28	0.21		0.30	0.30	
6	5.51	5.62	5.69	5.08	4.71	5.15	4.75	5.11	4.58	0.34	0.46	0.06	0.35	0.44	0.06	0.36	0.52	0.06
12	5.42	5.54	5.58	4.70	4.37	5.07	4.40	5.15	4.24	0.55	0.64	0.05	0.55	0.65	0.05	0.59	0.72	0.05
18	5.31	5.38	5.41	3.26	4.05	3.64	4.08	3.98	3.93	0.98	0.80	0.06	1.04	0.84	0.07	1.12	0.91	0.08
24	5.01	5.17	5.19	3.11	3.75	3.36	3.78	3.55	3.65	1.23	0.95	0.06	1.25	1.02	0.06	1.35	1.09	0.08
30	4.89	5.08	5.11	2.57	3.48	2.94	3.50	3.04	3.38	1.41	1.09	0.06	1.46	1.19	0.06	1.69	1.25	0.08
36	4.53	4.66	4.67	2.30	3.22	2.55	3.25	2.54	3.13	1.75	1.22	0.07	1.81	1.35	0.07	1.88	1.40	0.08
42	4.21	4.34	4.40	2.18	2.99	2.35	3.01	2.17	2.91	1.94	1.34	0.07	1.99	1.49	0.07	2.08	1.54	0.08
R^2 = coefficient of correlation				0.93		0.92		0.90		0.97			0.97			0.97		
Average values of K_3												0.06			0.06			0.07

Concentrations of raw samples were 5.12 mg/L, 5.21 mg/L, and 5.32 mg/L for runs 1, 2 and 3 respectively.

Table A.22 Makindu Catholic Sisters (MK10)

Time (Hrs)	Concentration of iron after aeration (mg/L)			Concentration of ferrous ions (mg/L)						Concentration of Ferric ions (mg/L)								
	Run 1	Run 2	Run 3	Run 1	Batch 1	Run 2	Batch 2	Run 3	Batch 3	Run 1	Batch 1	K_3	Run 2	Batch 2	K_3	Run 3	Batch 3	K_3
0	5.47	5.39	5.58	4.61	4.61	4.39	4.39	4.86	4.86	0.33	0.33		0.29	0.29		0.38	0.38	
6	5.61	5.48	5.82	4.82	4.27	4.51	4.07	4.95	4.51	0.55	0.52	0.11	0.51	0.47	0.10	0.50	0.54	0.09
12	5.32	5.10	5.26	4.66	3.96	4.47	3.77	4.62	4.18	0.61	0.69	0.06	0.59	0.64	0.06	0.46	0.70	0.04
18	4.89	4.82	4.97	4.15	3.67	4.11	3.50	4.31	3.87	0.69	0.85	0.05	0.66	0.79	0.05	0.62	0.84	0.04
24	4.37	4.24	4.44	3.30	3.40	3.21	3.24	3.54	3.59	0.96	1.00	0.05	0.89	0.93	0.05	0.87	0.97	0.04
30	3.99	3.91	4.10	2.62	3.16	2.62	3.00	2.79	3.33	1.31	1.13	0.06	1.24	1.07	0.06	1.23	1.09	0.05
36	3.49	3.54	3.69	1.74	2.92	1.92	2.79	2.15	3.08	1.64	1.26	0.07	1.59	1.19	0.07	1.50	1.20	0.06
42	3.11	3.18	3.28	1.18	2.71	1.32	2.58	1.46	2.86	1.75	1.38	0.07	1.83	1.30	0.08	1.79	1.30	0.07
R^2 = coefficient of correlation				0.88		0.86		0.90		0.93			0.91			0.88		
Average values of K_3												0.07			0.07			0.06

Concentrations of raw samples were 5.37 mg/L, 5.11 mg/L, and 5.46 mg/L for runs 1, 2 and 3 respectively.

Appendix XII : Batch Reaction Graphs

Sikh Temple (A) (MK3)

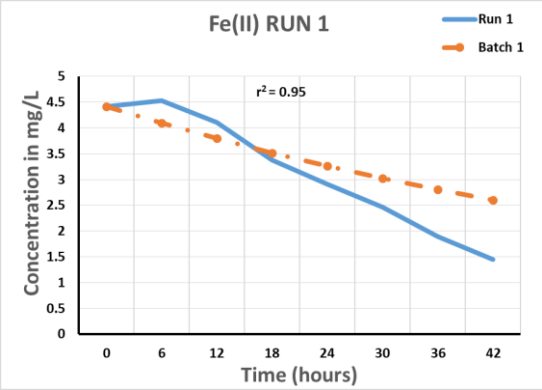

Figure A.27 MK3 Fe(II) Run 1

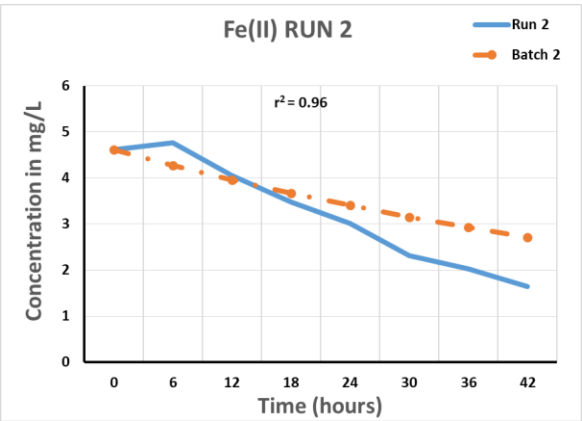

Figure A.28 MK3 Fe(II) Run 2

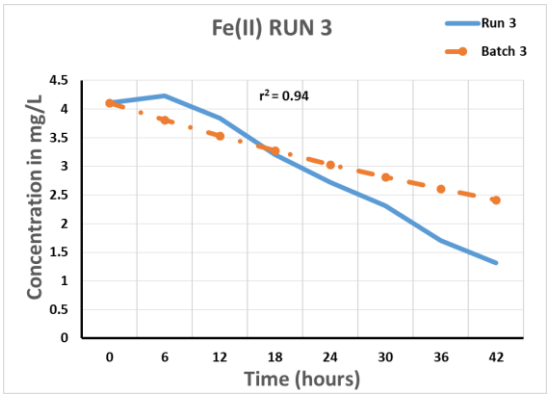

Figure A.29 Sikh MK3 Fe(II) Run 3

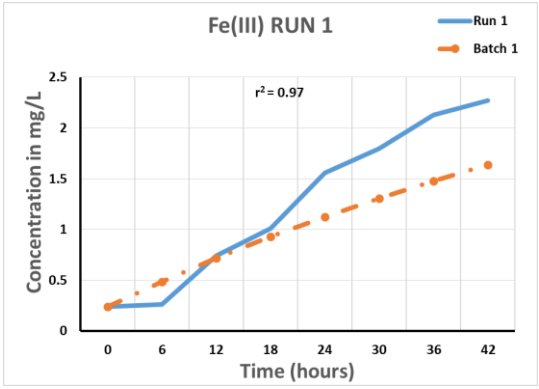

Figure A.30 MK3 Fe(III) Run 1

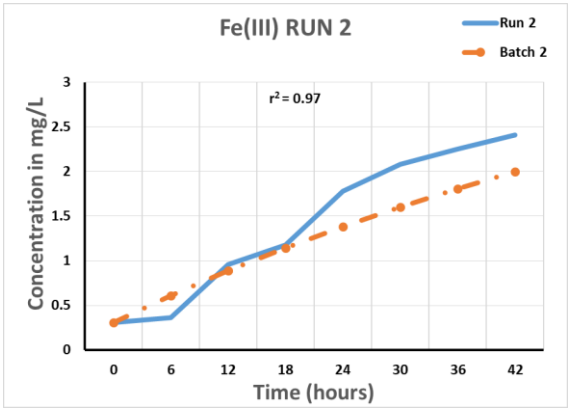

Figure A.31 MK3 Fe(III) Run 2

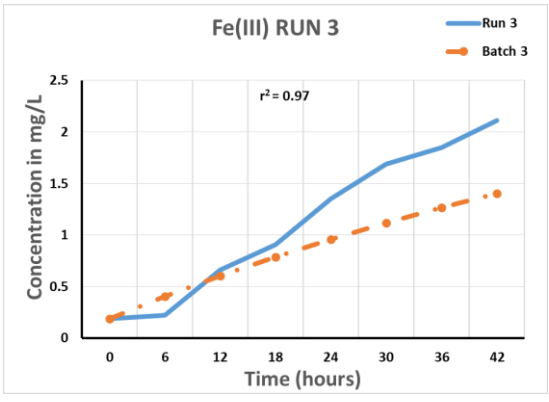

Figure A.32 MK3 Fe(III) Run 3

Sikh Temple (B) MK4

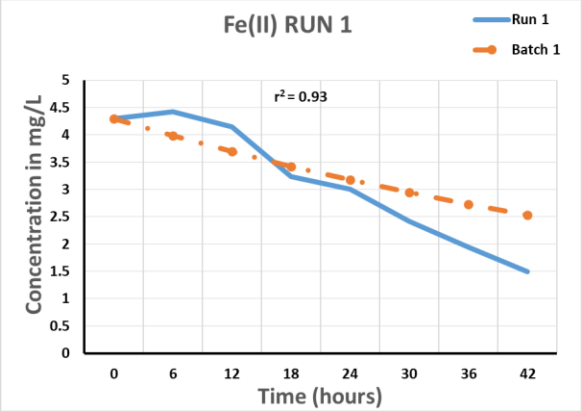

Figure A.33 MK4 Fe(II) Run 1

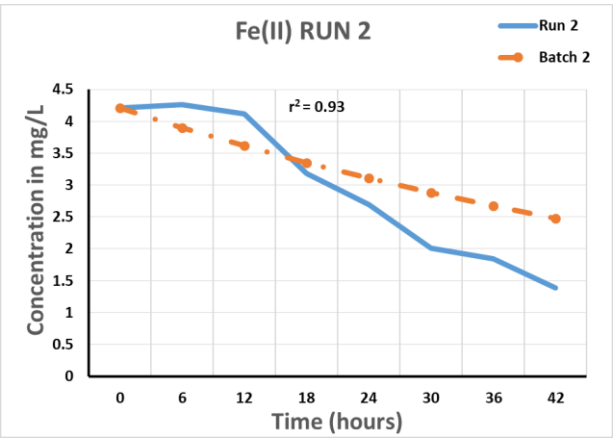

Figure A.34 MK4 Fe(II) Run 2

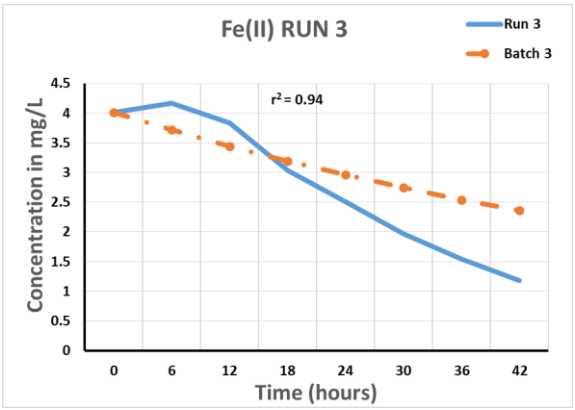

Figure A.35 MK4 Fe(II) Run 3

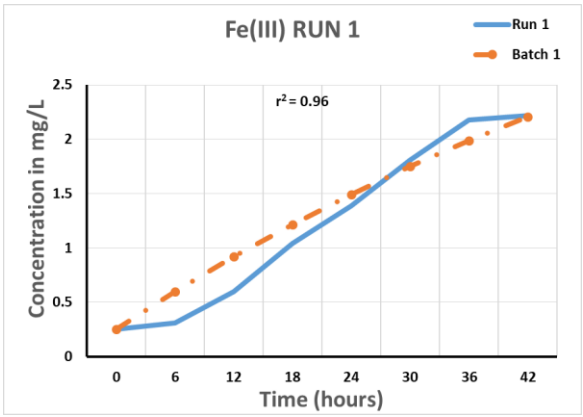

Figure A.36 MK4 Fe(III) Run 1

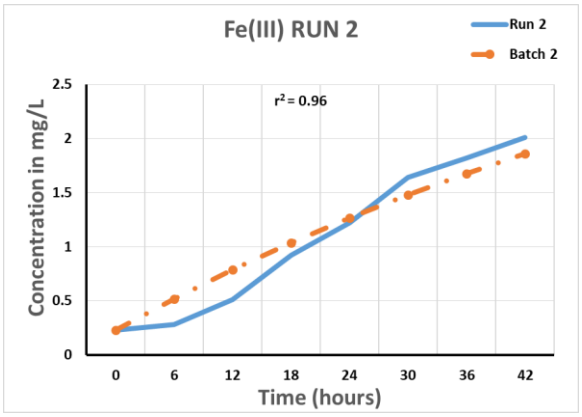

Figure A.37 MK4 Fe(III) Run 2

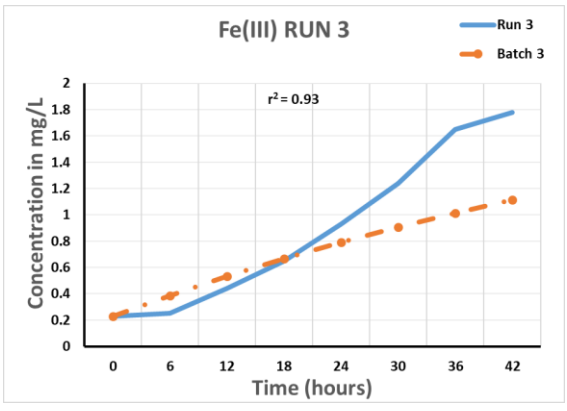

Figure A.38 MK4 Fe(III) Run 3

Jamia Mosque (A) MK1

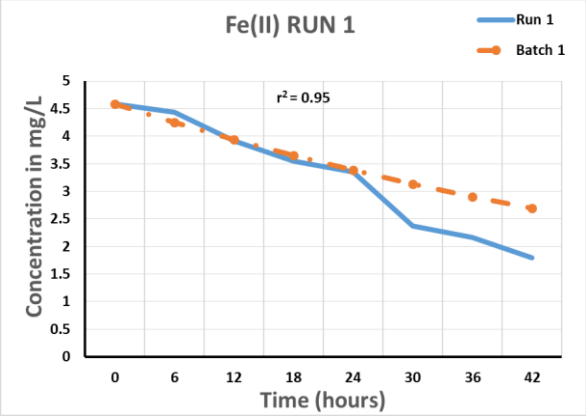

Figure A.39 MK1 Fe(II) Run 1

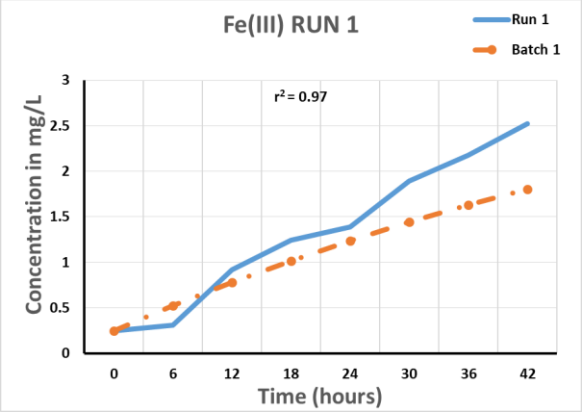

Figure A.42 MK1 Fe(III) Run 1

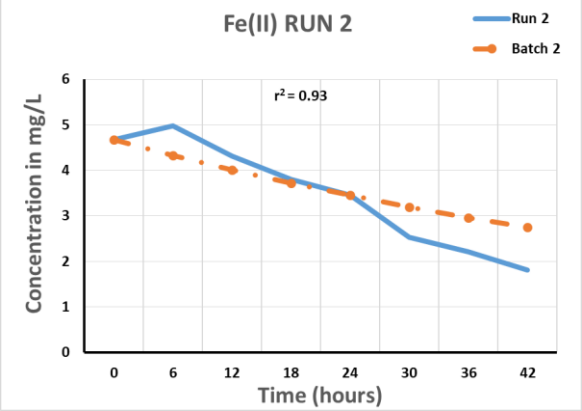

Figure A.40 MK1 Fe(II) Run 2

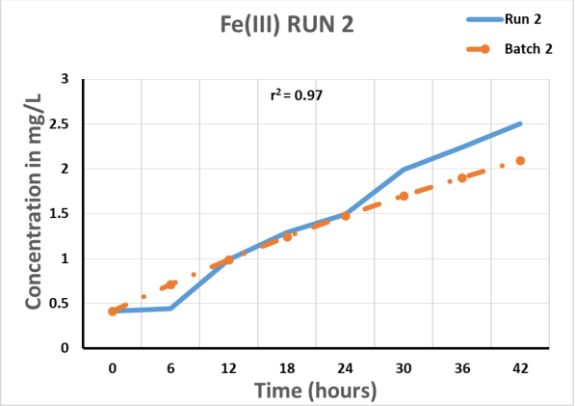

Figure A.43 MK1 Fe(III) Run 2

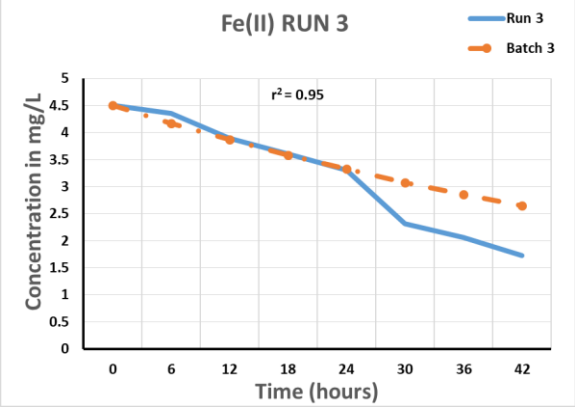

Figure A.41 MK1 Fe(II) Run 3

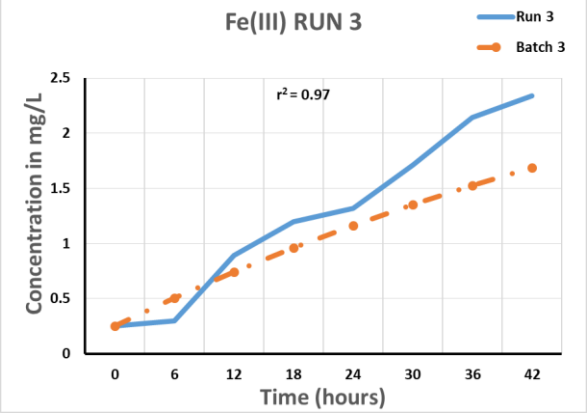

Figure A.44 MK1 Fe(III) Run 3

Jamia Mosque (B) MK2

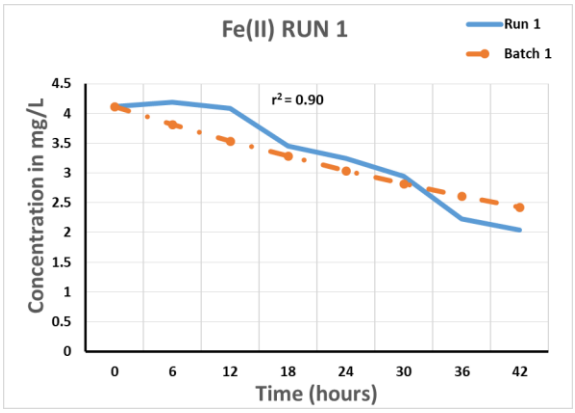

Figure A.45 MK2 Fe(II) Run 1

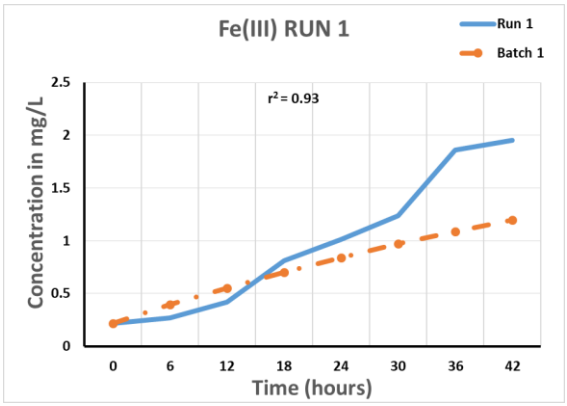

Figure A.48 MK2 Fe(III) Run 1

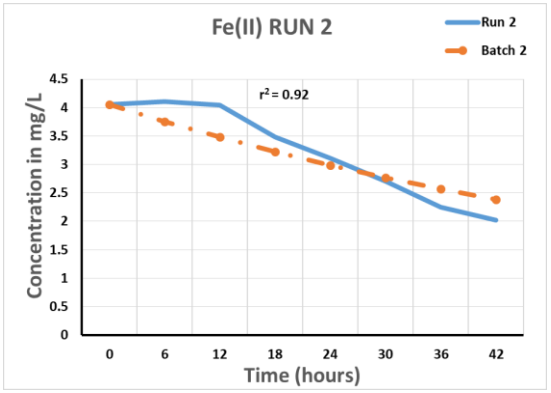

Figure A.46 MK2 Fe(II) Run 2

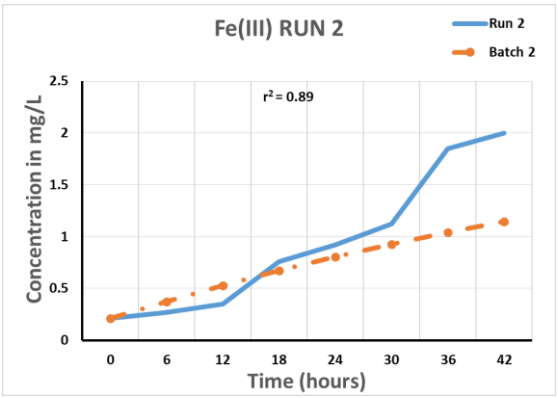

Figure A.49 MK2 Fe(III) Run 2

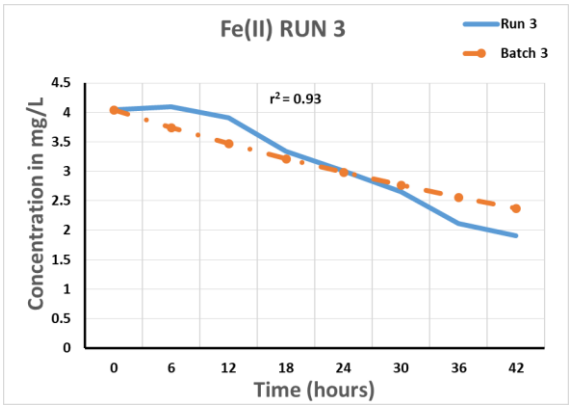

Figure A.47 MK2 Fe(II) Run 3

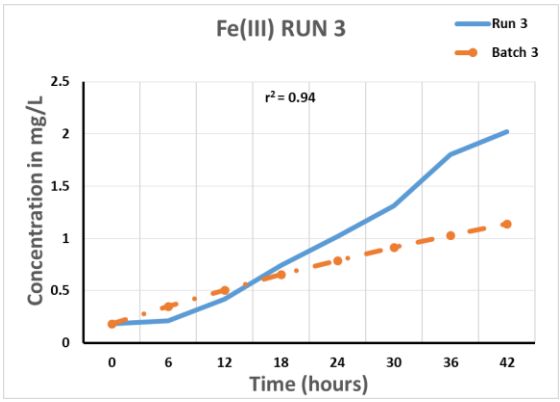

Figure A.50 MK2 Fe(III) Run 3

Makindu Hospital MK5

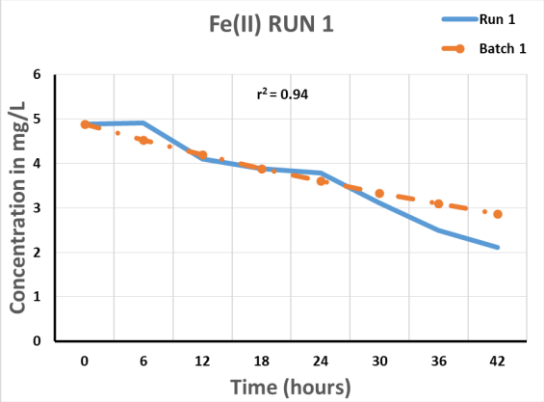

Figure A.51 MK5 Fe(II) Run 1

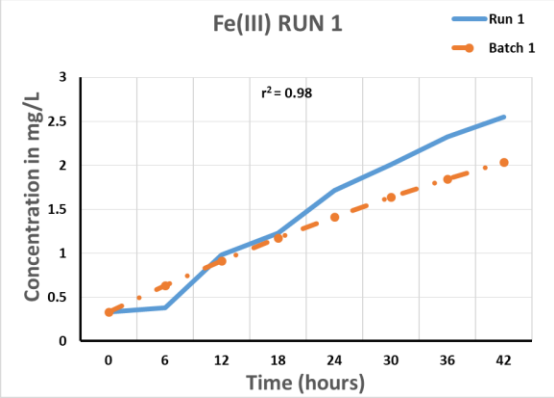

Figure A.54 MK5 Fe(III) Run 1

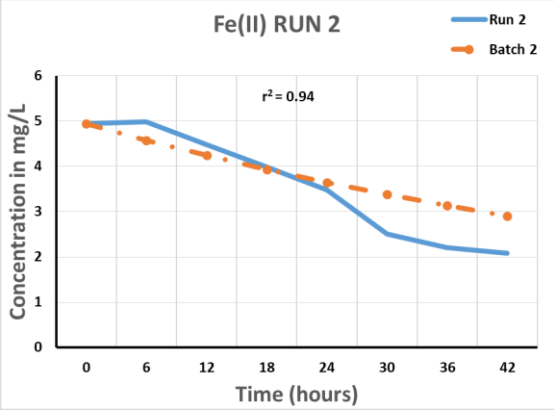

Figure A.52 MK5 Fe(II) Run 2

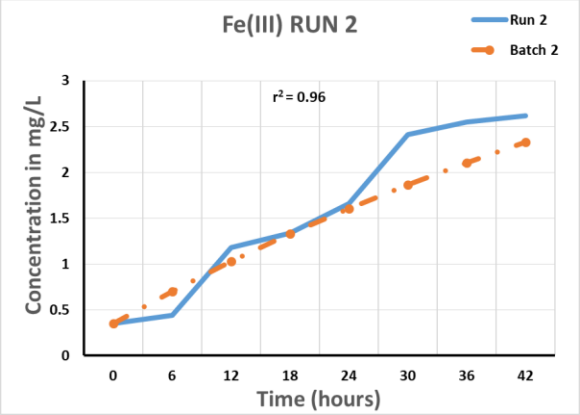

Figure A.55 MK5 Fe(III) Run 2

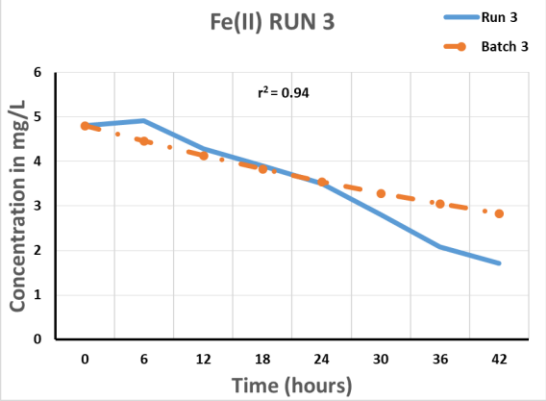

Figure A.53 MK5 Fe(II) Run 3

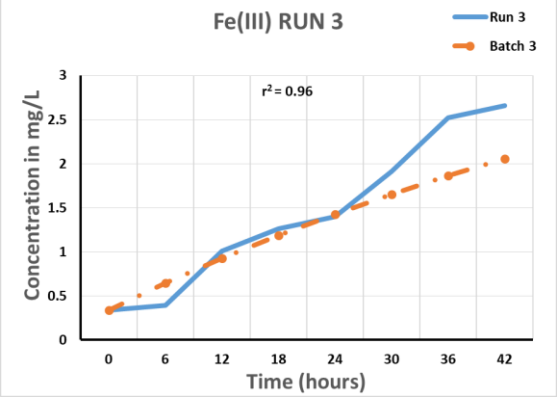

Figure A.56 MK5 Fe(III) Run 3

Makindu Railway MK6

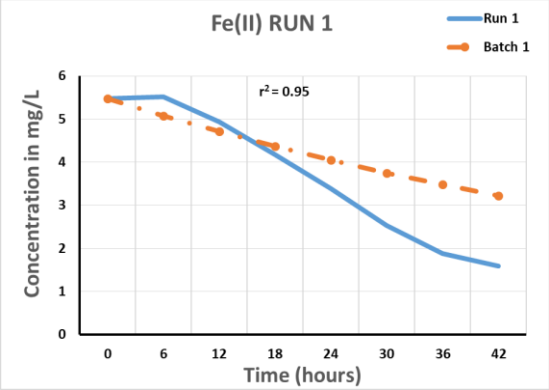

Figure A.57 MK6 Fe(II) Run 1

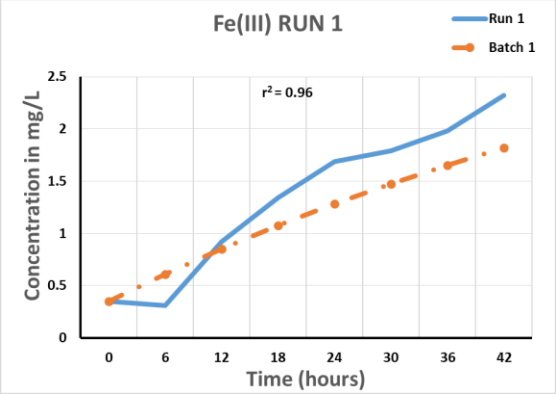

Figure A.60 MK6 Fe(III) Run 1

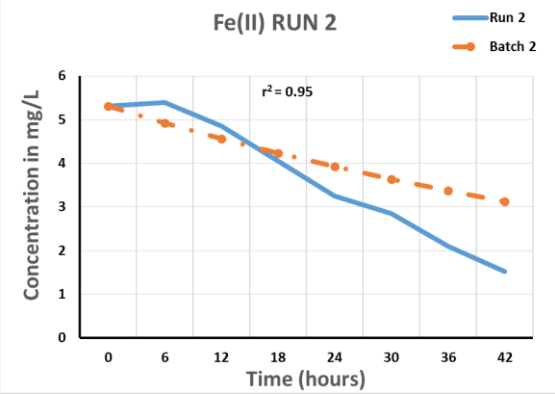

Figure A.58 MK6 Fe(II) Run 2

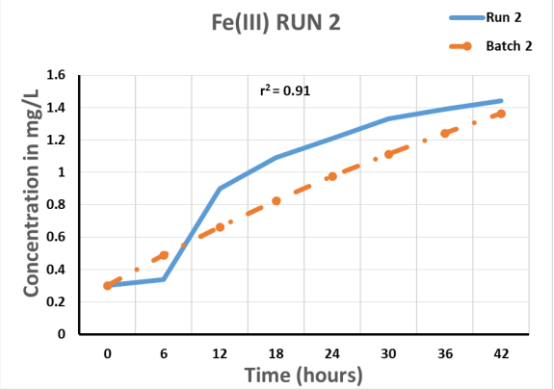

Figure A.61 MK6 Fe(III) Run 2

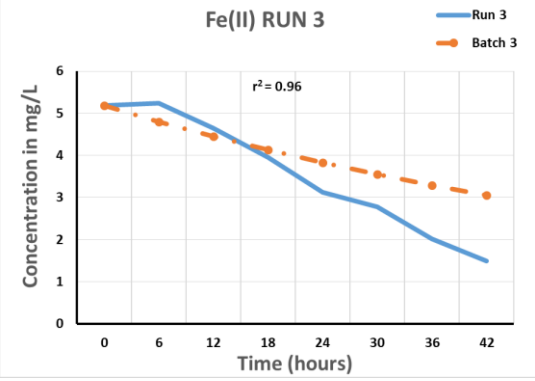

Figure A.59 MK6 Fe(II) Run 3

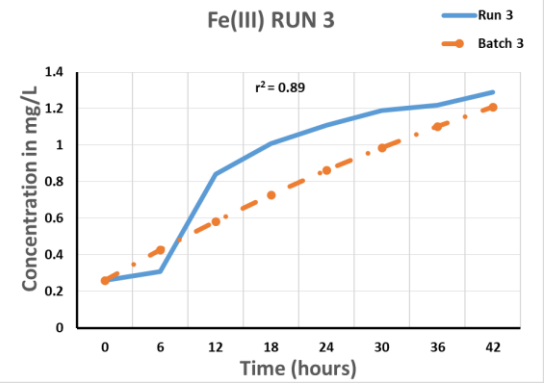

Figure A.62 MK6 Fe(III) Run 3

Ministry of Water, Makindu MK7

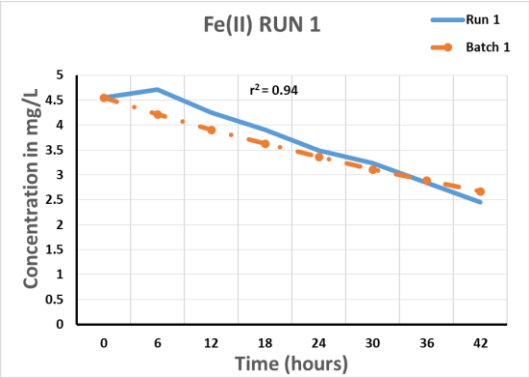

Figure A.63 MK7 Fe(II) Run 1

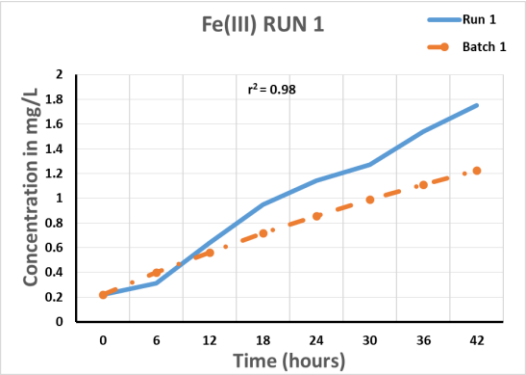

Figure A.66 MK7 Fe(III) Run 1

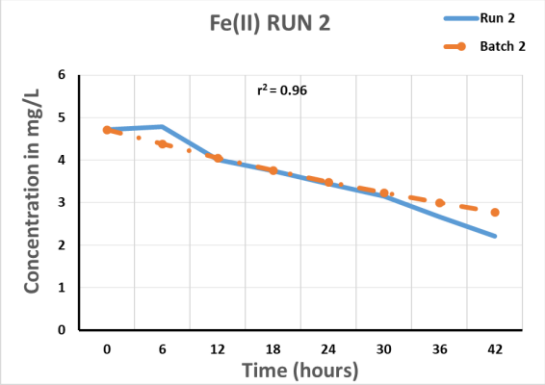

Figure A.64 MK7 Fe(II) Run 2

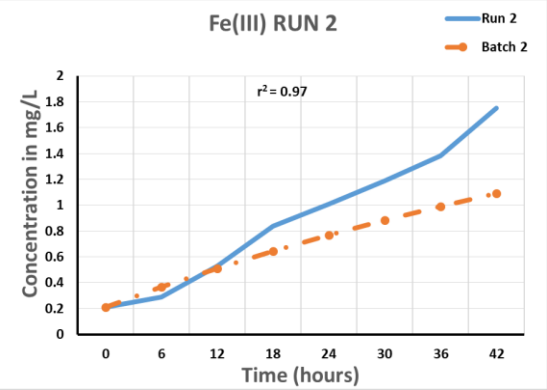

Figure A.67 MK7 Fe(III) Run 2

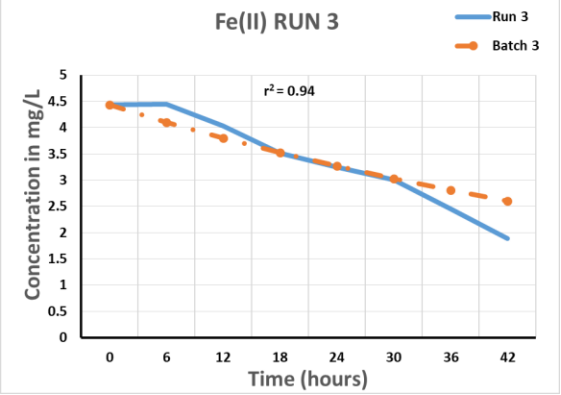

Figure A.65 MK7 Fe(II) Run 3

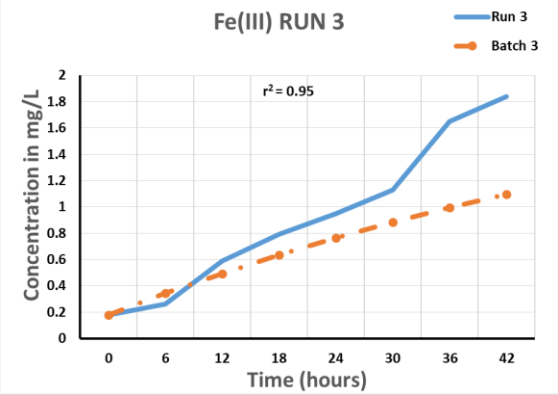

Figure A.68 MK7 Fe(III) Run 3

Makindu Mission MK8

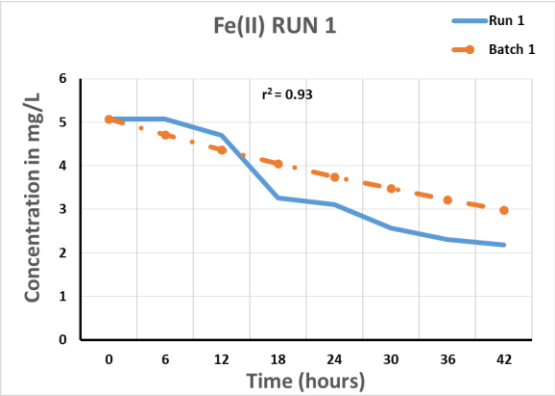

Figure A.69 MK8 Fe(II) Run 1

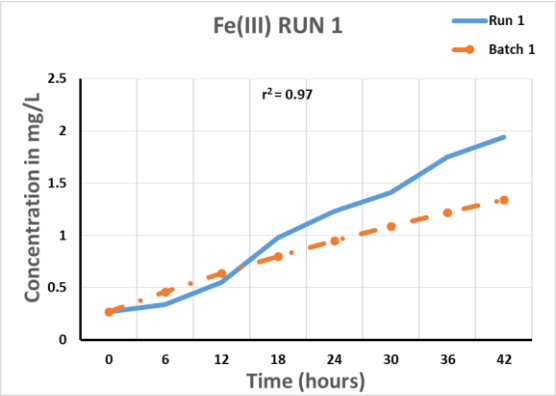

Figure A.72 MK8 Fe(III) Run 1

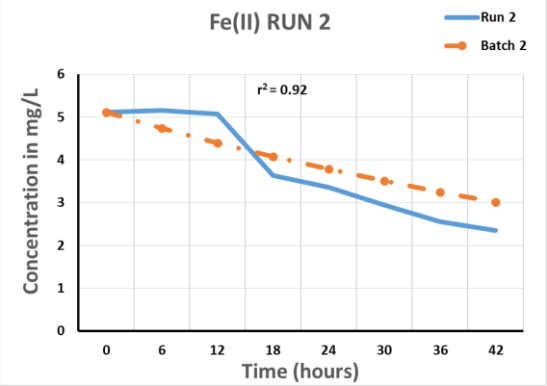

Figure A.70 MK8 Fe(II) Run 2

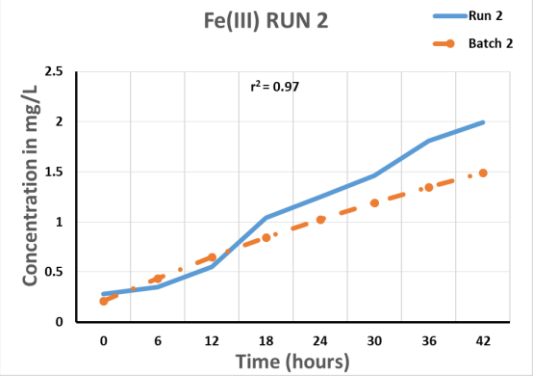

Figure A.73 MK8 Fe(III) Run 2

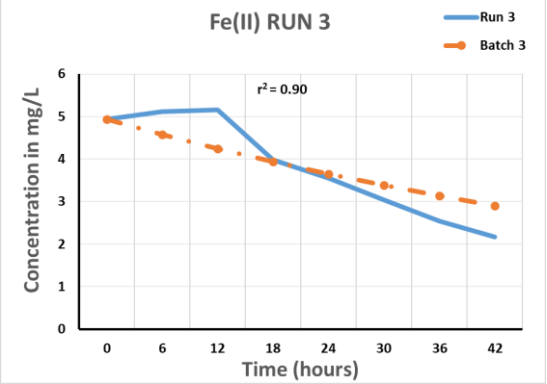

Figure A.71 MK8 Fe(II) Run 3

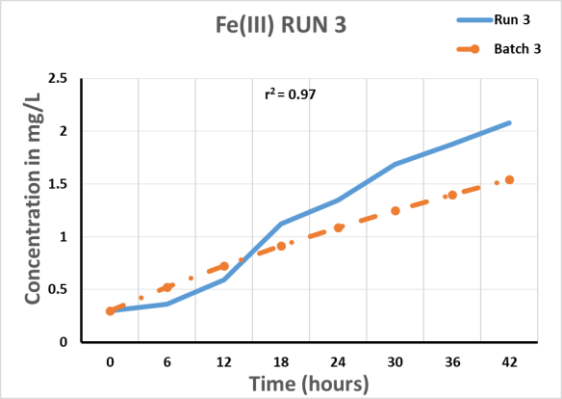

Figure A.74 MK8 Fe(III) Run 3

Makindu Sisters MK10

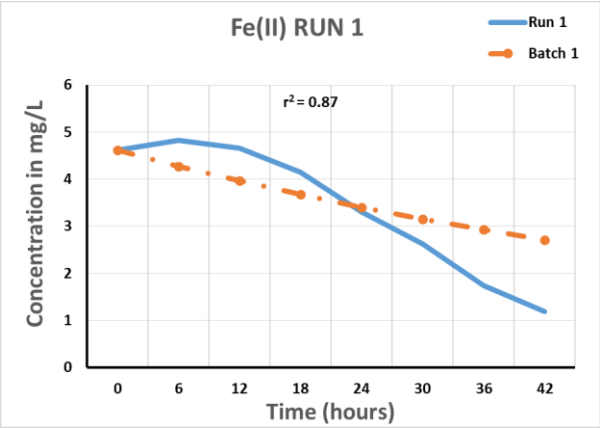

Figure A.75 MK10 Fe(II) Run 1

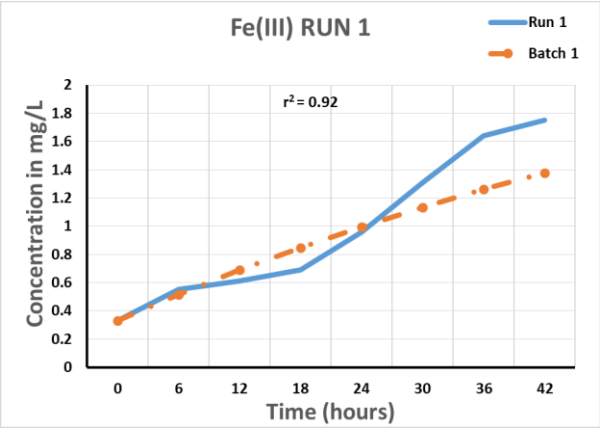

Figure A.78 MK10 Fe(III) Run 1

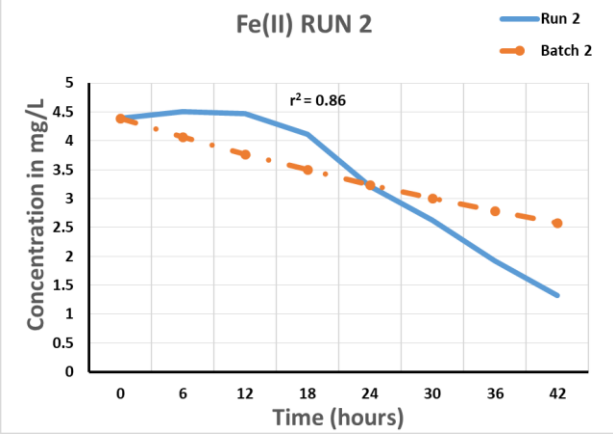

Figure A.76 MK10 Fe(II) Run 2

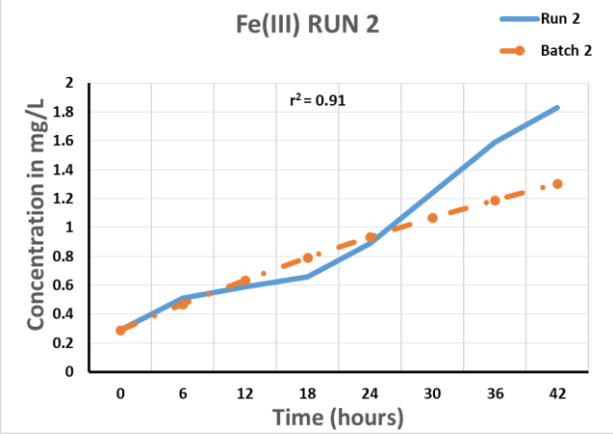

Figure A.79 MK10 Fe(III) Run 2

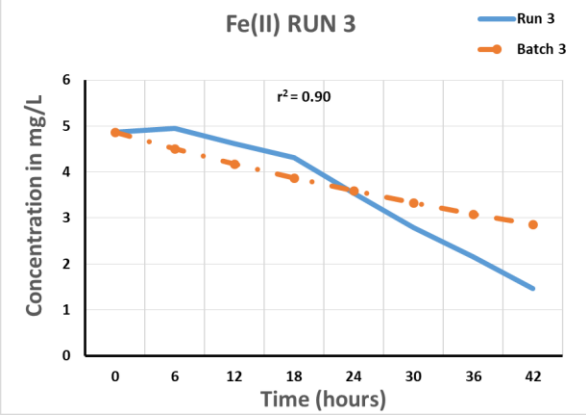

Figure A.77 MK10 Fe(II) Run 3

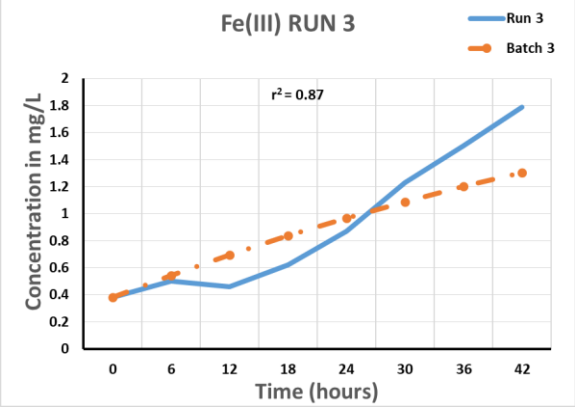

Figure A.80 MK10 Fe(III) Run 3

Appendix XIII : The Subroutine Code for Model Verification In The Aquifer

```
1  SUBROUTINE rxns (ncomp,nvrxndata,j,i,k,y,dydt,
2  $       poros,rhob,reta,rc,nlay,nrow,ncol,vrc)
3  c ***** Block 1: Comments block *******
4  c234567890123456789012345678901234567890123456789012345678901234567890123456789012
5  c ncomp - Total number of components
6  c nvrxndata - Total number of variable reaction parameters to be input via RCT file
7  c J, I, K - node location (used if reaction parameters are spatially variable)
8  c y - Concentration value of all component at the node [array variable y(ncomp)]
9  c dydt - Computed RHS of your differential equation [array variable dydt(ncomp)]
10 c poros - porosity of the node
11 c reta - Retardation factor [array variable dpreta(mcomp)]
12 c rhob - Bulk density of the node
13 c rc - Stores spatially constant reaction parameters (up to 100 values)
14 c nlay, nrow, ncol - Grid size (used only for dimensioning purposes)
15 c vrc - Array variable that stores spatially variable reaction parameters
16 c ***** End of Block 1 *******
17 c *** Block 2: Standard interface block ***
18 ! MS$ATTRIBUTES DLLEXPORT :: rxns
19 IMPLICIT NONE
```

```
20  INTEGER ncol,nrow,nlay
21  INTEGER ncomp,nvrxndata,j,i,k
22  INTEGER First_time
23  DATA First_time/1/
24  DOUBLE PRECISION y,dydt,poros,rhob,reta
        a.  DOUBLE PRECISION rc,vrc
        b.  DIMENSION y(ncomp),dydt(ncomp),rc(50)
25  DIMENSION vrc(ncol,nrow,nlay,nvrxndata),reta(50)
26  C ****** End of block 2 *******

27  C *** Block 3: Declare your problem-specific new variables here ***
28  C     INTEGER
29  DOUBLE PRECISION FE2,FE3,kFE2,kFE3
30  DOUBLE PRECISION O2,FL
31  C ***** End of Block 3 ******

32  C *** Block 4: INITIALIZE YOUR CONSTANTS HERE***
33  IF (First_time .EQ. 1) THEN
34  First_time = 0 !reset First_time to skip this block later
35  END IF
36  C ***** End of Block 4  ******
```

```
37  C  *** Block 5: Definition of other variable names ***
38  FE2 = y(1) !This is the concentration of Fe(II) (ferrous)
39  FE3 = y(2) !This is the concentration of Fe(III) (ferric)
40  kFE2 = vrc(j,i,k,1) !This is the rate constant of Fe(II) (ferrous)
41  kFE3 = vrc(j,i,k,2) !This is the rate constant of Fe(III) (ferric)
42  O2 = vrc(j,i,k,3) !This is the concentration of O2 (oxygen)
43  FL = vrc(j,i,k,4) !This is the concentration of F (fluoride)
44  C ***** End of Block 5  ******
45  c  *** Block 6: Definition of Differential Equations ***
46  c  *** concentration of Fe2 was assumed to be constant throughout the aquifer ***
47  IF (FE2 .GT. 1.0E-11) THEN
48  dydt(1) = ((-kFE2*FE2*O2*FL)) /reta(1) ! from equation (3.12)
49  ELSE
50  dydt(1) = 0
51  END IF
52  dydt (2) = ((kFE3*FE2*O2))/reta(2) ! from equation (3.13)
53  C ***** End of Block 6 ******
54  RETURN
53  END
```

Appendix XIV : Experimental Data Against Data Generated by the Subroutine Used For The Calibration

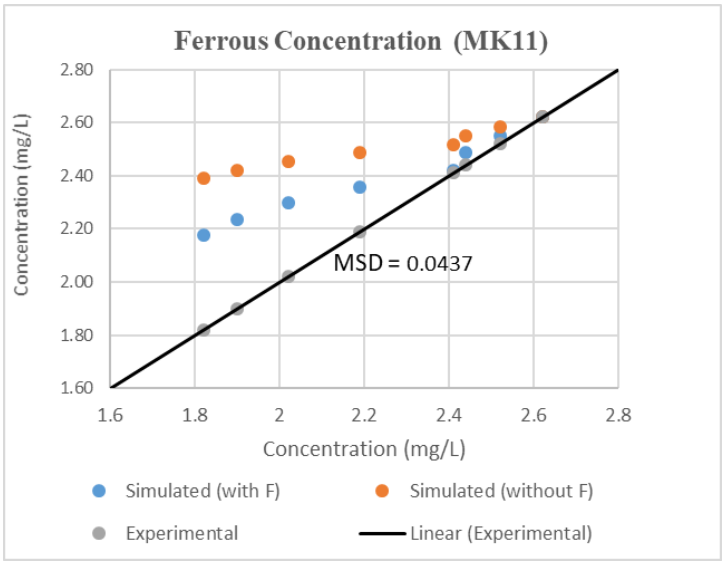

Figure A.81 Experimental against simulated data for ferrous ions for Musimba borehole (MK11)

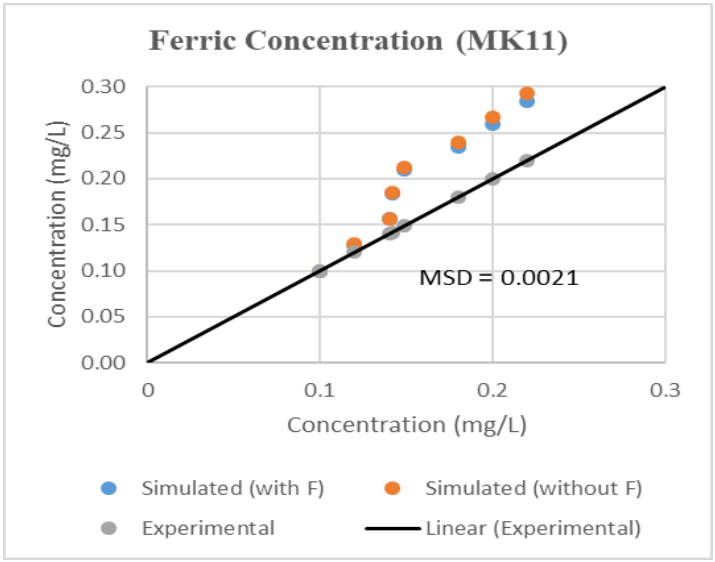

Figure A.82 Experimental against simulated data for ferric ions for Musimba borehole (MK11)

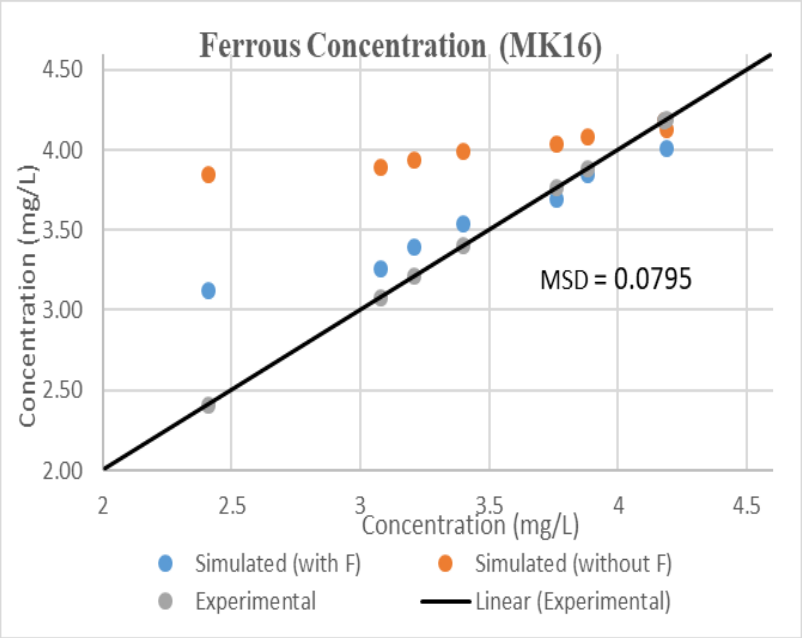

Figure A.83 Experimental against simulated data for ferrous ions for Makilya borehole (MK16)

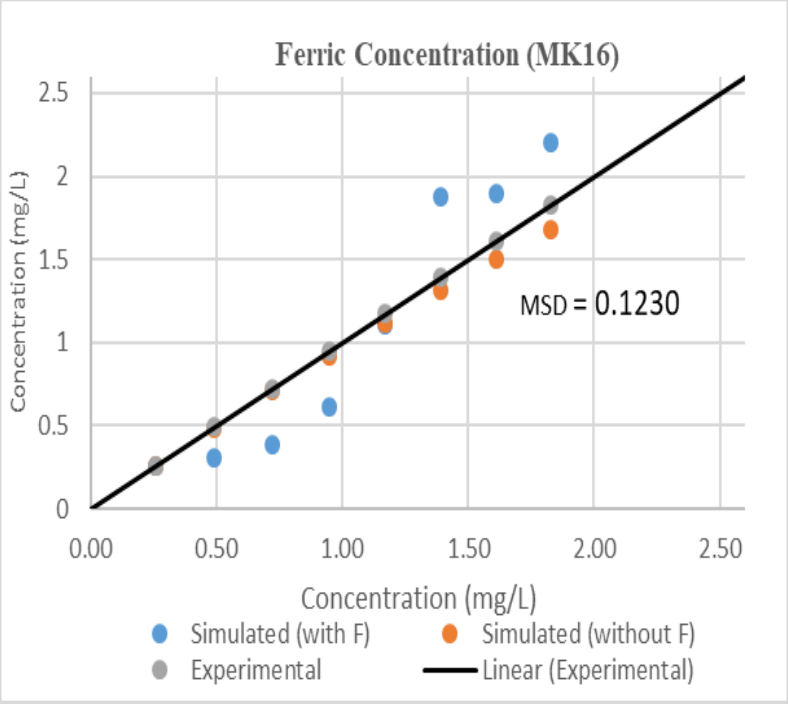

Figure A.84 Experimental against simulated data for ferric ions Makilya borehole (MK16)

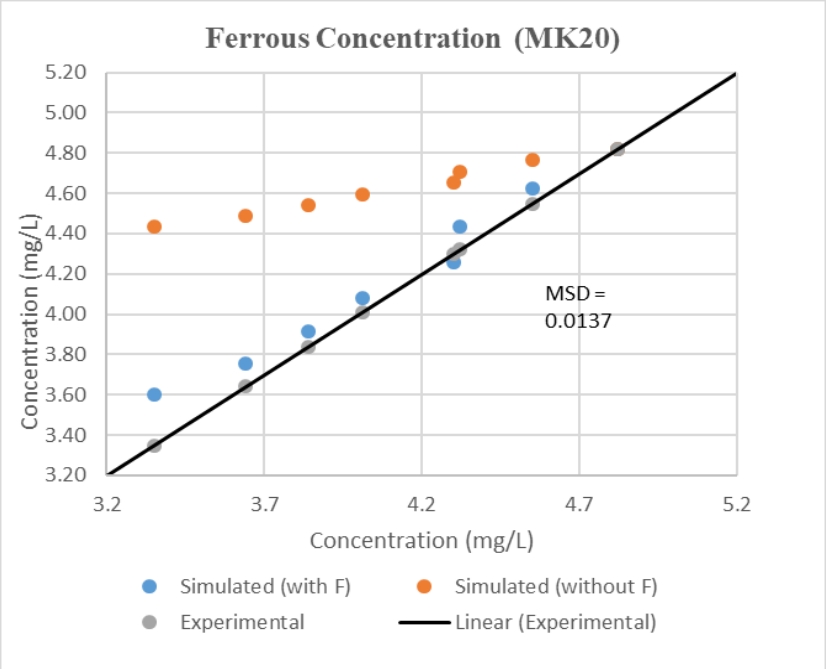

Figure A.85 Experimental against simulated data for ferrous ions for Ndivo & Co borehole (MK20)

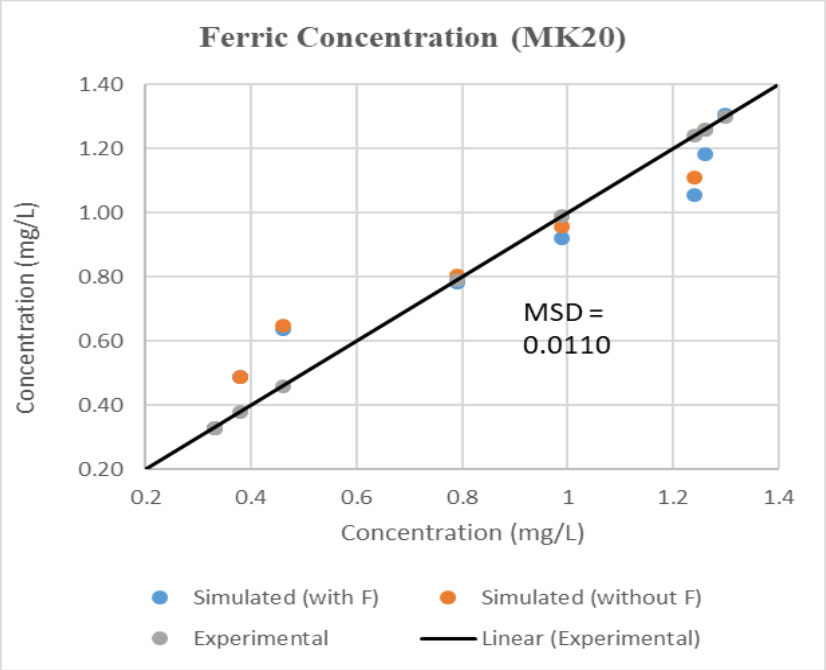

Figure A.86 Experimental against simulated data for ferric ions for Ndivo & Co borehole (MK20)

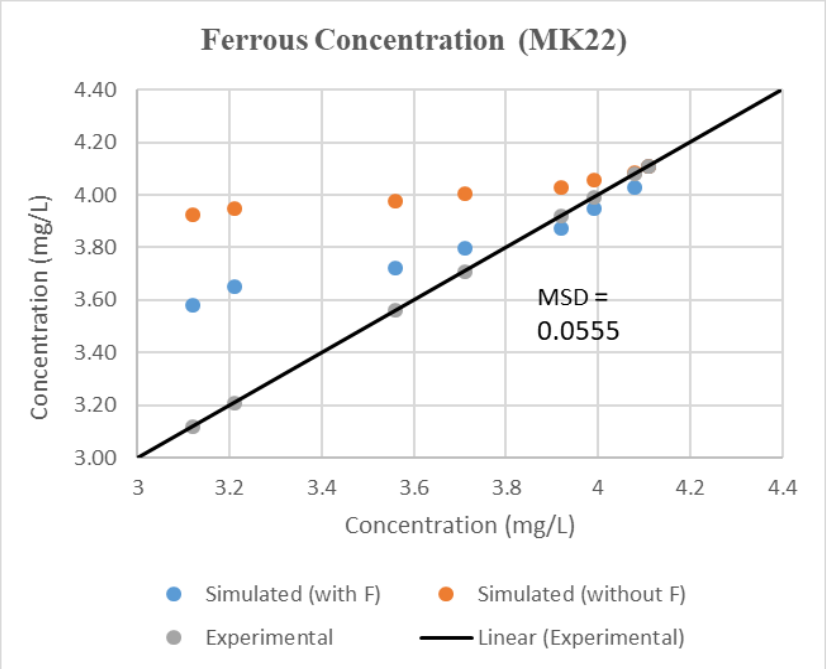

Figure A.87 Experimental against simulated data for ferrous ions for Kyeni borehole (MK22)

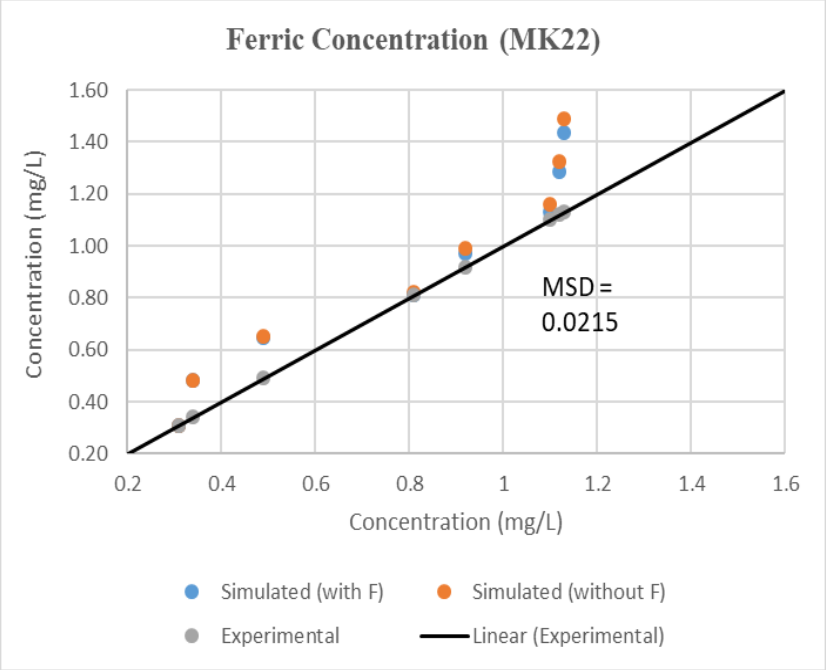

Figure A.88 Experimental against simulated data for ferric ions for Kyeni borehole (MK22)

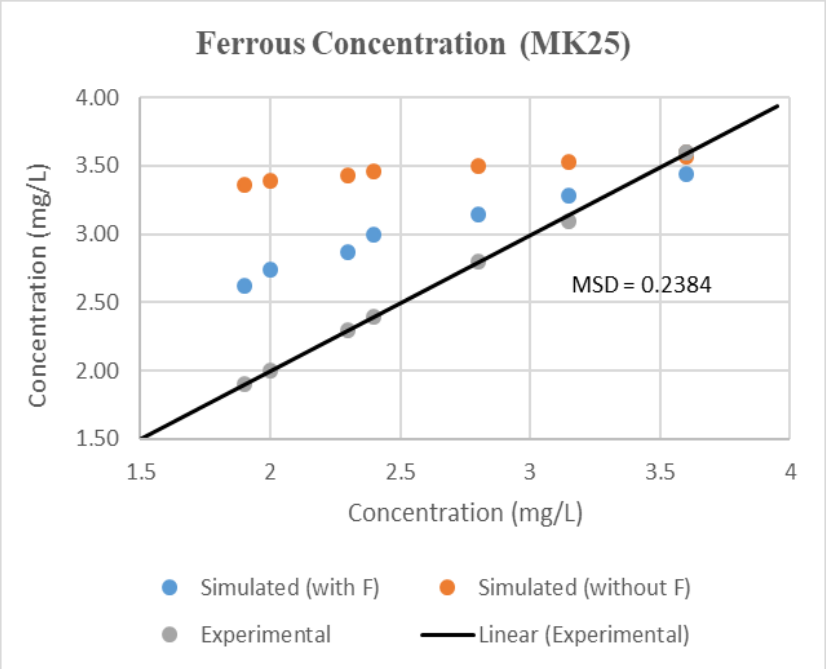

Figure A.89 Experimental against simulated data for ferrous ions for Mulili borehole (MK25)

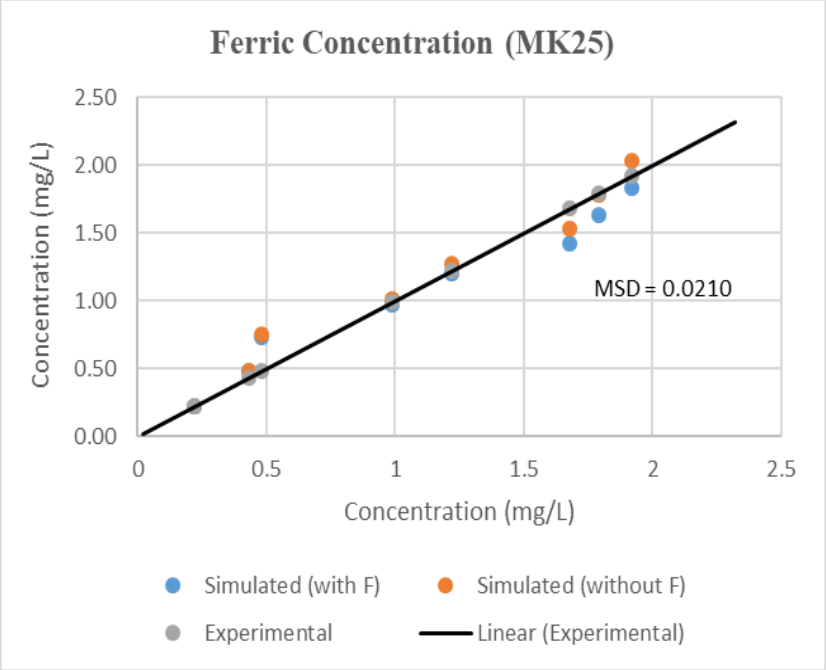

Figure A.90 Experimental against simulated data for ferric ions for Mulili borehole (MK25)

Appendix XV : Experimental and Simulated Data From June 2016 To December 2019 (Ferrous)

Table A.23 Table of experimental and simulated data for four (4) years from june 2016 to december 2019 (ferrous)

Time of sampling	Jamia Mosque (A) MK1)		Sikh Temple B (MK4)		Makindu Hospital (MK5)		Makindu Railway (MK6)		Makindu Mission 1 MK8)	
	Experimental	Simulated	Experimental	Simulated	Experimental	Simulated	Experimental	Simulated	Experimental	Simulated
June.2016	1.60	1.505	1.33	1.197	1.41	1.02	1.10	0.83	0.92	0.878
Dec.2016	1.43	1.427	1.23	1.110	1.24	0.965	0.92	0.744	0.76	0.705
June.2017	1.42	1.431	1.17	1.12	1.22	0.916	0.82	0.760	0.82	0.805
Dec.2017	1.39	1.424	1.10	1.11	1.234	0.89	0.84	0.760	0.81	0.800
June.2018	1.33	1.435	0.98	1.127	1.230	0.88	0.86	0.780	0.79	0.825
Dec.2018	1.28	1.398	0.86	1.186	1.19	0.837	0.78	0.724	0.78	0.766
June.2019	1.37	1.413	1.01	1.106	1.12	0.848	0.66	0.750	0.75	0.799
Dec.2019	1.39	1.410	0.86	0.99	1.10	0.842	0.75	0.750	0.77	0.795
Coefficient of Correlation **(R^2)**	**0.90**		**0.76**		**0.88**		**0.70**		**0.75**	

Appendix XVI : Experimental and Simulated Data From June 2016 To December 2019 (Ferric)

Table A.24 Table of experimental and simulated data for four (4) years from june 2016 to december 2019 (ferric)

Time of sampling	Jamia Mosque (A) MK1)		Sikh Temple B (MK4)		Makindu Hospital (MK5)		Makindu Railway (MK6)		Makindu Mission 1 MK8)	
	Experimental	Simulated	Experimental	Simulated	Experimental	Simulated	Experimental	Simulated	Experimental	Simulated
June.2016	3.185	4.058	2.44	2.494	2.93	2.737	2.75	2.254	2.51	2.118
Dec.2016	3.430	4.207	2.57	2.540	3.06	2.807	2.86	2.390	2.48	2.152
June.2017	3.640	4.218	2.48	2.53	2.95	2.854	2.68	2.38	2.73	2.150
Dec.2017	3.73	4.235	2.50	2.532	3.20	2.93	2.92	2.28	2.82	2.153
June.2018	3.59	4.224	2.510	2.520	3.21	2.98	2.82	2.28	3.01	2.146
Dec.2018	3.79	4.275	2.52	2.449	3.32	3.06	2.87	2.29	3.11	2.165
June.2019	3.87	4.252	2.532	2.534	3.39	3.10	3.01	2.28	3.15	2.156
Dec.2019	3.68	4.252	2.54	2.534	3.56	3.40	2.94	2.40	3.25	2.157
Coefficient of Correlation **(R^2)**	**0.91**		**0.70**		**0.94**		**0.72**		**0.83**	

MODELING SOLUTE DYNAMICS IN AQUIFERS: CASE STUDY OF IRON DISPERSION CHYULU AQUIFER, KENYA

ORIGINALITY REPORT

19%	17%	10%	6%
SIMILARITY INDEX	INTERNET SOURCES	PUBLICATIONS	STUDENT PAPERS

PRIMARY SOURCES

1	www.jiarm.com Internet Source	2%
2	ir.jooust.ac.ke:8080 Internet Source	1%
3	jiarm.com Internet Source	1%
4	"RT3D tutorials for GMS users", 'Office of Scientific and Technical Information (OSTI)' Internet Source	1%
5	technodocbox.com Internet Source	<1%
6	www.ijsr.net Internet Source	<1%
7	webapps.itc.utwente.nl Internet Source	<1%
8	etd.uwc.ac.za Internet Source	<1%
	bioprocess.pnl.gov	